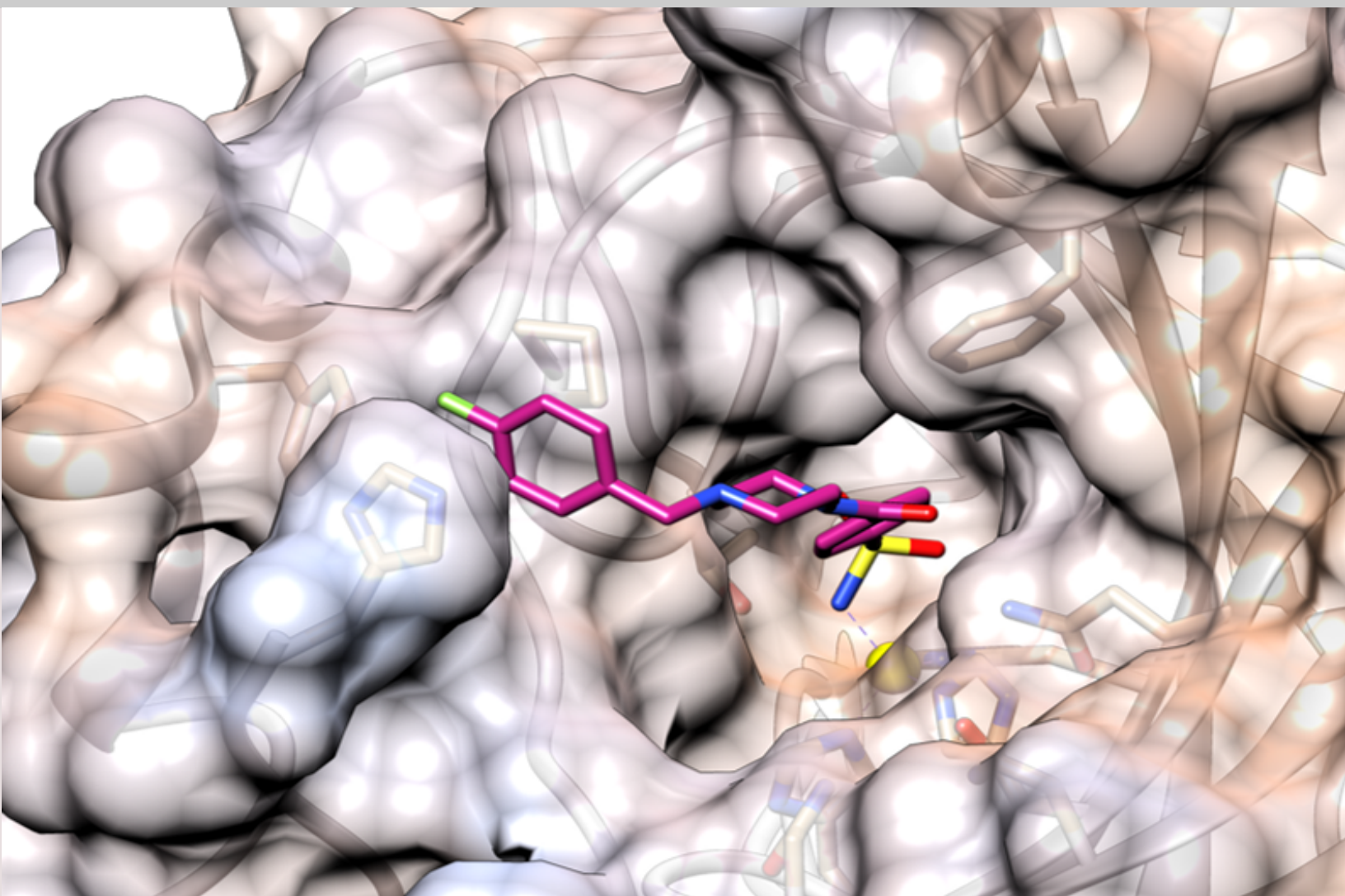# UNIVERSITY OF MESSINA

DEPARTMENT OF CHEMICAL, BIOLOGICAL, PHARMACEUTICAL AND ENVIRONMENTAL SCIENCES

DOCTORAL THESIS

Targeting Carbonic Anhydrases (CAs): Rational Design, Synthesis, Structural Studies and Biochemical Evaluation

Francesca Mancuso

PHD SCHOOL IN APPLIED BIOLOGY AND EXPERIMENTAL MEDICINE

Prof. Rosaria Gitto
Doctoral Thesis Supervisor

Prof. Nunziacarla Spanò
Head of PhD School

PhD Course in Pharmaceutical Sciences 2017–2020

UNIVERSITY OF MESSINA

DEPARTMENT OF CHEMICAL, BIOLOGICAL, PHARMACEUTICAL AND ENVIRONMENTAL SCIENCES

DOCTORAL THESIS

Targeting Carbonic Anhydrases (CAs): Rational Design, Synthesis, Structural Studies and Biochemical Evaluation

PhD SCHOOL IN
APPLIED BIOLOGY AND EXPERIMENTAL MEDICINE
• PHARMACEUTICAL SCIENCES •

XXXIII CYCLE

S.S.D. CHIM/08

CANDIDATE:
Francesca Mancuso

SUPERVISOR:
Prof. R. Gitto

HEAD OF PhD SCHOOL:
Prof. N. Spanò

PhD COURSE 2017–2020

Abbreviations

CA	Carbonic Anhydrase		**EtOH**	Ethanol
hCA	Human Carbonic Anhydrase		**MeOH**	Methanol
VchCA	Vibrio Cholerae Carbonic Anhydrase		**THF**	Tetrahydrofuran
CoCA	Coccomyxa Carbonic anhydrase		**DMF**	N,N-Dimethylformamide
SARs	Structure Activity–Relationships		**TFA**	Trifluoroacetic acid
CAI	Carbonic Anhydrase Inhibitor		**DBU**	1,8–Diazabicyclo[5.4.0]undec–7–ene
ZBG	Zinc Binding Group		**TEA**	Triethylamine
AG	Anchoring Group		**BzCl**	Benzoyl chloride
SG	Sticky Group		**HATU**	1–[Bis(dimethylamino)me-thylene]–1H–1,2,3–triazolo[4,5–b]pyridinium 3–oxid hexafluorophosphate
CAA	Carbonic Anhydrase Activator			
AAZ	Acetazolamide		**COMU**	(1–Cyano–2–ethoxy–2–oxoethylidenaminooxy)dime-thylamino–morpholino–carbenium hexafluorophos-phate
EZA	Ethoxzolamide			
TPM	Topiramate			
HIF	Hipoxia Inducible Factor			
HBTU	N,N,N,N–tetramethyl–O–(1H–benzotriazol–1–yl)uronium hexafluorophos-phate		**DMSO**	Dimethyl Sulfoxide
			EtOAc	Ethyl Acetate
			CyHe	Cyclohexane
			TLC	Thin Layer Cromatography
CDI	1'–Carbonyldiimidazole		**AUC**	Area Under Curve
PTZ	Pentilentetrazole		**ROC**	Receiver Operating Character-istic
DIPEA	N,N–Diisopropylethylamine			
DCM	Dichloromethane		**VS**	Virtual Screening
			RMSD	Root Mean Square Deviation

Preface

The title of the present Doctor of Philosphy (PhD) dissertation is "*Targeting Carbonic Anhydrases (CAs): Rational Design, Synthesis, Structural Studies and Biochemical Evaluation*".
This thesis describes the three–years research work aimed and develop novel Carbonic Anhydrase inhibitors (CAIs) by a combination of structural and computational techniques. The first chapter provides a brief overview of the different families of Carbonic Anhydrases (CAs) identified so far, their structural features, function, catalytic and inhibition mechanism. In the second chapter our efforts in the field of search of novel CAs inhibitors targeting the human and bacterial classes are presented. The discussion focuses on the rational design, synthetic procedures, the biochemical assessment, Structure Activity Relationships (SARs) analysis, and investigation of the binding poses of the novel CA inhibitors through theoretical (molecular docking) or experimental (X-ray crystallography) studies. In details, section 2.1–2.3. show the results obtained searching for new CAIs targeting the druggable human CA VII, CA IX and CA XII isoforms. These compounds have been rationally designed on the basis of structural information collected from literature. The following sections (2.4–2.7) shift the attention on the potential of CAIs as new agents to overcome the spreading phenomena of antimicrobial drug resistance. Specifically, these sections explain various drug design strategies that led us to identification of potent and selective inhibitors against the CAs classes expressed by the pathogenic species *Vibrio Cholerae*.
The third part provides a full description of the experimental protocols employed for the synthesis, the biochemical and pharmacological testing, molecular docking and X–ray crystallographic studies for the novel designed CAIs. The CA inhibition assays were performed at the University of Florence (Italy) in collaboration with the research group of Professor Claudiu T. Supuran. The *in vivo* testing has been carried out in the laboratory of Professor Giovanbattista De Sarro from the Magna Graecia University of Catanzaro (UniCZ, Italy). X–ray diffraction data were collected at the Institute of Biostructure and Bioimaging (IBB) of National Research Council (CNR, Italy) thanks to the collaboration with Dr. Giuseppina De Simone and coworkers.
A part of this project has been developed during my seven–months external experience at "The Institute of Organic Chemistry and Biochemistry" (IOCB, Czech Academy of Science) of Prague (Czech Republic) under the supervision of Dr. Milan Vràbel. In the Appendix of this dissertation, the research paper titled "*Transition Metal–Mediated vs. Tetrazine–Triggered Release Reaction. Direct Comparison and Combinations Thereof*" is attached. This manuscript documents the personal contribution given to the realization of a innovative project focused on bioorthogonal release reactions performed during IOCB period.

Keywords: *Carbonic anhydrase, inhibitor, sulfonamide, coumarin, synthesis, molecular docking, X–ray crystallography.*

List of Publications

[I] **F.Mancuso**, M. Rahm, R. Dzijak, H. Mertikova-Kaiserova, M. Vrabel, "Transition-metal-mediated versus tetrazine-triggered bioorthogonal release reactions: direct comparison and combination thereof" *ChemPlusChem*, **85**, (1669-1675) (2020).

[II] **F.Mancuso**, L.De Luca, A. Angeli, E. Berrino, S. Del Prete, C. Capasso, C. T. Supuran, R. Gitto, "In Silico-Guided Identification of New Potent Inhibitors of Carbonic Anhydrases Expressed in Vibrio cholerae" *ACS Medicinal Chemistry Letters*, Published online 1th Sept 2020.

[III] **F. Mancuso**, L. De Luca, A.Angeli, .Del Prete, C.Capasso, C. T. Supuran, R. Gitto, "Synthesis, computational studies and assessment of in vitro inhibitory activity of umbelliferon-based compounds against tumor-associated carbonic anhydrase isoforms IX and XIIs" *Journal of Enzyme Inhibition and Medicinal Chemistry*, 1442–1449 (2020).

[IV] **F.Mancuso**, A Di Fiore, L. De Luca, A. Angeli, S. M. Monti, G. De Simone, C. T. Supuran, R. Gitto, "Looking toward the Rim of the Active Site Cavity of Druggable Human Carbonic Anhydrase Isoforms" *ACS Medicinal Chemistry Letters*, **11**, 1000–1005 (2020).

[V] R. Gitto, L. De Luca, **F. Mancuso**, S. Del Prete, D. Vullo, C.T. Supuran, C. Capasso, "Seeking new approach for therapeutic treatment of cholera disease via inhibition of bacterial carbonic anhydrases: experimental and theoretical studies for sixteen benzenesulfonamide derivatives" *Journal of Enzyme Inhibition and Medicinal Chemistry*, **34**, (1186-1192) (2019).

[VI] G. Mandalari, C. Bisignano, A., M. Denaro, M. Musarra Pizzo, R. Pennisi, **F. Mancuso**, S. Ferro, D. Trombetta, A.M. Monforte, M. T. Sciortino, L. De Luca, "Simulated human digestion of N1-aryl-2-arylthioacetamidobenzimidazoles and their activity against Herpes-simplex virus 1 in vitro" *PLOS ONE*, **14**, e0216384, (2019).

[VII] M.R. Buemi, A. Di Fiore, L. De Luca, A. Angeli, **F. Mancuso**, S. Ferro, S.M. Monti, M. Buonanno, E. Russo, G. De Sarro, G. De Simone, C. T. Supuran, R. Gitto, "Exploring structural properties of potent human carbonic anhydrase inhibitors bearing a 4-(cycloalkylamino-1-carbonyl)benzenesulfonamide moiety" *European Journal of Medicinal Chemistry*, **163**, (443–452) (2019).

[VIII] L. De Luca, **F. Mancuso**, S. Ferro, M.R. Buemi, A. Angeli, S. Del Prete, C. Capasso, C. T. Supuran, R. Gitto, "Inhibitory Effects and Structural Insights for a Novel series of Coumarin-based Compounds that Selectively Target human CA IX and CA XII Carbonic Anhydrases" *European Journal of Medicinal Chemistry*, **143**, 276–282 (2018).

CONTENTS

ABSTRACT

Carbonic anhydrases (CAs, E.C. 4.2.1.1.) are ubiquitous metalloenzymes present throughout most organisms in all kingdom of life and they are classified in eight evolutionary unrelated gene families namely α–, β–, γ–, δ–, ζ–, η–, θ–, τ-CAs. CAs catalyze the reversible hydration of carbon dioxide to bicarbonate and proton. In many organisms, these enzymes are involved in CO_2 and pH homeostasis, transport of CO_2/HCO_3^-, respiration and a multitude of biosynthetic reaction [1, 2]. In humans, fifteen isoenzymes belonging to α–class have been identified (hCAs I–IV, VA and VB, VI–XIV) in numerous tissues and organs. Since many hCAs have been implicated and extensively studied in a multitude of physiological processes (gluconeogenesis, lipogenesis, bone resorption, calcification, tumorigenesis, etc.), the abnormal activity or deregulated expression of specific hCAs have been linked with a wide array of pathological consequences (epilepsy and others neuropathic pain, osteoporosis, glaucoma, obesity, cancer, etc.) [3, 4]. For these reasons, in the recent years several human CAs (hCA VII, hCA IX and hCA XII) became well-established drug targets for designing CAs modulators endowed with therapeutic and/or diagnostic applications. Although a large number of molecules have been designed, synthesized and tested for their affinity against human CAs to date, their use as drugs is still limited due to the lack of selectivity for a specific isoform and the related wide onset of side effects. Hence, the main challenge in the development of new CA inhibitors is to find selectivity against isoforms involved in human diseases and to prevent off-target related side effects that are caused by the inhibition of the ubiquitous isoforms hCA I and II.

In this scenario, the basis for the rational drug design of more selective compounds can be provided by structural data on human CA isoforms collected so far and by the inspection of their complexes with inhibitor molecules. A careful comparison between all the crystallized hCAs revealed that the main differences in terms of oligomeric structure and sequence among
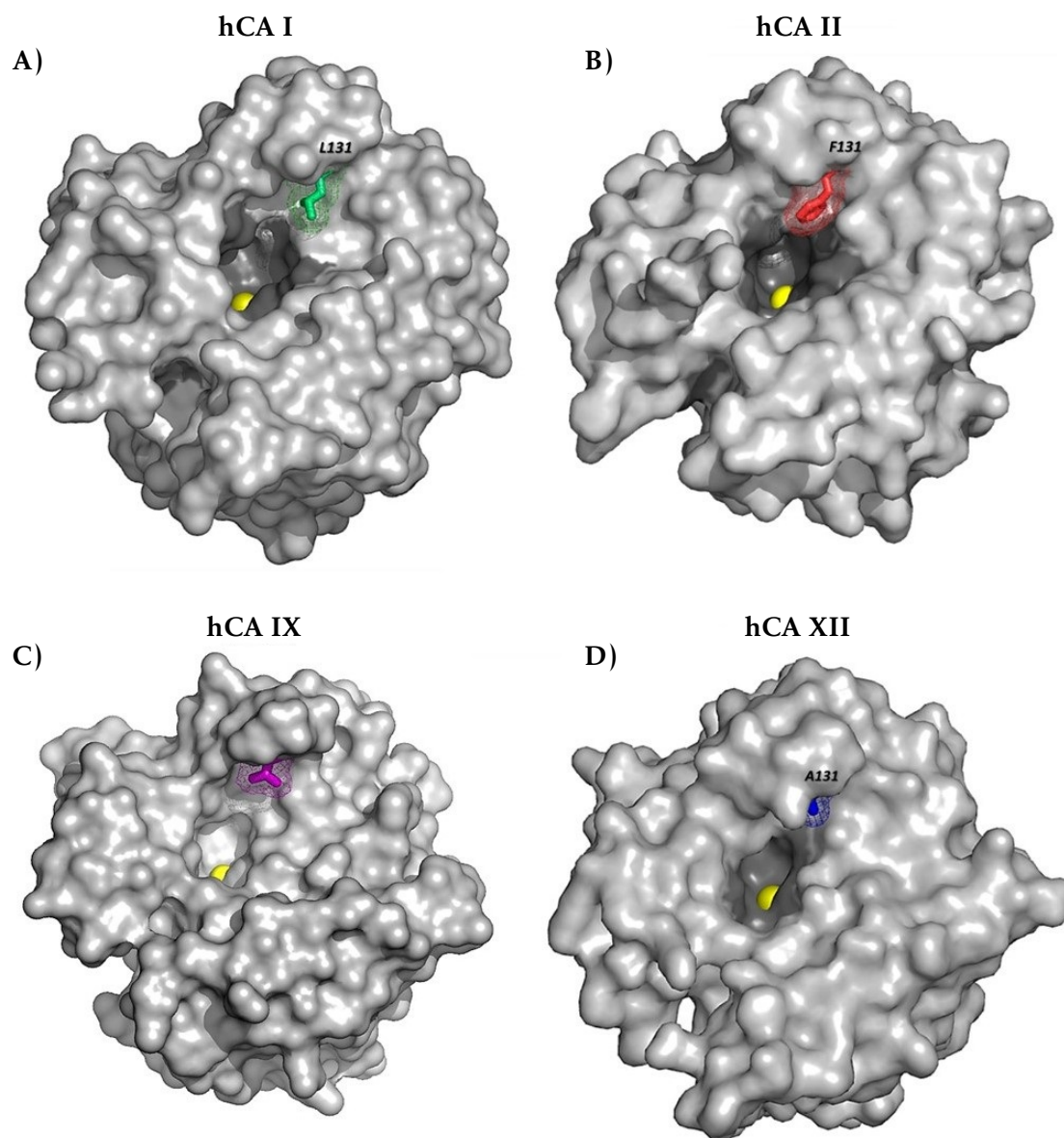
Figure A.1: *Representation of hCAs I, II, IX and XII binding site with focus on non–conserved residue 131. In the ubiquitous hCA I and II this residue is a leucine (L131) or phenylalanine (F131) which, due the bulky side chain, act as "steric blocker" reducing the accessible entrance to the active site (Panel A and B). The tumor–associated hCA IX and XII possess in this position a residue of valine (V131) or alanine (A131) which present shorter hydrophobic side chains (Panel C and D).*

the isoenzymes, are observed in the region comprising residues 127-136 located on protein surface [5], which thus has to be considered the main suggestion in the drug designing of novel selective hCAs inhibitors. For example, residue 131, located within this "*selective pocket*" is not conserved among the different isoforms and it has been well explained that it plays a critical role in determining compound selectivity (Figure A.1). In general, these structural differences allow the compounds to easily enter the active site cavity and bind in a conformation that favors interactions with residues in the hydrophobic pocket controlling isoform selectivity [6]. Then, it is clear that this "*selective valley*" located in the rim of the active site could be targeted to find isoform specific inhibitors. The most popular drug design strategy employed to strike this specific area is the so called "*tail approach*". This consists in the design of a molecular template containing the portion addressed to catalytic cavity through the zinc–binder group and an additional fragment (namely "*tail*") to the core structure molecule for enhancing interactions with specific hydrophobic or hydrophilic residues lined the middle area or the rim of the active site.

In the last decade Gitto R. and coworkers at University of Messina contributed to expand the chemical space of compounds which affect the catalytic activity of CAs, reporting a collection of classical CA inhibitors bearing sulfonamide moiety [7–14]. Among them, several inhibitors proved to be active in the low nanomolar range, but most of them were not characterized by a good selectivity profile against the druggable isoforms human CAs VII, IX and XII. Nonetheless, the discovery of these CAIs and the resolution of the X–ray complexes for the most promising compounds, highlighted new suggestions for the development of novel series of human CAIs that could specifically bind the target isoforms.

The first part of the research activity of this PhD project focused on the development of new class of compounds strictly related to previously discovered sulfonamides. Specifically, the main goal was the improvement of our knowledge about structure–affinity relation-ships (SARs). Thus, we planned the synthesis of novel sulfonamide–based CAIs bearing azepine/piperidine/piperazine core that differ mainly in the "*tail*" molecules. This wide set of cicloalkylamines were tested against selected hCAs constituting interesting drug targets. Then, structural and computational studies were carried out in order to investigate the binding pose of the most intriguing compounds and to identify residues within hCAs active site involved in the stabilization of the protein–ligand complexes.

As second project of this PhD period, a novel series of non-classical CAIs has been investigated. Based on the evidence that some coumarins showed high affinity and selectivity against the tumor associated hCA IX and XII, the natural compound Umbelliferon (7–hydroxycoumarin) was chosen as template for our novel design. By inserting different substituents on coumarin *core*, we obtained a small library of coumarin derivatives. Thus, the evaluation of the in-hibitory activity revealed that these compounds possessed nanomolar affinity and high selectivity toward tumor–associated hCA IX and XII.

As it was recently found, three classes of CAs that are α–, β–, γ–CAs, seem to play a crucial role in the growth, virulence and acclimation for several pathogenic bacteria in the host organism.

As consequence, prokaryotic CAs represent excellent drug targets for the development of novel chemotherapic agents. Based on this assumption, in the last part of this PhD course, we discovered potent and selective inhibitors against the α, β and γ classes of the pathogenic species *Vibrio Cholerae* (VchCAα, β, γ) by means of computer assisted drug design. Notably, we disclosed the first modelled *"open active site"* of VchCAβ, as useful tool for the investigation of binding mode of VchCAs inhibitors and as potential tool for a future structure-based drug design.

1.1   Overview on Carbonic Anhydrases

Carbon dioxide (CO_2) represents the primary source of carbon for all living organisms and it plays a key role in the global carbon cycle. When CO_2 dissolves in water and in absence of a catalyst, it forms the unstable carbonic acid (H_2CO_3) that spontaneously dissociates into bicarbonate and proton (Figure 1.1, reaction (I)). Carbon dioxide, bicarbonate and protons are essential molecules/ions in many physiologic processes and the equilibration of these species is assured by the action of a class of enzymes named carbonic anhydrases (CAs, EC 4.2.1.1). CAs are found in almost all organisms that require these biological catalysts to manage the great amount of carbon dioxide and to control the acid–base imbalance [2, 15–17].
CAs type also possess ability to hydrate further small molecules such as COS, CS_2, cyanamide leading to urea (Figure 1.1, reactions II–IV). In addition, the aldehydes have shown to be hydrated to gem diols by CAs, whereas the esterase activity with carboxylic acid esters, sulfonic acid esters, phosphate esters (Figure 1.1, reaction V–VII), and thioesters have been also reported. It is unclear if these additional reactions might be physiological relevant, although the reported thioesterase activity may interfere with the generation of acyl–coenzyme A, thus emerging derivatives thus possessing a relevant biological function.
So far eight CA genetic families are known: α–, β–, γ–, δ–, ζ–, η–, θ–, and the most recently reported τ–CAs. The α–CAs are expressed in vertebrates, in many Gram negative bacteria, protozoa, algae and green plants; the β–CAs are found in both Gram negative and positive bacteria, algae, chloroplasts of mono– as well as di–cotyledons, and also in many fungi and some Archaea. The γ–CAs were found in Archaea, cyanobacteria and most types of bacteria; the δ– and ζ–CAs seem to be present only in marine diatoms. A unique η–CA has been found in the protozoa *Plasmodium Falciparum*. A θ–CA has been identified in the marine diatom

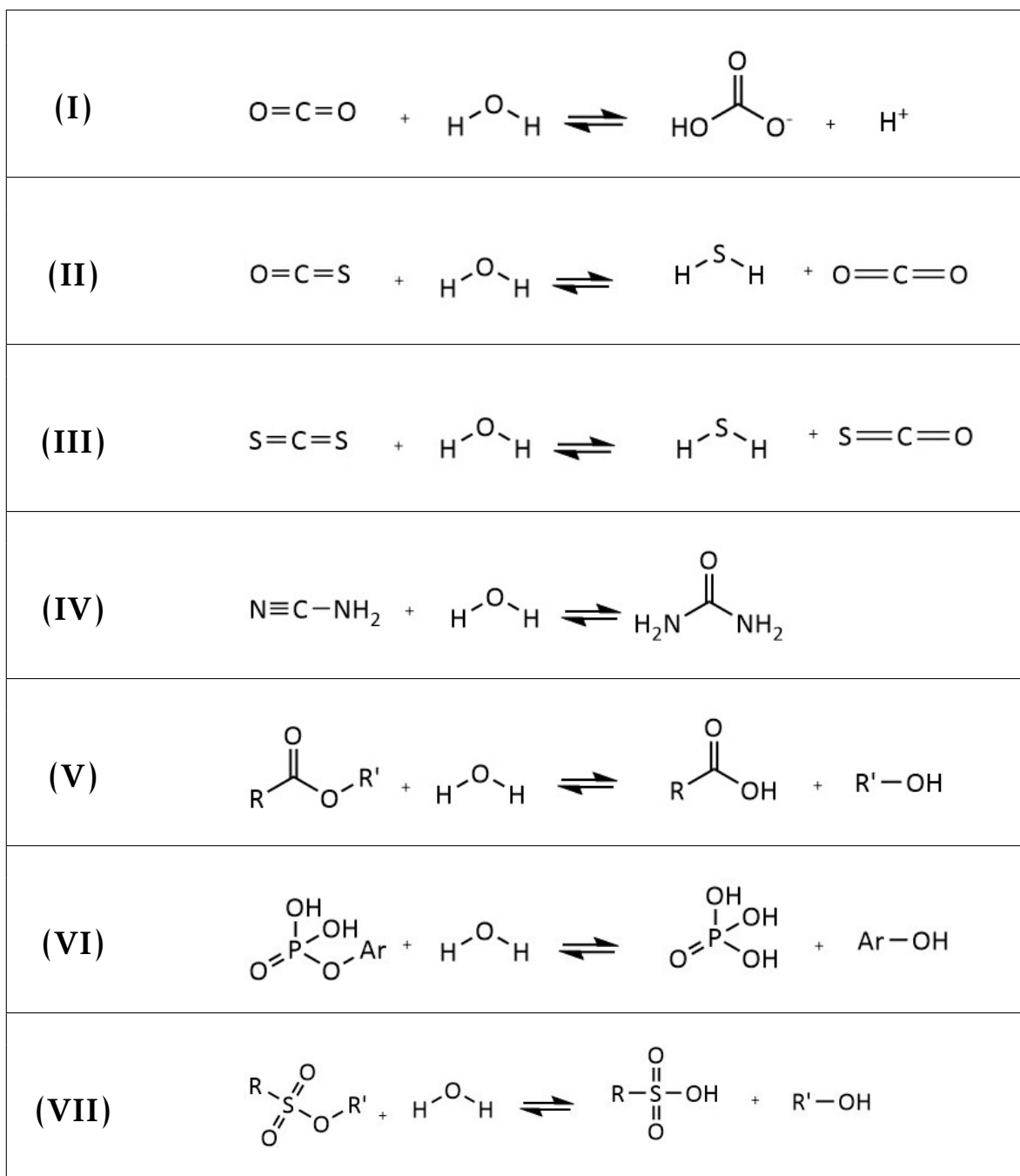|	
(I)	$O=C=O$ + $H-O-H$ ⇌ $HO-C(=O)-O^-$ + H^+
(II)	$O=C=S$ + $H-O-H$ ⇌ $H-S-H$ + $O=C=O$
(III)	$S=C=S$ + $H-O-H$ ⇌ $H-S-H$ + $S=C=O$
(IV)	$N≡C-NH_2$ + $H-O-H$ ⇌ $H_2N-C(=O)-NH_2$
(V)	$R-C(=O)-O-R'$ + $H-O-H$ ⇌ $R-C(=O)-OH$ + $R'-OH$
(VI)	$O=P(OH)(OH)-O-Ar$ + $H-O-H$ ⇌ $O=P(OH)(OH)-OH$ + $Ar-OH$
(VII)	$R-S(=O)(=O)-O-R'$ + $H-O-H$ ⇌ $R-S(=O)(=O)-OH$ + $R'-OH$

Figure 1.1: *CA–catalyzed hydrolytic reactions.*

Phaedaodactylum tricornutum. Recently, a τ–CA has been found in marine phytoplankton *Thalassiosira pseudonana* [16, 18–21].

In many organisms, these enzymes are involved in crucial physiological processes such as CO_2 homeostasis, transport of CO_2/HCO_3-, respiration and a multitude of biosynthetic reaction, such as gluconeogenesis, lipogenesis and ureagenesis. In addition, in mammals, CAs are involved in secretion of electrolytes in tissues and organs, in many metabolic reactions and others physio–pathological processes. In plants, algae and cyanobacteria, CAs play a crucial role in photosynthesis; in marine diatoms, they play a role in CO_2 fixation and in the SiO_2 cycle [1, 16].

1.2   Structural features and catalytic mechanism of CAs

A large number of crystallographic and kinetic data elucidated the relationship between CAs structures and their function. The CAs are metalloenzymes catalytically effective when a metal ion is bound within the active site cavity, assuming a characteristic pattern of coordination for which the metal ion(II) displays a tetrahedral geometry, three coordinating amino acid residues and one water molecule or hydroxide ion that complete the coordination sphere.

In all eight genetically distinct families Zn (II) can be found, although it is exchangeable with Co (II) in α–CAs without a significant loss of catalytic activity; Cd (II) has been found in ζ class and Fe (II) in γ–CAs in anaerobic conditions [16, 22]. In the α, γ and δ–CAs the Zn (II) is tetrahedral coordinated by three residues of histidine (His) and a water molecule/hydroxide ion (Figure 1.2, Panel A). Regarding the β and ζ classes, the amino acid residues are two cysteine (Cys) and one His (Figure 1.2, Panel B)[1, 2, 16].

Among the β–CAs class it is possible to distinguish two different subtypes: in the type I–β-CAs (i.e. enzyme with an "*open*" active site) a water molecule or hydroxide ion represents the fourth zinc ligand (Figure 1.2, Panel B), whereas in the type II– β–CAs (i.e. enzymes with a "*locked*" active site) OH– is replaced by an aspartate (Asp) residue (Figure 1.2, Panel C).

Covarrubias et al. [23] highlighted that the "*locked*" active site of the II– β-CAs subtype is transformed in a corresponding "*open*" form at pH values > 8.3 with cooperation of arginine (Arg) residue that participates in the formation of a salt bridge with the coordinating Asp residue. The formation of this bond makes free the metal ion for an incoming water molecule/hydroxide ion, obtaining so a catalytically active species. By computational studies it has been suggested the distinctive coordination mode for η–CAs, for which two His, glutamine (Gln) and a water molecule/hydroxide ion are bound to Zn (II) [24]. CAs are among the fastest enzymes known, they displaying a maximum catalytic efficiency approaching the diffusion limit of 10_8 $M^{-1}s^{-1}$ in some α– and ζ–CAs. The efficient catalytic activity is also linked to a singular architecture shared by all CAs. There are two different environments, one constituted by hydrophobic residues and the other one lined by hydrophilic amino acidic residue. A plausible explanation attributes to the hydrophobic wall the role of CO_2 trapping. In turn, the hydrophilic region is the way out for the polar species (bicarbonate and protons)
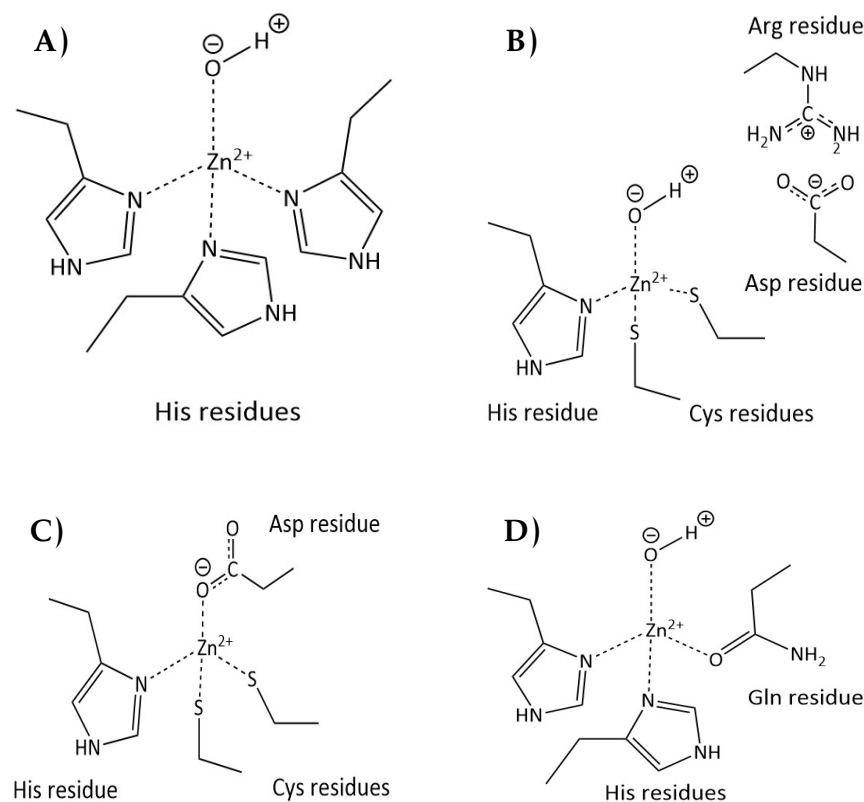
Figure 1.2: *Metal ion coordination pattern in the different CAs families. Panel A): α–, γ– and δ–CAs: the three His residues in α and δ classes come from the same monomer, whereas in the γ–CAs one residue is from an adjacent monomer. Panel B): β–CAs type I in its "opened" active site form; the Cd–bound ζ–CAs shared the same coordination pattern. Panel C): β–CAs type II in its "closed" active site form; an Asp residue constitutes the fourth zing ligand. Panel D): η–CAs class.*

generated by CO_2 hydration. This aspect has been confirmed at least for the proton release pathway, in which a network of His residues and water molecules were shown to be involved.

As depicted in the following Equation 1.1a–1.1b, CAs employ a two steps catalytic mechanism, in which the main active species is the metal hydroxide complex (EZnOH⁻). In the first reaction step the nucleophilic species EZnOH⁻ attacks the CO_2 molecule located to a hydrophobic pocket thus generating EZnHCO3⁻ species. Then, HCO_3^- is removed from the active site by an incoming water molecule that determines the generation of the zinc bound water molecule (EZnH₂O). In the second and rate–determining step, EZnH₂O is deprotonated to regenerate the EZnOH⁻ nucleophilic species by means of a proton transfer reaction from

the EZn–H$_2$O to an exogenous proton acceptor or to an active site amino acidic residue.

$$1^{st} \, step : \text{EZnOH}^- + \text{CO}_2 \rightleftharpoons \text{EZnH}_2\text{O} + \text{HCO}_3^- \tag{1.1a}$$

$$2^{nd} \, step : \text{EZnH}_2\text{O} + \text{B} \rightleftharpoons \text{EZnOH}^- + \text{BH}^+ \tag{1.1b}$$

Figure 1.3: *Panel A): Monomeric α–CA: human CAs II (PDB code: 1F2W); Panel B): dimer of dimers (tetramer) β–CA: Vibrio cholerae carbonic anhydrases (VchCAs; PDB code: 5CXK); Panel C): trimeric γ–CAs from the archeon Methanosarcina Termophila (PDB code: 1THJ); Panel D): monomeric ζ–CAs: R3 domain Cd(II)–bound from diatom Thalassiosira Weissflogii (PDB code: 3UK8).*

The oligomer state of CAs superfamily, is highly variable. Most of α–CAs enzymes exist as monomers (Figure 1.3A), but homodimers are also reported for several human and bacterial enzymes. The protein fold of β–CAs consists of a dimer, despite for some isoforms have been observed a tetrameric state (dimers of dimers) (Figure 1.3B) or multiples of such homodimers (mainly in higher plants). The catalytically active unit of γ–CAs has been characterized from the methanogenic archeon *Methanosarcina Termophila* and it consists of a trimer with three zinc–containing active sites, each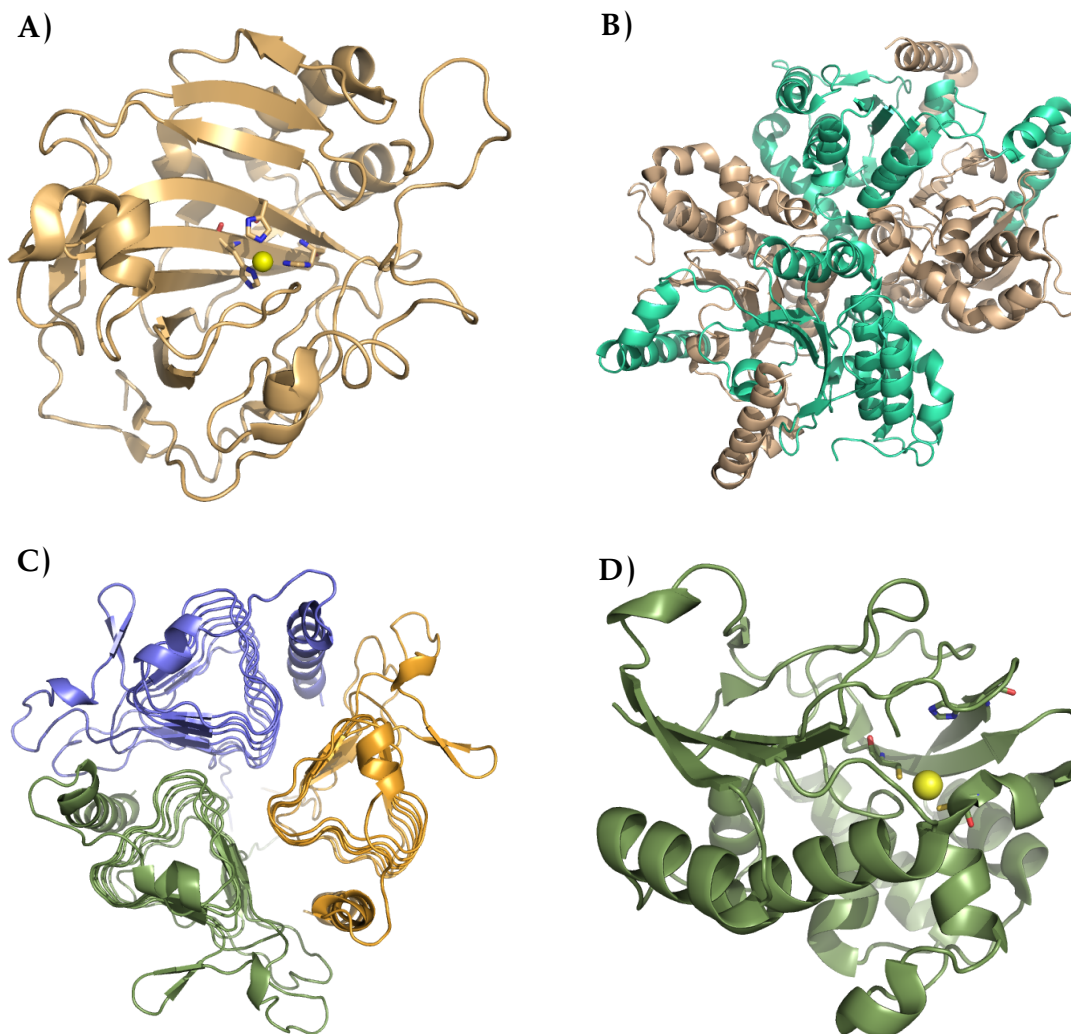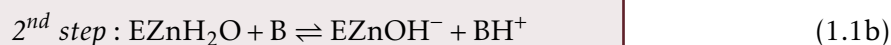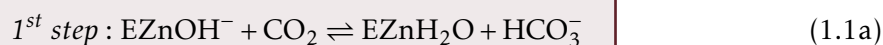 located at the interface between two monomers (Figure 1.3C) [25]. The ζ–CAs seems to be monomeric enzymes (Figure 1.3d), as observed for the enzyme isolated from the marine diatom *Thalassiosira Weissflogii*, but the full–length enzyme consists of three almost identical units (R1, R2 and R3) [22]. To date, representative isoforms for the classes δ–, η–, θ– and τ–CAshave not yet been crystallized. However, preliminary homology models have been reported for η–CAs from the pathogenic *Plasmodium falciparum*.

1.3   Inhibition and activation of carbonic anhydrase activity

CAs inhibition and activation mechanisms are well–understood processes; even though new findings continue are emerging in this area. Inhibitors of these metalloenzymes (CAIs) started to be studied more than 60 years ago and they found pharmacological application for the treatments of a wide range of human diseases; the activators of CAs (CAAs) have not yet found a clinical use.

To date, five different inhibition mechanisms are known so that they include:

i)   The zinc–binders, including sulfonamides and their bioisosters (sulfamates, sulfamides, etc), inorganic anion, hydroxamates, carboxylic acids, benzoxaboroles, phosphates, dithiocarbamates and bioisosters, etc [4, 17, 26–30].

ii) Compounds anchoring to the zinc-coordinated water/hydroxide ion species, among which are phenols, phenolic derivatives, polyamines, sulfocoumarins, etc [31–34].

iii) Compounds that produce active site entrance occlusion coumarins, six–membered lactones, thiolactones and quinolinones [35–37].

iv) Compounds that bound out of the active site as for 2–(benzylsulfonyl)–benzoic acid [38].

v)   Compounds that act with an unknown mechanism, tertiary sulfonamides, imatinib and nilotinib, N–substituted saccharin, and so on [39].

The deprotonated form of primary sulfonamide ($R–SO_2NH_2$) is the most efficient and commonly use zinc binding group (ZBG) useful to design CAIs [1, 16]. Indeed, at least twenty sulfonamides are in clinical use for decades and some of them have recently entered the clinical trial phase [2, 4]. A detailed discussion about the pharmacological activity of CA inhibitors, their actual clinical uses and the potential future medical applications, is reported in Section 2.1.2.
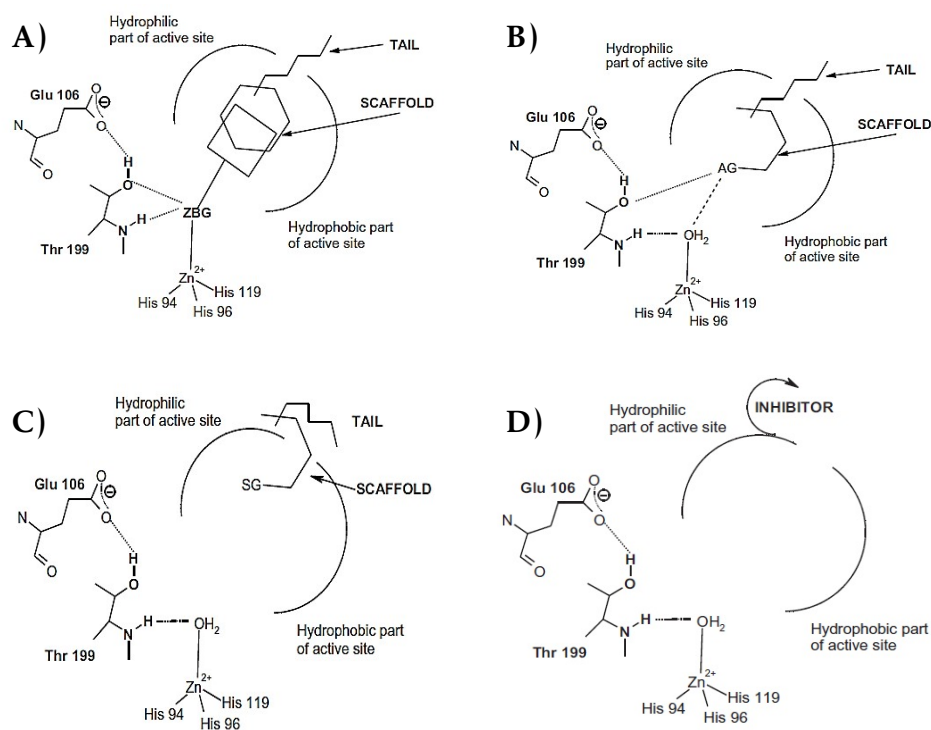
Figure 1.4: *Schematic representation of inhibitory mechanism within CAs. Panel A): Zn–binders: compounds which anchor to the Zn ion through a metal binding group (MBG). Panel B): Compounds which anchor to the Zn(II)–coordinate water molecule/hydroxide ion. Panel C): Compounds that occlude the active site entrance. Panel D): Compounds that bind out of the active site.*

The first evidence that sulfonamides could act as efficient CAIs came from a study on the simple prototype sulfanilamide as reported in literature in 1940 [41]. Since this pioneering work, this class of compounds has been widely investigated by means of kinetic, crystallographic and pharmacological studies. Subsequently, a large number of substituted-sulfonamides have been designed and tested for their CAs inhibitory activity. Benzenesulfonamide derivatives represent the most common and well–characterized class of zinc–binders [17]. The literature reports a large number of structural studies of sulfonamides in complex with different classes of CAs, especially with for predominant human α–CA isoform II. It has been demonstrated that benzenesulfonamides shared similar the interactions found for prototype benzenesulfon-amide 1: the sulfonamide group is involved in the canonical interaction with Zn (II) metal ion and the gate-keeper T199, whereas the phenyl ring establishes van der Waals interactions with the key amino acid residues Q92, V121, F131, L198 and T200 (Figure 1.5).

The main sulfonamide bioisosters are sulfamide and sulfamate ones as ZBGs, in which an additional electron–withdrawing atom/group (NH or O respectively) is connected to the
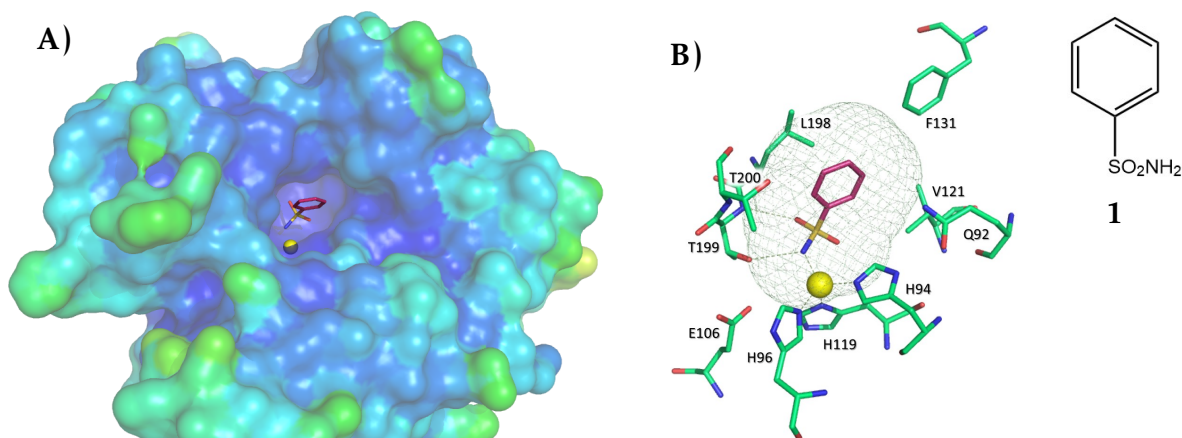
Figure 1.5: *Panel A): Benzenesulfonamide (1) complexed with hCA II (PDB code: 2WEJ) [40]. The protein backbone is represented as surface. Panel B): Representation of the binding pocket of hCA II/1 complex showing residues involved in the recognition process of the inhibitor molecule; Chemical structure of compound 1.*

sulfamoyl moiety, thus originating compounds with the general formula R–NH–SO$_2$NH$_2$ and R–O–SO$_2$NH$_2$ [4, 17]. Structural studies demonstrated that the presence of this additional heteroatom improves the network of hydrogen interactions as more efficient CA ligands [2] (Figure 1.6).

Over the years, carboxylates, hydroxamates (Figure 1.7, compound 2 [28]) phosphonates (phosphonoformic acid, compound 4 [42]) have been considered novel ZBGs. Most recently,
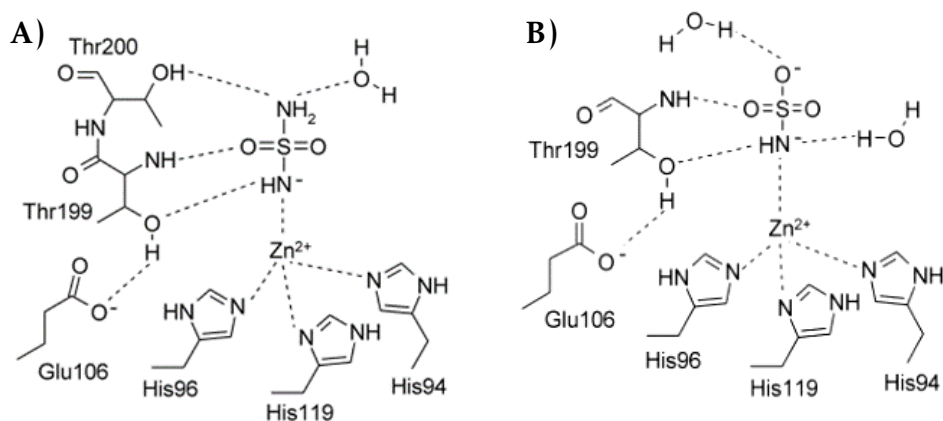
Figure 1.6: *Schematic representation of the binding pose of sulfamide (Panel A) and sulfamate (Panel B) within hCA II active site.*
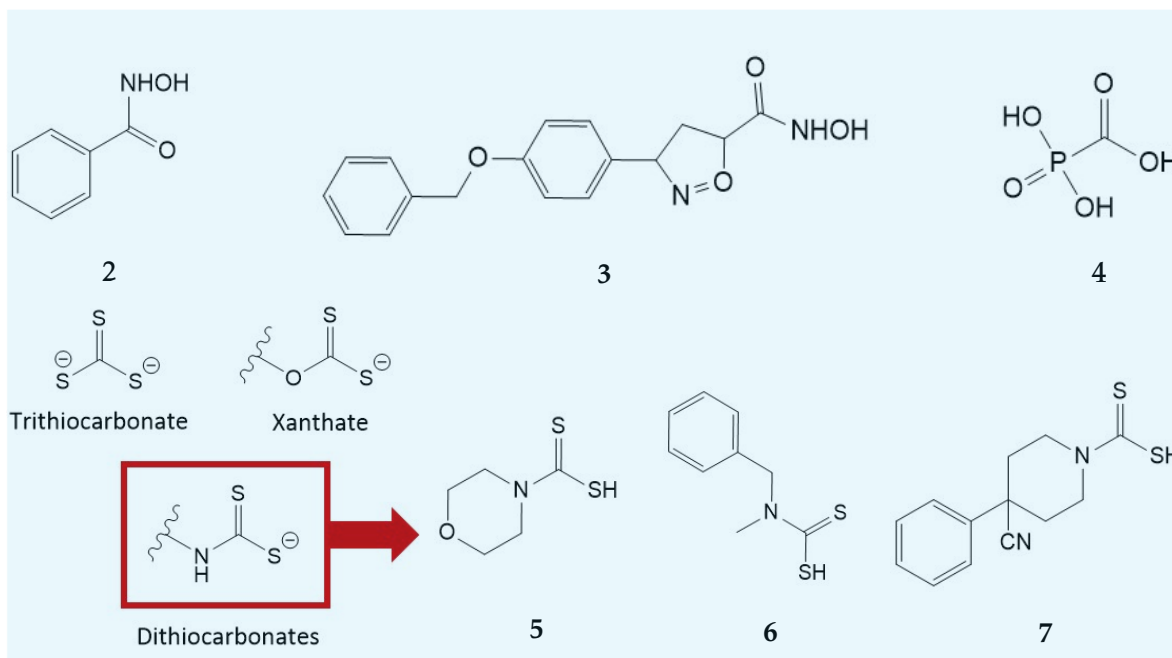
Figure 1.7: *Chemical structures of non-classical zinc binders (derivatives 2–7).*
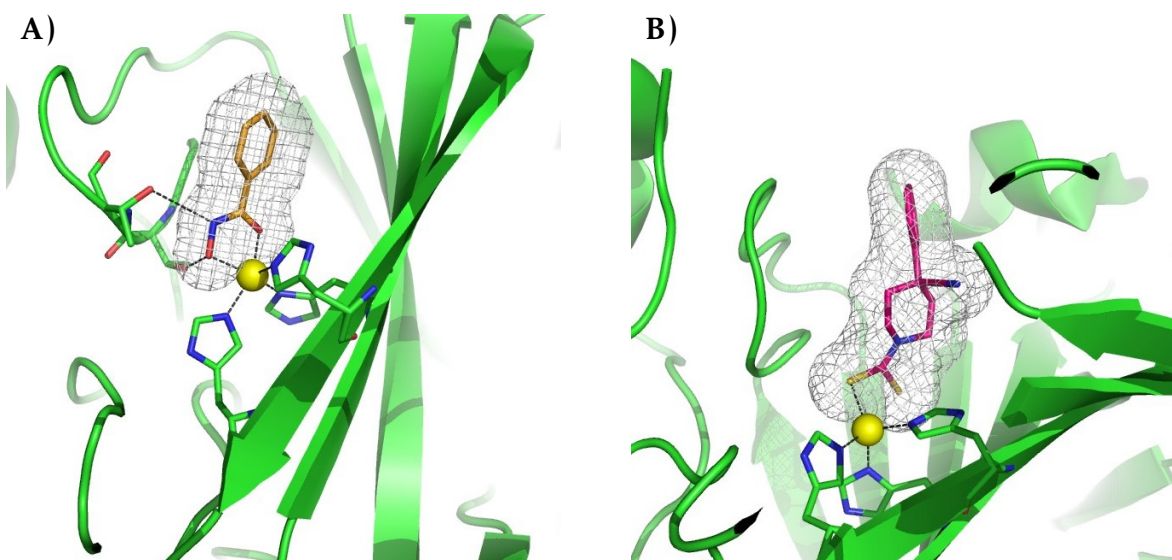
Figure 1.8: *X–ray adducts of non–classical zinc binders. Panel A): N–(Hydroxy)–benzamide (2) in complex with hCA II (PDB code: 4FL7) [28]; Panel B): 4–cyano–4–phenylpiperidine–1–carbodithioate (7) in complex with hCA II (PDB code: 3P5L) [27].*

the X–ray adduct of simple inorganic anion trithiocarbonate (PDB code: 3K7K) with hCA II inspired novel zinc binders chemotypes as dithiocarbamates (DTCs) (see Figure 1.8), xanthates and thioxanthates [43]. In addition, the salycilaldoxime scaffold has been recently identified as new intriguing ZBGs for the development of new CAIs. These prototypes generally bind to the CAs active site as in their deprotonated state; they coordinate the Zn (II) ion in the bottom of the catalytic pocket and replace the nucleophile water molecule/hydroxide ion. A schematic representation of CA inhibition mechanism within hCAs with zinc binders is shown in Figure 1.4. X–ray crystallographic studies confirmed this for all the chemotypes of CAIs above mentioned (Figure 1.8), except for the xanthates and salycilaldoxime for which computational docking methods revealed a hypothetical inhibition mechanism.

An increasing number of non zinc-binding CAs inhibitors has been recently reported. The simple molecule of phenol (Figure 1.9, compound 8) was the first compound for which it was investigated the ability to inhibit CAs by anchoring to the zinc–bound water molecule. This alternative mechanism of action has been confirmed for various phenolic derivatives (Figure 1.9, compound 8–9), some carboxylates (Figure 1.9, compound 10), polyamines
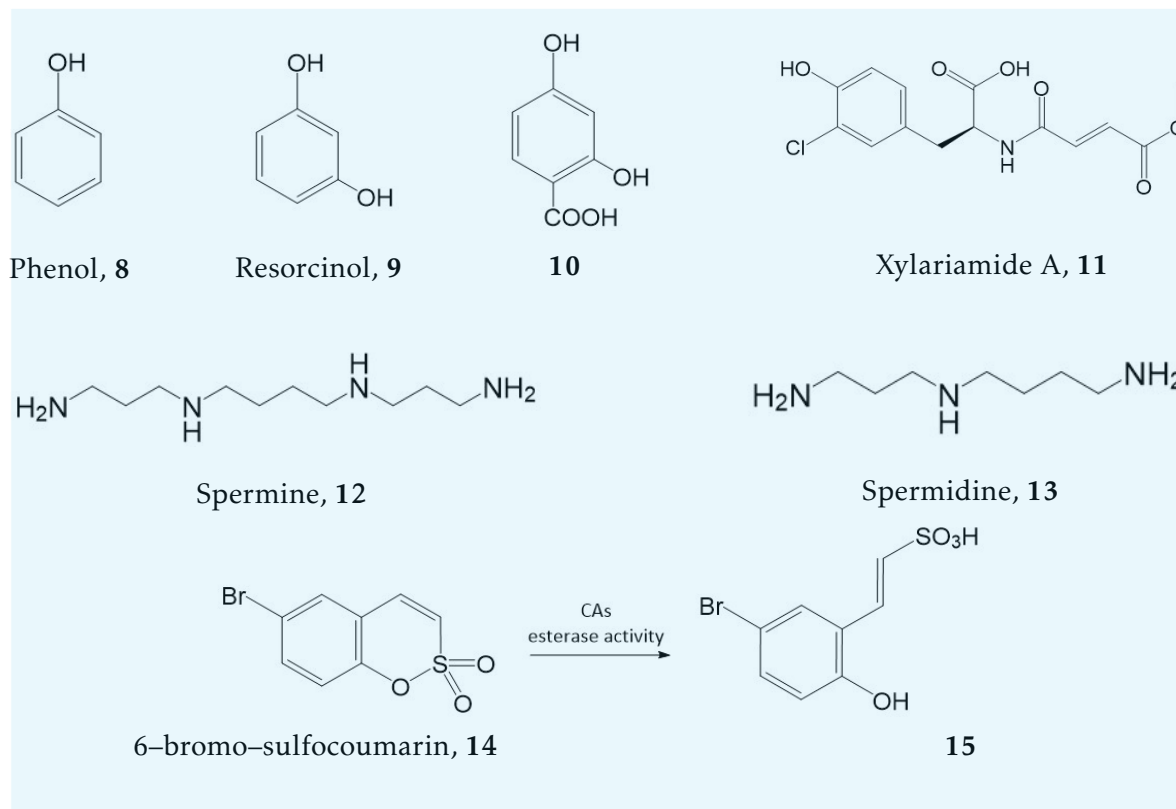
Figure 1.9: *Chemical structures of non–zinc binding inhibitors 8–15.*
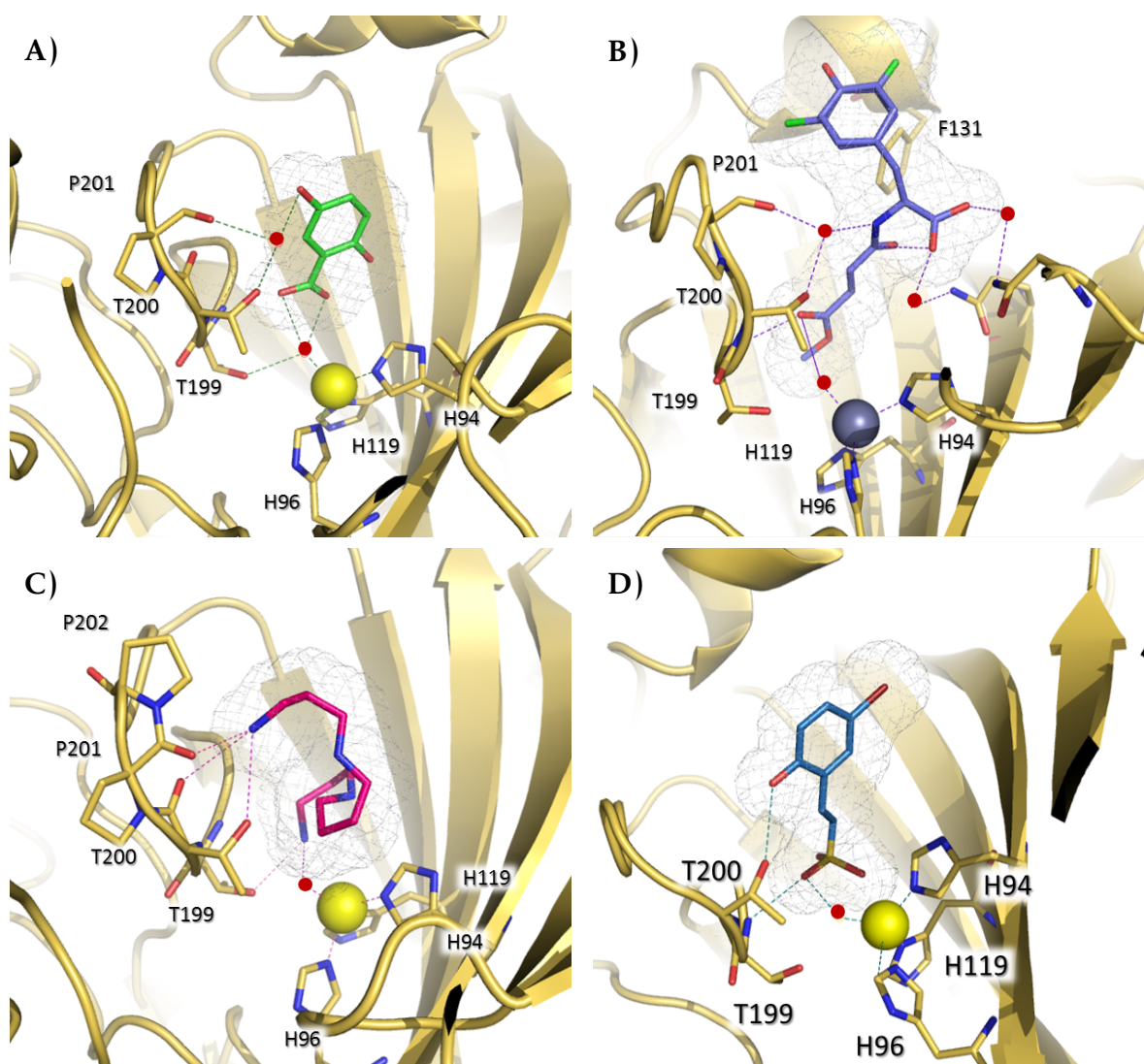
Figure 1.10: *Several X–ray adducts of CAIs and the peculiar water–mediated binding to zinc–. Active site view of hCA II in complex respectively with 2,5–dihydroxybenzoic acid (10) (Panel A, PDB code: 4E3D) [44], Xylariamide A (11) (Panel B, PDB code: 3P4V) [45], spermine (12) (Panel C, PDB code: 3KWA) [32] and with the hydrolysis product of 6–bromo–sulfocoumarin (14) (Panel D, PDB code 4BCW) [33]. The protein backbone is depicted as yellow–orange ribbon. Amino acidic residues involved in the recognition processes are shown as sticks. Zinc is showed as yellow sphere. Water molecules are shown as red circles.*

(spermine 12 and spermidine 13), and sulfocoumarins (Figure 1.9, compound 14 [33]) by means of kinetic and X–ray crystallographic studies. As depicted in Figure 1.4 (Panel B), this class of CAIs is characterized by the presence of an anchoring group (AG) through which they bind to the zinc coordinated water molecule/hydroxide ion. These AGs include OH, primary amines, COOH, COOMe, SO_3H moieties. The AG is generally attached to a scaffold bearing a tail, which can interact with the two halves of the catalytic pocket (as seen or the zinc–binders) catching additional interactions. X–ray crystal adducts of various isoforms in complex with these chemotypes are available and some of them are reported in Figure 1.10.

Particularly, the X–ray crystal structure of spermine (12) in adduct with hCA II was solved (Figure 1.10 [32], Panel C); the analysis of this structure clearly shows that spermine binds CAs active site in a completely different orientation when compared to canonical binding mode of sulfonamides. Indeed, the polyamine assumes a coiled conformation within hCA II active site, and it binds the hydroxide ion by means of a strong hydrogen bond involving one of its ammonium moiety. The same chemical moiety is able to create a further hydrogen bond contact with the crucial gatekeeper residue T199. Additional hydrogen bonds with T200 and P201 and several van der Waals interactions with different residues contribute to stabilize the complex and exert CA isoform selectivity. As shown in Figure 1.11, X–ray crystallographic experiments evidenced a similar binding pose for 2,5–dihydroxybenzoic acid (10) [44] and Xylariamide A (11) [45] as well as for the hydrolysis product of 6–bromo–sulfocoumarin (14) [33]. In this latter case the AGs is identifiable in the SO_3H moiety.

The occlusion of the active site entrance can be considered the third mechanism of CAs inhibition. A schematic representation is reported in Figure 1.4 (Panel C). It was evidenced for the first time for coumarins, but thereafter other compounds have shown to act with a very similar mechanism of action (quinolinones, six–membered lactones and thiolactones, the anti–epileptic drug lacosamide and substituted coumarins) [35, 36, 46]. The first derivative for which it was observed this singular mechanism of inhibition was the natural product 16 isolated from the Australian plant *Leionema Ellipticum*. X–ray crystallographic studies on the 6–(1S–hydroxy–3–methylbutyl)–7–methoxy-2*H*–chromen–2–one (17) or the simple coumarin (16), in complex with hCA II demonstrated that coumarins (and sulfocoumarins) can act as prodrugs in human CAs (Figure 1.11, Panel B). Indeed, the α–CAs possess esterase activity which is responsible for the formation of 2-hydroxycinnamic acid derivatives (Figure 1.11, Panel A). Interestingly, the binding interaction occurs in a region of the CA active site far away from the metal ion. In particular, coumarins bind at the entrance of catalytic site which is the region with the minor number of conserved residues among the different CAs and this aspect justify the advantageous selectivity profile detected for a large number of coumarin derivatives. In detail, several coumarins bind the enzyme cavity through a sticky group (SG) attached to the heterocyclic scaffold which can also incorporate a tail which may be potentially able to establishes additional interaction away from the catalytic hole (Figure 1.4C) [17].

The last known mechanism concerns compounds able to bind out of the active site (Figure 1.3, Panel D). A structural study of the adduct of 2–(benzylsulfonyl)benzoic acid (18) with hCA
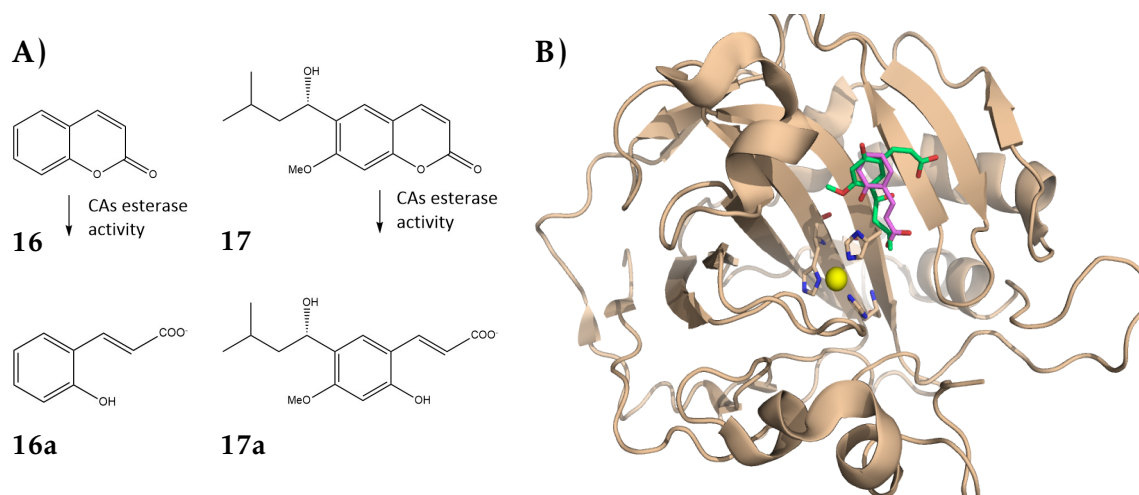
Figure 1.11: *Panel A) Chemical structures of 2H–chromen–2–one (16, coumarin) and 6–(1S–hydroxy–3–methylbutyl)–7–methoxy–2H–chromen–2–one (17) and their corresponding hydrolytic products. Panel B) Binding mode of the hydrolytic products of coumarins 16 (16a, in pink stick) and 17 (17a, in green stick) within hCA II active site. The protein backbone is represented as wheat ribbon, the Zn (II) ion is depicted as yellow sphere. The catalytic triad (His95, His96 and His119) is evidenced as wheat sticks.*
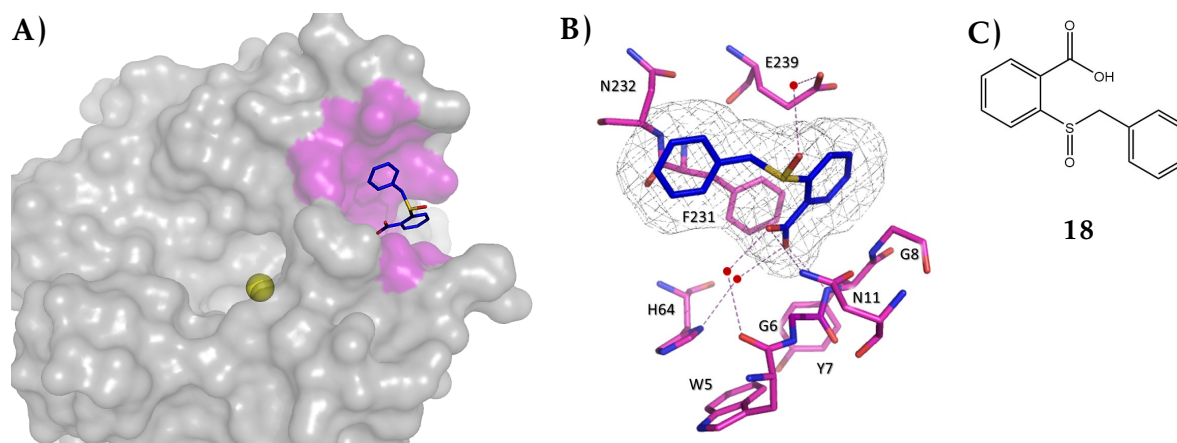
Figure 1.12: *Panel A): 2–(benzylsulfonyl)benzoic acid (18) in complex with hCA II. The protein backbone is represented as grey surface. Residues delimiting the cavity are highlighted in pink. Panel B): Representation of the binding pocket of hCA II/(18) complex (PDB code: 4QY3) showing residues involved in the recognition process. Panel C): Chemical structure of compound 18.*

II (Figure 1.12) suggests that there is not the binding of any inhibitors to the metal ion and not even to adjacent amino acid residues. Indeed, the carboxylate of compound 18 binds in a suitable pocket located near to protein surface at a distance of about 14 Å from the Zinc ion; polar interactions created an additional stabilizing network. In particular, one oxygen atom of the carboxylate moiety accepted a H–bond interaction from the amino function of Y7, whereas the other oxygen atom interacts with N11 (Figure 1.12, Panel B). Furthermore, the two oxygen atoms are involved in two strong hydrogen bonding interactions with water molecules which in turn are linked to G6 and to the proton shuttle H64. This latter water-mediated interaction with the hCA *proton shuttle*, exerts a blockage for this crucial residue in its "out" conformation disabling the entire catalytic cycle. Additional details for the key function of H64 residue in hCAs are reported in Section 2.1.1. Moreover, the organic scaffold of 18 is stabilized into hCA II binding pocket by means of numerous van der Waals contacts involving W5, G6, Y7, G8 and E239. Finally, the benzyl moiety interacts with F231 and N232.

The binding of inhibitors in this surface cavity had already been observed for other carboxylates [44], namely 19 and 20. The structural superposition of the binding poses of these two latter and of the 2–(benzylsulfonyl)benzoic acid (18) (Figure 1.13) [38], highlighted that the phenyl ring assumes the same conformation and that the two water–mediated interactions and the H-bonds network with Y7 and N11 are well conserved. Nonetheless, hCA II–19 and hCAII–20 complexes evidenced that a further inhibitor molecule is bound to the zinc ion.

The fourth inhibition mechanism above described is well understood and several inhibitors

A)

B)

19   **20**
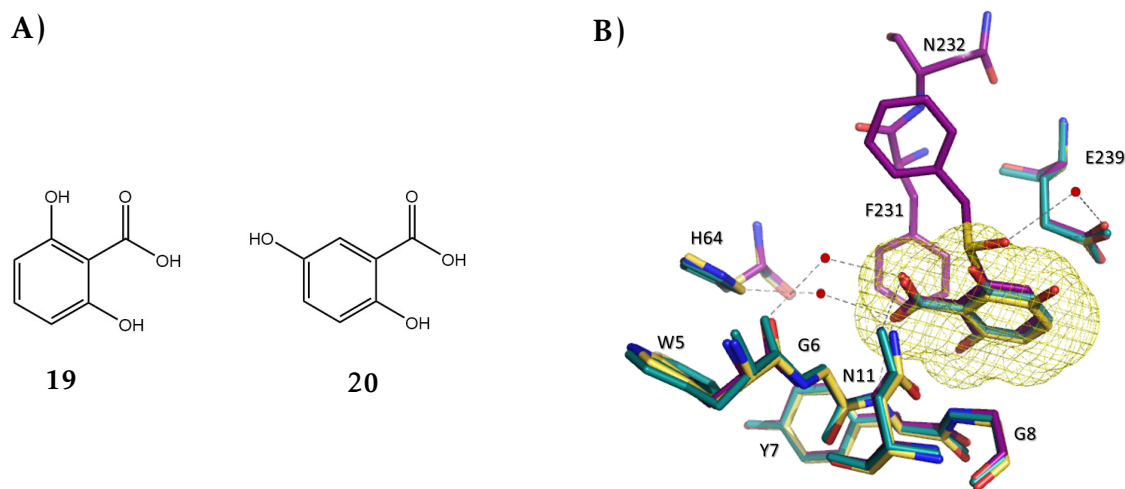
Figure 1.13: *Panel A) Chemical structures of carboxylates 19 and 20. Panel B) Structural superposition of 18– (purple sticks), 19– (deepteal sticks) and 20–hCA II (yellow sticks) complexes. Residues involved in the binding recognition process are shows as sticks.*
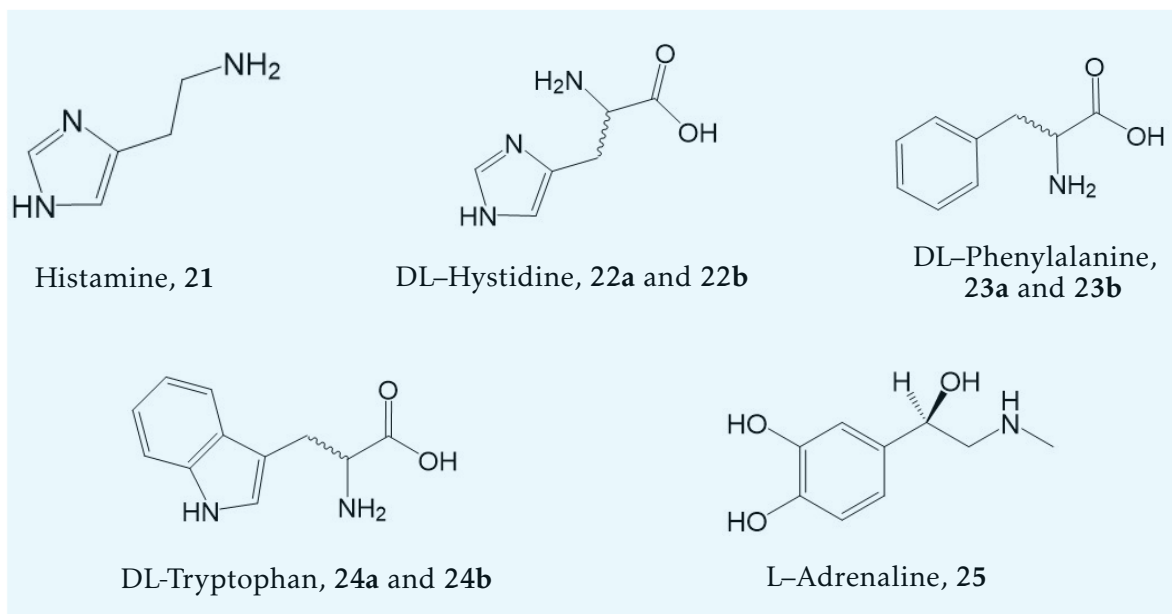
Figure 1.14: *Chemical structures of several CAAs.*

were highly investigated by means of X–ray crystallographic studies and kinetic measurements. However, to date many classes of compounds that show inhibitory CAs activity with an unknown mechanism of action have been reported. Generally, the non-understanding mechanism of action is related to the low solubility of these CAIs. The secondary sulfonamides, as well as the tertiary, represent a classical examples of CAIs which act with an unknown mechanism of action. Although some of these derivatives showed CA inhibitory properties, their mechanism is still unclear. These compounds are unable to bind within the active site due to the steric hindrance of side chain bound to sulfonamide moiety [39].

CAs activators (CAAs) have been a controversial topic for long time and their potential clinical application started to be recently investigated . The CA activation phenomena was reported for the first time in 1940s, for amines, amino acids and peptides. Since these early discoveries, it started a long period of disputes because many researchers claimed that an efficient catalyst, such as CAs, did not need to be activate. Only since 1990s, when it became possible to work with extremely pure enzymes and accurate biochemical techniques, such as stopped–flow assay, the existence of CAAs was then confirmed [16]. Following this, a general CAAs mechanism of action has been proposed and it is summarized in the Equation 1.2:

$$ EZnH_2O + A \rightleftharpoons [EZnH_2O - A] \rightleftharpoons [EZnOH^- - AH^+] \rightleftharpoons EZnOH^- + AH^+ \qquad (1.2) $$

The activation mechanism of CAs has been investigated by kinetic, electronic spectroscopy, crystallographic measurements. The binding of CAAs to several CAs isoenzymes, evidenced
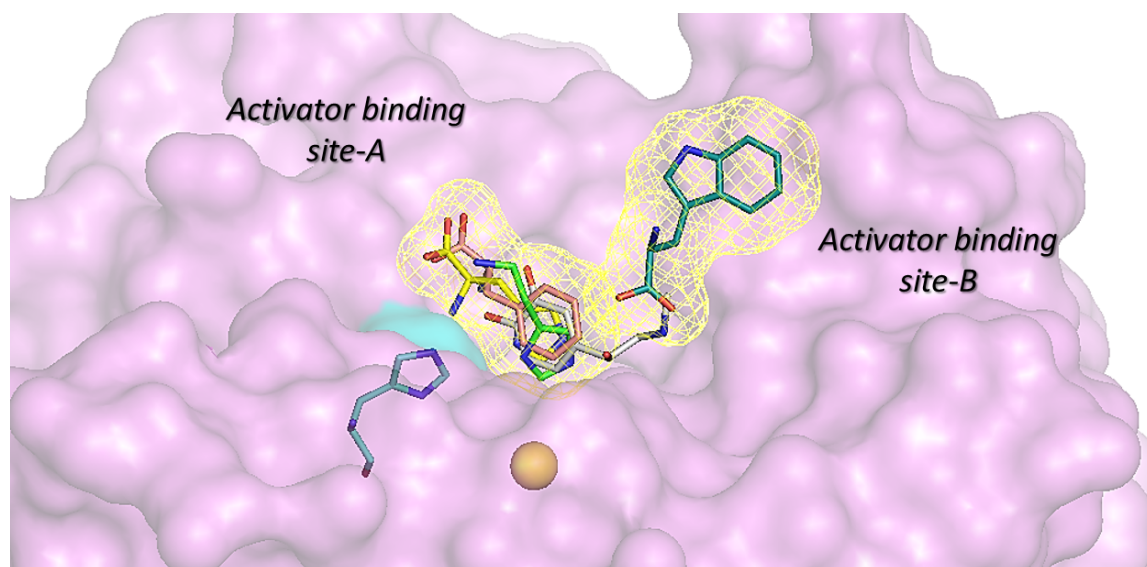
Figure 1.15: *Superposition of CAAs in complex with hCA II. The selected activators are: histamine 21 in green (PDB code: 1AVN) [49], D–Hys (22a) in yellow (PDB code: 2EZ7) [50], D–Phe (23a) in salmon (PDB code: 2FMZ) [51], D–Trp (24a) in deepteal (PDB Code: 3EFI) [52]. The enzyme backbone is shown as pink surface, the zinc ion as yellow sphere. The enzyme proton shuttle His64 is evidenced as cyan stick.*

activator to interfere with the rate–determining step of catalytic cycle that is the protons shuttling between the Zn bound water molecule (EZnH$_2$O) and the medium. CAAs hve been hypothesized to act as exogenous proton acceptors as demonstrated by means of X–ray data for histamine (21) in complex with hCA II. These data were corroborated by further experiments for D– and L–Hys (22a and 22b respectively) bound to hCA I and II (Figure 1.15), D– and L–Phe (23a and 23b), D–Trp (24a) and L–adrenaline (25) bound to hCA II [47, 48].

As shown in Figure 1.15, activators generally establish profitable contacts in the same region of CAs catalytic cavity, also known as "Activator binding site A". This binding area is located in the opposite part of the active site region and in proximity of proton shuttle H64; it has been supposed that the CAAs are able to create interactions with amino acids/water molecules. It has been reported for D–Trp (24a) a further binding site named "Activator binding site B" (see Figure 1.15). However, the amino and carboxylic moiety of D-Trp is retained in almost the same region of the active site occupied by the other activators. Currently, X–ray adducts are reported exclusively for hCA I and hCA II and CAAs, a wide panel of compounds has been screened for the activation of all CAs classes (α–, β–, γ–, δ–, ζ–, η– and τ–CAs).

Therefore, the CAAs research field might be exploited in a near future. Actually, CAAs could be employed for the treatment of CAs–deficiency syndrome for many mammal isoforms,

that is a recessive disorder that produce renal tubular acidosis, osteopetrosis and cerebral calcification, but also potential cognitive defects, short stature, development delay and history of multiple facture by adolescence [53]. Again, interestingly CAAs could be useful to fight memory disorder, considering that several animal models showed that the administration of CAAs induced an enhancement of spatial memory and learning.

2.1 The family of α–Carbonic anhydrases

Among the CA gene families, the α–CAs was the first to be discovered in 1933 in human erythrocytes [54], then, different α–CA isoforms have been identified in many living organisms. The α–CAs from vertebrates have been largely investigated from a structural/biochemical point of view [16, 21, 24, 54–60]. These numerous studies led to the identification of 15 different α–CAs isoforms, which differ for catalytic properties, oligomeric structure, tissue and cellular distribution in mammals and others in nonmammalian vertebrates [3]. Nevertheless, despite the biochemical heterogeneity, α-CAs present the same active site scaffolding (for more details see section 1.2).

2.1.1 hCAs: distribution, kinetic properties and physio-pathological roles

Among the 15 human α–CAs (hCAs) identified so far, only twelve isoforms are catalytically active (CAs I–IV, VA and VB, VI, VII, IX, XII and XIV), whereas the so called CA–related proteins (CARPs, VIII, X and XI) are devoid of any catalytic activity due to the absence of the crucial three histidine residues coordinating the zinc ion in catalytic cycle [3, 16]. Based on the different cellular localization the hCAs are classified in five cytosolic isoforms (hCAs I, II, III, VII and XIII), four membrane–bound isoforms (CAs IV, IX, XII and XIV), two mitochondrial ones (CAs VA and VB) and one single isoform secreted in milk and saliva (CA VI) [55]. Several kinetic studies have highlighted the different catalytic effectiveness of these isoenzymes, showing that the most efficient catalyst for the CO_2 hydration process is the hCA II with a K_{cat}/K_M equal to 1.5×10^8 $M^{-1}s^{-1}$ (meaning that 10^8 CO_2 molecules are hydrated to bicarbonate in one second) [2]. The other measured kinetic constants are summarized in Table 2.1. The molecular determinants responsible for their very different

	K_{cat}/K_M $(M^{-1}s^{-1})$	ORGAN/TISSUES DISTRIBUTION	CELLULAR/SUBCELLULAR LOCALIZATION	PATHOLOGIES IN WHICH THE ISOFORMS ARE INVOLVED
hCA I	5.0×10^7	Erythrocytes, eye, gastrointestinal tract	Cytosol	Retinal/cerebral edema [61]
hCA II	1.5×10^8	Erythrocytes, eye, gastrointestinal tract, bone osteoclasts, kidney, lung testis, brain	Cytosol	Glaucoma, edema, epilepsy, altitude sickness, cancer [62–66]
hCA III	2.5×10^5	Adipocytes, skeletal, muscle	Cytosol	Oxidative stress [67]
hCA IV	5.1×10^7	Kidney, lung, colon, heart muscle, pancreas, brain capillaries, eyes	Membrane-bound	Glaucoma, retinis pigmentosa, stroke [66]
hCA VA	2.9×10^7	Brain, liver	Mitochondria	Diabetic cerebrovascular disease, obesity [68, 69]
hCA VB	9.8×10^7	Gastrointestinal tract, spinal cord, kidney, pancreas, skeletal muscle and heart	Mitochondria	Obesity [69]
hCA VI	4.9×10^7	Salivary and mammary glands	Secreted	Cariogenesis [70]
hCA VII	8.3×10^7	Central nervous system (CNS)	Cytosol	Epilepsy, neuropathic pain [71]
hCA IX	5.4×10^7	Gastrointestinal mucosa, tumoratumors	Trans–membrane	Cancer [72]
hCA XII	3.5×10^7	Intestinal, reproductive and renal epithelia, eye, tumors	Trans–membrane	Cancer, glaucoma [66, 72, 73]
hCA XIII	1.1×10^7	Reproductive tract, gut, lung, brain, kidney	Cytosol	Sterility [55]
hCA XIV	3.9×10^7	Skeletal muscle, liver, kidney	Trans–membrane	Epilepsy, retinopathies [63, 74]

Table 2.1: *Organ/tissues distribution, cellular localization and diseases in which hCAs are involved.*

catalytic efficiency have been identified in the presence of the histidine–64 residue that facilitates the rate-limiting step acting as proton shuttle. Indeed, H64 is not present in the

inefficient catalytic isoform, hCA III. The rate of the proton transfer process is also dependent by the network of water molecules that connect the zinc–bound water molecule to the proton shuttle residue: these molecules are stabilized by polar interaction with amino acid residues of the active cavity. Therefore, it is clear that even few amino acid variation can significantly affect catalytic efficiency for the isoforms [75–77]. The human CAs tissue distribution and their physiological roles have been widely investigated. These studies highlighted that some isoforms, such as hCA I and hCA II, are ubiquitous, whereas the distribution of many others is confined to specific organs or tissues as summarized in Table 2.1.

The presence of hCAs in so many tissues and organs justify the plethora of physio-patological processes in which these enzymes play an important role, among which pH and CO_2 home-ostasis, respiration and transport of CO_2/HCO_3^- between metabolizing tissues and excretion sites (lungs, kidneys), electrolytes secretion, biosynthetic reaction, calcification, bone resorption and tumorigenicity [16, 55, 60–69, 71–74]. Therefore, it is evident that a wide array of pathological consequences might occur as a result of a dysregulated expression or abnormal activity of the various CAs. Table 2.1 collects the diseases in which the twelve catalytically active human α–CAs isozymes play a determinate role. Therefore, in the last decades CAs have been identified as molecular target for the development of inhibitors (CAIs) or activators (CAAs) with diagnostic and/or therapeutic applications [2, 16].

2.1.2   CAIs in pre–clinical and clinical use

CAIs are mainly diuretic drugs with a wide variety of FDA-approved applications which include the treatment of elevated intraocular pressure (glaucoma), idiophatic intracranial hypertension (IIH), edema due to congestive heart failure, epilepsies and prophylaxis of altitude sickness. Acetazolamide (AAZ, 26), methazolamide (27), ethoxzolamide (28), dichlorophenamide (29) and sulthiame (30) represent the first generation of CAIs, which are still in use as systemic drugs for the management of the above mentioned disorders. Unfortunately, the systemic use of CAIs is limited, due to the risk of serious adverse effects, such as metabolic acidosis, hepatic failure, hypokalemia and so on. The topically active agents dorzolamide (31) and brinzolamide (32) belong to the second generation of CAIs and they are drugs of choice for the treatment of glaucoma [4, 16, 65, 78–83]. This class of drugs also includes compounds for which the CA inhibitory properties were discovered after they were launched for other therapeutics applications, such as the anticonvulsants topiramate (TPM, 33) [84] and zonisamide (34) [85], the COX-2 inhibitors celecoxib and valdecoxib (35-36) [86], the dopamine antagonist sulpiride (37), the sweetener saccharine (38) [87], as well as the indoleamine–2,3–dioxygenase inhibitor epacadostat (actually in Phase III clinical trials as antitumor agents) [88]. All these derivatives share the presence of sulfonamide, sulfamate or sulfamide moieties. The main drawback of most of the above–mentioned sulfonamides and congeners is the lack of isoform selectivity that justifies their side effects and limited their use. Nonetheless, these compounds resulted essential for the development of the third generation of CAIs from which the ureido

substituted-benzenesulfonamide SLC–0111 43 is a promising antitumor agent that selectively targets the two tumor–associated isoforms hCA IX and XII [89].

SLC-0111 entered in Phase I clinical trials for the treatment of metastatic solid tumors in 2014, whereas Phase Ib/II are still ongoing in open-label study in combination with IV gemcitabine in CA IX positive subject. Apart from the applications mentioned up to here, in the last years the CAIs demonstrated to be useful for the treatment of other human disorders [90].

2.1.3   Human α–CAs as drug targets

Although the role of CA I is still obscure, several evidences demonstrated that this isoform is involved in diabetic macular edema, proliferative diabetic retinopathy and anemia [16, 91].

Acetazolamide, 26

Methazolamide, 27

Ethoxzolamide, 28

Dichlorophenamide, 29

Sulthiame, 30

Dorzolamide, 31

Brinzolamide, 32

Topiramate, 33

Zonisamide, 34
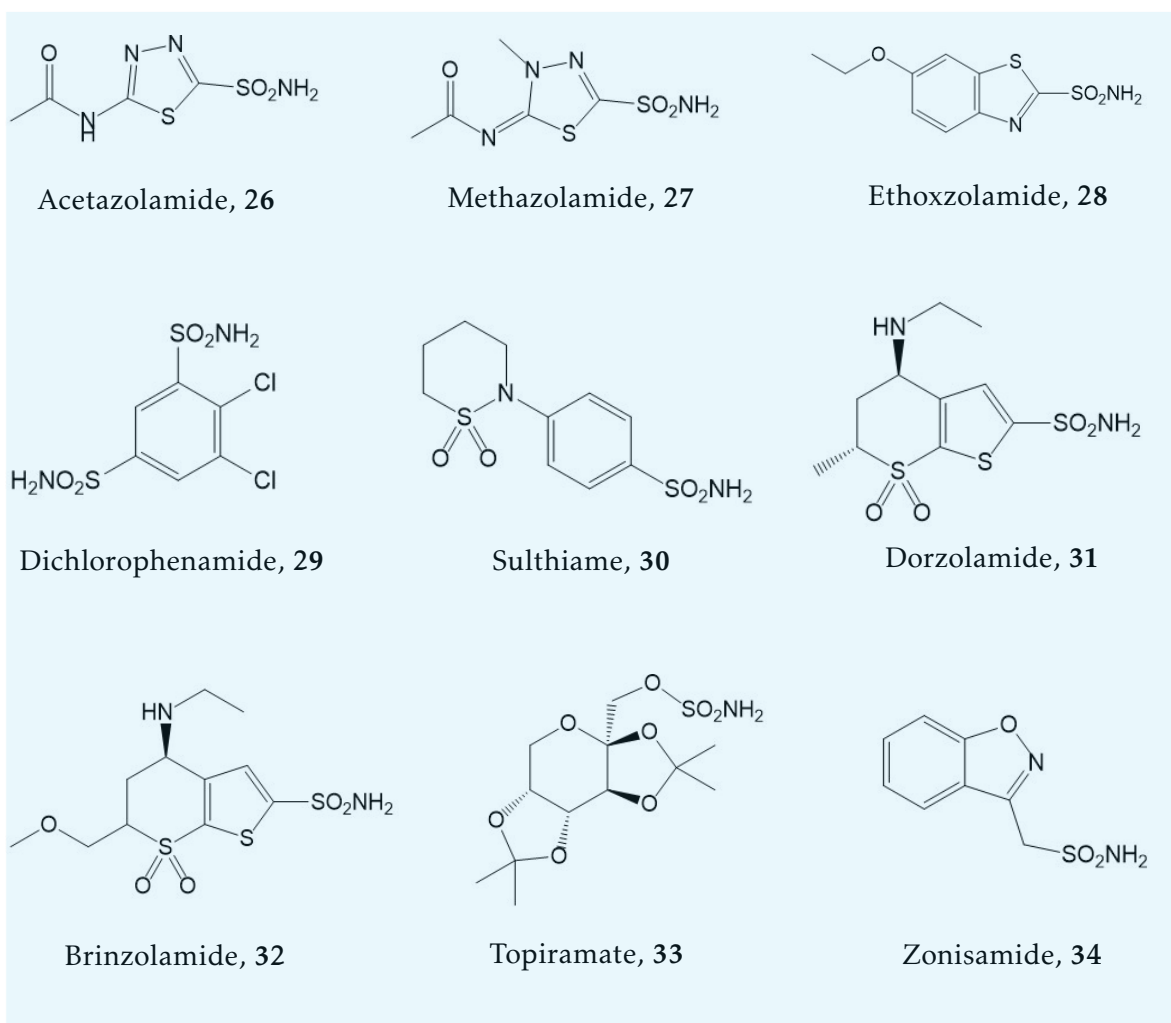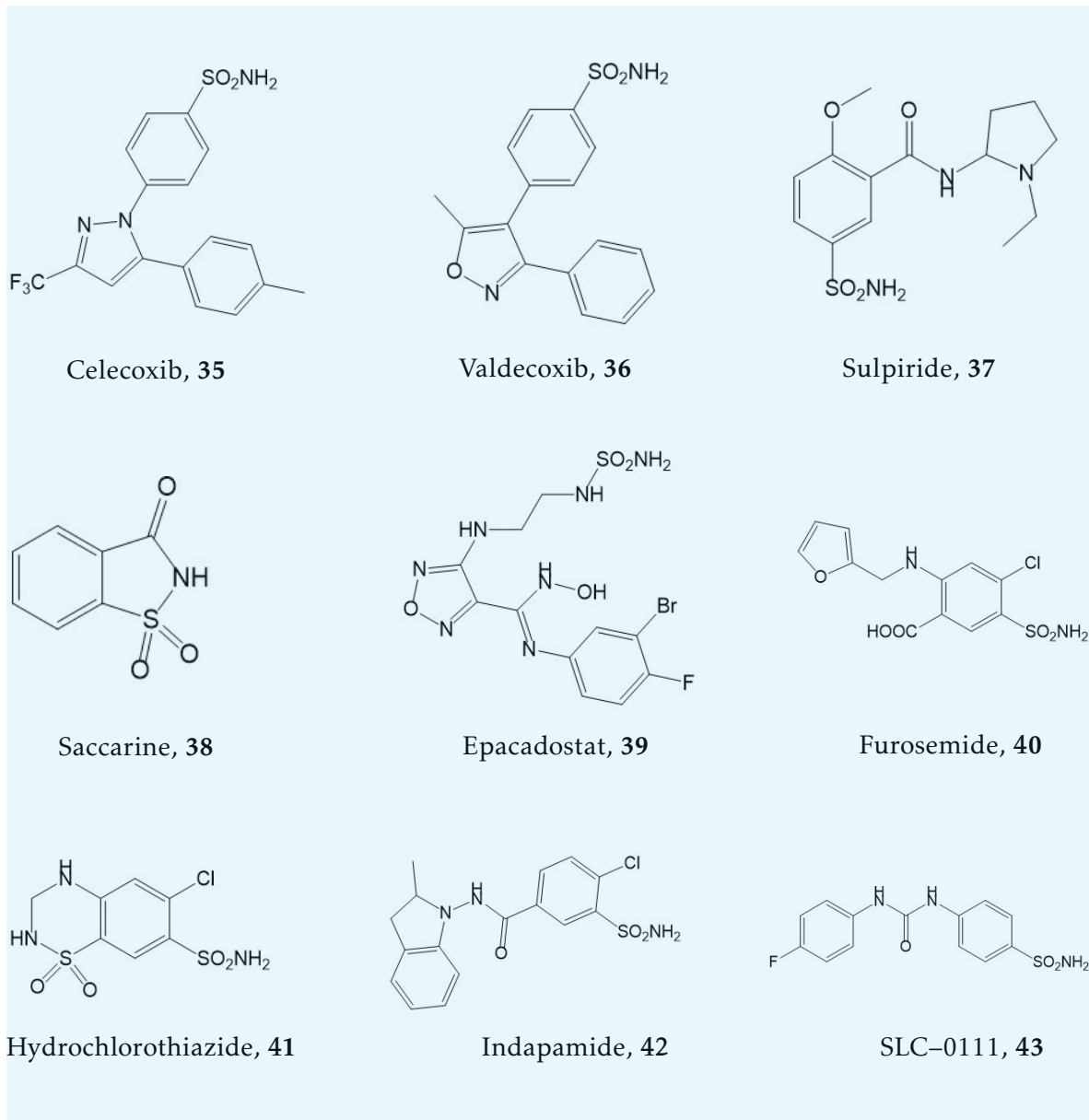
Figure 2.1: *Chemical structures of sulfonamides and sulfamates CAIs (26–42) in therapy or clinical trials (43).*

Altered levels of activity of the physiologically dominant CA II have well-known pathological consequences, such glaucoma, edema, epilepsy, some form of cancers, mountain sickness and, plausibly, also osteoporosis and atherosclerosis[65, 66, 72, 81, 92, 93]. CA III has been recently proposed to be associated with acute myeloid leukemia and carcinoma progression, so CA III

specific inhibitors may be useful against tumor proliferation and invasiveness in myeloid and liver tissue [94]. Data are available on the involvement of CA IV in retinal pathogenesis and the ability of dorzolamide (31) to provide protection against cell death; based on this evidence CA IV inhibitors might be efficient agents for managing retinitis pigmentosa [95, 96]. The involvement of CA VA and VB in metabolic processes and the evidence that the antiepileptic drugs topiramate (33) and zonisamide (34) induce severe weight loss in obese patients led to a growing interest in CA V as novel target for the treatment of obesity [69, 97]. It could speculate that CA VI is involved in the onset of caries and therefore that its inhibition could reduce cariogenesis [70]. In the aforementioned scenario of CAIs application as anticonvulsant agents, isoforms specific inhibitors of CA VII may represent safe and efficient drugs in the management of febrile seizure or other epileptic syndromes [98]. Considering that the use of acetazolamide in combination with midazolam affect positively neuropathic allodynia after spinal nerve damage, CAVII together with CAII can represent new targets for the management of neuropathic pain [99]. The two tumor-associated CA IX and XII are object of intense drug design campaigns, since they are validated as both therapeutic and diagnostic targets [60, 100]. Among these, CA IX is the most investigated one because the constitutive expression of this isoenzyme is limited, reducing the potential off target effects on normal tissues [101]. Its expression in tumors is modulated by hypoxia–inducible factors (HIFs) as response to decreasing oxygen levels and increased cell density. CA IX has been observed in many aggressive tumors (brain, breast, bladder, cervix, colon, etc.) and an overexpression is linked to poor prognosis, chemotherapeutic resistance, and poor clinical outcome. This aspect explains why this isoform serves as prognostic/predictive factor for hypoxic and malignant tumors [102]. Contrary, CA XII has been observed in many organs/healthy tissues (pancreas, appendix, colon and so on) and its expression in tumors is not controlled by HIFS, though observed in hypoxic condition. Because CA XII is regulated by estrogen, this isoform is strongly associated with breast cancer. The use of selective CA IX and CA XII inhibitors was shown to lead to the inhibition of primary tumors growth and metastatic processes, as well as reduction of cancer stem cell population. It is therefore clear why there is an increasing interest in new class of CAIs, prevalently for application in oncologic area. In addition, the discovery of the overexpression of CA IX and XII in the inflamed synovium of patients with arthritis paved the way to a new and unexplored research area. Considering the relevance of pH and ion homeostasis in reproductive organs to ensure a normal fertilization, the use of CA XIII inhibitors could be used for the development of anti–contraceptive agents. Finally, several studies reported the involvement of CA XIV in the onset of seizures and some types of retinopathies. Although CA I, III, IV, XIII and XIV are involved in serious pathological conditions, these isoforms have not been studied in depth and are still considered "orphan targets". On the contrary, many drug design and structural biology efforts have been focused on the well explored isoforms CA VII, IX and XII.

2.2   Our focus on classical CAIs targeting druggable hCAs: discovery of a promising template and structural modifications

In the last decade, Gitto and coworkers contributed to improve the knowledge about the structure–affinity/activity relationships (SARs) of CAIs bearing sulfonamide moiety [7–14]. In particular, previous studies allowed the identification of a large numbers of potent hCAIs. Among them, the arylsulfonamide N–(3,4–dimethoxyphenethyl)–4–sulfamoylbenzamide (44), showed relevant inhibitory activity in the nanomolar range against hCA isoforms in the a stopped flow CO_2 hydration assay as a well–established screening procedure by Supuran and coworkers at Univeristy of Florence (Italy). The X–ray adduct of compound 44 with the ubiquitous hCA II has been solved (Figure 2.2), suggesting the mechanism of action of this compound. However, compound 44 was not characterized by a good selectivity profile against the druggable isoforms hCA VII, IX and XII (Table 2.2). Based on flexible prototype 44, a series of corresponding cyclic analogues , constituted by isoquinoline/quinoline derivatives, has been designed and tested, thus identifying the promising compound 4–(1,2,3,4–tetrahydroquinoline–1–carbonyl)benzenesulfonamide (45).

The following sections report details about the design, synthesis, SARs, structural and computational studies for a newer series of cycloalkylamino–1–carbonylbenzenesulfonamide derivatives inspired by the quinoline prototype 45. The chemical characterization for all final compounds was supported by spectroscopic measurements (^{1}H–NMR and ^{13}C–NMR). The purity of tested compounds was confirmed by elemental analysis (C, H, N).

2.2.1   Design and synthesis of cycloalkylamino–1–carbonylbenzenesulfonamide derivatives

In order to understand the role of the benzene fused ring of the isoquinoline core in the binding recognition process, we designed a novel series of compounds strictly related to our lead compound 4–(1,2,3,4–tetrahydroquinoline–1–carbonyl)benzenesulfonamide (45) containing piperidine, piperazine and azepine nucleus in place of isoquinoline one. Our drug design was inspired by the visual inspection of the binding pose of inhibitor 45 within hCA II active site, for which the heterocyclic portion was located into the hydrophobic cleft delimited by the amino acid residues F131 and P202. Therefore, we have decorated the cycloalkylamine core with hydrophobic substituents capable to establish additional contacts in the middle and top area of CA cavity, thus addressing both affinity and isoform selectivity toward several druggable human CAs. Indeed, the most used drug design method in the field of CAs is the so called "*tail approach*", which consists in the introduction of a "*tail*" to the scaffold of sulfonamide–based inhibitors. The numerous inhibitors designated by tail approach and the huge number of corresponding X–ray complexes to date available, validated it as one of the most versatile method to readily develop a large variety of CA inhibitors.

Following this approach, we designed cycloalkylamino–1–carbonylbenzenesulfonamides

A)

Table 2.2: *K_i values (nM) against hCA I, hCA II, hCA VII and hCA XIV for compound 44–45.*

	K_i (nM)[a]				
	hCA I	hCA II	hCA VII	hCA IX	hCA XIV
44	8.7	2.7	5.8	3.8	4.3
45	78.6	6.8	8.5	9.4	39.0
AAZ	250	12.1	2.5	25.8	41.0

44   45

B)

C)
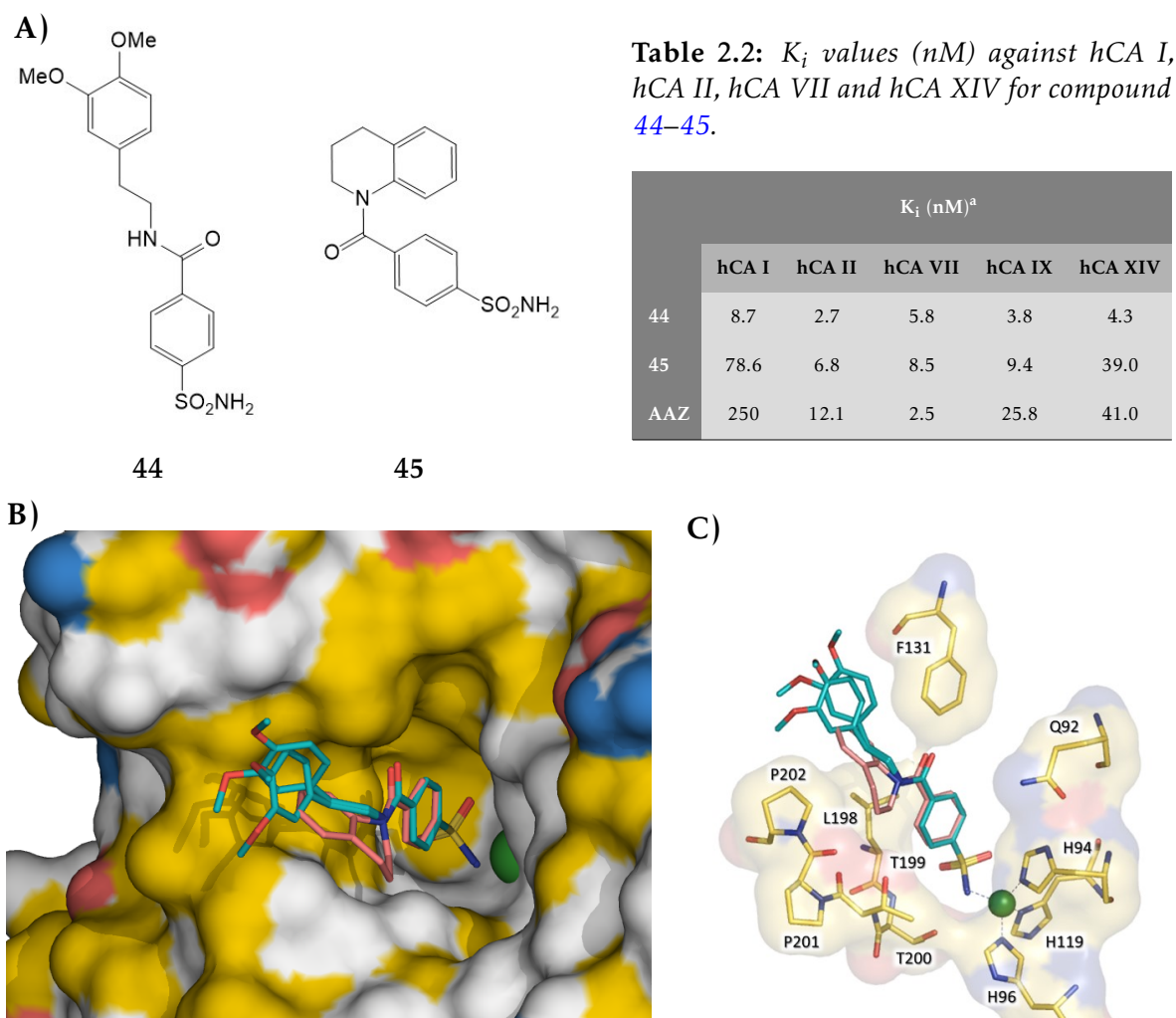
Figure 2.2: *Panel A): Chemical structures of arylsulfonamide 44 and quinoline derivatives 45. Panel B): Superposition of binding pose of 44 (deepteal stick) and 45 (deepsalmon stick) into the active site of CA II (PDB code: 3V7X and 4Z0Q respectively). The protein backbone is represented as surface and colored by hydrophobicity. The Zn(II) in depicted as green sphere. Panel C): Representation of the CA II binding pocket in complex with 44 and 45, showing residues involved in the recognition process of the inhibitors.*

47a–e, 48a, 49a–f, 50a–c and 50d, which were obtained by following the procedure depicted in Scheme 2.1. In particular, the commercially available 4–sulfamoylbenzoic acid (46) and suitable cycloalkylamines were coupled at room temperature, in alkaline medium and in presence of N,N,N,N–tetramethyl–O–(1*H*–benzotriazol–1–yl)uranium hexafluorophosphate

	R₁
a	H
b	2–CH₃
c	3–CH₃
d	4–CH₃
e	4–CH₂–Ph

	R₂	R₃
a	H	H
b	OH	H
c	OH	Cl
d	OH	Br
e	CN	H
f	COCH₃	H

	R₄	R₅
a	H	Ph
b	H	4–FC₆H₄
c	Ph	Ph
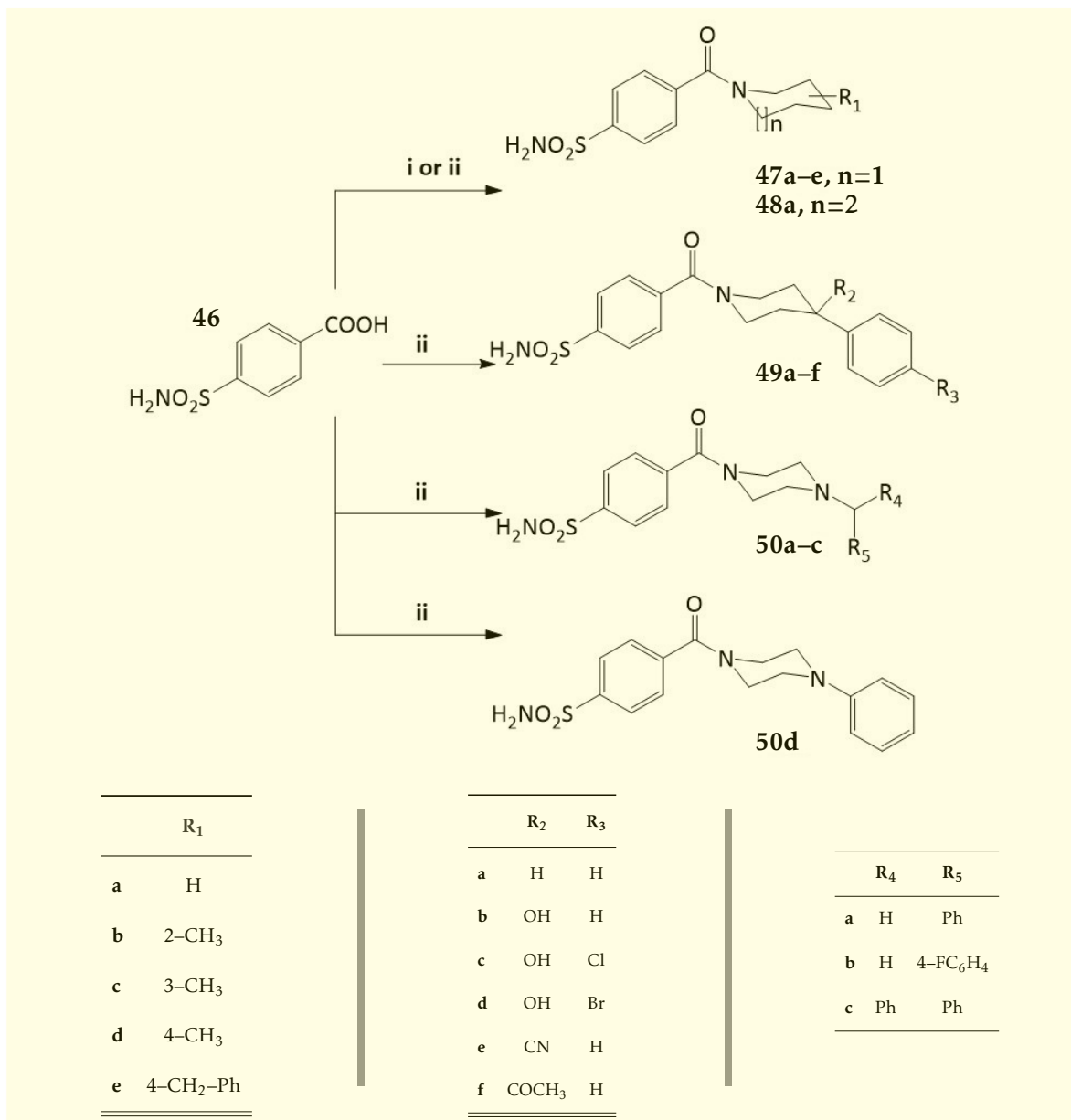
Scheme 2.1: *Reagents and conditions: i) carbonylimidazole (CDI), THF, r.t., 3h, then RR'NH, DMF, rt, 2hs; ii) RR'NH, HBTU, TEA, DMF, rt, overnight.*

(HBTU) (pathway i). For compound 47a and 47d, carbonylimidazole (CDI) was used in order to optimize the yield (pathway ii).

2.2.2 *In vitro* and *in vivo* profiling of sulfonamides 47a–e, 48a, 49a–f and 50a–d

For all compounds thus obtained, the CA inhibitory effects were measured for human CA I, CA II and the druggable isoforms CA VII, CA IX, CA XII and CA XIV by the before mentioned stopped flow CO_2 hydration assay and the potencies were expressed in terms of K_i values (lower is more effective). The K_i value is equivalent to the dissociation constant (K_d) of the enzyme–inhibitor complex for reversible inhibitor that competes for the same binding pocket of the substrate. The obtained results are reported in Table 2.3 and compared with K_i values of prototype 45 and two well–known inhibitors AAZ 26 and TPM 33 as reference compounds. As shown in Table 2.3, the four 4–(piperidine–1–carbonyl)benzenesulfonamides (47a–e) and the cyclohomologous 4–(azepane–1–carbonyl)benzenesulfonamide (48a) displayed significant inhibitory effects towards all studied CA isoforms when compared to well–known inhibitors 26 and 33. They generally demonstrated inhibitory activity at low nanomolar concentration, except for outlier compounds 47c, 47e and 48a against CA I. Moreover, all tested compounds resulted poorer inhibitors of CA XIV to respect other studied isoforms. By removing the benzene fused ring of prototype 45, it was registered an enhancement in affinity toward human CA II isoform by an order of magnitude for 4–(2–methylpiperidine–1–carbonyl)benzenesulfonamide (compound 47b) and 4–(4–methylpiperidine–1–carbonyl)benzenesulfonamide (compound 47d), suggesting an optimized orientation within CA II active site cavity. Notably, for the 4–(4–benzylpiperidine–1–carbonyl)benzenesulfonamide (47e) an improvement of affinity toward druggable isoform hCA VII has been found (K_i value of 0.63 *nM*), thus suggesting a crucial role of additional 4–benzylpiperidine moiety to address hCA VII selectivity. By incorporating a phenyl moiety at C–4 position of piperidine nucleus, a further increased affinity against CA II and CA VII was registered for compound 49a (K_i values of 0.5 *vs* 5.7 *nM*) in comparison with analogous 47a (K_i values 5.7 *nM* and 8.3 *nM*). The installation of additional hydroxyl group, nitrile or acetyl functionalities at C–4 position, did not lead to significant improvement against CA II inhibition. As result the SAR analysis was very flat for compounds 49a–f concerning CA II inhibitory activity. In contrast, the affinity against CA VII has been optimized for compounds 49d ($R_1 = OH$ and $R_2 = 4 - BrC_6H_4$) and 49e ($R_1 = CN$ and $R_2 = Ph$) showing K_i values of 0.55 and 0.68 *nM*, respectively. In particular, compounds 49a, 49d and 49e proved high inhibitory effects toward brain–expressed CA VII with K_i values comparable to those of the anticonvulsant agent TPM 33. For other studied isoforms, no linear correlation between Ki values and structural modifications has been observed for inhibitors 49a–f. The screening of piperazinyl derivatives 50a–d revealed that all compounds generally displayed inhibitory effects towards the selected isoforms in the nanomolar range. It appears that the installation of a 4–fluorobenzyl moiety on piperazine core optimizes the affinity toward CA I and CA II isoforms for compound 50b.

To evaluate the *in vivo* effects of the most efficacious inhibitors against the brain expressed hCA VII isoform 49a, 49d, 50b, and 50c, we carried out additional pharmacological studies. Specifically, it has been evaluated the ability of these compounds to prevent seizures in mice using pentylentetrazole (PTZ) as chemical proconvulsant agent. The four chosen compounds

	hCA I	hCA II	hCA VII	hCA IX	hCA XII	hCA XIV
47a	9.2	5.7	8.3	3.1	7.9	23.8
47b	4.4	0.63	4.6	2.6	7.8	31.4
47c	187	6.1	16.5	2.4	4.5	41.7
47d	7.7	0.79	6.9	3.4	3.1	13.7
47e	75.5	1.5	0.63	7.0	9.4	53.7
48a	85.0	3.8	13.3	16.8	2.7	37.9
49a	1.7	0.5	0.45	3.3	6.6	46.9
49b	9.3	0.6	2.6	22.6	7.8	52.5
49c	6.6	0.6	1.0	24.9	8.5	7.8
49d	6.3	0.7	0.55	4.7	8.1	7.7
49e	6.5	0.6	0.68	18.4	6.4	11.0
49f	7.7	0.6	4.4	3.1	59.4	29.8
50a	6.8	3.0	10.4	33.1	3.8	34.6
50b	0.69	0.5	7.8	45.1	5.6	15.2
50c	50.1	5.7	7.8	28.2	8.5	42.8
50d	91.1	2.0	9.5	4.8	7.3	41.5
AAZ (26)	250	12.1	2.5	25.8	5.7	41.0
TPM (33)	250	10	0.9	58	ND	1460
45	78.6	6.8	8.5	9.4	ND	39.0

Column group header: K_i $(nM)^a$

[a]Errors in the range of ±10% of the reported value, from 3 different assays. Recombinant full–length hCA I, hCA II and hCA VII and catalytic domains of hCA IX, hCA XII and hCA XIV were used.

Table 2.3: *K$_i$ values against hCA I, II, VII, IX, XII and XIV isoforms showed by derivatives 47a–e, 48a, 49a–f, 50a–d, the prototype 45 and the well–known CAIs AAZ 26 and TPM 33.*

were tested at the doses of 20 and 30 *mg/kg*, according to the knowledge that the ED50 values of TPM 26 and AAZ 33. Unfortunately, none of the tested compounds was able to prevent the occurrence of clonus. However, some signs of sedation were observed at the dose of 20 *mg/kg*, effect that was confirmed at the higher dose of 30 *mg/kg* by which animals were clearly sedated. This effect may be potentially related to the toxicity of the tested compounds. Therefore no higher doses were tested. Considering latency to clonus (time to reach the third stage of seizure after PTZ administration), all compounds were able to increase significantly ($p < 0.05$) this parameter, although no significant differences were observed at different doses and between the tested molecules. All screened compounds seem to possess some neuronal effects considering the sedation signs and the increase in latency to clonus. However, the unexpected *in vivo* effects limit further studies in this animal model. The obtained results suggested that for this class of benzenesulfonamides, the significant potency against the brain enzyme CA VII might be not corroborated with anticonvulsant activity. Anyway, we cannot exclude a potential onset of pharmacological effect with higher concentrations.

2.2.3 X–ray studies for Compounds 49a, 49b and 50b in complex with CA II and CA VII

To gain more information about the mode of action of the novel synthesized compounds, the crystal structures of some representative molecules in complex with the isozymes CA II and CA VII were solved. hCA II was generally chosen as model isoform for crystallization, since it readily forms crystals and many studies have been reported on its adducts with different classes of inhibitors. The data collection and refinement statistics for these six crystal adducts are summarized in Table 4.1 (Chapter 4) and deposited in the Protein Data Bank [103, 104] with the codes 6H2Z, 6H33, 6H34, 6H36, 6H37 and 6H38. Since piperidine derivatives 49a–d and 49a–f piperazine displayed very high inhibitory activity against CA II and CA VII with respect to the pioneer compound 45, the crystallographic structures of the 4–(4–phenylpiperidine–1–carbonyl)benzenesulfonamide (49a) in complex with both enzymes were initially solved. Inspection of (Fo–Fc) and (2Fo–Fc) electron density maps at various stages of the crystallographic refinement showed features compatible with the presence of compound 49a within the active site of hCA II and hCA VII (Figure 2.3A and 2.3B). These maps were very well defined in both cases, thus indicating absence of inhibitor flexibility within enzyme active sites. As generally observed for sulfonamide–based CA inhibitors, in these adducts compound 49a was anchored to the catalytic zinc ion via the primary sulfonamide moiety, replacing the zinc–bound water molecule and creating hydrogen bond interactions with T199. The benzene-sulfonamide core established strong hydrophobic interactions (distance < 4.0 Å) with residues H94, L198 and V121 in the case of hCA II and with H94, V121 L198 and T200 in the case of CA VII (Figure 2.4A and 2.4C). Furthermore, the carbonyl group was hydrogen bonded to Q92 in the CA VII active site, but this interaction is not detectable in the case of CA II. Finally, 4–phenylpiperidine *tail* was oriented toward the hydrophobic cavity of the
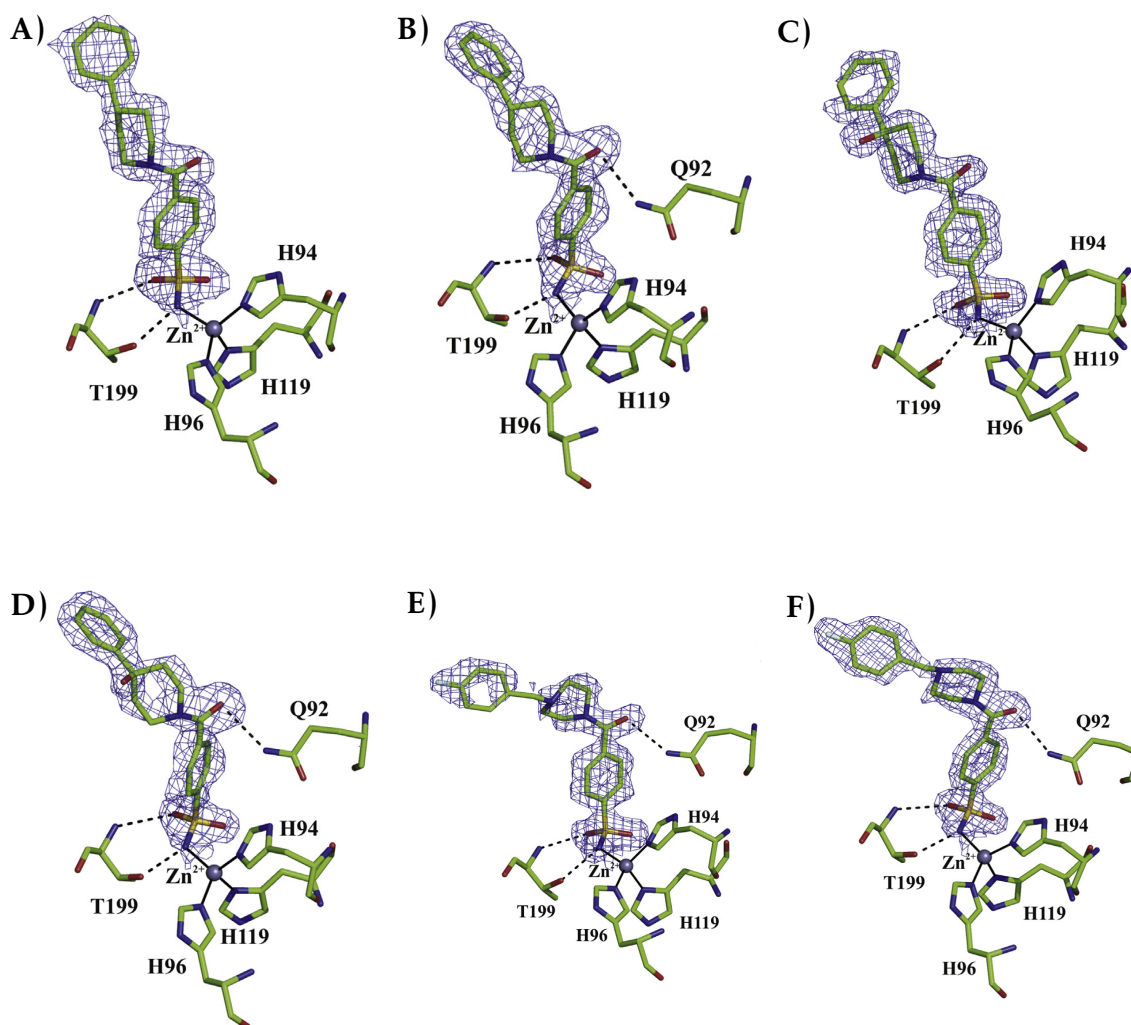
Figure 2.3: *Electron density maps of CAIs. Sigma–A weighted |2Fo–Fc| simulated annealing omit map of inhibitors bound in hCA II and VII active sites. A) hCA II/49a, B) hCA VII/49a, C) hCA II/49b, D) hCA VII/49b, E) hCA II/50b and F) hCA VII/50b. Zinc is represented as a grey sphere.*

active site establishing many hydrophobic interactions with residues of both proteins. It is therefore clear that the binding poses assumed by 49a within CA II and VII and the network of interactions that it forms with the two isoforms were very similar, with exception for the H-bond established with Q92 in CA VII. Nonetheless, it appears that this additional hydrogen bond did not influence the binding affinity since the K_i values of the inhibitor against the two isoenzymes are comparable. Successively, it was investigated the binding pose of compound

49b bearing an additional hydroxyl group at C4 position of the piperidine nucleus to respect of parent derivative **49a**. It has been found that the introduction of a polar moiety did not significantly affect the interaction mode of the inhibitor with CA II and CA VII active sites (Figure 2.4B and 2.4D) if compared with the unsubstituted **49a**.

This evidence results in good agreement with the very closely K_i values against CA II (0.5
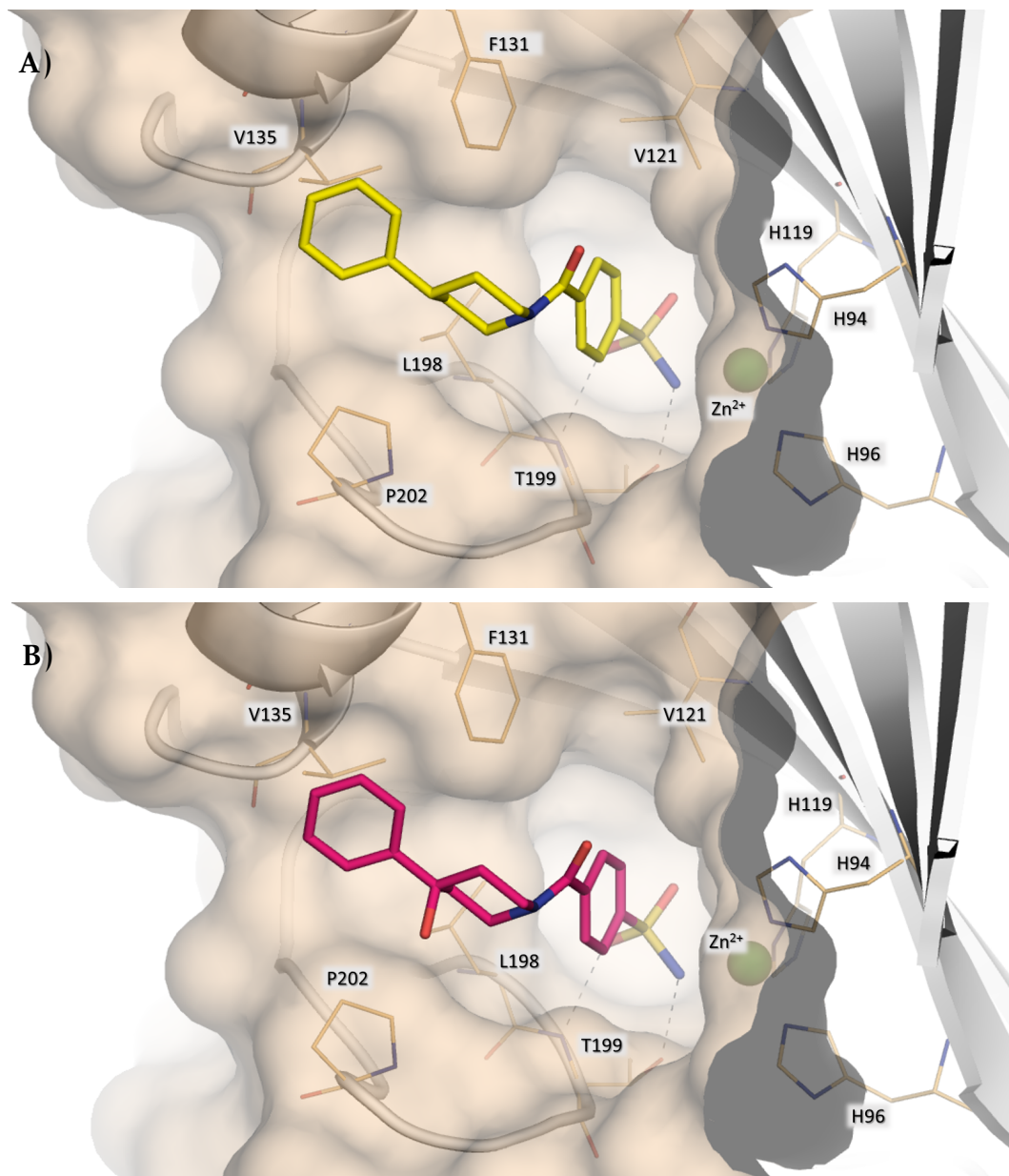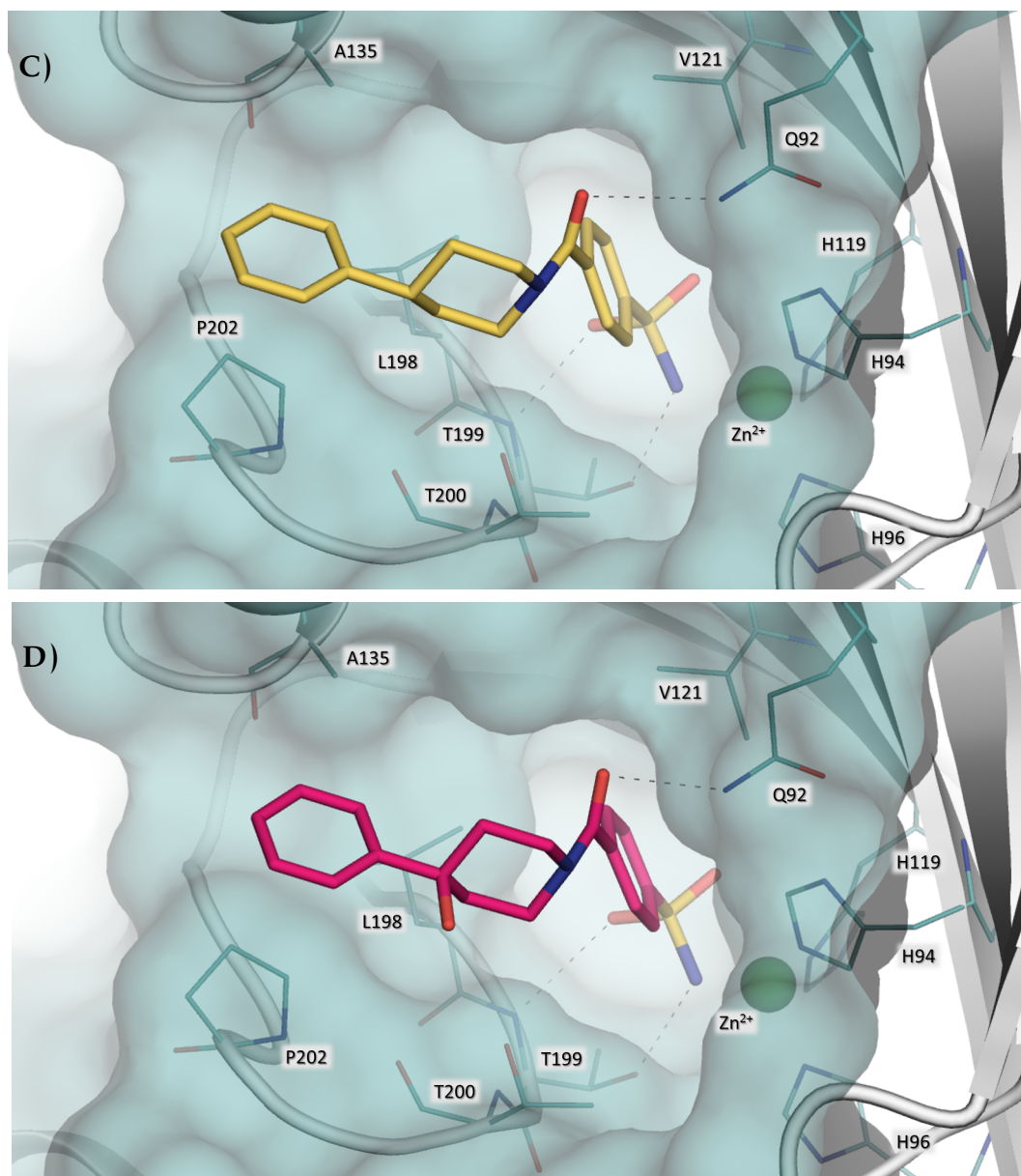
Figure 2.4: *Piperidine–1–carbonyl–benzenesulfonamides bound to the active site of hCA II (wheat) and hCA VII (light teal). A) and C): compound 49a (yellow). B) and D): compound 49b (hotpink). Zinc ion is depicted as dark green sphere. Residues involved in hydrophobic interactions and hydrogen bonds (grey dashed lines) are shown. The figure was made using PyMol.*

nM and 0.6 nM for 49a and 49b, respectively); whereas the slight divergence found for K_i values against CA VII (0.45 nM and 2.6 nM for 49a and 49b, respectively) is not consistent
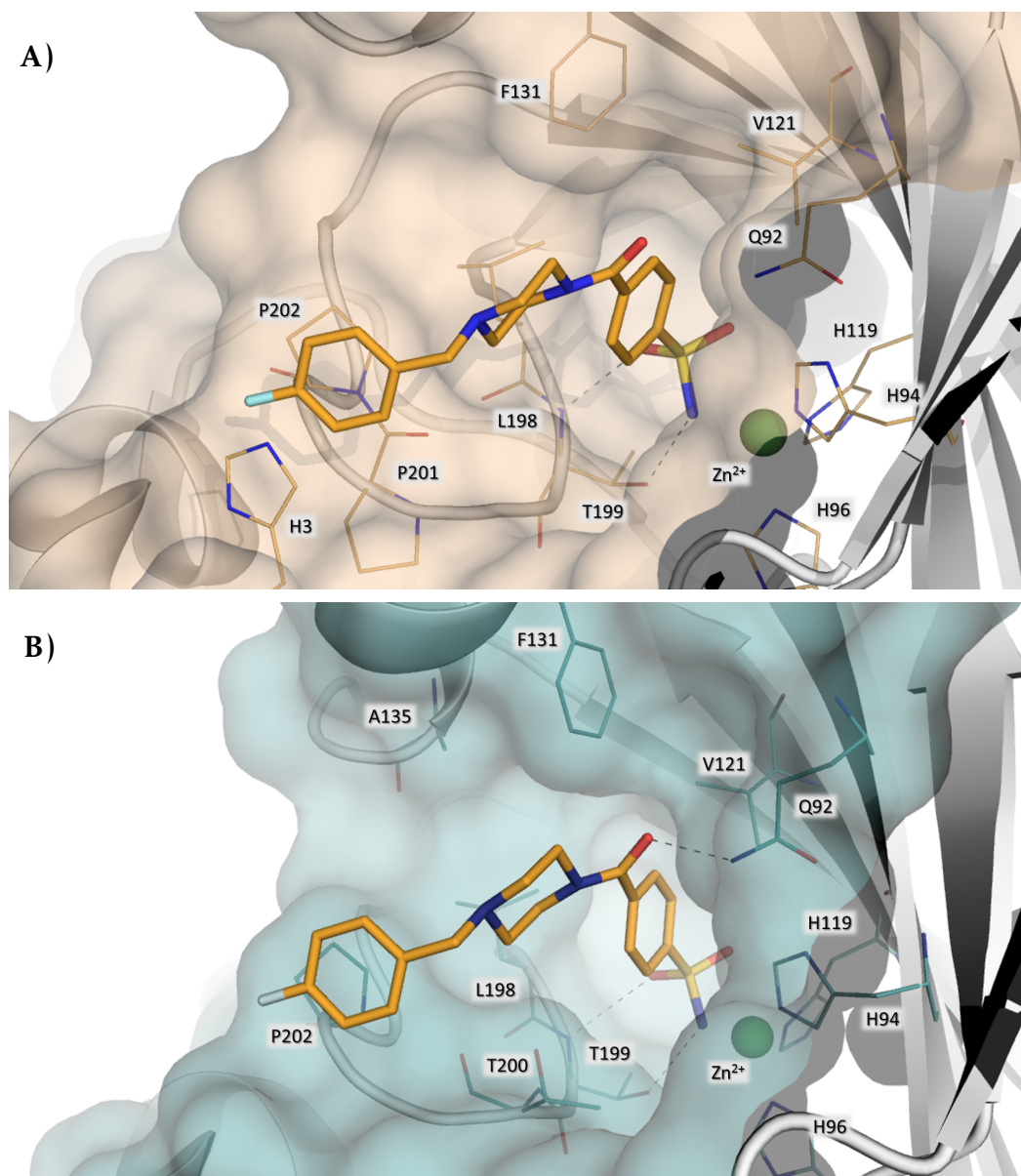
Figure 2.5: *(4–Fluorophenyl–piperazine–1–carbonyl)benzenesulfonamide 50b (orange) bound to the active site of hCA II (wheat) (A) and hCA VII (light teal) (B). Residues involved in hydrophobic interactions and hydrogen bonds (gray dashed lines) are shown.*

with their very comparable binding pose within the CA II and CA VII active sites. Thus, we can hypothesize that the higher affinity of 49a with respect to 49b for the brain–expressed isoform should be ascribed to other molecular factors. To understand how the replacement of piperidine *core* with piperazine one could influence the binding process, the crystal structures of the most active molecule of the series 50b in complex with CA II and CA VII were solved. Surprisingly, despite kinetic experiments indicated for this molecule a higher binding affinity for CA II with respect to CA VII, the electron density maps of the inhibitor were better defined in the case of the adduct with the brain enzyme with respect to the adduct with the ubiquitous CA II (Figure 2.3E and 2.3F). The analysis of the structures of the two adducts furnished an explanation to this apparent inconsistency. Indeed, in both cases the inhibitor is bound to the enzyme active site establishing the canonical interactions of the benzenesulfonamide moiety with CA active site. Moreover, polar and hydrophobic interactions between the phenyl-carbonyl-piperazine moieties and residues which delimit the cavity (see Figure 2.5A and 2.5B) are detectable. However, in the case of CA VII/50b complex, additional interactions are found between the inhibitor and residue R159 of a symmetry-related macromolecule. Thus, it is obvious that the lower conformational flexibility of 50b is related to the crystal packing and thus it is not present in solution. Finally, it is worth noting that both in CA II/50b and in CA VII/50b the benzylpiperazine *tail* is oriented toward a rather unexplored region of the active site located at the surface protein. Indeed, it has been reported that the majority of hCAIs orient their tail toward either the hydrophobic or the hydrophilic region of the catalytic cavity. Due to this unusual orientation, these piperazine–derivatives have been further investigated to address selectivity issues.

2.2.4 From methylene to carbonyl bridge: design and synthesis of a new series of 4-(4-aroylpiperazine-1-carbonyl)benzenesulfonamides

We designed a further set of 4–(4–aroylpiperazine–1–carbonyl)benzenesulfonamides obtained by the replacement of the N–benzyl moiety with the N-benzoyl one (Figure 2.6). Our initial idea was to explore how this slight chemical modification could affect the binding pose within CA pocket. For instance, we focused our interest on CA IX and CA XII isoforms bearing smaller residues (V131 and A131 in CA IX and XII, respectively) when compared to CA II (F131), thus forming a more accessible subpocket site in CA cavity. Secondly, to improve isoform selectivity over the ubiquitous CA I and CA II, our efforts have been addressed to decorate the benzoyl tail by incorporating hydrophobic/hydrophilic substituents, for enhancing interactions with residues located on the rim of the active site cavity characterized by the highest diversity among the different isoforms. This region has been termed as "*selective pocket*" because several amino acids present in this area are unique across the CA isoenzymes.

The short and efficient synthetic pathway that has been employed to obtain the designed 4–(4–benzoylpiperazine–1–carbonyl)benzenesulfonamide is depicted in Scheme 2.2. In detail, the coupling of suitable benzoyl chlorides 52a–p with 1-Boc-piperazine 51 and the N–Boc deprotection was performed by a one pot procedure thus giving the N–aroylpiperazines 53a–p in good yields. In the last step, the intermediates 53a–p reacted with the 4–sulfamoylbenzoic acid to give desired 4–(4–aroylpiperazine–1–carbonyl)benzenesulfonamides 54a–p. This reaction was carried out at room temperature, in alkaline medium for DIPEA and by using in HBTU as coupling reagent. To study the influence of introduction of polar group on outer benzoyl ring, it was also performed the nitro reduction of compounds 54n–p into the corresponding amine derivatives 54q–s, by treatment with hydrazine hydrate (NH_2–$NH_2 \cdot H_2O$) as reductive agent, in ethanol (EtOH) and in the presence of carbon supported palladium catalyst (Pd/C).

2.2.5 Carbonic anhydrase inhibition assays against hCA isoforms and structural studies

The K_i values have been determined for all the synthesized 54a–p benzenesulfonamides toward selected hCAs and the obtained results are summarized in Table 2.4, in comparison with the K_i values of the structurally related amines 50a–50b, the well–known inhibitor AAZ (26) and the ureido derivative SLC–0111 (43). By analyzing data reported in Table 2.4, some hint of structure–activity relationships (SARs) can be described. Most of the synthesized 4–(4–aroylpiperazine–1–carbonyl)benzenesulfonamides have shown inhibitory effects in the low nanomolar range towards druggable CA isoforms. However, it was not possible to find a linear correlation between K_i values and the nature/position of groups on the phenyl ring. A comparison of the K_i values measured for the amide derivative 4–(4–benzoylpiperazine–1–carbonyl)benzenesulfonamide 54a with the corresponding amine–derivative 50a, showed that introducing of this slight chemical modification did not lead to significant impact on affinity for the druggable CA VII, CA IX and CA XII. At the same time, no improvement in selectivity profile toward target isoforms over the physiologically dominants CA I and II was observed. To compare the binding mode of this novel series of benzenesulfonamides with the previously reported, X–ray crystallographic studies were carried out. In particular, the crystal structure
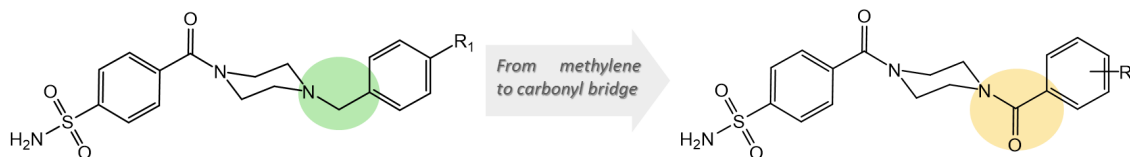
Figure 2.6: *Designed hCAIs structurally related to the lead compounds 50a–50b.*
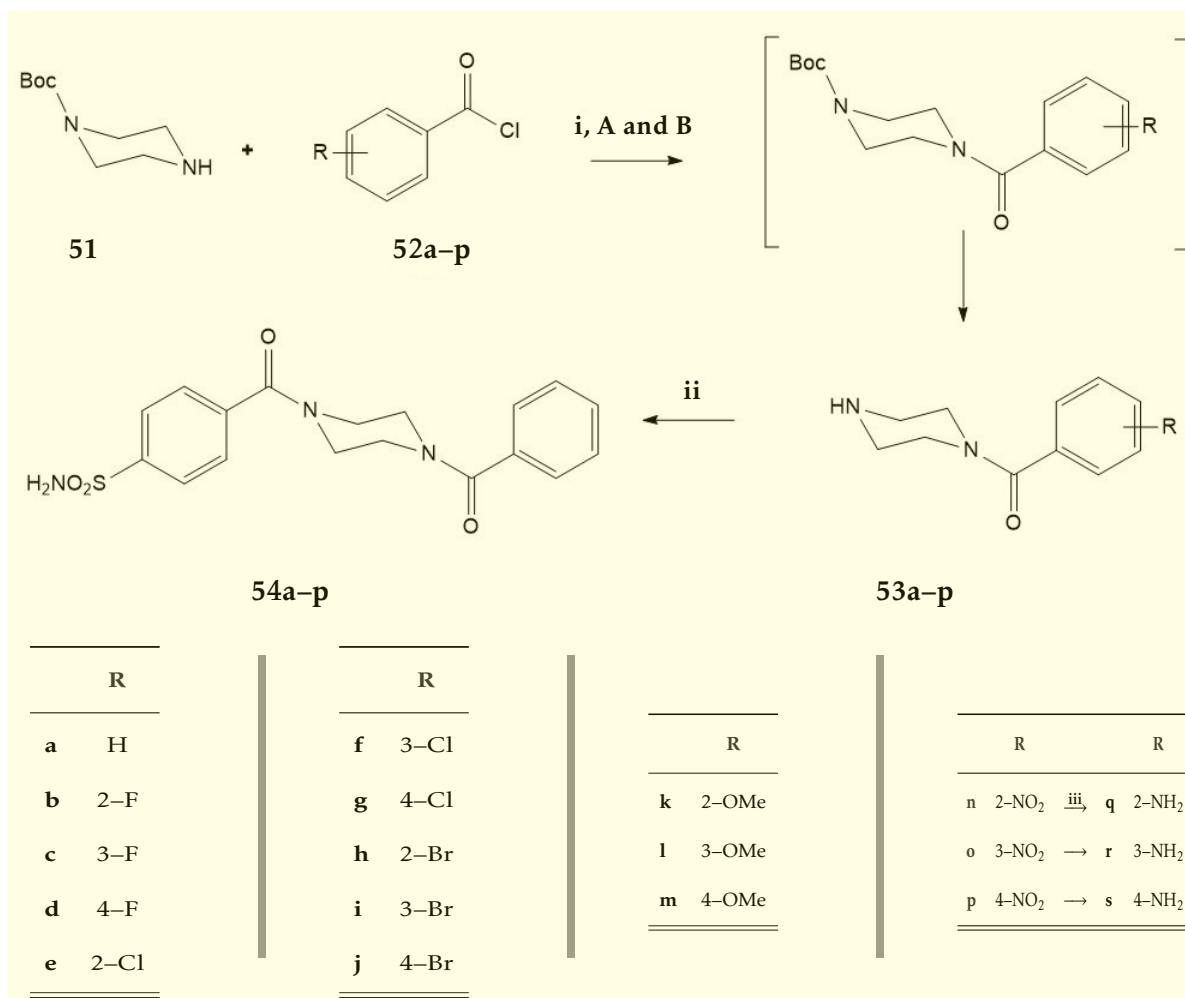
Scheme 2.2: *Reagents and conditions: i) A: DCM, DIPEA, rt, 3hs; i) A: TFA, 0°C to rt, 4 hs; ii) DMF, HBTU, 4–Sulfamoylbenzoic acid, DIPEA, rt, overnight; iii) EtOH, NH_2-$NH_2 \cdot H_2O$, Pd/C, rt to reflux, 1 h.*

of CA II in complex with unsubstituted compound 43a (Figure 2.7) was determined at 1.0 Å. The data collection and refinement statistics for the crystal structure are summarized in Table 2.4 and deposited in the PDB with code 6XXT. The electron density maps highlighted the presence of inhibitor 54a within the hCA II catalytic site. As shown in Figure 2.7A, it is possible to distinguish that 4–(4–benzoylpiperazine–1–carbonyl)benzenesulfonamide assumed two slight different conformations, differing only for the orientation of the carbonyl group between benzenesulfonamide and the piperazine ring. The electron density maps were well defined for the entire inhibitor molecule with the exception of phenyl tail that showed a
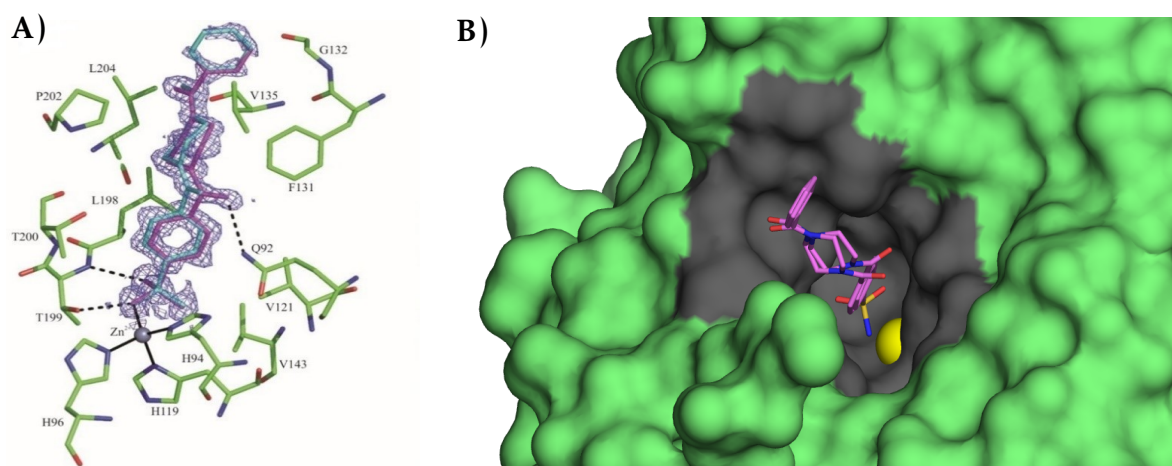
Figure 2.7: *A) hCA II/54a active site showing the σA–weighted |2Fo–Fc| electron density map (contoured at 1.0 σ) relative to the inhibitor with the conformer A colored in cyan and the conformer B in magenta. The zinc ion coordination and residues involved into polar and hydrophobic interactions with 54a molecule are also depicted. B) Representation of hCA II surface showing the inhibitor 54a located in the enzyme active site. The Zn²⁺ ion within the catalytic cavity is represented as a yellow sphere. The amino acids constituting the catalytic pocket are colored in grey.*

greater conformational variability. Inhibitor binding did not alter CA II 3D structure.

As expected, compound 54a was anchored to the active site by means of the deprotonated sulfonamide moiety, which coordinated the catalytic zinc ion and established two hydrogen bonds with the *gate keeper* T199. The inner phenyl ring engaged strong hydrophobic interactions (distance < 4.0 Å) with residues Q92, V121, L198 and T199. The carbonyl group of one conformer formed a weak hydrogen bond with of Q92NE2 atom, whereas in the case of the other conformer the oxygen atom was involved into a polar interaction with a glycerol molecule. Moreover, in both conformers the 4–carbonylpiperazine moiety was stabilized by van der Waals interactions with F131, V135 and P202 residues. Finally, the phenyl tail was located as expected on the border of the active site cavity establishing only few and weak hydrophobic interactions (distance < 4.2 Å) with F131 and G132 (Figure 1.2A and 1.2B). The structural data obtained encouraged us to further explore the aromatic "tail" by the introduction of further hydrophobic/hydrophilic substituents.

This new series of CAIs in general exhibited medium inhibitory potency toward ubiquitous CA I, isoform except for derivatives 54c, 54d and 54q for which the K_i values fall in low nanomolar range. It is worth to note that the *meta*–amine 54o and *meta*–bromine 54i derivatives showed a potency over five times lower than the unsubstituted 54a, with measured K_i values of 404.9 and 460.0 *nM*. Since the inhibition of CA I, with clinically use CAIs is related to the onset of serious side effects, this aspect can be considered a positive feature for these two
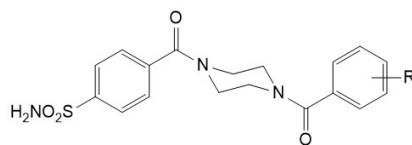
Cmpd		K_i (nM)[a]					
	R	hCA I	hCA II	hCA VII	hCA IX	hCA XII	hCA XIV
50a	H	6.8	3.0	10.4	33.1	3.8	34.6
50b	4–F	0.69	0.5	7.8	45.1	5.6	15.2
54a	H	69.1	3.7	70.7	37.1	8.5	85.5
54b	2–F	22.4	28.4	6.8	68.7	3.1	6.9
54c	3–F	0.84	0.41	66.1	3.8	29.1	35.7
54d	4–F	7.7	32.4	39.5	332.4	26.4	69.6
54e	2–Cl	94.4	5.6	2.9	62.2	63.1	86.1
54f	3–Cl	72.5	22.5	7.5	54.4	66.9	58.3
54g	4–Cl	87.5	7.2	61.7	29.2	6.3	63.4
54h	2–Br	58.0	3.0	45.3	60.4	48.7	73.9
54i	3–Br	460	0.6	3.5	16.2	8.5	85.3
54j	4–Br	85.1	4.4	9.1	8.0	37.4	86.0
54k	2–OMe	81.9	19.8	27.7	250.0	39.6	78.1
54l	3–OMe	87.6	36.3	46.7	360.3	26.5	48.0
54m	4–OMe	81.9	5.5	9.3	223.0	86.3	9.7
54n	2–NO_2	81.2	42.4	39.2	9.8	6.9	61.6
54o	3–NO_2	93.8	28.6	41.7	2.2	8.2	66.5
54p	4–NO_2	60.8	23.9	64.2	11.2	6.2	46.1
54q	2–NH_2	9.4	4.1	9.0	19.1	27.4	86.4
54r	3–NH_2	404.9	51.1	65.0	15.2	7.7	91.7
54s	4–NH_2	173.5	78.8	69.3	14.3	8.2	66.5
AAZ (26)	–	250	12.5	2.5	25.8	5.7	41
SLC–0111 (33)		5080	960.0	8550	45.0	4.5	ND

[a]Errors in the range of ±10% of the reported value, from 3 different assays.

Table 2.4: *K_i values against hCA I, hCA II, hCA VII, hCA IX, hCA XII and hCA XIV isoforms showed by new benzenesulfonamides 53a–s and reference compounds AAZ and SLC-0111.*

benzenesulfonamides. The cytosolic CA II is strongly inhibited by all the tested compounds, with K_i values ranging from 0.41 to 78.8 *nM*. Toward CA II, the two most active derivatives were 54c (K_i value of 0.41 *nM*) and 54i (K_i value of 0.6 *nM*) bearing fluorine or bromine in the *meta* position of the benzoyl ring. Regarding the brain–expressed CA VII, all compounds displayed a remarkable inhibitory activity for this isoform with K_i value ranging from 6.8 to 70.7 *nM*. Undoubtedly, worth mentioning is the advantageous selectivity profile of some compounds revealed by a careful interpretation of the collected data. For example, compound 54e (R=2–Cl) showed a good affinity (K_i value of 2.9 *nM*) and selectivity toward the brain–expressed CA VII isoform, resulting more then 20–fold more potent against the brain isoenzyme if compared with the prototype 54a (K_i value of 70.3 *nM*). The crystal structure for compound 54e in complex with the brain isoform CA VII was recently solved (not yet deposited in the RCSB Protein Data Bank). Figure 2.8 shows the binding pose of 4–[4–(2–chlorobenzoyl)piperazine–1–carbonyl]benzenesulfonamide 54e superimposed with the binding mode of the parent compound 54a assumed within the catalytic cavity of CA II.

With regard to the data collected by the biochemical screening against two tumor–associated isoforms CA IX and CA XII, the data suggested the ability of all the tested compounds to affect the inhibitory activity with Ki values spanning from the low-nanomolar to the medium-nanomolar range (3.1–360 *nM*). By incorporating a methoxy group on the benzoyl tail, obtaining so compound 54k–5m, a decreased affinity against CA IX was measured with respect to unsubstitued compound 50a. The same effect was observed also for the
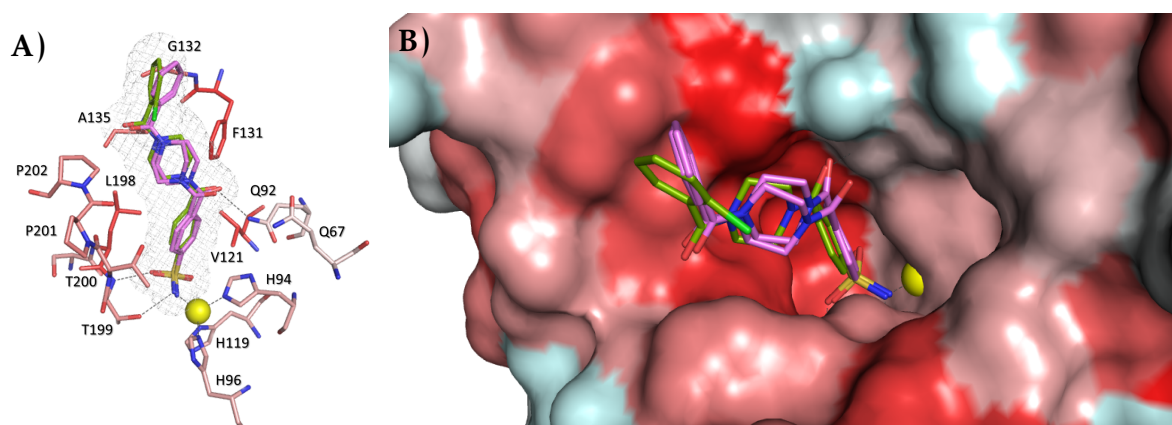
Figure 2.8: *A) Binding pose of 4–[4–(2–Chlorobenzoyl)piperazine–1–carbonyl]benzenesulfonamide 54e (green stick) assumed into hCA VII superimposed with the binding mode assumed by 54a into hCA II. Amino acid residues from hCA VII active site involved in hydrophobic interactions and hydrophilic bonds (grey dashes) are represented in stick. Zinc ion is shown as yellow sphere. B) Representation of hCA VII surface colored according to hydrophobicity, showed the alignement of 54a and 54e located in the catalytic pocket.*

4–fluorine substituted 54d. The three nitro–substituted compounds 54n–5p and the two amino derivatives 54r (R=3–NH$_2$) and 54s (R=4–NH$_2$) display the best selectivity toward the tumor–expressed CA IX and CA XII.Specifically, the introduction of 3–nitro substituent on phenyl ring significantly improved CA IX affinity, so that the inhibitor 54o (K_i = 2.2 *nM*) was more active than the promising anti–tumour agent SLC–0111 (K_i value of 45.0 *nM*). Interestingly, the 2–fluorosubstituted derivative 54b was very active inhibitor of CA XII isoform (K_i value of 3.1 *nM*) displaying an inhibitory activity similar to that of SLC–0111 (K_i = 4.5 *nM*). Furthermore, compound 54b demonstrated also an enhanced selectivity over the off-target isoforms CA I and CA II with respect to amine parent compounds 54a–b.

In order to decipher the chemical requirements which have determined the improvement in CA XII affinity, molecular docking analysis for compounds 54b and SLC–0111 have been performed. In detail, the crystal structure of hCA XII in complex with the inhibitor AAZ was retrieved from the RCBS Protein Data Bank (PDB code: 1JD0) and used for docking simulation carried out by Gold Suite 5.7.1. It should be note that today the number of crystallographic complexes of CAIs bound to the tumors–associated isoenzymes CA IX and XII is really limited, due to the technical difficulties in expression and purification of these membrane–bound proteins. Figure 2.9 displays the plausible binding mode for compounds SLC–0111 and 54b.

The docking results suggested that some similarities are present between the binding mode
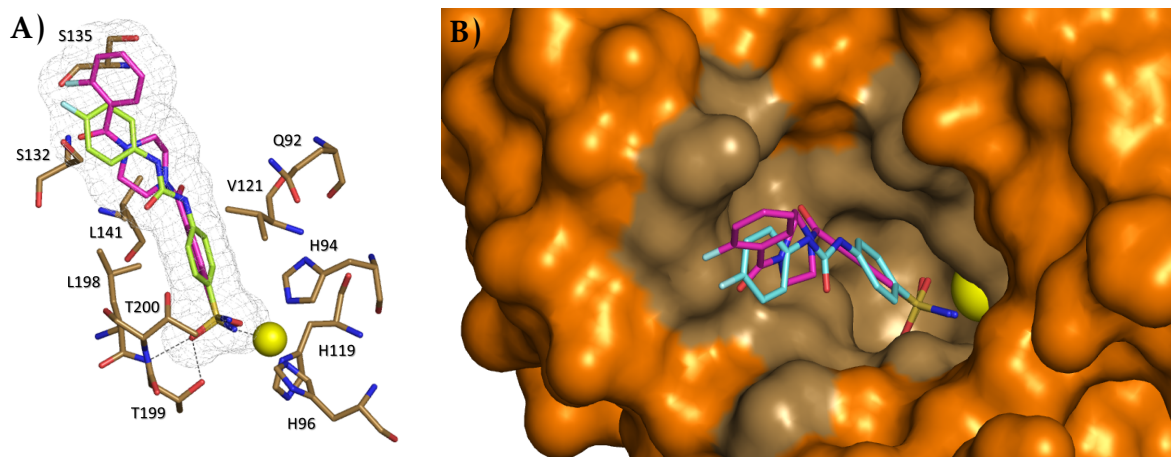
Figure 2.9: *Panel A) Superposition of the suggested binding modes of compounds SLC–0111 (lime stick) and 54b (magenta stick) docked into the hCA XII structure (PDB code: 1JD0). The key residues of the pocket are presented, and the hydrogen-bond interactions are showed by grey dotted lines. Panel B) Representation of hCA XII orange surface showing the inhibitor 54b located in the enzyme active site. The Zn^{2+} ion within the catalytic cavity is represented as a yellow sphere. The amino acids constituting the catalytic pocket are colored in sand.*

of SLC–0111 (colored in magenta) and compound 54b (colored in limegreen) within hCA XII catalytic cleft. Indeed, in both cases, the benzenesulfonamide moiety engages canonical H–bond contacts with T199 and T200 residues and establishes hydrophobic interaction with V121, L141 and L198 residues of the active site, whereas the fluoro–substituted tail is oriented toward amino acids S132 and S135. These two residues are located in the so called "*selective pocket*" near the entrance of the active site cavity and they are a unique structural characteristic of CA XII, since they are not conserved cross the other isoforms.

2.2.6   Different heteroaromatic systems in place of benzoyl ring of compound 54

Our previous studies evidenced that a suitable substituent on aromatic tail of lead compound 4–(4–benzoylpiperazin–1–carbonyl)benzene–1–sulfonamides (54a) endowed to an improvement of affinity for brain expressed CA VII or the tumor–associated CA IX and XII. Furthermore, the visual inspection of X–ray complexes furnished useful information for a new drug design, thus prompting us to continue exploring this class of benzenesulfonamides with the aim to improve the knowledge in terms of SARs and to identify novel CA inhibitors. In particular, starting from the prototype 54a it was carried out the isosteric substitution of the benzene ring with different hetero–aromatic systems, including naphthalene, thiophene, furan, pyrrole and indole.

In the Scheme 2.3 it was reported the synthetic pathway to afford the 4–(4–heteroaroylpiperazine–1–carbonyl)benzene–1–sulfonamides (57a–m). Specifically, the choice of the substituents on aromatic ring was driven by the commercial availability of the different aryl chlorides and aryl carboxylic acids. The procedure is similar to that previously reported for derivatives 54a–s, but in this case the both two reaction steps were promoted by microwave irradiation. In Table 2.5 have been summarized the results of a preliminary biochemical screening collected for compounds 56a–c, 56h–i and 55k, whereas for other synthesized compounds 56d–g, 56j and 56m the biochemical screening is still in progress.

Notably, these preliminary findings showed that the tested 4–(4–heteroaroylpiperazine–1–carbonyl)benzene–1–sulfonamides 57a–m are more potent inhibitors of CA VII when compared to the parent compound 54a. However, they generally showed poor affinity against the both tumor–associated CA IX and CAXII suggesting that the introduction of different aromatic systems in place of benzene ring is detrimental for these isoforms.

Concerning CA VII, the best outcome was obtained for compound 57h moiety that resulted 17–fold up more active than the starting compound 54a with a K_i values of 4.3 *nM*. In addition, it showed a significant selectivity ratio (CA I/CA VII ratios of 106 and CA II/CA VII of 8) comparable with those of the classical anticonvulsant TPM (33). Molecular docking was used to analyze the mode of binding of 57h within CA VII active site, with the aim to gain
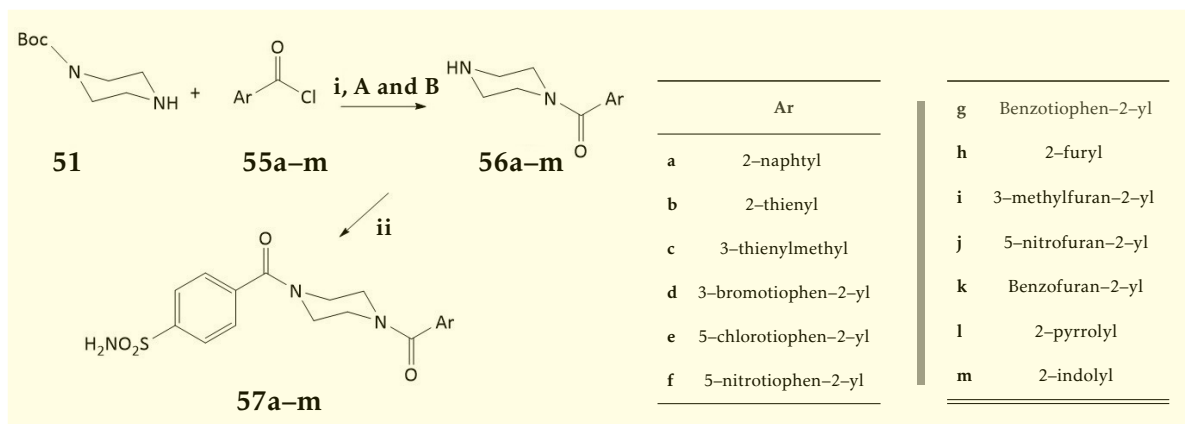
Scheme 2.3: *Reagents and conditions: i, A) RCOCl, DIPEA, DCM/DMF (2:1, v/v), MW, 25°C, 10 min; then, TFA, 0°C to rt, 4 hs; B) RCO$_2$H, HBTU, DIPEA, DCM/DMF (2:1, v/v), MW, 25°C, 25 min; then, TFA, 0°C to rt, 4 hs; ii) DMF, HBTU, 4-Sulfamoylbenzoic acid, DIPEA, MW, 25°C, 25 min.*

	K$_i$ (nM)[a]				
	hCA I	hCA II	hCA VII	hCA IX	hCA XII
57a	66.2	3.4	8.3	2989	91.8
57b	425.8	38.0	21.5	3279	644.3
57c	8.1	14.2	7.1	2920	481.9
57h	454.8	33.7	4.3	3175	494.6
57i	78.3	20.2	15.5	3045	49.6
57k	51.9	2.8	7.2	2938	240.6
54a	69.1	3.7	70.7	37.1	8.5
TPM (33)	250	10	0.9	58.0	1460

[a]Errors in the range of ±10% of the reported value, from 3 different assays.

Table 2.5: *K$_i$ values against hCA I, hCA II, hCA VII, hCA IX and hCA XII for the benzenesulfon-amides 57a–c, 57h–l and 57k, compared to the reference compounds 54a, AAZ and TPM.*
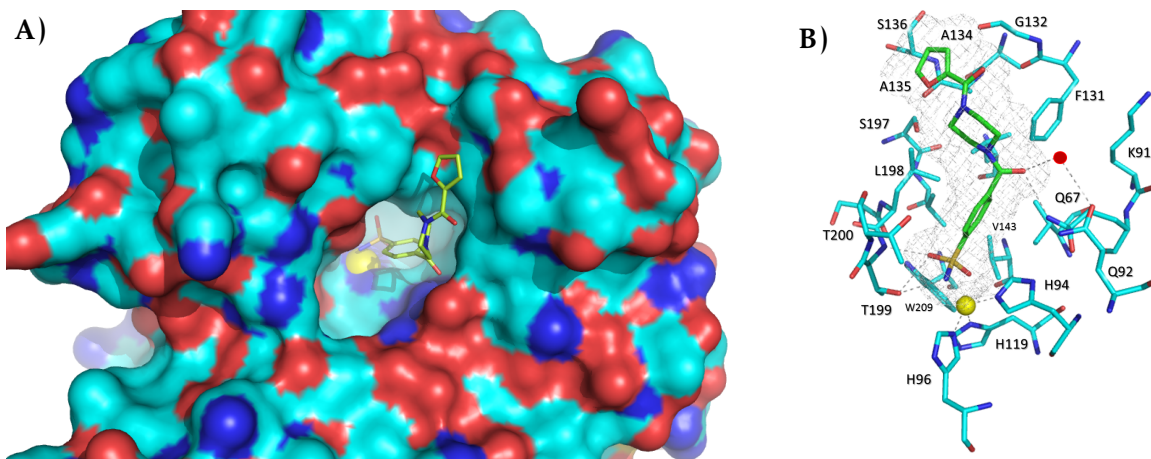
Figure 2.10: *Representation of hCA VII surface colored according to hydrophobicity, showed 4–(4–(Furan–2–carbonyl)piperazine–1–carbonyl)benzenesulfonamide (57h) (limegreen sticks) located in the catalytic pocket. Panel B. Predicted binding pose of 57h into CA VII active site. Residues around 6 Å are showed as cyan sticks. Hydrogen bond interactions are reported as grey dashed lines; zinc ion and water molecule are are depicted as yellow and red sphere respectively.*

insight about the enhanced 17–fold up affinity with respect to the parent compound 54a. The computational analysis reveals that 57h binds via the primary sulfonamide group interacting directly with catalytic zinc ion. In addition, the ZBG is engaged in a network of H–bond with T199 and T200. The carbonyl group of the benzamide portion acts as H–bond acceptor to Q92, whereas it establishes a water–mediated bond Q67. The furyl function targets the so called "*selective pocket*", mainly delineated by hydrophobic residues.

2.3 Breakthrough in CAIs drug design: coumarins as selective CA IX and XII inhibitors

The real breakthrough in the drug design process of isoform-specific CAIs came in the last decade with the discovery of coumarins CAs inhibitory activity. Since then, a large number of substituted coumarin/thiocoumarin derivatives were investigated as CAIs and they showed a high level of isoform selectivity against many enzymes, such as CA VA, VII, IX, XII and XIV. In many cases, a strong inhibitory effect on the tumor–associated isoforms CA IX and XII were observed without significant inhibition of the physiologically dominant CA I/II. The basis for the optimal selectivity profile of coumarins resides in the peculiar mechanism of action which does not involve the coordination of the prosthetic zinc ion. Indeed, they

are hydrolyzed by esterase activity of the enzyme and subsequently bind at the entrance of the active site cavity, acting as pro-drug (for a more detailed discussion on Coumarines mechanism of action see section 1.3). We stress again that this is the most variable region between the various mammalian isoforms and this aspect determines important consequences in the drug design of CAIs, since compound binding in this area could interact differently with the various mammalian isoforms and thus exhibit high isoform–selectivity.

The main factor influencing CA inhibitory activity was the substitution pattern on coumarin core. A preliminary structure–activity relationship investigation highlighted that most effective coumarin-based CAIs are compounds with no substituents or small substituents in the C–3 and C–4 position of coumarin, whereas in the second ring (from C–5 to C–8 position) a large variety of groups could be introduced without loss of CA affinity. Many of the most potent coumarins, in fact, carry substituents on C6–C7 positions. Among which, the natural compound Umbelliferon and its substituted analogues, were shown to be endowed with a good selectivity/affinity toward the tumor–expressed isoforms CA IX and XII, with some representative compounds demonstrating also cytotoxicity in different cancer cell lines.

2.3.1 Our focus on non-classical CAIs targeting tumors–associated CA IX and XII: discovery of umbelliferone–based compounds

With the purpose to expand the chemical space of known coumarin–based CAIs and to improve the knowledge in terms of SARs, we focused our interest on the development of novel umbelliferon–based potentially able to produce anticancer effects through the inhibition of the two tumor–associated isoforms CA IX and XII. We report the synthesis of a novel series of coumarin derivatives designed to study the influence of substituents introduction in the C4 and C6–C8 positions (R1–R4 respectively, see Figure 2.12) on coumarin scaffold.

To achieve this goal, initially attention has been paid to 7–hydroxycoumarin (commonly named Umbelliferon, 59), 6–hydroxycoumarin and 6,7–dihydroxycoumarin (namely Esculetin, 60) which have been converted in the corresponding esters in order to explore the role of hydroxyl group in the binding affinity. In particular we synthesized the acetate 62a–64a and benzoate 62–64b analogues by the reaction with acetic anhydride (pathway A) or benzoyl chloride (pathway B).
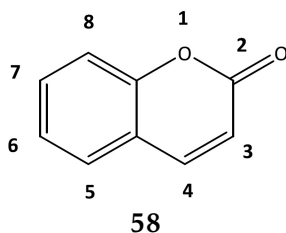
Figure 2.11: *Chemical structure of simple coumarin 58*
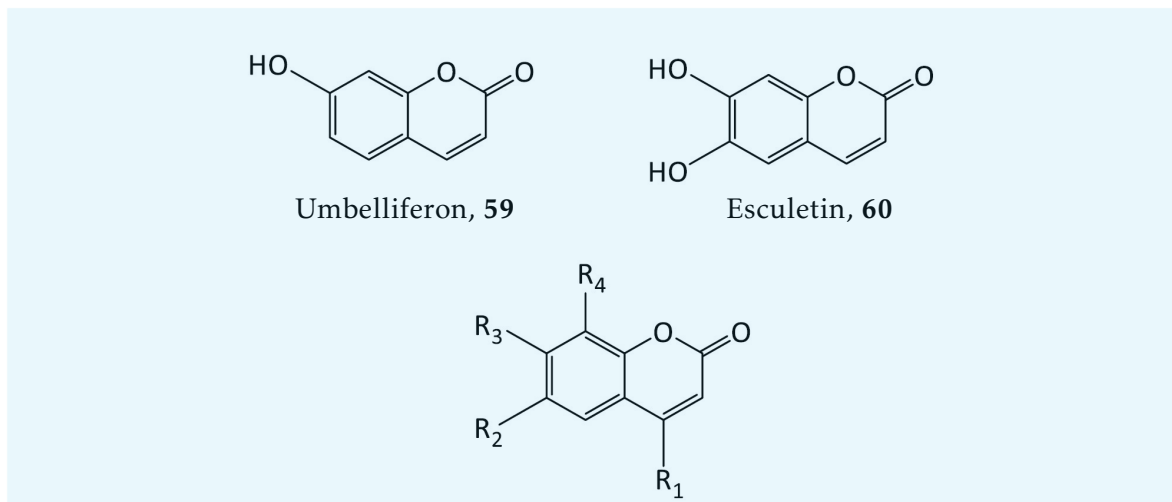
Figure 2.12: *Chemical structures of natural coumarins Umbelliferon (59) and Esculetin (60). A general structure for the new designed compounds is also showed.*

The inhibitory effects of the hydroxyl coumarins and the corresponding esters as acetate (62–64a) and benzoate (62–64b) were evaluated against the target isoforms CA IX and CA XII and the ubiquitous CA I and II. The collected K_i inhibition values are summarized in Table 2.6 in comparison with the promising anti–tumors agent SLC–0111.

The analysis of the obtained results suggested that all the tested compounds showed a good inhibitory activity against CA IX and CA XII with affinity in the range 23.1–116.2 and 9.3–814.4 *nM* respectively; on the contrary, none of these compounds affect the catalytic activity of the off–target isoforms CA I and II up to the 10,000 *nM* concentration. A preliminary analysis of structure-affinity-relationships (SARs) for the esters 62–64a and 52–64b suggested that the presence of acetyl or benzoyl groups, which mask the hydroxyl moieties of the parent compounds 62–64, gave an opposite kinetic behavior against CA IX and XII. Specifically, the

59, R_1=OH, R_2=H   **62a**, R_1=OAc, R_2=H   **62b**, R_1=OBn, R_2=H
60, R_1=R_2=OH   **63a**, R_1=R_2=OAc   **63b**, R_1=R_2=OBn
61, R_1=H, R_2=OH   **64a**, R_1=H, R_2=OAc   **64b**, R_1=H, R_2=OBn
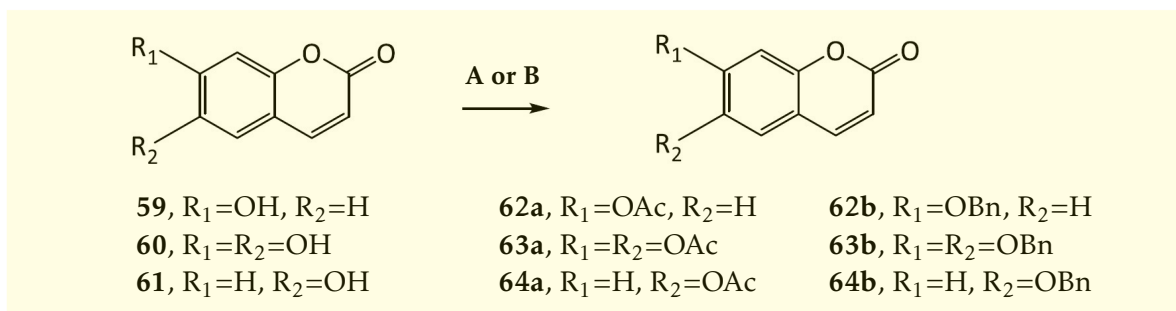
Scheme 2.4: *Reagents and conditions: A) Ac_2O, TEA, H_2SO_4, 0°C to rt; B) BzCl, TEA, DCM, rt.*

	K_i (nM)[a]			
	hCA I	hCA II	hCA IX	hCA XII
62	>10,000	>10,000	24.9	45.1
63	>10,000	>10,000	36.4	9.3
64	>10,000	>10,000	30.5	33.9
62a	>10,000	>10,000	40.2	573.2
63a	>10,000	>10,000	116.2	48.2
64a	>10,000	>10,000	23.1	47.0
62b	>10,000	>10,000	51.4	814.4
63b	>10,000	>10,000	38.4	292.4
64b	>10,000	>10,000	29.9	87.4
SLC–0111	5080	960.0	45.0	4.5

[a] Errors in the range of ±10% of the reported value, from 3 different assays.

Table 2.6: K_i *values against hCA I, hCA II, hCA IX and hCA XII isoforms for the coumarin derivatives 62–64, 62–64a and 62–64b, compared to the candidate anti–tumors agent SLC–0111.*

lack of the 6–, 7– or 6,7– hydroxyl groups lead only to a slight modification of inhibition potency against CA IX, except for the 2–oxo–2H–chromene–6,7–diyl dibenzoate 63b (K_i of 116.2 *nM*) that resulted 3–fold less active with respect to the precursor esculetin 60 (K_i of 36.4 *nM*). Surprisingly, the same substitution pattern has greatly influenced the inhibition affinity toward CA XII especially for umbelliferon and esculetin esters. In fact, moving from umbelliferon (K_i of 45.1 *nM*) to the corresponding acetate 62a (K_i value of 573.2 *nM*) and benzoate 62b (K_i of 814.4 *nM*) it was registered a decrease of affinity value of 12 and 18–fold up respectively. A similar effect has been observed for the esculetin benzoate derivatives 59b. Surprisingly, the masking of 6–hydroxil moiety of coumarin 60 did not have a marked influence on CA XII catalytic activity. Thus, we can speculate that the 7–hydroxyl polar group might play a crucial role in the binding recognition process within CA XII active site.

From this first subseries of coumarin–based CAIs, it was chosen umbelliferon as lead compound for further chemical optimization. In particular, in the second step of our study the

tail approach drug design method was exploited on this class of non-classical CAIs. Therefore, the second and the third subseries of 4–aryl–hydroxy–2H–chromen–2–ones [69a–i] and 4–aryl–hydroxy–8–methyl–2H–chromen–2–ones [70a–i] has been designed by introducing a phenyl moiety in the C–4 position as well as a methyl group into the C–8 position of coumarin ring. Successively, to in depth explore the role of C–8 substituent we synthesized few representative compounds bearing chlorine atom in this position [71a,hi]. To synthesize the designed coumarins 69a–i, 70a–i, 71a, h–i, the classical Peachmann condensation has been employed. Thus, selected commercially available ethyl benzoylacetates [65a–h] reacted with resorcinol 66, 2–methylresorcinol 67 or 2–chlororesorcinol 68 in strong acidic condition to provide the desired products 69a–h, 70a–h, 71a and h. To study the influence of the introduction of a polar group on the phenyl tail, it was performed the nitro–reduction of compounds 69h, 70h and 71h affording the corresponding amine derivatives 69i, 70i and 71i.

The K_i values measured for 4–arylcoumarins 69a–i, 70a–i, 70a and h–i are summarized in Figure 1.7 in comparison with the lead compound Umbelliferon. As you can see in Figure 1.7, all compounds from this library of 4–aryl–7-hydroxy–2H–chromen–2–ones proved to be potent and selective inhibitors toward the tumor–associated CA IX and XII. Among the first subseries of compounds 69a–i, we found that the introduction of an unsubstituted phenyl moiety on C–4 position of lactam ring led to a slight decrease of inhibitory activity toward both the trans-membrane isoforms CA IX and XII if compared with the prototype Umbelliferon. An in–depth analysis of inhibition values collected for compounds 69a–i and 70a–i against CA IX, showed that the introduction of electron–withdrawing as well as donating group on different position of the phenyl ring has not led to significant variations in terms of affinity against this isoform. In fact, the K_i values are included in a very narrow range between 17.0–95.9 nM, so this subseries is generally characterized by a flat SAR. Therefore, we can hypothesize that the 4–arylsubstituent occupies a very large area of CA IX catalytic pocket thus failing to establish profitable contacts with specific amino acid residues in the rim of cavity. Again, concerning the inhibitory effects on CA IX an unexpected result has been obtained through the introduction of chlorine atom in C8 position. Indeed, chemical modification resulted extremely detrimental for the interaction with CA IX.

Significant inhibitory effects toward CA XII were observed for the subseries of the 4–aryl–7–hydroxy–2H–chromen–2–ones 69, within which we can identified several compounds active in the low nanomolar range with K_i values ranging from 6.5 to 8.9 nM. Specifically, the less active compound is the unsubstituted 4–arylcoumain 69a, suggesting that the introduction of substituents is advantageous for the interaction with this isoform. For compounds belonging to the subseries 4–aryl–7–hydroxy–8–methyl–2H–chromen–2–ones of 70 it has been generally observed a decrease of affinity, with exception of derivatives 70e, 70h and 70i that were very potent inhibitors sharing a comparable K_i values with non–methylated analogues 69e and 69h–i. Finally, the introduction of a chlorine atom in C8, affording the small set of 8–chloro–7–hydroxy–4–phenyl–2H–chromen–2–ones 71a and 71h–i, led to divergent results. In order to confirm the role of the 7–hydroxyl group in the binding recognition process
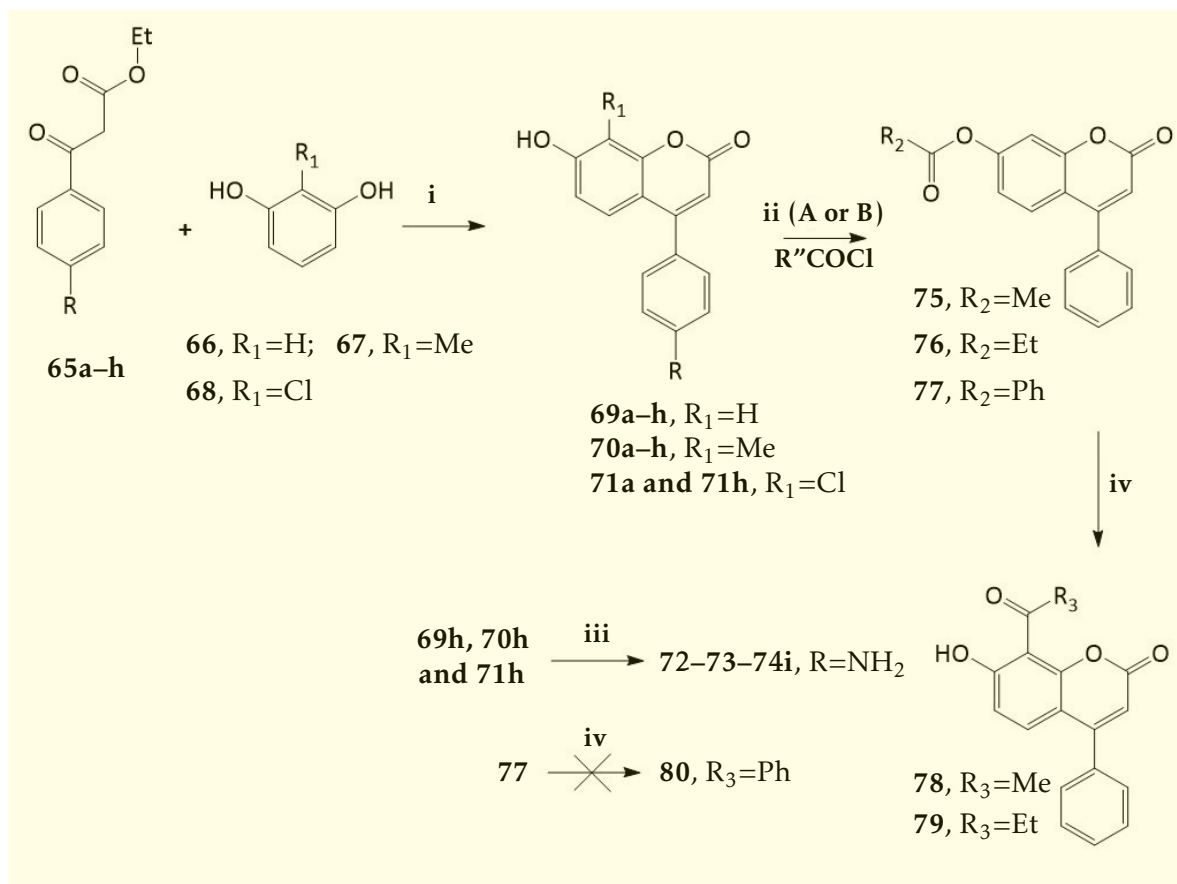
Scheme 2.5: *Reagents and conditions. i) H_2SO_4, 0°C to rt, 18–22 hs; ii) A: $(MeCO)_2O$, H_2SO_4, Et_3N, 0°C to rt, 2 hs; B: BzCOCl or EtCOCl, Et_3N, DCM, rt, 24 hs; iii) $AlCl_3$, 320°C, 6 h; iv) $NH_2NH_2–H_2O$, Pd/C, EtOH, 70°C, 1 h.*

with CA XII also for the 4–arylcoumarin derivatives, we have synthesized the corresponding acetate 75, propanoate 77 and benzoate 77 of 7–hydroxy–4–phenyl–2*H*–chromen–2–one (69a) employing the same reaction conditions above mentioned (Scheme 2.4, ii). The obtained esters 76–77 were further subjected to Fries rearrangement reaction conditions (Scheme 2.5, iii) by employing as Lewis acid $AlCl_3$, thus giving the desired 78 and 79 derivatives bearing 8–acetyl or 8–propionyl substituent, respectively. Unfortunately, we failed in all attempts to obtain 8–benzoyl derivative 80 from corresponding benzoate 77.

In Table 2.8 the results of the biochemical screening for compounds 75–79 are summarized. As observed for esters 62–64a and 62–64b the esterification of the 7–hydroxyl moiety did not affect significantly CA IX inhibitory effects whereas negatively affected those towards CA XII. Moreover, the K_i values measured for compounds 78 and 79 suggested that the introduction

	R	R$_1$	K$_i$ (nM)^a		
			hCA I–II	hCA IX	hCA XII
69a	H	H	>10,000	47.2	90.8
69b	2–Cl	H	>10,000	30.8	7.8
69c	3–Cl	H	>10,000	31.0	7.6
69d	4–Cl	H	>10,000	31.5	8.9
69e	2–F	H	>10,000	31.8	8.0
69f	3–Me	H	>10,000	17.0	7.8
69g	4–Me	H	>10,000	35.8	64.7
69h	4–NO$_2$	H	>10,000	20.3	6.5
69i	4–NH$_2$	H	>10,000	21.6	7.7
70a	H	Me	>10,000	39.5	402.2
70b	2–Cl	Me	>10,000	27.5	31.0
70c	3–Cl	Me	>10,000	36.6	369.2
70d	4–Cl	Me	>10,000	35.3	293.7
70e	2–F	Me	>10,000	95.9	9.0
70f	3–Me	Me	>10,000	37.4	89.1
70g	4–Me	Me	>10,000	38.2	44.9
70h	4–NO$_2$	Me	>10,000	30.9	9.3
70i	4–NH$_2$	Me	>10,000	24.2	5.5
71a	H	Cl	>10,000	261.3	32.0
71h	4–NO$_2$	Cl	>10,000	302.0	648.1
71i	4–NH$_2$	Cl	>10,000	180.3	29.3
Umbelliferon	–	–	>10,000	24.9	45.1

Table 2.7: *K$_i$ values collected for compounds 69a–i, 70a–i and against 71a, 71a–i against hCA I, hCA II, hCA IX and hCA XII. Umbelliferon is reported as reference compound.*

of MeCO– or EtCO– moiety at the C8 position of coumarin scaffold was detrimental for the binding to hCA IX isoform. Concerning CA XII, it was observed an improvement of inhibitory
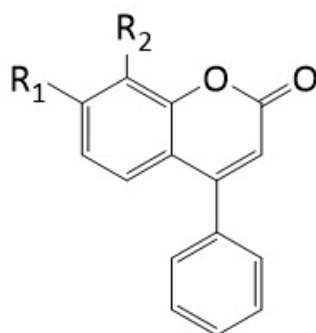
	R$_1$	R$_2$	K$_i$ (nm)[a]			
			hCA I	hCA II	hCA IX	hCA XII
75	OCOMe	H	>10,000	>10,000	56.2	734.1
76	OCOEt	H	>10,000	>10,000	97.8	523.5
77	OCOPh	H	>10,000	>10,000	21.8	384.6
78	OH	COMe	>10,000	>10,000	176.5	24.9
79	OH	COEt	>10,000	>10,000	3042	868.5
67a	OH	H	>10,000	>10,000	47.2	90.8
Umbelliferon[b]	–	–	>10,000	>10,000	24.9	45.1

[a]Errors in the range of ±10% of the reported value, from 3 different assays.

Table 2.8: *Inhibition data for hCA I, II, IX and XII with compounds 75–79 as well as umbelliferon and the prototype 17a.*

activity for 8–acetyl–7–hydroxy–4–phenyl–2H–chromen–2–one 78. However, moving to the homologue 79 we found a considerable decrease of affinity against CA XII when compared to the starting compound 69a (K_i of 868.5 *nM* vs 90.8 *nM*). We can speculate that the presence of a longer carbon chain prevents the access to the active site generating steric hindrance.

2.3.2 Molecular docking studies for the most active coumarines

Docking analysis were carried out in order to gain further insight about the hypothetical interaction mode into CA XII catalytic cleft for this class of 4-arylcoumarins. *In silico* studies were performed by using AutoDock 4.2. software and the crystal structure of CA XII was retrieved from the RCSB Protein Data Bank (PDB code: 1JCZ). Considering the CA esterase activity, it was chosen to analyze the binding pose of the tested coumarins and the corresponding 2–hydroxycinnamic acid derivatives ad *Z*– and *E*–isomers. Figure 2.13 summarizes the hydrolitic ring opening of the lactone mediated by CAs for the most active compound 70i to afford the related hydrolyzed cis–/trans–hydroxycinnamic acid derivatives (70i–*Z* and 70i–*E*).
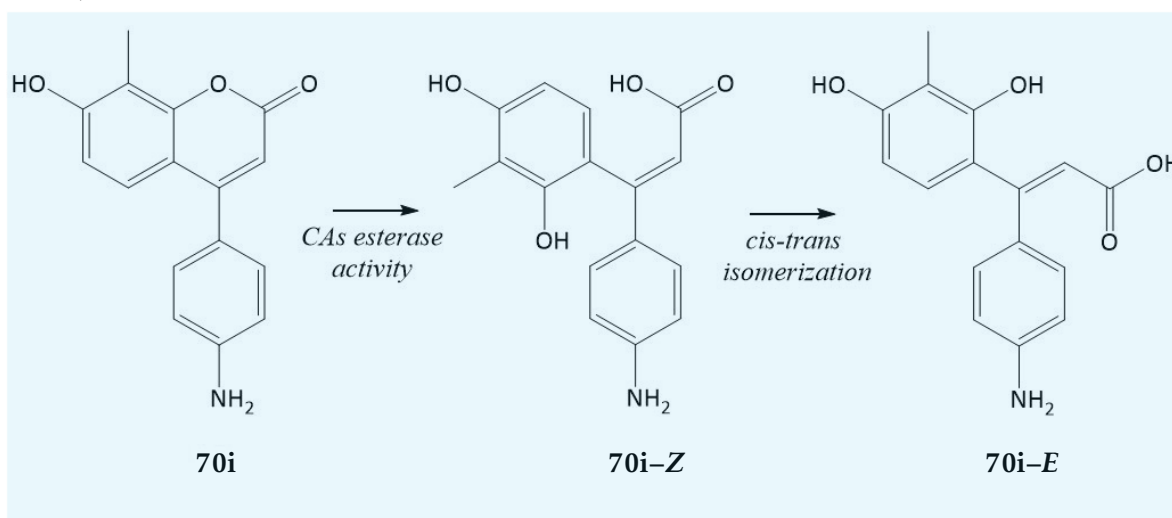
Figure 2.13: *CAs mediated hydrolitic process of coumarin derivative 70i leading to (Z)– or (E)–hydroxycinnamic acid derivatives 70i–Z and 70i–E.*

Docking simulations suggested that all active coumarins shared a very similar binding pose. Figure 2.14 showed the superposition of the putative binding mode for three representative compounds 69i, 70i and 78 in the "close" form toward CA XII (K_i values of 5.5, 29.3, 24.9 *nM* respectively). As an example, we discuss the result obtained for the most active compound of the series that is 4–(4–aminophenyl)–7–hydroxy–8–methyl–chromen–2–one (70i).
As above mentioned, initially it was predicted the binding mode of coumarin 70i in the lactone form. It is clear the ability of this compound to deeply occupy the middle area of CA XII catalytic cavity, interacting closely with hydrophilic residues from the active site. In particular, the benzopyrone system establishes a dense hydrogen bond network with N62, H94 and T199. The 4–phenyl ring is projected toward hydrophobic wall in the middle area of the pocket, lined by V121 and 141, L142, V143 and L198. In addition, the 4–amino functional moiety engages H–bond donor interaction with the crucial residue S135 in the rim cavity.
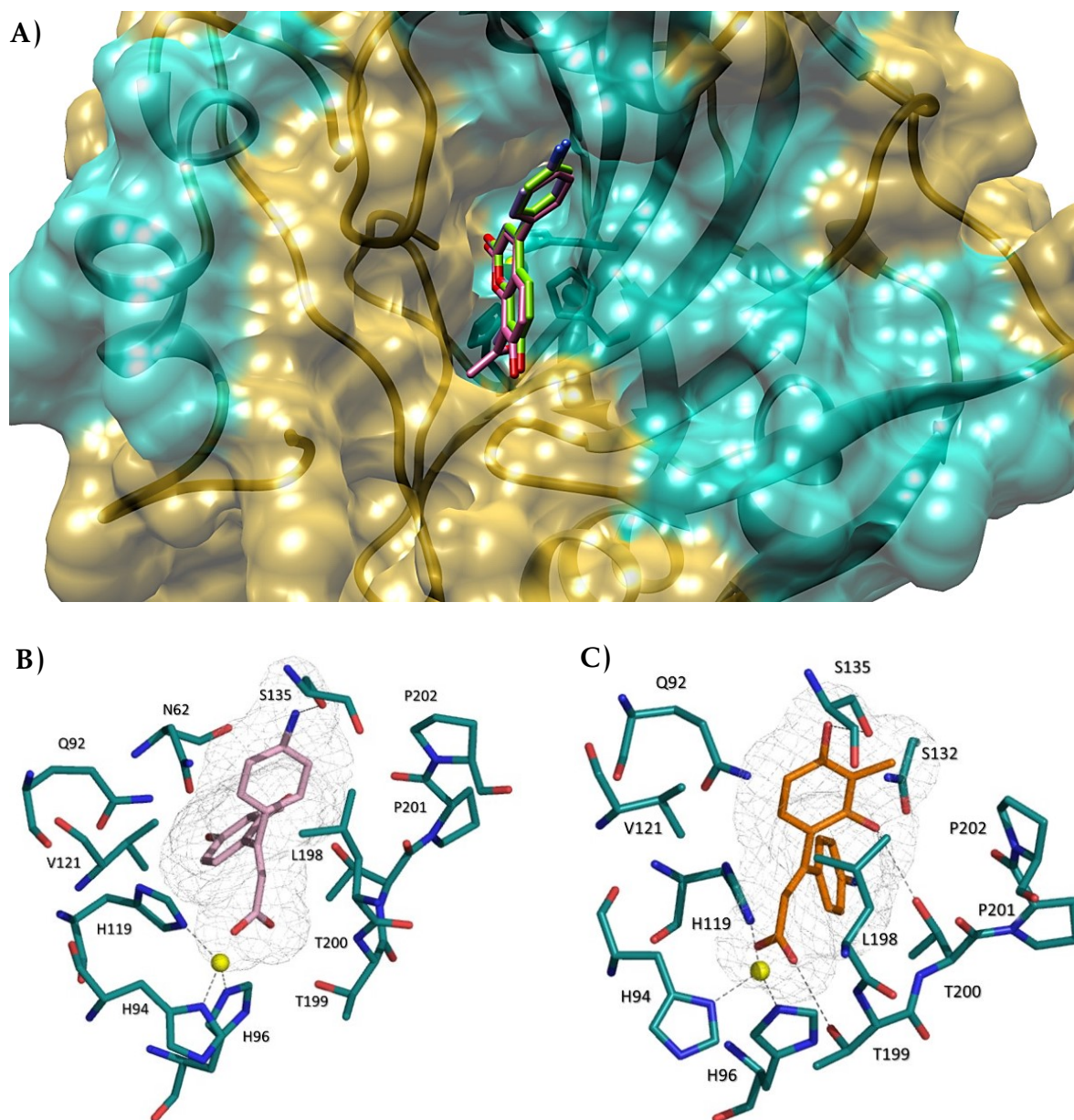
Figure 2.14: *Panel A) Superposition of predictive binding mode for compounds 69i, 70i and 77 within CA XII active site. Panel B and C) Representation of the CA XII binding pocket in complex with 70i–Z (light pink) and 70i–E (orange), showing residues involved in the recognition process of the inhibitors. Polar interactions are evidenced as grey dashes.*

It is worth to note that the studied coumarin 70i oriented the lactone ring toward the Zn ion, creating a favorable scenario for the hydrolytic process. Considering this hypothetical binding mode, we can hypothesize that these selective inhibitors might be not capable to access to the CA I and CA II active site, since these isoforms are characterized by the presence of bulkier residues as gatekeeper of the enzymatic cleft if compared with CA IX and XII. Specifically, L131 or F131 act as "*steric–blocker*" in CA I and CA II respectively. In the membrane-bound CA IX and XII this residue corresponds to V131 and A131 ones, both amino acids characterized by the presence of small hydrophobic chain which allows a more favorable binding.

A very similar binding mode was observed for (*Z*)–3–(4–aminophenyl)–3–(2,4–dihydroxy–3–methylphenyl)acrylic acid 70i–*Z* with respect to the corresponding coumarin 70i. Indeed, the phenyl ring is orientated in the proximity of the hydrophobic wall in the middle area of cavity, whereas the 4–aminophenyl group maintains the hydrogen bond interaction with S135.

In contrast, the (*E*)–3–(4–aminophenyl)–3–(2,4–dihydroxy–3–methylphenyl)acrylic acid 70i–*E* binds to CA XII active site assuming a different orientation: this isomer turns the 4–aminophenyl substituent toward the catalytic triad (H94, H96 and H119). The resorcinol moiety assumes a peculiar disposition establishing two relevant H–bonds with S135 and T200 which lead the aromatic ring lying on hydrophobic wall. To conclude, the carboxylic moiety establishes a strong bidentate interaction with the amino acid residues H119 and T199.

2.4 Carbonic anhydrases as a drug target for the development of novel antibacterial agents

The antimicrobial resistance (AMR) is one of the most complex global health challenge due to the increasing incidence of infectious diseases that are untreatable with known antimicrobial agents. This issue has raised enormous scientific interest towards the identification of novel molecular targets controlling the life cycle of several pathogens. In the last years the DNA sequencing method applied to microbial genome allowed the identification of numerous genes encoding for enzymes involved in the bacterial central metabolism as bacterial CAs. A key physiological reaction for the microbial survival is the CO_2 hydration/dehydration essential reaction for their biosynthetic processes and energy metabolism. Herein, the discussion will be focused on the role of CAs in the survival/virulence of microorganisms and therefore in their potential as drug targets.

2.4.1 Bacterial CAs: distribution, kinetic properties and physio–pathological roles

Across the eight genetically distinct families of CAs, bacterial genome encodes for α–, β- and γ–CAs. The distribution pattern of CAs is peculiar for each bacterium: some organisms frequently express only one family, whereas others encode for two or three different classes of CAs. Specifically, α-CAs have been detected only in the genome of gram negative bacteria, where they seems to play a key function for bacterial growth and survival. Instead, β– and γ–CAs are the most widespread classes in all bacterial species. Figure 2.15 displays the transport of CO_2 and HCO_3^- by bacterial CAs: it has been supposed that in gram negative bacteria the α–CA is able to convert the metabolic CO_2 or atmospheric diffused into the periplasmic space; the β– and γ–CAs are cytosolic classes and are responsible for CO_2 replenishment for carboxylase enzymes, pH homeostasis and other intra–cellular functions, ensuring survival and the metabolic needs of the microorganism [105].
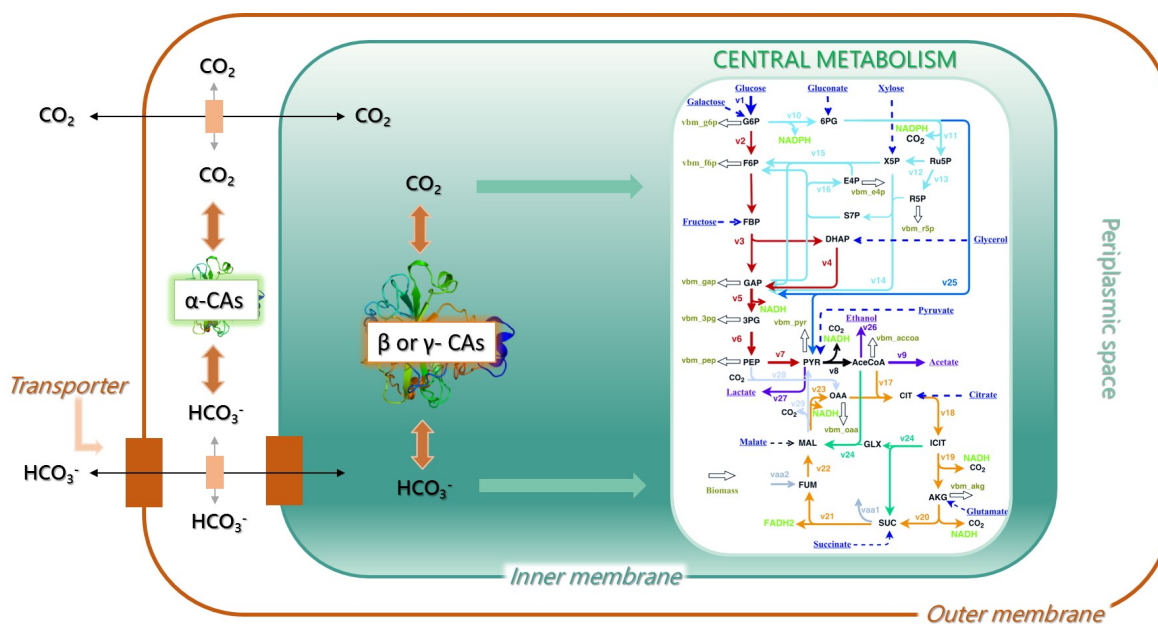
Figure 2.15: *The CAs role in Gram-negative bacteria. The α-CAs have a periplasmic localization and can convert the diffused CO_2 inside the periplasmic space into HCO_3^-. The feeding of CO_2 and HCO_3^- to the central microbial metabolism depends on the action of the cytosolic β– and γ–CAs.*

In vivo experiments demonstrated that pathogenic and nonpathogenic gram negative bacteria require functional CAs not only for their survival, but also for manifesting their virulence in host organism. In this scenario, have emerged the pathogenic microorganisms *Helicobacter pylori* [106, 107], *Vibrio cholerae*, *Brucella suis*, *Mycobacterium tuberculosis*, *Neisseria gonorrhoeae*

and *sicca*, and the nonpathogenic bacterium *Escherichia Coli* and *Ralstonia eutropha* [108, 109]. The role of CAs in bacterial growth and virulence is well explained by the two striking examples as follow. The pathogen *H. Pylori* requires functional α– and β–CAs for its acid acclimation within the human stomach. The inhibition of these two CAs classes led to the pathogen death and a plausible eradication of *H. Pylori* by its environment and therefore has found clinical use for the treatment of gastric ulcers. *Vibrio Cholerae* uses all the three classes of CAs (VchCA α, β and γ) to produce bicarbonate that induces its virulence. On this basis, it is immediately apparent that prokaryotic CAs may be identified as excellent drug targets for obtaining novel antibacterial agents characterized by a singular mechanism of action, although many of them were not yet validated *in vivo* as drug targets.

2.4.2   CAs inhibition to fight cholera disease

Cholera is an acute diarrheal infection caused by the pathogenic gram-negative bacterium *Vibrio Cholerae*, causing characteristic rice–water stool, dehydration, hypovolemic shock, acidosis, and if not well–treated leads to death. The treatment of cholera infection actually consists on the re–hydration using saline–glucose solutions that can be combined with antibiotics, in order to stabilize highly dehydrated patients and reduce the duration of illness. Tetracycline and quinolones have been widely used, but numerous multidrug–resistance phenomena have been observed. On this basis, the development of new drugs with different mechanisms of action become an important approach to fight a global public health problem. There is evidence that protein ToxT is one of the transcription factors activating the *V. Cholerae* virulence gene expression; therefore, ToxT represents a target for the development of cholera therapeutics. ToxT activity is (i) negatively controlled by the unsaturated fatty acids (UFAs) of the bile and (ii) enhanced by the presence of bicarbonate in the upper small intestine where *V. Cholerae* preferentially colonizes. Therefore, bicarbonate is likely an important chemical stimulus during the cholera infection. Figure 2.16 shows the virulence cycle of *V. Cholerae*. Due to the lack of specific transporter proteins, *V. Cholerae* increases cytosolic HCO_3^- levels through the hydration of CO_2 by the action of CAs.

As above mentioned, *V. Cholerae* genome encodes for VchCAα, β and γ classes. VchCAα has been cloned, purified and characterized. The sequence analysis suggested that VchCAα retains all the common features from enzyme belonging to α class, such as the amino acid residues of the catalytic triad, the proton shuttle and the gate–keeping residues. The only singular macrofeature in the primary structure of the bacterial α–CA is the deletion of three amino acid loops, a feature shared by all the bacterial α–CA investigated so far. The absence of these loops makes the bacterial proteins more compact and smaller [110]. To date no crystal structures have been reported so far for VchCAα and only recently a homology model was constructed by identifying the α–CA from *Photobacterium profundum* as template [111]. The VchCAβ X–crystal structure has been recently solved; it has been showed that the biologically active molecule is a homotetramer with the active site located at the interface
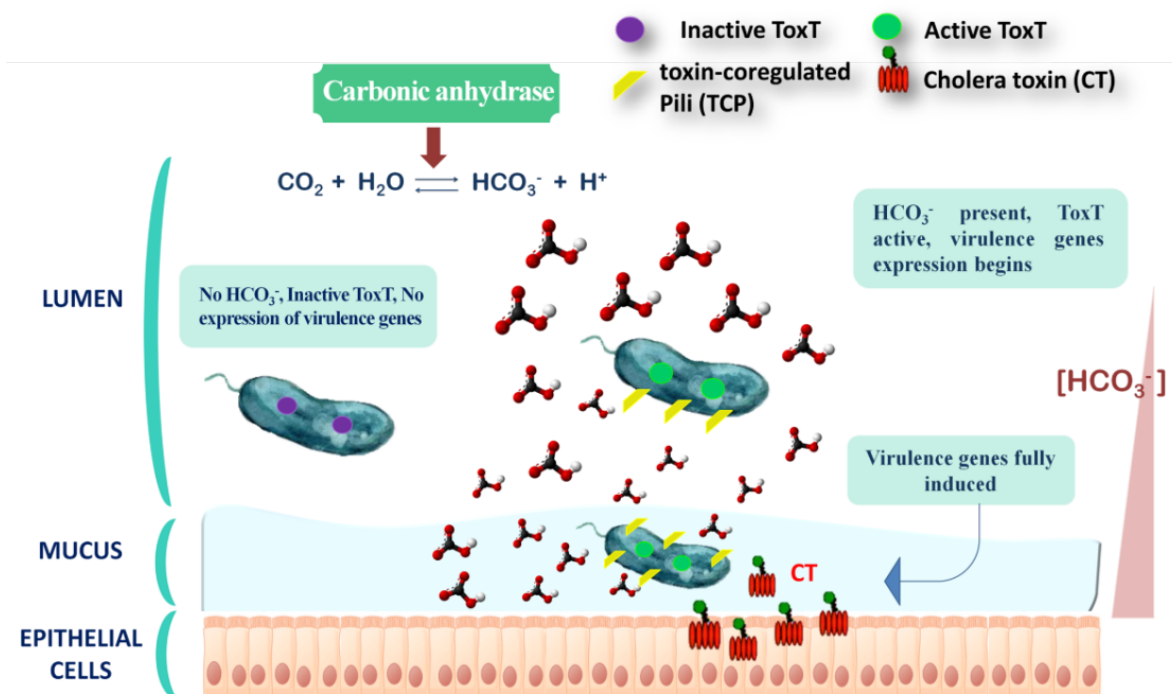
Figure 2.16: *Model for induction of virulence gene expression by bicarbonate in vivo. On the left, motile Vibrio Cholerae containing inactive ToxT protein enters the upper small intestine. In the center, Vibrio Cholerae in the intestinal lumen encounters bicarbonate, ToxT becomes active, and TCP production begins. Bacteria across the mucus layer, encountering higher levels of bicarbonate. Virulence genes are fully induced and Cholera toxin production begins. The gradient of increasing bicarbonate levels from the lumen to the mucosal surface is indicated by the triangle on the right.*

of one dimer[112]. The active site displays the zinc (II) coordinated by C42, D44, H98 and C101, with an approximate tetrahedral geometry (Figure 2.17). Therefore, VchCAβ belongs to the type II subclass of β–CAs that are characterized by the presence of four protein-derived ligands which coordinate zinc, in contrast with the type I subclass in which the fourth zinc–coordination sphere is occupied by a water molecule/hydroxide ion. It is worth to stress that also the β–CAs class employs a Zn–hydroxide mediated two steps mechanism like α–CAs.

In the type I subclass the residue D44 is employed in the formation an aspartate–arginine dyad, whereas in type II this dyad is broken making D44 free to coordinate the zinc metal ion and R46 is oriented away. It has been hypothesized that this *"closed"* conformation corresponds to an allosteric form of the enzyme that is called *"T–state"*: this is an inactive form present at pH values below 8. In fact, an elegant work demonstrated that at pH values
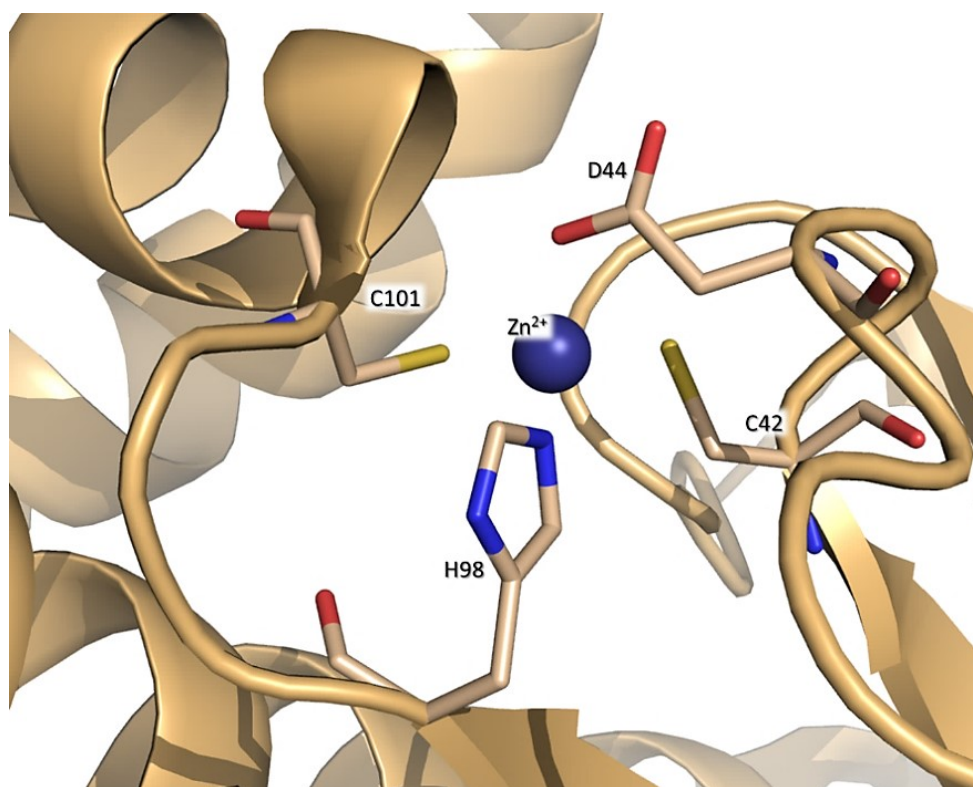
Figure 2.17: *Structural representation of active site of VchCAβ (PDB code: 5CXK) exhibiting a 'closed' conformation*

> 8, the carboxylic moiety of D44 and the guanidine group of R46 form a strong salt–like interaction, thus making free the fourth coordination position on the Zinc (II), in turn this allows the binding of an incoming water molecule. This latter species is further activated by the proton shuttle residue Y83, thus generating the nucleophile enzyme active species.

Interestingly, in VchCAβ, as well as in β–CAs from *H. Influenzae* and *E. Coli*, it has been identified an allosteric bicarbonate binding site at a distance of 8 Å from the zinc located between the residues W39, R64, Y181 and V47. Each residue forms a hydrogen bond with HCO_3^-, with the exception of the carbonyl moiety of V47 which acts as hydrogen bond acceptor. As result, the bicarbonate bound to this allosteric site enforces the "*T–state*" conformation: the bicarbonate expels the side chain of V47, causing a reorganization of the 44-48 loop and a consequent break of aspartate–arginine dyad (D44-R46), allowing the carboxylic group of D44 to displace the zinc–bound water molecule. Unfortunately, the alternative open conformation of VchCAβ has not been determined. Anyway, the kinetic data suggest that these enzymes adopt an "*open*" form in order to work in a cooperative manner.

Recently, VchCAγ has been cloned and purified. It showed an identity of about 25–26% with the γ–CAs prototype isolated by *Methanosarcina thermophile* (CAM), an anaerobic methane–producing species from Archaea domain. However, the γ class lacks of an extended structural characterization due to the limited numbers of available crystal structures. In fact, the only deposited crystal structure of γ–CAs from bacteria is Yrda encoded by *E. Coli* (PDB code: 3TIS), obtained in a "*closed*" conformation like to the "*T–state*" form described for VchCAβ. The following sections describe the drug design strategies employed by us to identify potent and selective inhibitors against α, β and γ classes of the pathogenic species *V. Cholerae*. Specifically, our pilot study began with the biochemical investigation of selected sulfonamides from our database in house. This work led to the identification of some weak VchCA inhibitors. With the aim to expand the chemical diversity of VchCA inhibitors and to improve the knowledge in terms of SARs, two novel series of benzenesulfonamides were developed: the first one was designed through a molecular simplification of already reported compounds, whereas the second one was rationally developed through a computer-aided drug design strategy. Like to previous designed CAIs all compounds were characterized by spectroscopic measurements, investigated by computational studies and biochemically tested.

2.5 Starting point: discovery of promising VchCAs inhibitors from our in house database

VchCAs were recently investigated with a panel of sulfonamides and sulfamates, detecting a large number of nanomolar VchCA inhibitors, including acetazolamide (AAZ, 26), methazo-lamide (27) and ethoxzolamide (EZA, 28), brinzolamide (32), etc. However, they generally displayed low selectivity over human off–target α–class CAs (CA I and II), reducing their potential therapeutic in humans [113]. Among the tested sulfonamides, EZA (28) proved to decrease the HCO_3^-–mediated virulence gene expression impairing the growth of pathogen. Previous studies (Section 2.2.1) allowed the identification of a small set of compounds containing azepine/piperidine/piperazine nucleus linked to benzenesulfonamide fragment able to act as CAI in the low nanomolar range. By considering the high inhibitory effects of this series of potent benzenesulfonamides as human CAIs, we decided to further study their CA inhibitory profile thus exploiting their capability to act as potential anti–infectives. In particular, this set of sixteen sulfonamides 47a–e, 48a, 49a–f and 50a–d were assayed for their inhibitory activity against VchCAα, –β and –γ . The three bacterial enzymes were prepared by the novel protonography techniques established by C. Capasso and co-workers from the National Council Research (NCR) of Naples (Italy) [114]. The VchCA inhibitory data are summarized in Table 2.9 and compared with K_i values for the AAZ (26). For a comparative purpose the inhibitory profiles against the ubiquitous hCA I and hCA II are also reported. All tested compounds generally showed to be high potent inhibitors of the VchCAα class (K_i ranging from 43.3–843.2 *nM*), whereas they are medium potent inhibitors toward VchCAβ,

	K_i (nM)[a]				
	hCA I[b]	hCA II[c]	VchCAα	VchCAβ	VchCAγ
47a	9.2	5.7	843.2	>10,000	>10,000
47b	4.4	0.63	296.4	>10,000	>10,000
47c	187	6.1	528.8	>10,000	>10,000
47d	7.7	0.79	588.9	>10,000	>10,000
47e	75.5	1.5	241.9	3754	>10,000
48a	85.0	3.8	275.4	>10,000	>10,000
49a	1.7	0.5	43.3	3308	>10,000
49b	9.3	0.6	193.8	3714	>10,000
49c	6.6	0.6	45.1	3945	>10,000
49d	6.3	0.7	58.8	2776	>10,000
49e	6.5	0.6	89.9	806.4	>10,000
49f	7.7	0.6	72.1	6612	>10,000
50a	6.8	3.0	470.4	>10,000	>10,000
50b	0.69	0.5	95.7	5008	>10,000
50c	50.1	5.7	275.5	4816	>10,000
50d	91.1	2.0	47.0	4156	>10,000
AAZ (26)	250.0	12.1	6.8	451	473

[a]Mean from three different assays (errors were in the range of ±5–10 % of the reported values).

Table 2.9: *Inhibition of hCA I, hCA II, VchCAα, VchCAβ, and VchCAγ for compounds 47a–e, 48a, 49a–f and 50a–d and acetazolamide (26, AAZ).*

with the exception of compounds 47a–d, 48a and 50a ($K_I s > 10,000 \ nM$). Finally, all the investigated sulfonamides did not affect the CO_2 hydrase activity of the VchCAγ subclass. For the VchCAα, the data collected in Table 2.9 suggested that the unsubstituted 4–(piperidine–1–carbonyl)benzenesulfonamide (47a), the three methyl–substituted analogs 47b, 47c, 47d as well as cyclohomologue compound 48a were less active than corresponding 4–aryl–substituted compounds 49a, 49b, 49c, 49d, 49e and 49f. Compound 49a (VchCAα, K_i value of 43.3 nM) demonstrated the best activity having the phenyl ring linked to 4–position of piperidine nucleus. The introduction of an additional hydroxyl group, nitrile or acetyl functionalities at C-4 position of piperidine nucleus induces a weak decrease of affinity. The presence of 4'-chlorophenyl ring and hydroxyl group at 4–position of piperidine nucleus of compound 49c afforded equi–active inhibitor of unsubstituted 4–phenyl analogue 49a. Among the series of benzenesulfonamides 50a–d containing the piperazine core, the 4–(4–phenylpiperazine–1–carbonyl)benzenesulfonamide (50d) displayed the best inhibitory effect (K_i value of 47.0 nM), thus confirming that the presence of a bulky aromatic group anchored to the 4–position of cycloalkylamine nucleus generally improves the affinity against VchCAα. It is interesting to note the impact of the introduction of a methylene spacer between piperazine core and phenyl moiety: it was found a ten–fold reduction of activity of the compound 4–(4–benzylpiperazine–1–carbonyl)benzenesulfonamide (50a) (K_i value of 470 nM) when compared to the parent compound 50d. This evidence might be due to a different binding within the catalytic cavity. Moreover, the introduction of a fluorine atom in the *para* position of the phenyl ring of benzylpiperazine–sulfonamide 50b (K_i value of 95.7 nM) improves the affinity toward VchCAα. The presence of a benzhydryl moiety (compound 50c, K_i value of 275.5 nM) seems well tolerated to respect the benzyl–fragment (compound 50a).

Concerning the activity against VchCAβ several tested compounds proved to be inhibitors at low micromolar concentration showing inhibition data ranging from 806.4 to 6612 nM value.

Overall, the presence of a 4–aryl moiety resulted advantageous for inhibitory effects toward VchCAβ. The best affinity was found for 4–(4–cyano–4–phenyl–piperidine–1–carbonyl)benzenesulfonamide compound 49e (K_i value of 806.4 nM). The presence of other small substituents, such as acetyl for compound 49f or hydroxyl group for compounds 49b, 49c and 49d did not significantly influence the inhibitory effects toward VchCAβ. Moreover, the replacement of piperidine nucleus with piperazine one resulted in divergent effects: (a) it was found a completely loss of inhibitory activity for unsubstituted compound 50a; whereas compounds 50b, 50c, and 50d shared similar potency as moderate inhibitors of VchCAβ class. On the contrary, all studied compounds were totally ineffective inhibitors against VchCAγ class. We can speculate that the incapability to inhibit γ–CAs may be related to smaller size of the catalytic pocket of enzymes belonging to γ–class if compared with α and β–CAs.

Despite these compounds showed high affinity against VchCAα to respect β– and γ–classes, they proved to be active inhibitors of ubiquitous expressed hCAI and hCA II at low nanomolar concentration, thus impairing their potential employment as therapeutics in humans.

2.5.1 Construction of a hypothetical "open active site" form of VchCAβ as first *in silico* model

The structure–based drugs design is hampered by the lack of available crystal structures for α and γ–CAs from *Vibrio Cholerare*. Despite the wealth of structural information reported for VchCAβ class, to date it is not yet available a structure of its alternative "*open*" conformation. However, other β–CAs crystal structures from different species have been obtained in the active conformations and among them it was found a high level of sequence homology.
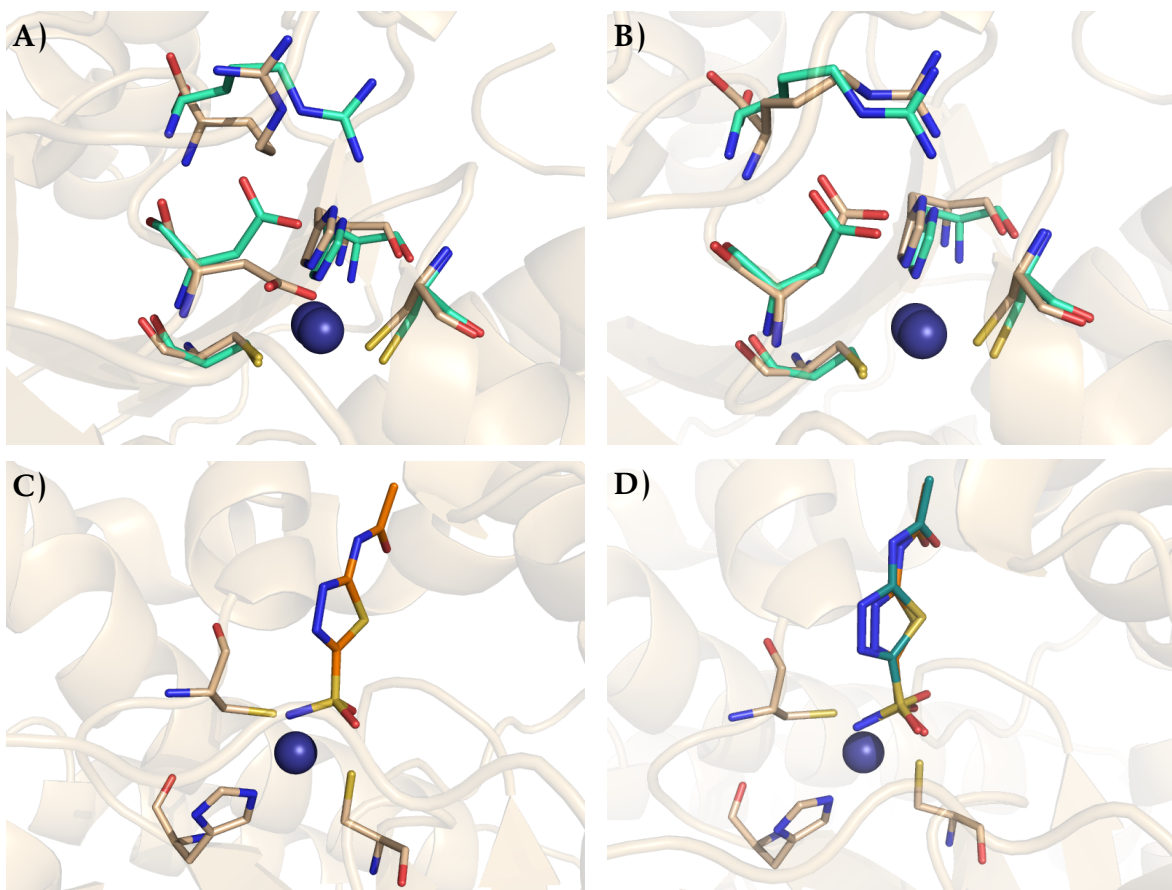
Figure 2.18: *A) Superposition of active site residues from the recombinant VhCAβ (PDB code: 5CXK, wheat sticks) with those of β–CA from Co–CA (PDB code: 3UCJ, palecyan sticks). Zinc is represented as blue sphere. B) Redesign of D44 and R46 side chains orientation using D49 and R51 from Co–CA as template. C) Inserting of the X–ray conformation of AAZ retrieved by Co–CA into VhCAβ active site (orange stick). D) Alignment of the X–ray conformation of AAZ (orange stick) with the hypothetical binding pose suggested by docking studies within VhCAβ active site.*

By using the β–CA encoded by the green alga Coccomyxa (*Co*–CA) as template (PDB code: 3UCJ), we obtained a modelled structure of the accessible active site of VchCAβ (Figure 2.18). In the first step of our theoretical study, we performed a simulation for the opening of the catalytic site of β–CA from *V. Cholerae*. In more details, a superimposition of the 3D X–ray structure of VchCAβ in its "*closed*" form (PDB code: 5CXK) to the "*open*" state of *Co*–CA in complex with inhibitor AAZ (26) was performed. Based on the conformation of side chains of the crucial residues D49 and R51 of β–CA from *Coccomyxa* (Figure 2.18, palecyan sticks), the orientation of the corresponding side-chains of D44 and R46 (wheat sticks) was modified in order to make free the fourth zinc coordination sphere. By assuming that the inhibitor AAZ (26) displays a similar binding mode in these two β–CAs, AAZ X–ray conformation from *Co*CA was positioned in the catalytic site of VchCAβ. Then, the side–chains of residues
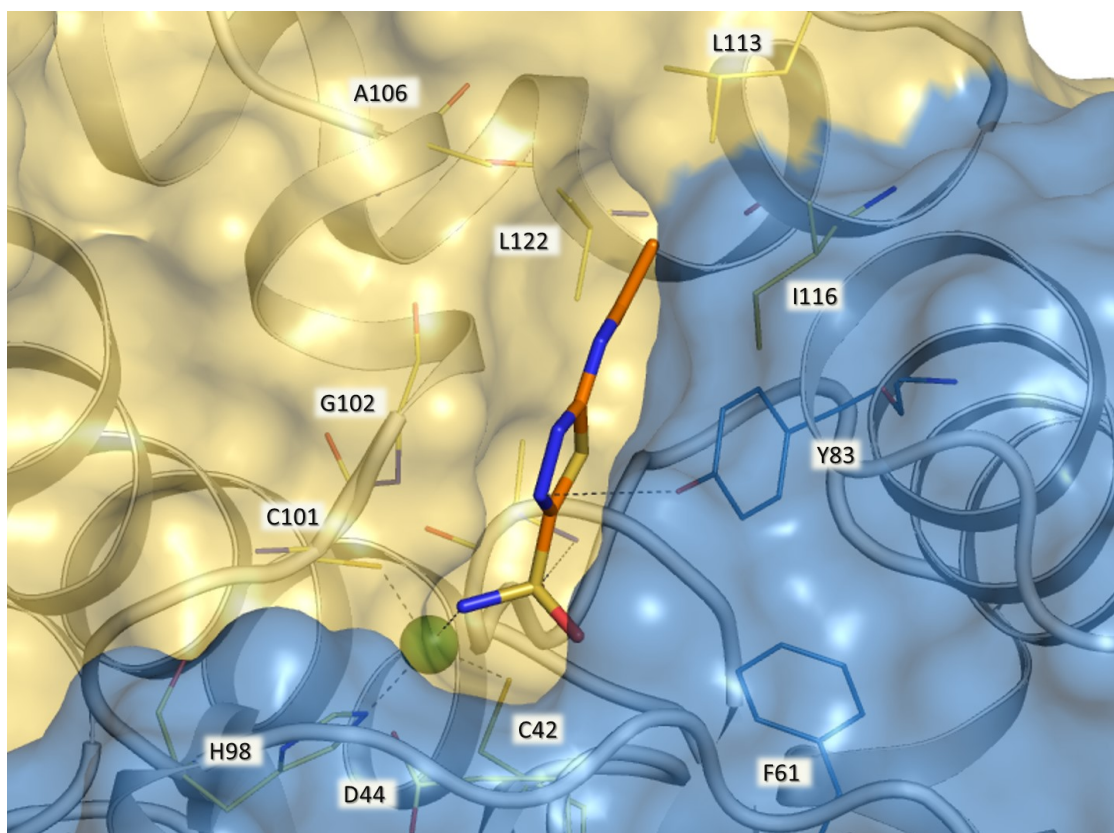
Figure 2.19: *Docking poses into our "modelled" VchCAβ catalytic cavity for acetazolamide (AAZ, 26). The VchCAβ backbone is showed as surface: chain A is colored in gold, chain B in sky blue. Residue involved in hydrophobic and hydrophilic interactions are highlighted as lines. Zinc ion is depicted as yellow sphere. Dark grey dashed lines represent hydrogen bond interaction.*

close to the inhibitor AAZ have been minimized. In the last step of our study, AAZ was discarded from the theoretical complex with VchCAβ. The obtained protein was used to perform docking studies on AAZ, in order to assess the ability of our protocol to restore a similar binding pose. We found that the binding pose suggested by docking studies is perfectly superimposable with the native conformation of AAZ, confirming the robustness of our model (Figure 2.18). As result, we obtained a hypothetical structure of "*open active site*" from VchCAβ as the "*first in silico model*" useful for mapping the inhibitor binding interactions and to perform a structure–based drug design of potential anticholera agents.

As expected, the sulfonamide moiety anchors the catalytic zinc ion; additionally, the nitrogen of the N-acetamido group forms a H–bond to the oxygen atom of G102, the thiadiazole ring establishes π/π interaction with Y83 which is reinforced by further hydrogen bond contacts between heterocyclic nitrogen atoms and hydroxyphenyl substituent. This network of interactions might explain the affinity for VchCAβ at submicromolar concentration (K_i value of 451 *nM*, Table 2.9), thus supporting the reliability of our modelled VchCAβ. Then we investigated the docking poses into our "*modelled*" VchCAβ catalytic cavity for all 4–(cycloalkyl–1–carbonyl)benzensulfonamide derivatives (47a–e, 48a, 49a–f and 50a–d).
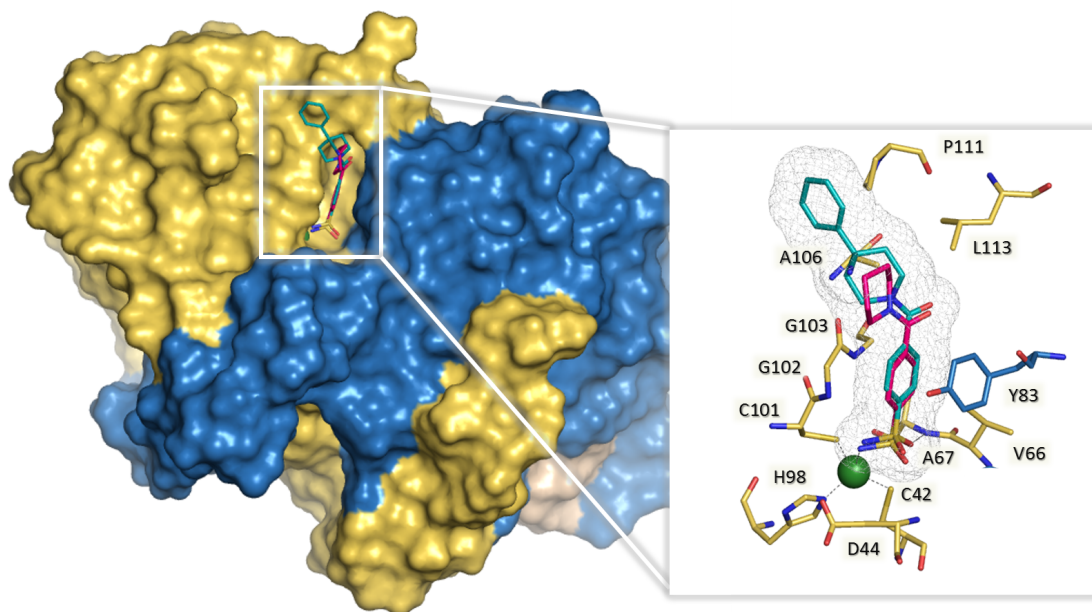
Figure 2.20: *Superposition of predicted binding mode for sulfonamide derivatives 47a and 49e into "modeled" VchCAβ catalytic cavity. Residues involved in hydrophobic and hydrophilic interactions are shown as gold (chain A) and sky blue (chain B) stickS. Zinc ion is depicted as dark green sphere. Dark grey dashed lines represent hydrogen bond interactions.*

In Figure 2.20 we described the best pose of prototype unsubstituted sulfonamide 47a showing the ability to create a network of interactions with the deep area of the catalytic site near to zinc ion, establishing few contacts with residues located in the middle area and top of CA cavity. We found hydrophobic interactions only with Y83, L113 and A106. Therefore, we hypothesized that these interactions could be not sufficient to inhibit VchCAβ (K_i > 10,000 nM). This consideration might justify the low efficacy demonstrated by sulfonamide derivatives 47b–d and 48a structurally related to parent compound 47a. Interestingly, the best active inhibitor 49e (K_i value of 806.4 nM) demonstrated the ability to form additional interactions with a cluster of hydrophobic residues A106, P111 and L113 when compared with unsubstituted analogue 47a, thus suggesting that the 4–phenylsubstituent of compound 49e is a crucial fragment to make more favorable hydrophobic contacts in the top of the cavity. This result indicates that the ligands having a good affinity towards VchCAβ are expected to establish additional H–bond interactions or hydrophobic contacts in the middle or top region of the enzymatic cavity.

2.6 Design and synthesis of new VchCAs inhibitors by molecular simplification approach

It has been suggested that the three bacterial CAs classes are characterized by a different spatial reorganization, since a progressive reduction of catalytic pocket width has been observed moving from α, to β and γ class [115] (Figure 2.21). This structural feature could justify the poor affinity toward β and γ classes for bulky inhibitors.
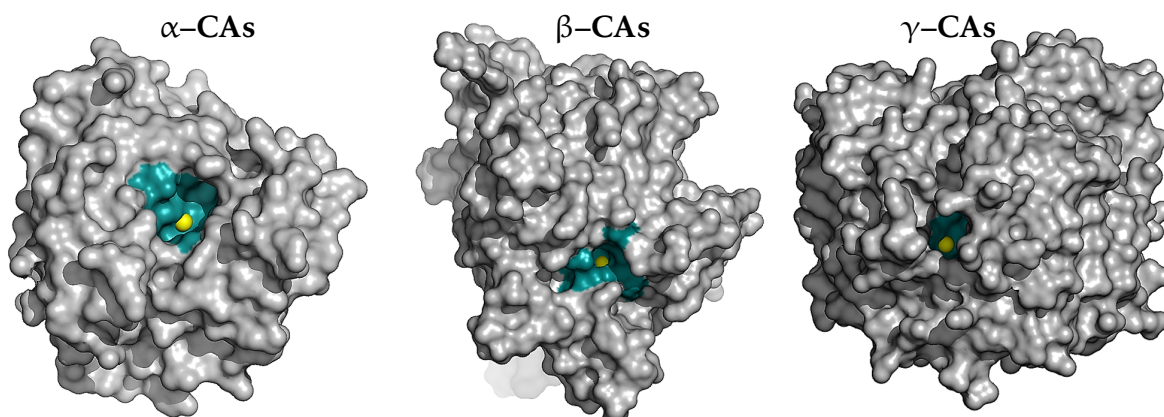
Figure 2.21: *3D–structures of bacterial α–, β–, γ–CAs with focus on catalytic pocket size.*

In light of the above findings and as continuation of our research project to develop effective antibacterial candidates targeting VchCAs, it was thought to extend our investigation. In particular, the visual inspection of the bacterial CAs pockets prompted the design of a new series of more flexible molecules based on benzenesulfonamide scaffold in which the cycloalkylamine nucleus of compounds 47a–e, 48a, 49a–f and 50a–d, was replaced by glycine linker (Figure 2.22). The follow up of this work was the investigation of the phenyl *tail* by the addition of lipophilic substituents and the replacement of the phenyl ring with different aryl systems. Successively, attention has been paid to linker modification through the substitution of the glycine fragment with different amino acids. Finally, it was planned the synthesis of a homologous series for which the biochemical screening is still in progress.
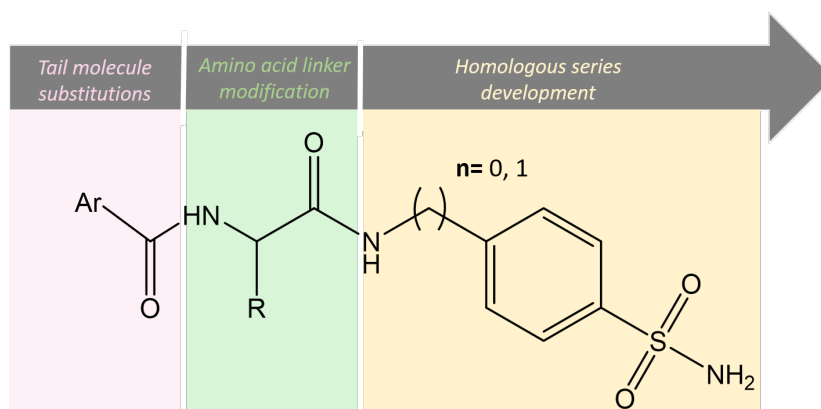
Figure 2.22: *Schematic representation of the multi–step approach used for the design of N–(2–oxo–2–((4–sulfamoylphenyl)amino)ethyl)benzamides [85a–g].*

Initially, it was planned the synthesis of a small set of glycine derivatives. The route followed to afford the N–(2–oxo–2–((4–sulfamoylphenyl)amino)ethyl)benzamides [85a–g] is depicted in Scheme 2.6. The key intermediates N–aroyl glycine 83a–g were obtained from glycine (80) and the appropriate aroyl chloride (79a–g) in alkaline water medium. In the second and last step, the aroyl glycine intermediates 83a–g were treated with the activating agent HBTU and coupled with *p*–aminobenzenesulfonamide (84) affording final compounds 85a–g.
The small set of N–(2–oxo–2–((4–sulfamoylphenyl)amino)ethyl)benzamides 85a–g thus obtained has been then biochemical screened against VchCAα, –β and –γ and the collected data are summarized in Table 2.10 in comparison with K_i values measured for the most active compound of previous series 49e and AAZ. The inhibitory profiles against the physiologically dominant isoenzymes CA I and II have been also measured in order to evaluate the ability of this compounds to discriminate the bacterial CAs over human off-target isoforms.
All these data evidenced how changes in *core* molecules significantly impact the inhibitory profile toward VchCAs. Indeed, all the tested compounds proved to affect the carbon dioxide hydrase activity of the three classes of CAs encoded by the pathogen *V. Cholerae*. In particular,

Cmpds	Ar
a	phenyl
b	2–chlorophenyl
c	3–chlorophenyl
d	4–chlorophenyl
e	2–fluorophenyl
f	2–furyl
g	2–thienyl
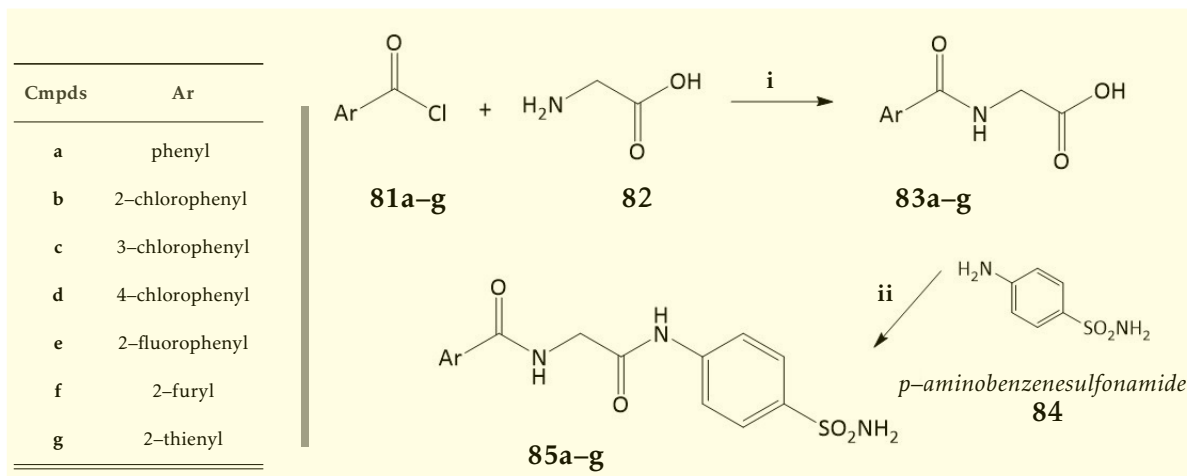
Scheme 2.6: *i) NaOH, H_2O/CH_3CN, 2.5 h, 0° C to rt; ii) HBTU, p–aminobenzenesulfonamide (84), DBU, DMF, 12 h, rt.*

N–(2–oxo–2–((4–sulfamoylphenyl)amino)ethyl)benzamides 85a–g revealed inhibitory effects in the low nanomolar range towards VchCAα with K_i ranging from 0.4–18.5 *nM*, whereas they are medium potent inhibitors of VchCAβ (K_i comprises between 59.7–884 *nM*).

	K_i (nM)[a]				
	VchCAα	**VchCAβ**	**VchCAγ**	**hCA I**	**hCA II**
85a	0.4	884	562.8	524.3	19.9
85b	8.9	795.5	8933	564.1	29.6
85c	18.5	82.8	363.6	127.2	14.7
85d	9.6	59.7	282.2	81.3	3.3
85e	9.2	311.6	70.0	162.7	3.1
85f	4.8	635.7	6025	429.6	38.5
85g	6.8	460.0	7750	620.8	22.2
49e	89.9	806.4	>10,000	6.5	0.6
AAZ	6.8	451.0	470.0	250	12.1

[a]Mean from three different assays (errors were in the range of ±5–10 % of the reported values).

Table 2.10: *Inhibition data for VchCAα, β–and γ and for the human hCA I and II with compounds 83a–g. Compound 49e and AAZ are reported only for comparative for a comparative purpose.*

Confirming the proof–of concept that a flexible linker might improve the binding affinity toward γ–CAs, these new series of compounds showed to be effective inhibitors also against the class (K_i comprises between 70.0–8933 nM). The screening toward VchCAα evidenced that any structural modification introduced on *tail* molecule of parent compound 85a did not significantly affect the inhibitory potency of derivatives 85b–g. The inhibitory trend toward VchCAβ revealed that the introduction of a chlorine atom in meta (85c) or para (85d) position resulted advantageous for the interaction with this CA class. As result, we can speculate that additional hydrophobic interactions can greatly contribute to stabilize these two ligands, 85c and 85d, within VchCAβ active site. With the aim to corroborate this hypothesis, molecular docking studies were carried by using the previously validated protocol. The hypothetical binding pose for the most active compound 85d is shown in Figure 2.23. As expected, docking analysis revealed that the sulfonamide moiety participates in the canonical interactions with the catalytic zinc ion. Furthermore, the sulfonamide is engaged in a network of H–bond interactions involving residues C101, G102 and A67 (chain A, colored in wheat). Interestingly, the aromatic ring of the benzenesulfonamide portion is stabilized by a π–π interaction with the enzyme proton shuttle Y83 (chain B, colored in sky blue) [112]. In addition, the hydroxyl group of Y83 acts as H-bond donor to the carbonyl group of the glycine spacer. Finally, it was found that the tail extends towards the rim cavity and it is retained by interactions mediated by T105, A105, I108 lining the hydrophobic valley along chain A (in gold).
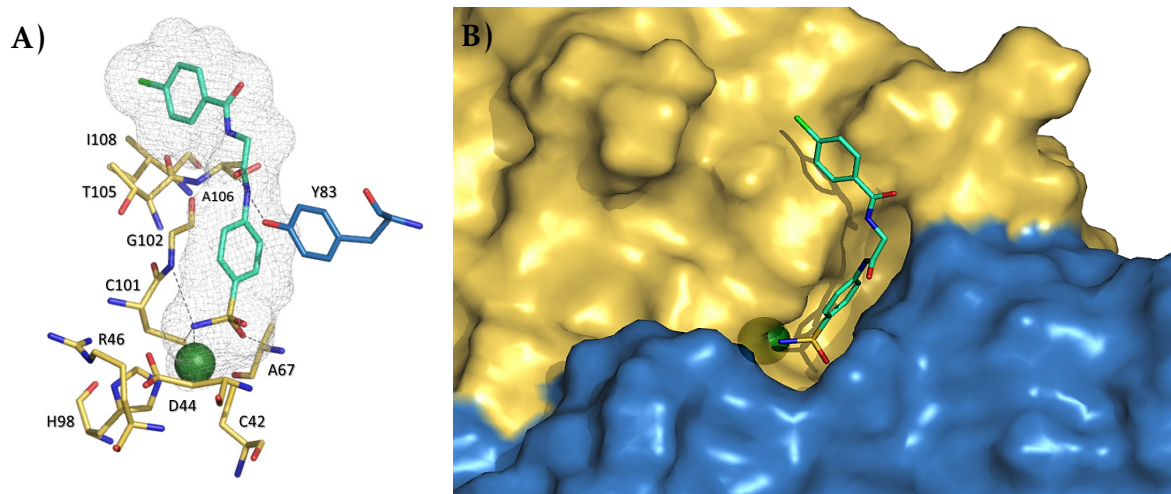
Figure 2.23: *A) Predicted binding pose of the inhibitor 4–chloro–N–(2–oxo–2–((4-sulfamoylphenyl)amino)ethyl)benzamide 85d into a "modelled" VchCAβ. The key residues of catalytic pocket are presented as gold (Chain A) and sky blue sticks (Chain B). The zinc (II) is depicted as dark green sphere. Hydrogen bond interactions are showed as dark grey dashed lines. B) Representation of VchCAβ surface showing compound 85d located in the active site.*

Concerning VchCAγ, the best outcome has been obtained for fluorinated derivative (85e) that resulted 7–fold up more active then reference compound AAZ. The lack of VchCAγ crystal structure did not allow to explore the 85e binding pose and, as consequence, to identify the key amino acid residues regulating the affinity towards this CA class. As continuation, several structural modifications have been introduced to the linker of compound 85a with the aim to catch new profitable contacts in the middle area of VchCAs catalytic

86a, R=Me
86b, R=iPr
86c, R=iBu

88a, R=Me
88b, R=iPr
88c, R=iBu

89a, R=Me
89b, R=iPr
89c, R=iBu

87a, R=Me
87b, R=iPr
87c, R=iBu

90a, R=Me
90b, R=iPr
90c, R=iBu

91a, R=Me
91b, R=iPr
91c, R=iBu
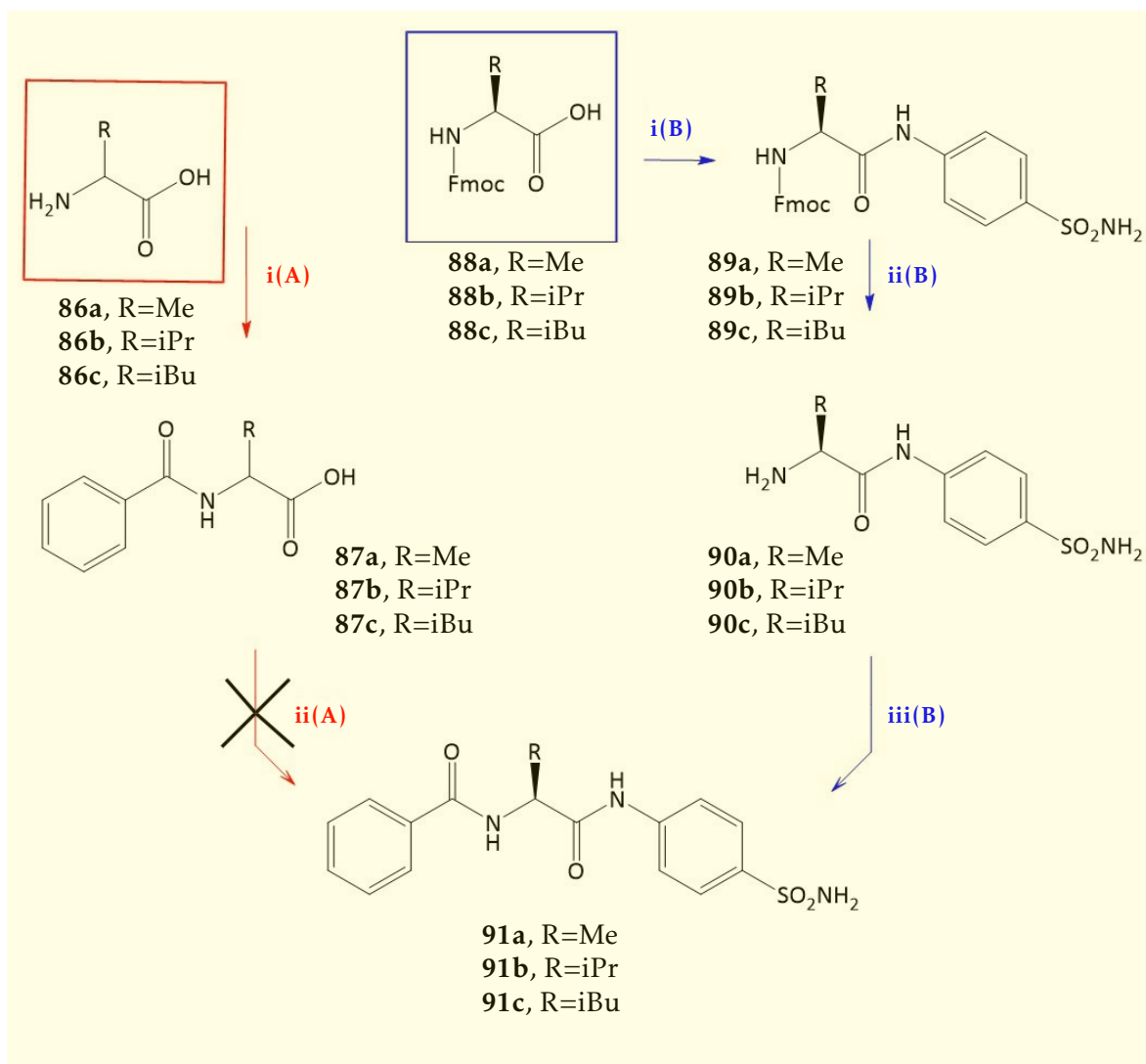
Scheme 2.7: *Reagents and conditions. i(A): NaOH, H_2O/CH_3CN, 0° C to rt, 2.5 h; i(B) HBTU, p–aminobenzenesulfonamide (84), DBU, DMF, rt, 12 h. ii(A) HATU, DIPEA, DMF, 0° C to rt, overnight; ii(B) DBU, DMF, rt, 10 min.; iii(B) EDIPA, DCM/DMF mixture (4:1), 0° C to rt, 3h.*

cavity, thus improving the binding potential. Therefore, a second subseries of N–(2–oxo–2–((4–sulfamoylphenyl)amino)ethyl)benzamides has been designed. The new compounds bear aliphatic amino acids including alanine, valine and leucine fragments (91a–c) in place of glycine building block. Many experimental attempts of synthesis have been made to afford the new designed derivatives 91a–c by following the same synthetic route of glycine analogues 85a–g, but the final coupling between the N–benzoyl amino acids 86a–c and *p*–aminobenzenesulfonamide (84) did not lead to desired compounds (Scheme 2.7, pathway A). Different coupling conditions have been used to overcome this obstacle, but in any case it was observed the formation of final products in a low percentage due to the high percentage of unreacted sulphanilamide and to the side-reactions occurred. Therefore, a highly effective synthetic procedure has been developed and it is described in Scheme 2.7 (pathway B).

In particular, the intermediates 89a–c have been obtained via a coupling reaction between the commercially available Fmoc–L–amino acids 86a–c and *p*–aminobenzenesulfonamide (84). This first step of reaction was performed in DMF solution by using different coupling reagent as well as (1–[Bis(dimethylamino)methylene]–1H–1,2,3–triazolo[4,5–b]pyridinium–3–oxide––hexafluorophosphate) (HATU) , HBTU or (1–Cyano–2–ethoxy–2–oxoethylidenaminooxy)di-methylamino–morpholino–carbenium hexafluorophosphate) (COMU), and DIPEA as base. The best result was obtained by using HATU and by adding this in different time in ice bath. Following this procedure, it was possible to minimize the formation of side products and to increase consistently the yield. The derivatives 89a–c were then subjected to a deprotection reaction using different bases as well as TEA, piperidine, DBU to afford compounds 90a–c.

83a, R=H
87a, R=Me
87b, R=iPr
87c, R=iBu

92

i

93a, R=H
93b, R=Me
93c, R=iPr
93d, R=iBu
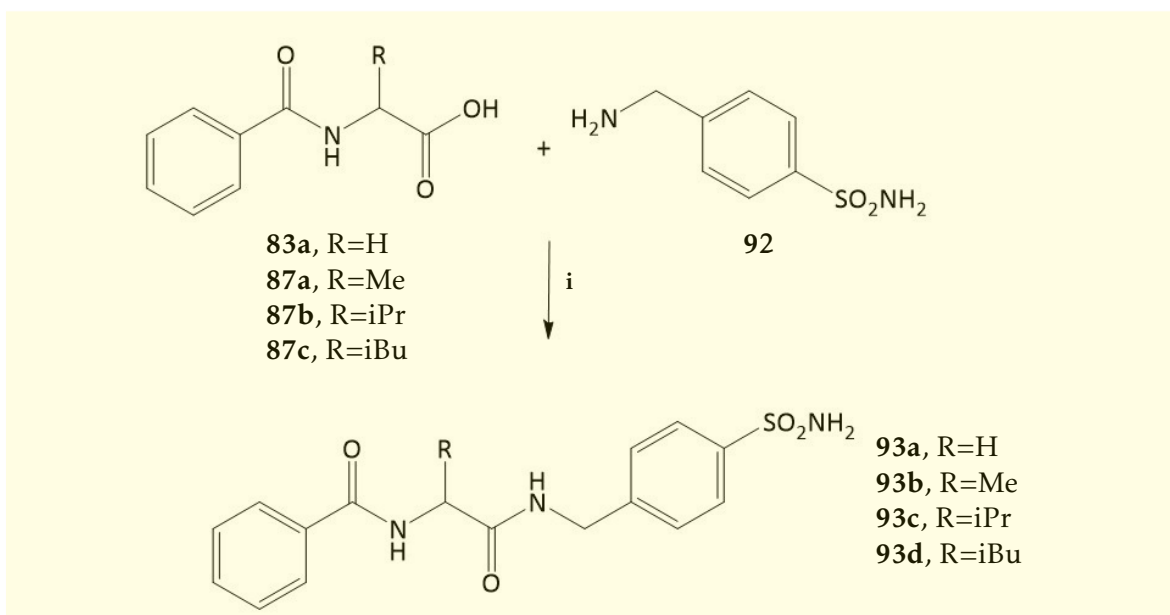
Scheme 2.8: *Reagents and conditions. i) HBTU, DIPEA, DMF, rt, 12 h.*

Finally, the intermediates 90a–c were dissolved in DMF/DCM mixture and treated with benzoyl chloride (81a) in order to achieve the final compounds 90a–c in excellent yield.

The K_i values measured for compounds 92a–c against VchCAα, β– and γ and the ubiquitous hCA I and II are summarized in Table 2.11. In order to investigate the role of the benzoyl tail in regulation the binding affinity toward the bacterial CAs and the selectivity over the human off–target isoforms, also the intermediates of synthesis 92a–c were screened.

The SAR analysis pointed out the introduction of methyl 90a or isopropyl 90b side chains weakly affected the affinity against VhCAα compared to the not–branched derivative 85a; whereas the replacement with bulkier isobutyl group of leucine derivative 91c highly reduced the binding affinity. As regard VhCAβ, there is not a linear correlation between the increase of side chain steric hindrance and the variation of affinity. Unexpectedly, compounds 91a–c proved to be high potent inhibitor of VhCAγ, suggesting that this aliphatic side chains could
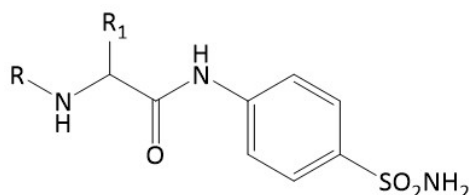
	R	R$_1$	K$_i$ (nm)[a]				
			VchCAα	VchCAβ	VchCAγ	hCA I	hCA II
90a	H	Me	869.3	382.7	35.7	380.6	23.7
90b	H	iPr	608.7	182.6	658.8	362.5	88.6
90c	H	iBu	86.9	5.4	323.5	237.0	770.9
91a	Bz	Me	9.5	3000	80.5	46.1	4.4
91b	Bz	iPr	9.2	389.3	24.3	51.5	3.7
91c	Bz	iBu	690.2	642.4	87.7	4.7	2.5
85a	Bz	H	0.4	884	562.8	524.3	19.9
AAZ	–	–	6.8	451.0	470.0	250	12.1

[a]Mean from three different assays (errors were in the range of ±5–10 % of the reported values).

Table 2.11: *Inhibition data for VchCAα, β–and γ and for the human hCA I and II with compounds 90a–c and 92a–c. Compound 85a is reported for comparison reasons.*

provide hydrophobic stabilizing interactions within the middle area of VhCAγ. It is worth to note that the ramification led to an enhanced inhibitory activity against the, in this case, human off–target isoforms CA I and II, hinting that the affinity and selectivity profile of this small set of compounds could be in future investigate for different clinical applications.

The biochemical test of the intermediates 90a–c has led to amazing results in terms of both affinity and selectivity; indeed, the 2–amino–4-methyl–N–(4–sulfamoylphenyl)pentanamide 90c (K_i of 5.4 nM) resulted about 84– and 120–fold up more active than the classical CAI inhibitor AAZ and the parent compound 91c respectively. In addition, compound 90c showed a low affinity towards the ubiquitous isoforms CA I and II, making it a promising lead compound for more in-depth biological studies aimed to identify agents useful in treatment of cholera disease. However, considering the highest level of sequence homology found for VchCAβ to the β–CAs from *Salmonella enterica* (63% identity), from *E. coli* (61% identity) and from *H. influenzae* (58% identity), it is possible to suppose that VchCAs inhibitors reported so far could potentially be employed in the management of other human infectious diseases.

Continuing our exploration of the chemical space of VchCAs inhibitors, in the last part of this study we planned the synthesis of a homologous subseries (93a–d) identifying as useful synthon the 4–(aminomethyl)benzenesulfonamide (92). The synthetic approach used to afford compounds 93a–d is depicted in Scheme 2.8. The intermediates 83a, 87a–c were easily coupled with 4–(aminomethyl)benzenesulfonamide 92, in alkaline medium for DIPEA and using HBTU as coupling reagent. All the designed compounds 90a–c were easily obtained in good yields thanks to the high nucleophilicity of 4–(aminomethyl)benzenesulfonamide 92; on the contrary this approach failed to furnish branched derivatives 91a–c. The biochemical screening for this last series of compounds is still in progress.

This part of project has been carried out during the period abroad at the Institute of Organic Chemistry and Biochemistry (IOCB) of Prague under the supervision of Dr. Milan Vrabel.

2.7 Generation of pharmacophore model for the development of new VchCAs inhibitors

Computer-aided drug design strategies have been successfully applied to attempt the identification of novel CA inhibitors. Herein we report the first ligand-based pharmacophore model as computational tool to identify novel scaffold for VchCAβ target. By applying this strategy, it was initially obtained a three–dimensional pharmacophore model which has been validated to confirm its robustness as valuable tool to identify potent inhibitors. Then, a structure–based virtual screening of 3D–databases allowed us to select hypothetical drug–like sulfonamides able to establish favorable interaction within catalytic cavity. Finally, several compounds were synthesized and screened to confirm the reliability of our computational protocol and to reach new information about the Structure Activity Relationships (SARs).
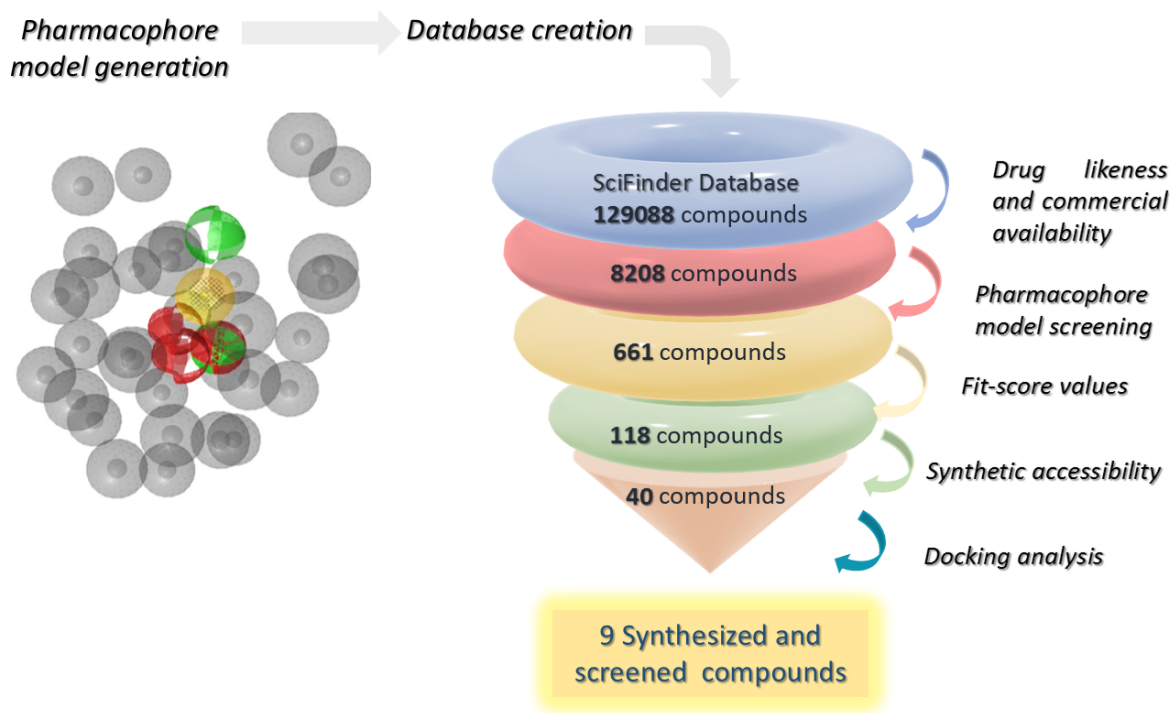
Figure 2.24: *Our workflow to develop VchCAβ inhibitors.*

It is well known that the virtual screening of compound libraries is a process that can be divided into well–defined steps. Figure 2.24 describes the screening workflow that was applied by us to discern novel VchCAβ inhibitors. The first step of our method was the creation of a query pharmacophore model for CA inhibitors targeting VchCAβ class. For this purpose, we selected from literature nineteen well–known inhibitors (Figure 2.25 and Figure 2.26) that possess the RSO_2NHR chemical moiety as common ZBG. In order to guarantee the best reliability of the pharmacophore hypotheses, it has been selected a homogenous series of inhibitors that have been assayed by employing the stopped–flow CO_2 hydrase assay. The K_i values for the chosen compounds range from 68 to 6000 *nM*. The data set compounds were distributed in two subsets, that are the training set (Figure 2.25) and the test set (Figure 2.26). The two data set of sulfonamides have been employed to generate a collection of ten pharmacophore model by means of LigandScout. The pharmacophore hypothesis with the best score value (72.7165) has been chosen from the ten generated models. To validate this model, its discriminatory ability has been assessed by considering the enrichment factor and the area under the curve (AUC) of the Receiver Operating Characteristic (ROC) curve. The model displays a preference for active compounds with an AUC value of 0.97 and EF of 11.5. As

shown in Figure 2.27A the obtained ligand–based pharmacophore consists of one aromatic ring feature (blue ring), two H–bond donors (green spheres), one hydrophobic feature (yellow sphere), three H–bond acceptors (red spheres), one negative ionizable (red star) and thirty-one exclusion volumes (gray sphere).

The superposition of the 3D coordinates of the classical inhibitor AAZ (K_i value of 451 nM) on generated pharmacophore (see Figure 2.27B) highlighted that the deprotonated sulfonamide moiety (RSO_2NH^-) is defined by two oxygen atoms as H–bond acceptors as well as one nitrogen atom corresponding to a H–bond donor or a negative ionizable group. Furthermore, the thiazolidine core of AAZ well fitted hydrophobic/aromatic ring features. Additionally, the nitrogen atom of amide portion corresponds the the other H–bond donor feature. The above described features corroborated with previously reported interactions found for AAZ docked into our modelled open conformation of VchCAβ. This strong matching found between the hypothetical binding pose of AAZ and the pharmacophore model, prompt us to exploit this plausible model as virtual screening (VS) tool to identify potential VchCAβ inhibitors.

The second step of our computational study involved the construction of a plausible database
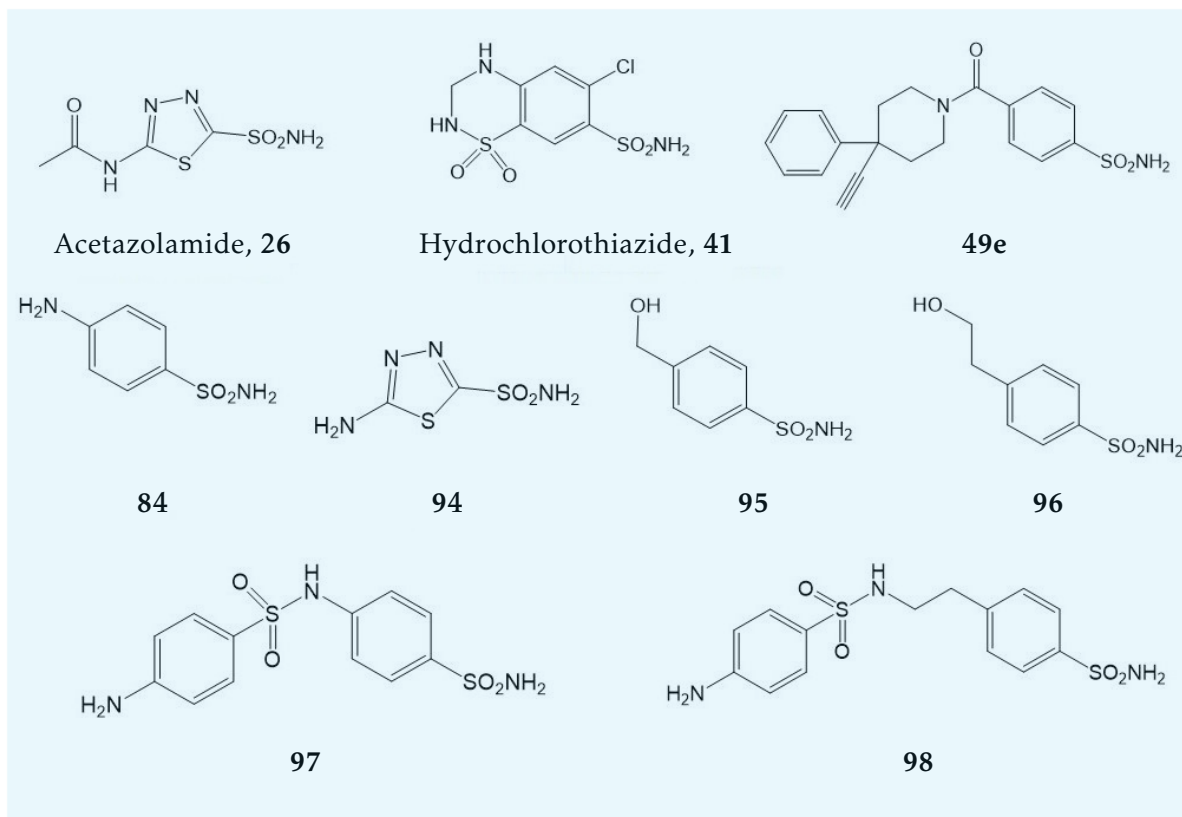
Figure 2.25: *Chemical structure of selected VchCAβ inhibitors constituted the training set.*
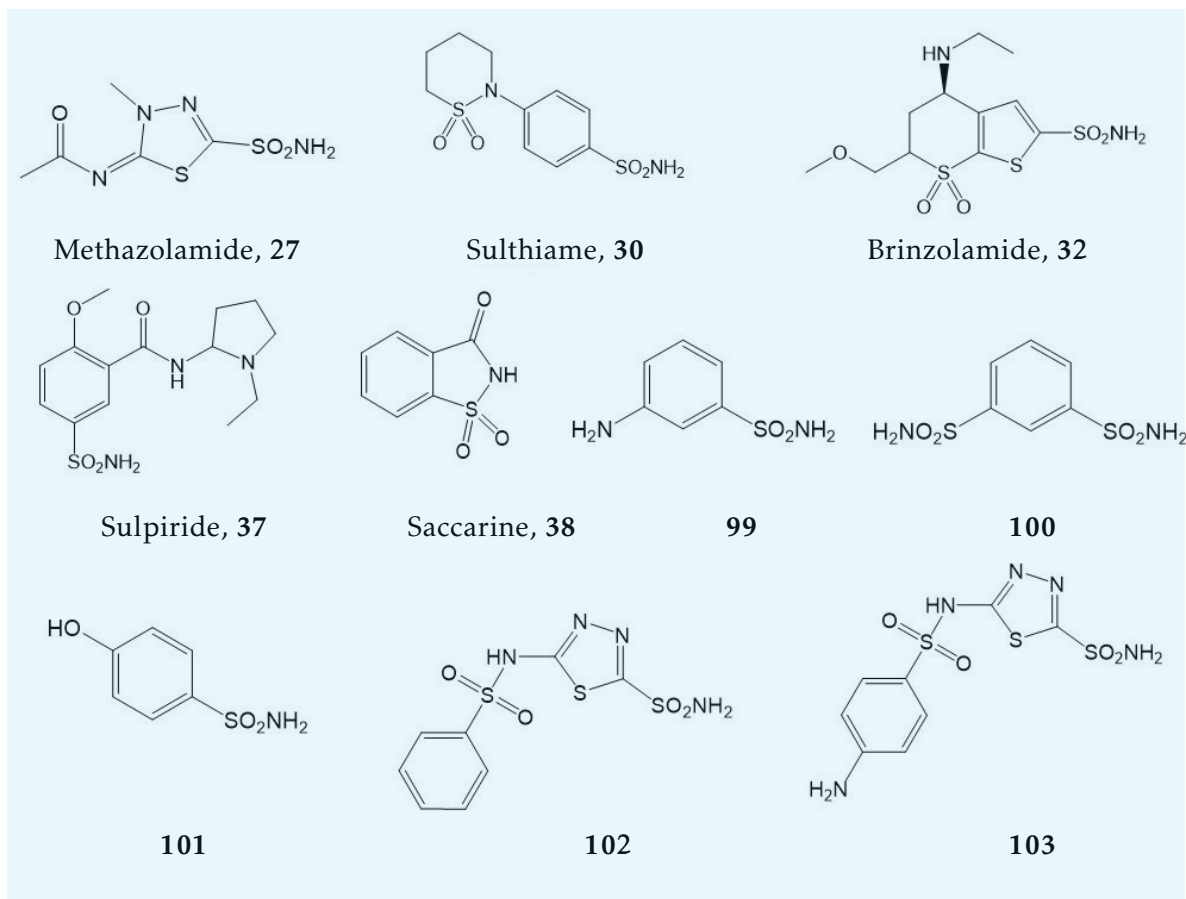
Figure 2.26: *Chemical structure of selected VchCAβ inhibitors constituted the test set.*

of VchCAβ inhibitors through the collection of *para*–benzenesulfonamide derivatives retrieved from SciFinder chemical database (https://scifinder.cas.org). Specific filters have been applied to select commercially available compounds with drug–likeness properties. Therefore, 8.208 molecules were collected and thus screened on pharmacophore model, thus obtaining 661 compounds. Among them, a set of 118 sulfondamides was chosen on the basis of fit-score values (major than 72.86). A visual inspection has allowed the selection of a subseries concerning of 40 compounds, that were docked into our modelled β–CA cavity by Gold software. Therefore, docking analysis afforded to nine sulfonamides that were selected on the basis of easy synthetic accessibility. The chemical structures of the selected hits compounds can be generalized as reported in Figure 2.28. Compounds 104a–i are characterized by the canonical ZBG linked to the lipophilic cap–group by an amide spacer as crucial motif to bind VchCAβ catalytic cavity through the requested hydrogen bond donor group; additionally, the cap group might furnish a selective interaction with VchCAs over other CA classes.
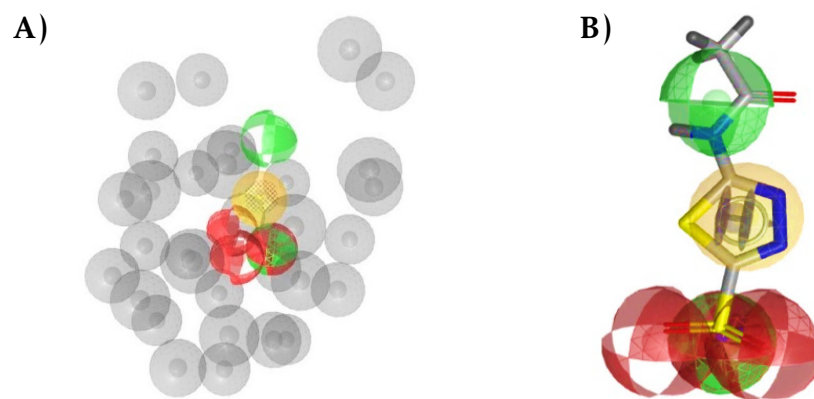
Figure 2.27: *Panel A) Representation of the best generated pharmacophore hypothesis. Panel B) AAZ mapped into pharmacophore model.*

It was performed the synthesis of the desired compounds by following the easy on step procedure reported in Scheme 2.9. The computationally designed N–(4–sulfamoylbenzyl)amide derivatives 104a–i were readily obtained by coupling the 4–aminomethylbenzenesulfonamide (92) with commercially available carboxylic acids or aroyl chlorides.

The N–(4–sulfamoylbenzyl)amide derivatives 104a–i thus obtained, were assayed for their inhibitory activity against VchCAα, –β and –γ. The collected biochemical data are summarized in Table 2.12 and compared with K_i values of AAZ as reference compound. For a comparative purpose the inhibitory profiles against the ubiquitous hCA I and hCA II have been also investigated. All computationally–inspired compounds 104a–i affected the CO_2 hydrase activity of VchCA classes showing K_i values ranging from 6.2 to 6442 *nM*. The screening toward VchCAα
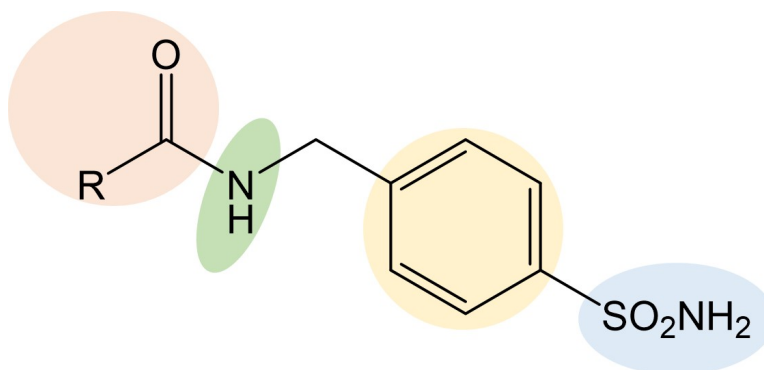
Figure 2.28: *Schematic representation of structural moieties shared by sulfonamides 104a–i.*
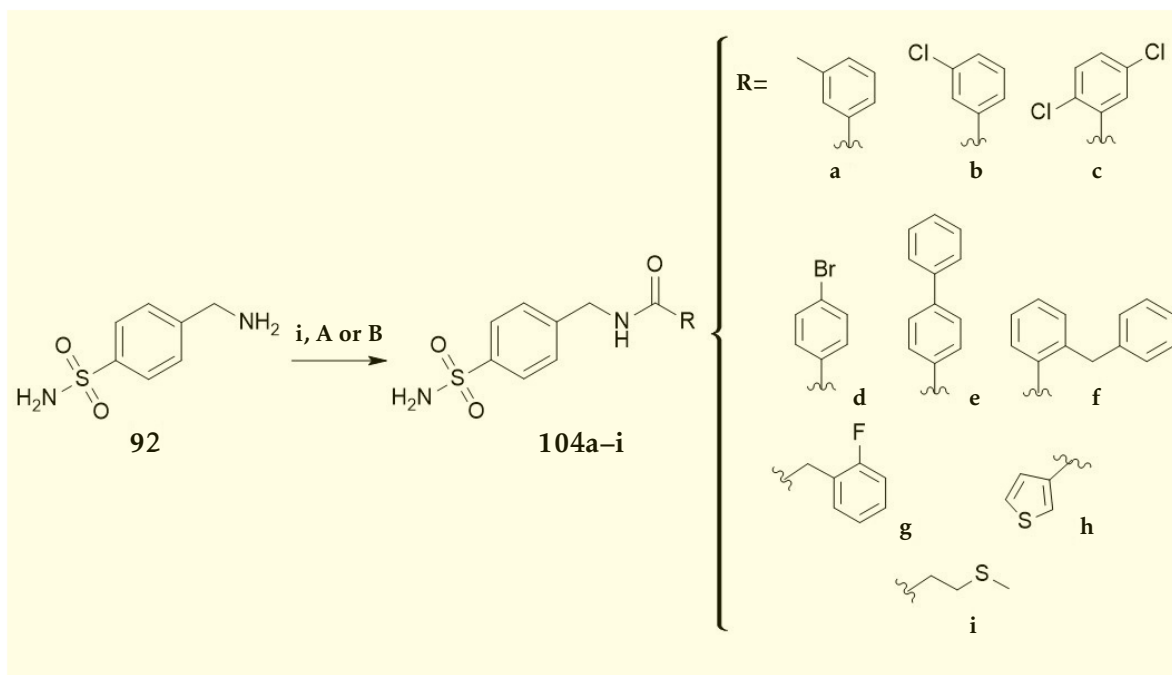
Scheme 2.9: *Reagents and conditions: i, A) RCOCl DIPEA, DCM/DMF (2:1, v/v), MW, 25° C, 10 min; B) RCO$_2$H, HBTU, DIPEA, DCM/DMF (2:1, v/v), MW, 25° C, 25 min.*

highilighted that the R substituent not significantly affected the inhibitory potency of tested compounds 104a–i. Notably, the 1–(biphenyl–4–yl)–substituted compound 104e resulted the most active VchCAβ inhibitor with a K_i value of 95.6 *nM*. Compounds 104b, 104f, 104g and 104i were about 5–fold less active VchCAβ inhibitors when compared with analogue 104e. The presence of *m*–tolyl or 2,5–chlorophenyl as hydrophobic cap group, respectively in compounds 104a and 104c, proved to be dramatically detrimental for VchCAβ binding potential. On the contrary, compounds 104d and 104h were more active when compared with 104a and 104c, whereas they were weakly active if compared with the most interesting inhibitor 104e. All these data evidenced how changes in the size and/or shape of the hydrophobic *tail* can strongly affect the affinity toward VchCAβ. The inhibitory trend against VchCAγ revealed that compounds 104a, 104d, and 104i were active at low nanomolar concentration, whereas no intriguing results have been found for the remaining compounds of the series. Taken together these data confirmed that VchCAα is more able to accommodate the various R–substituents compared the other tested classes VchCAβ and VchCAγ, certainly due to the wider size of its catalytic pocket. Overall, the most relevant result was the identification of compound 104e as a potent and selective VchCAβ inhibitor that displayed very low affinity toward hCAs I and II (K_i values of 2113.0 and 919.7 *nM*, respectively).

A further step of our study has been to analyze the hypothetical orientations into VchCAβ

	K$_i$ (nm)^a				
	VchCAα	**VchCAβ**	**VchCAγ**	**hCA I**	**hCA II**
104a	45.0	6442.0	56.1	60.7	3.3
104b	9.1	626.7	250.8	65.9	5.1
104c	8.8	3596.0	722.4	77.8	31.6
104d	18.1	179.2	98.4	95.0	63.0
104e	11.6	95.6	174.6	2113.0	919.7
104f	12.1	586.1	657.4	98.3	54.4
104g	6.2	553.9	593.0	269.3	26.3
104h	10.0	200.4	775.0	44.2	83.8
104i	7.7	538.5	79.6	571.5	69.5
AAZ	6.8	451.0	470.0	250.0	12.1

^{a}Errors in the range of ±10% of the reported value, from 3 different assays.

Table 2.12: *Inhibitory effects against VchCAα, VchCAβ, VchCAγ, hCA I and hCA II collected for benzenesulfonamides 104a–i and reference compound acetazolamide (AAZ, 26).*

cavity for synthesized compounds by docking analysis, that were performed by using the same protocol employed for the already investigated VchCAβ inhibitors. The docking results confirmed that N–(4–sulfamoylbenzyl)amide derivatives 104a–i adopted the canonical orientation of sulfonamide-based CAIs for which the deprotonated form of sulfonamide moiety is anchored to the zinc ion coordinated by residues C42, H98 and C101 (chain A, colored in blue). As expected, the aromatic ring of the benzenesulfonamide portion is stabilized through a π–π interaction with Y83 (chain B, colored in wheat). In addition, the –NH– group of amide spacer establishes H–bond interaction with the oxygen atom of G102 backbone. Our studies suggested that the cap–group might be involved in a network of interactions with a cluster of residues T105, A106, A139, I108 lining the hydrophobic subpocket along the rim of chain A. The network of above–mentioned interactions is displayed in Figure 2.29 for the most active inhibitor N–(4–sulfamoylbenzyl)biphenyl–4–carboxamide (102e, *K$_i$* value of 96.5 *nM*).

The screening and the docking efforts established that this compound might be a promising lead compound for further biological studies and structural optimization aimed to the
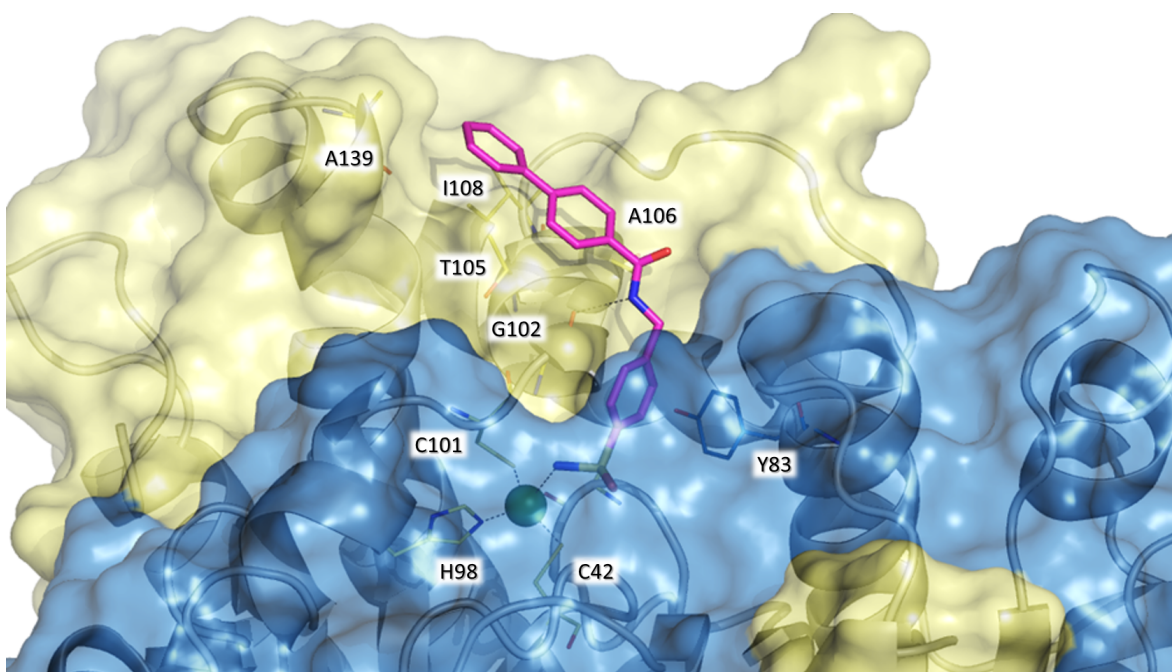
Figure 2.29: *Plausible binding mode of 104e within VchCAβ active site. VchCAβ backbone is represented as surface and cartoon. Amino acid residues involved in hydrophobic and hydrophilic interactions are showed as lines. Zinc ion is depicted as dark green sphere. Dark grey dashed lines represent hydrogen bond interaction.*

identification of novel anti–infective agents characterized by a peculiar mechanism of action, in order to overcome the global threat of antibiotic resistance.

> *The data collected in this last part of our research are reported in F. Mancuso et al. ACS Medicinal Chemistry Letters, 1 September 2020, In press, (doi: 10.1021/acsmedchemlett.0c00417).*

In attempt to carefully investigate the structure–activity relationships (SARs) of novel human CA inhibitors containing benzenesulfonamide scaffold, a series of forty–two compounds has been synthetized and tested for their CA inhibitory activity by a stopped–flow carbon dioxide hydrase assays against selected human CAs. The design of the CAIs has been performed by a structure–guided drug discovery method, thus taking into account the visual inspection of the X–ray crystallographic complexes previously obtained from our group.

Among the first series of cycloalkylamino–1–carbonylbenzenesulfonamides (47a–e, 48a–b, 49c–f and 50a–d), the most potent compounds demonstrated excellent inhibitory effects against several CA isoezymes at subnanomolar concentration. These findings were corroborated by crystallographic structures of the hit compounds 49a, 49b and 50b in complex with both hCA II and hCA VII isoforms. These structural analysis confirmed that the combination of the crucial benzenesulfonamide moiety with a suitable "*tail*" can enhance the affinity profile toward specific isoforms, suggesting the design of 4–[4–(aroylpiperazine–1–carbonyl]benzenesulfonamides series (54a–p). The best outcome has been the identification of for 4–[4–(2–fluorobenzoyl)piperazine–1–carbonyl]benzenesulfonamide (54b) and 4–(4–(furan–2–carbonyl)piperazine–1–carbonyl)benzenesulfonamide (57h). Interestingly, compound 54b showed very high affinity against the tumor–associated isoform, displaying an inhibitory activity similar to that of the promising anti–tumour agent SLC–0111. The binding interaction and the chemical requirements which have determined the improvement in hCA XII affinity, have been investigated by docking analysis. Concerning the furyl derivative 57h, it combines an advantageous affinity and selectivity profile against the brain–expressed human CA VII comparable with that of the clinical use anticonvulsant agent Topiramate (33).

Furthermore, we identified a novel series of thirty–two coumarins structurally related to the natural compound Umbelliferon, possessing high affinity toward the tumor–expressed hCA

IX/XII and selectivity over hCA I/II isoforms. The most relevant result has been obtained for 4–(4–Aminophenyl)–7–hydroxy–8–methyl–chromen–2–one (70i), for which docking analysis
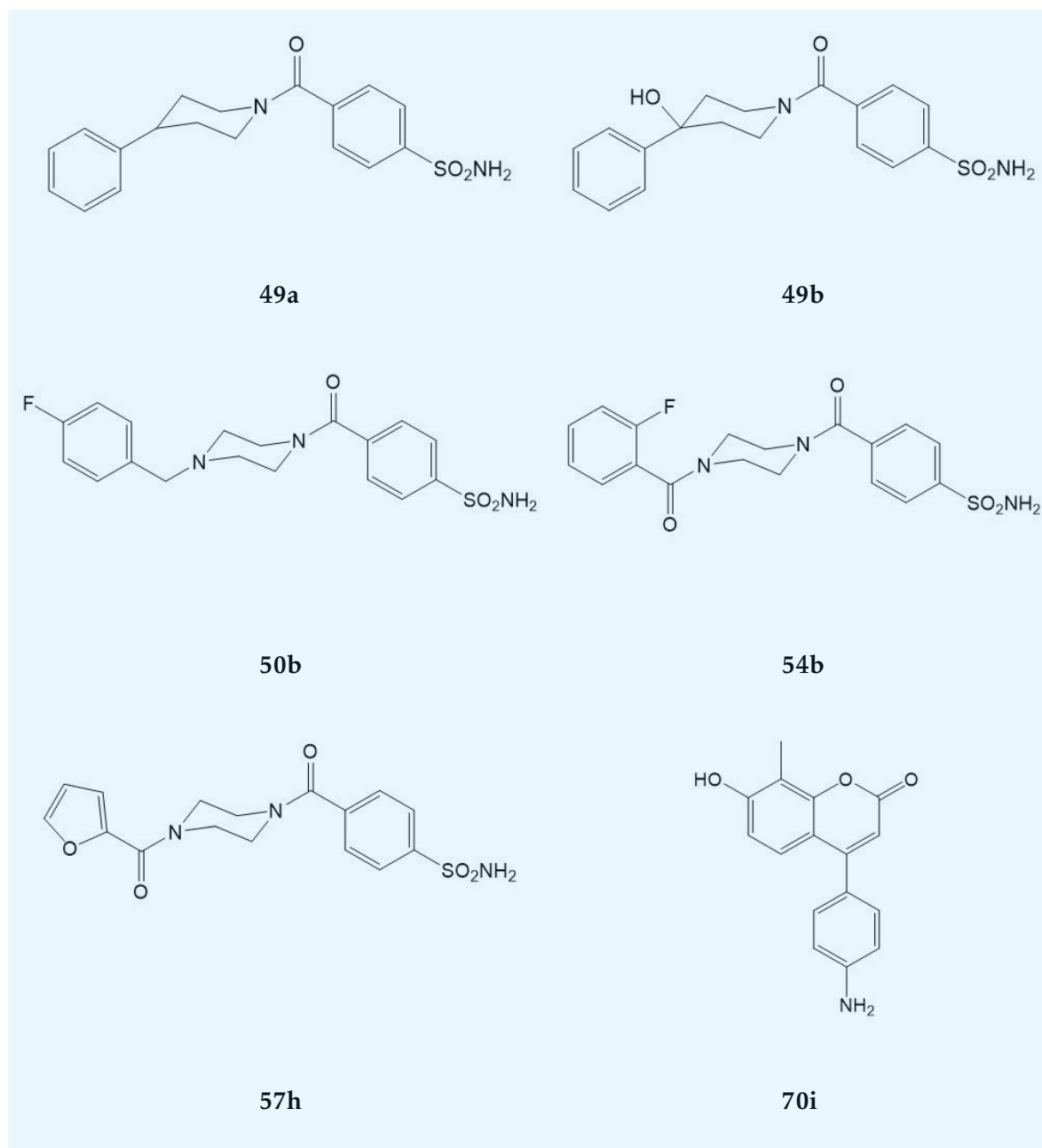
Figure 3.1: *Chemical structures of novel promising human CAI inhibitors.*

confirmed the relevance of the amino group in the binding process within CA XII active site. This evidence confirms that coumarins represent useful heterocyclic system for further chemical optimization in order to obtain CAIs characterized by a singular mechanism of CA inhibition which does not involve the coordination of zinc ion within catalytic site.

Finally, our efforts have been also addressed to the development of novel inhibitors targeting α, β and γ classes from the pathogen *Vibrio Cholerae* (VchCAα, β, γ) potentially useful in the management of cholera disease. In order to identify a new class of VchCAs inhibitors, different drug design strategies have been applied. All the designed compounds were synthesized and tested for their *in vitro* inhibitory activity against VchCAα, –β and –γ classes in comparison with ubiquitous hCA I and II. Overall, these studies led to the identification of three promising hit compounds: 4–chloro–N–(2–oxo–2–((4–sulfamoylphenyl)amino)ethyl)benzamide (83d), 2–amino–4–methyl–N–(4–sulfamoylphenyl) pentanamide (90c), N–(4–sulfamoylbenzyl)–[1,1'–biphenyl]–4–carboxamide (104e). Across them, hit compound 104e has been found to combine high affinity toward VchCAs with surprising selectivity over the human off–target isoforms. This result makes 104e a promising lead compound for further biological studies and structural optimization. Indeed, it could represent the starting point for the identification of novel anti–infective agents characterized by a peculiar mechanism of action, in order to overcome the global threat of antimicrobial drug resistance.
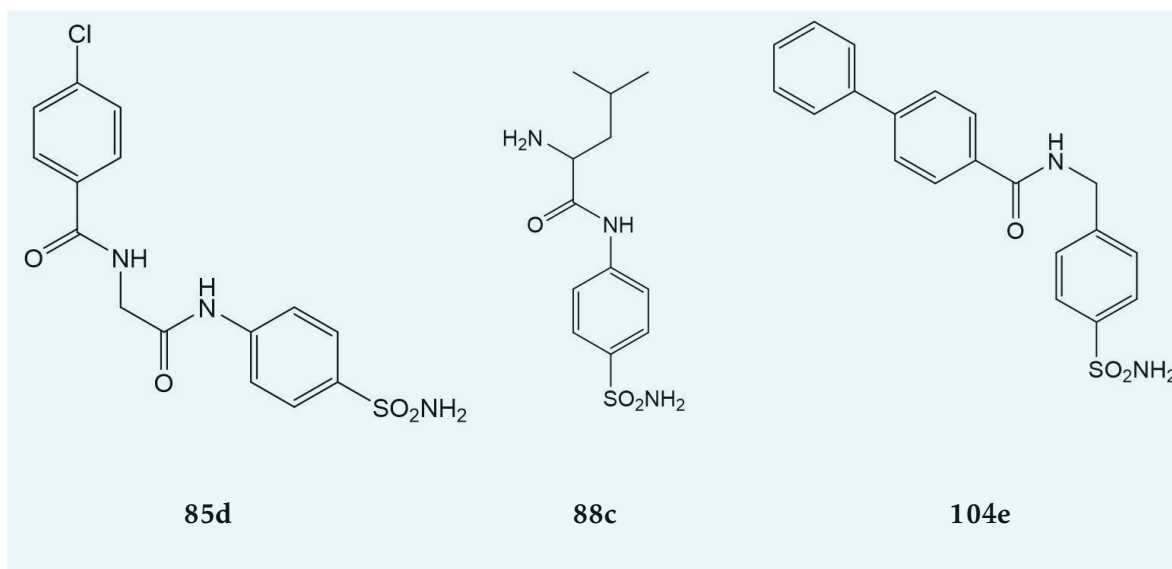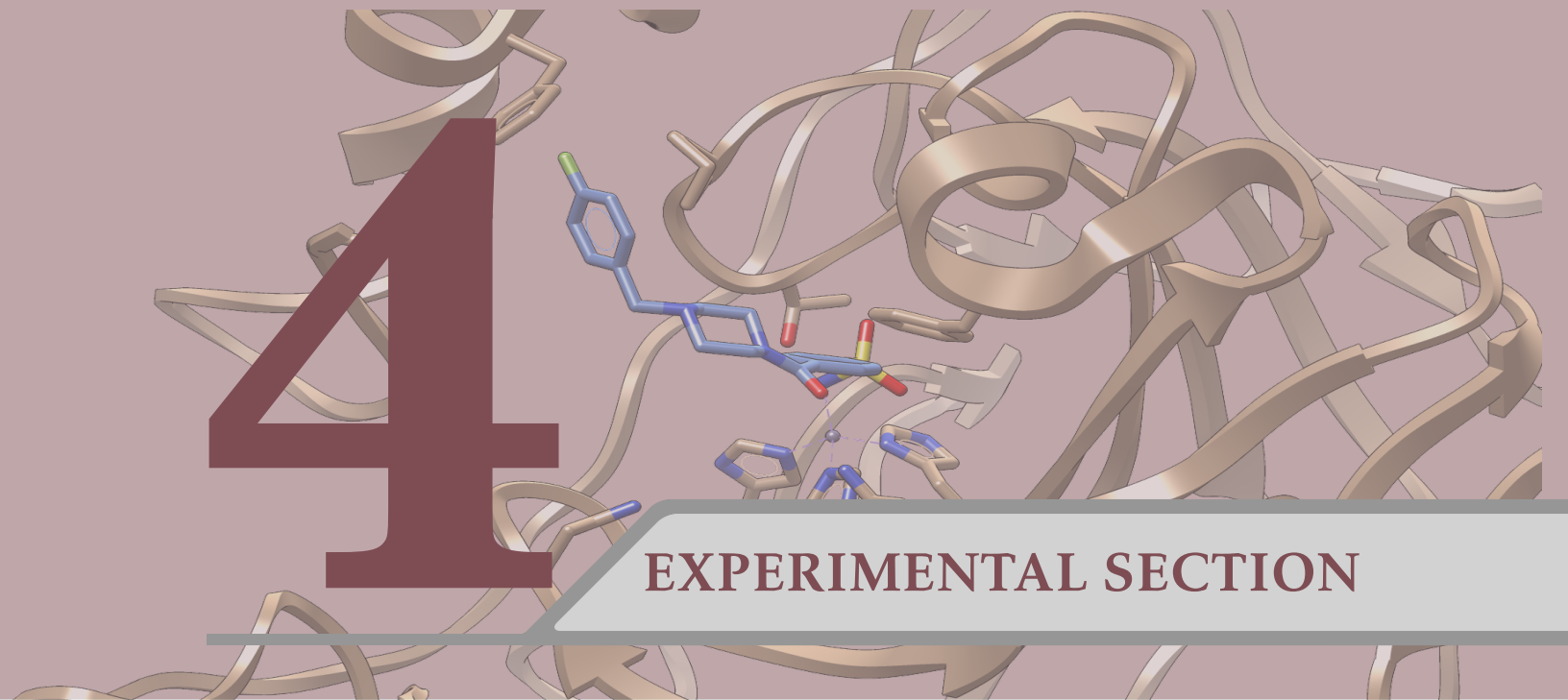
Figure 3.2: *Chemical structures of novel bacterial CAI inhibitors.*

Overall, the results of this three years PhD research project might contribute to expand the chemical space of both human and bacterial CA inhibitors. At the same time, the synthetic accessibility for all the discovered compunds has been ensured. The analysis of the many collected biochemical data furnished relevant knowledge about structure–activity relation-

ships (SARs) of benzenesulfonamide and coumarine derivatives. Structural investigation by means of computational or X–ray crystallographic studies have shed light on to the crucial interactions which affect affinitiy/selectivity towards the CA druggable isoforms. All the biochemical and the structural data reported so far, may provide useful insight for the future discovery of CAIs potentially employable in the treatment of important human diseases.

4.1   Chemistry

All starting materials and reagents commercially available (Sigma–Aldrich Milan, Italy; Alfa Aesar Karlsruhe, Germany) were used without further purification. Microwave–assisted reactions were carried out in a focused Microwave Synthesis System (CEM Technology Ltd Buckingham, UK). Melting points were determined on a Buchi B–545 apparatus (BUCHI Labortechnik AG Flawil, Switzerland) and are uncorrected (±0.4). Elemental analyses (C, H, N) were carried out on a Carlo Erba Model 1106 Elemental Analyzer (Carlo Erba Milano, Italy); the results confirmed a ≥ 95% purity. Thin–layer chromatography was performed on aluminum sheets from Merk (Silica gel 60 F254, 20 × 20). Chromatograms were visualized by UV light ($\lambda = 254$ *nm*/366 *nm*) or by staining with ninhydrin or vanilline solution. Merck silica gel 60 F254 plates were used for analytical TLC (Merck KGaA, Darmstadt, Germany). Flash Chromatography (FC) was carried out on a Biotage SP1 EXP (Biotage AB Uppsala, Sweden). High–resolution mass spectra were recorded on an Agilent 5975C MSD Quadrupol, Q–Tof micro from Waters or LTQ Orbitrap XL from Thermo Fisher Scientific. HPLC–MS measurements were performed on an LCMS–2020 system from Shimadzu equipped with a Luna® C18(2) column (3μm, 100 A, 100 × 4.6 *mm*) using a linear gradient of CD_3CN+0.05% HCOOH ($5 \rightarrow 95\%$ in 9 *min*) in H_2O +0.05% HCOOH at a flow rate of 1.0 *mL/min*. ^{1}HNMR and ^{13}CNMR spectra were measured in dimethylsulfoxide-d_6 (DMSO-d_6) or or Deuterochloroform (CDCl-d_3) with a Varian Gemini 500 spectrometer (Varian Inc. Palo Alto, California USA) or with a a Bruker Avance III [TM] HD 400 *MHz* NMR system equipped with Prodigy cryo–probe; chemical shifts are expressed in δ (ppm) and coupling constants (J) in hertz. All exchangeable protons were confirmed by addition of D_2O.

4.1.1 General synthetic procedure for compounds 47a–e, 48a, 49a–f, 50a–d

Pathway I: To a solution of 4–(aminosulfonyl)benzoic acid 46 (6 molar equivalents) in tetrahydrofuran (THF) (15 *mL*) the 1'-carbonyldiimidazole (CDI) (6 molar equivalents) at $0°C$ was added. The obtained mixture was stirred at room temperature for 3h and then the appropriate amine derivative (15 molar equivalents) in N,N–Dimethylformamide (DMF) (5 *mL*) was added drop wises. The reaction mixture was stirred vigorously at 350 rpm and room temperature for two hours. The solvent was removed *in vacuum*. The addition of aqueous solution of $NaHCO_3$(5 *mL*) to the crude led to compounds 47a and 47d, which were purified through crystallization by a mixture of diethyl ether (Et_2O) and ethanol (EtOH) (50%, v/v).

Pathway II: A mixture of 4–sulfamoyl benzoic acid 46 (2 molar equivalents) and N,N,N,N–tetramethyl–O–(1H-benzotriazol–1–yl)uronium hexafluorophosphate (HBTU) (2 molar equivalents) in DMF (2 mL) was stirred at room temperature for 1 h. Then, a solution of the appropriate amine derivative (2 molar equivalents) in triethylamine (TEA) (2 *mmol*) was added drop wises. The reaction mixture was left overnight and then quenched with water (10 *mL*) and extracted with EtOAc (3×5 *mL*). The organic phase was dried over sodium sulphate (Na_2SO_4) and then the solvent was removed in vacuum. The residue was purified by flash chromatography using a linear gradient of methylene chloride (DCM)/ + methanol (MeOH) (100% DCM to 96% DCM–4% MeOH), crystallized by treatment with a mixture of Et_2O and EtOH (1:1) to give the desired final compounds 47b–c, 48a, 49a–f, 50a–d as white powders. For compounds 47a–d,48a, 50a, and 50d registered CAS numbers have been already assigned. However, their synthetic procedures, chemical properties and structural characterization are not available in literature.

47a **4–(Piperidine–1–carbonyl)benzenesulfonamide**
(CAS Number: 4302–78–7)

Yield: 40%; m.p.: $206 - 208°C$; R_f (DCM/MeOH 96:4 v/v): 0.45; ^{1}H–NMR (DMSO–d_6) (δ): 1.43–3.57 (m, 10H, CH_2), 7.45 (bs, 2H, NH_2), 7.53 (d, J= 8.2 *Hz*, 2H, ArH), 7.83 (d, J= 8.2 *Hz*, 2H, ArH). Anal. for $C_{12}H_{16}N_2O_3S$: C 53.71%; H 6.01%; N 10.44%. Found: C 53.79%; H 6.13%; N 10.54%.

47b **4–(2–Methylpiperidine–1–carbonyl)benzenesulfonamide**
(CAS Number: 1097096–08–6)

Yield: 60%; m.p.: $186 - 188°C$; R_f (DCM/MeOH 96:4 v/v): 0.47; ^{1}H-NMR (DMSO-d_6) (δ): 1.15 (d, J=7.1 *Hz*, 3H, CH_3), 1.43-3.40 (m, 9H, CH and CH_2), 7.42 (bs, 2H, NH_2), 7.50 (d, J=8.2 *Hz*, 2H, ArH), 7.83 (d, J= 8.2 *Hz*, 2H, ArH). Anal. for $C_{13}H_{18}N_2O_3S$: C 55.30%; H 6.43%; N 9.92%. Found: C 55.35%; H 6.40%; N 9.97%.

47c **4–(3–Methylpiperidine–1–carbonyl)benzenesulfonamide**
(CAS Number: **4367–75–3**)

Yield: 35%; m.p.: $190 - 192°C$; R_f (DCM/MeOH 96:4 v/v): 0.49; ^{1}H-NMR (DMSO-d_6) (δ): 1.06 (d, $J=$ 7.1 Hz, 3H, CH$_3$), 1.10-2.94 (m, 9H, CH and CH$_2$), 7.43 (bs, 2H, NH$_2$), 7.52 (d, $J=$ 8.2 Hz, 2H, ArH), 7.84 (d, $J=$ 8.2 Hz, 2H, ArH). Anal. for C$_{13}$H$_{18}$N$_2$O$_3$S: C 55.30%; H 6.43%; N 9.92%. Found: C 55.40%; H 6.53%; N 10.02%.

47d **4–(4–Methylpiperidine–1–carbonyl)benzenesulfonamide**
(CAS Number: **1096951–92–6**)

Yield: 40%; m.p.: $212 - 214°C$; R_f (DCM/MeOH 96:4 v/v): 0.51; ^{1}H-NMR (DMSO-d_6) (δ): 0.91 (d, $J=$ 7.0, 3H, CH$_3$), 1.06-3.00 (m, 9H, CH and CH$_2$), 7.44 (bs, 2H, NH$_2$), 7.53 (d, $J=$ 8.2 Hz, 2H, ArH), 7.84 (d, $J=$ 8.2 Hz, 2H, ArH). Anal. for C$_{13}$H$_{18}$N$_2$O$_3$S: C 55.30%; H 6.43%; N 9.92%. Found: C 55.40%; H 6.40%; N 9.80%.

47e **4–(4–Benzylpiperidine–1–carbonyl)benzenesulfonamide**
(CAS Number: **2260622–11–3**)

Yield: 44%; m.p.: $156 - 158°C$; R_f (DCM/MeOH 96:4 v/v): 0.59; ^{1}H-NMR (DMSO-d_6) (δ): 1.47-3.44 (m, 9H, CH and CH$_2$), 2.50 (m, 2H, CH$_2$Ph), 7.15-7.16 (m, 3H, ArH), 7.24-7.27 (m, 2H, ArH), 7.42 (bs, 2H, NH$_2$), 7.52 (d, $J=$ 8.2 Hz, 2H, ArH), 7.84 (d, $J=$ 8.2 Hz, 2H, ArH). Anal. for C$_{19}$H$_{22}$N$_2$O$_3$S: C 63.66%; H 6.19%; N 7.81%. Found: C 63.56%; H 6.09%; N 7.71%.

48a **4–(Azepane–1–carbonyl)benzenesulfonamide**
(CAS Number: **1015627–49–2**)

Yield: 30%; m.p.: $200 - 202°C$; R_f (DCM/MeOH 96:4 v/v): 0.53; ^{1}H-NMR (DMSO-d_6) (δ): 1.50-3.53 (m, 12H, CH$_2$), 7.43 (bs, 2H, NH$_2$), 7.51 (d, $J=$ 7.6 Hz, 2H, ArH). 7.83 (d, $J=$ 7.6 Hz, 2H, ArH). Anal. for C$_{13}$H$_{18}$N$_2$O$_3$S: C 55.30%; H 6.43%; N 9.92%. Found: C 55.40%; H 6.53%; N 9.82%.

49a **4–(4–Phenylpiperidine–1-carbonyl)benzenesulfonamide**
(CAS Number: **2260622–14–6**)

Yield: 73%; m.p.: $222 - 224°C$; R_f (DCM/MeOH 96:4 v/v): 0.55; ^{1}H-NMR (DMSO-d_6) ($\delta\delta$): 1.86-4.60 (m, 9H, CH and CH$_2$), 7.18-7.28 (m, 5H, ArH), 7.45 (s, 2H, NH$_2$), 7.61 (d, $J=$ 8.00 Hz, 2H, ArH), 7.86 (d, $J=$ 8.00 Hz, 2H, ArH). Anal. for C$_{18}$H$_{20}$N$_2$O$_3$S: C 62.77%; H 5.85%; N 8.13%. Found: C 63.10%; H 5.65%; N 8.47%.

49b **4–(4–Hydroxy–4–phenylpiperidine–1–carbonyl)benzenesulfonamide**
(CAS Number: 226-0622–15–7)

Yield: 34%; m.p.: $135 - 137°C$; R_f (DCM/MeOH 96:4 v/v): 0.37; ^{1}H-NMR (DMSO-d_6) (δ): 1.51-4.45 (m, 8H), 5.20 (bs, 1H, OH), 7.18-7.32 (m, 3H, ArH), 7.45 (bs, 2H, NH$_2$), 7.51 (m, 2H, ArH), 7.63 (d, J= 8.2 Hz, 2H, ArH), 7.86 (d, J= 8.2 Hz, 2H, ArH). Anal. for C$_{18}$H$_{20}$N$_2$O$_4$S: C 59.98%; H 5.59%; N 7.77%. Found: C 60.18%; H 5.79%; N 7.87%.

49c **4-[4-(4-Chlorophenyl)-4-hydroxypiperidine-1-carbonyl]benzenesulfonamide**
(CAS Number: 2260622–16–8)

Yield: 31%; m.p.: $215 - 217°C$; R_f (DCM/MeOH 96:4 v/v): 0.38; ^{1}H-NMR (DMSO-d_6) ($\delta\delta$): 1.52-4.44 (m, 8H), 5.31 (bs, 1H, OH), 7.36 (d, J= 8.5 Hz, 2H, ArH), 7.44 (bs, 2H, NH$_2$), 7.54 (d, J= 8.5 Hz, 2H, ArH), 7.63 (d, J= 7.6 Hz, 2H, ArH), 7.86 (d, J= 7.6 Hz, 2H, ArH). Anal. for C$_{18}$H$_{19}$ClN$_2$O$_4$S: C 54.75%; H 4.85%; N 7.09%. Found: C 54.93%; H: 5.13%; N: 7.37%.

49d **4-[4-(4-Bromophenyl)-4-hydroxy-piperidine-1-carbonyl]benzenesulfonamide**
(CAS Number: 2260622–17–9)

Yield: 35%; m.p.: $219 - 221°C$; R_f (DCM/MeOH 96:4 v/v): 0.40; ^{1}H-NMR (DMSO-d_6) (δ): 1.48-4.45 (m, 8H), 5.31 (bs, 1H, OH), 7.44 (bs, 2H, NH$_2$), 7.49-7.52 (m, 4H, ArH), 7.63 (d, J= 8.8 Hz, 2H, ArH), 7.86 (d, J= 8.8 Hz, 2H, ArH). Anal. for C$_{18}$H$_{19}$BrN$_2$O$_4$S: C 49.21%; H %4.36; N 6.38%. Found: C 49.58%; H 4.67%; N 6.44%.

49e **4–(4–Cyano–4–phenylpiperidine–1–carbonyl)benzenesulfonamide**
(CAS Number: 2260-622–19–1)

Yield: 22%; m.p.: $285 - 287°C$; R_f (DCM/MeOH 96:4 v/v): 0.59; ^{1}H-NMR (DMSO-d_6) (δ): 2.07-4.67 (m, 8H), 7.34-7.39 (m, 1H, ArH), 7.42 (bs, 2H, NH$_2$), 7.45-7.47 (m, 4H, ArH), 7.66 (d, JJ= 8.2 Hz, 2H, ArH), 7.87 (d, JJ= 8.2 Hz, 2H, ArH). Anal. for C$_{19}$H$_{19}$N$_3$O$_3$S: C 61.77%; H 5.18%; N 11.37%. Found: C 6.83%; H 5.47%; N11.62%.

49f **4–(4–Acetyl–4–phenyl–piperidine–1–carbonyl)benzenesulfonamide**
(CAS Number: 2260-622–21–5)

Yield: 20%; m.p.: $232 - 234°C$; R_f (DCM/MeOH 96:4 v/v): 0.52; ^{1}H-NMR (DMSO-d_6) (δ): 1.89 (s, 3H, CH$_3$), 1.96-3.92 (m, 8H), 7.28-7.38 (m, 5H, ArH), 7.44 (bs, 2H, NH$_2$), 7.55 (d, J= 8.2 Hz, 2H, ArH), 7.83 (dJJ= 8.2 Hz, 2H, ArH). Anal. for C$_{20}$H$_{22}$N$_2$O$_4$S: C 62.16%; H 5.74%; N 7.25%. Found: C 62.10%; H 5.84%; N 7.15%.

50a **4–(4–Benzylpiperazine–1–carbonyl)benzenesulfonamide**
(CAS Number: **1032228–25–3**)

Yield 40%; m.p.: $204 – 206°C$; R_f (DCM/MeOH 96:4 v/v): 0.43; ^{1}H-NMR (DMSO-d_6) (δ): 2.32- 3.60 (m, 8H), 3.47 (s, 2H, CH$_2$Ph), 7.22-7.26 (m, 5H, ArH), 7.44 (bs, 2H, NH$_2$), 7.56 (d, J= 8.2 Hz, 2H, ArH), 7.83 (d, J= 8.2 Hz, 2H, ArH). Anal. for C$_{18}$H$_{21}$N$_3$O$_3$S: C 60.15%; H 5.89%; N 11.69%. Found: C 60.25%; H 5.99%; N 11.99%.

50b **4–[4–[(4–Fluorophenyl)methyl]piperazine–1–carbonyl]benzenesulfonamide**
(CAS Number: **2260622–24–8**)

Yield: 30%; m.p.: $206 – 208°C$; R_f (DCM/MeOH 96:4 v/v): 0.45; ^{1}H-NMR (DMSO-d_6) (δ): 2.35-3.78 (m, 8H), 3.50 (s, 2H, CH$_2$Ph), 6.99-7.28 (m, 4H, ArH), 7.48 (bs, 2H, NH$_2$), 7.50 (d, J= 8.2 Hz, 2H, ArH), 7.97 (d, J= 8.2 Hz, 2H, ArH). Anal. for C$_{18}$H$_{20}$FN$_3$O$_3$S: C 57.28%; H 5.34%; N 11.13%. Found: C 57.55%; H 5.43%; N 11.34%.

50c **4–(4–Benzhydrylpiperazine–1–carbonyl)benzenesulfonamide**
(CAS Number: **2260622–26–0**)

Yield: 60%; m.p.: $228 – 230°C$; R_f (DCM/MeOH 96:4 v/v): 0.58; ^{1}H-NMR (DMSO-d_6) (δ): 2.26-4.32 (m, 9H), 7.16-7.39 (m, 10H, ArH), 7.41(bs, 2H, NH$_2$), 7.52 (d, J= 8.2 Hz, 2H, ArH), 7.81 (d, JJ= 8.2 Hz 2H, ArH). Anal. for C$_{24}$H$_{25}$N$_3$O$_3$S: C 66.18%; H 5.79%; N 9.65%. Found: C 66.28%; H 5.69%; N 9.55%.

50d **4–(4–Phenylpiperazine–1–carbonyl)benzenesulfonamide**
(CAS Number: **1015405–80–7**)

Yield 84%; m.p.: $231 – 232°C$; R_f (DCM/MeOH 96:4 v/v): 0.59; ^{1}H-NMR (DMSO-d_6) (δ): 3.10-3.89 (m, 8H), 6.80-7.24 (m, 5H, ArH), 7.42 (bs, 2H, NH$_2$2), 7.58 (d, J= 8.2 Hz, 2H, ArH), 7.84 (d, J= 8.2 Hz, 2H, ArH). Anal. for C$_{17}$H$_{19}$N$_3$O$_3$S: C 59.11%; H 5.54%; N 12.16%. Found: C 58.81%; H 5.24%; N 12.06%.

4.1.2 General procedures for the synthesis of phenyl(piperazin–1–yl)methanone derivatives 53a–p

To a well–stirred solution of 1-Boc-piperazine 51 (1 molar equivalent) in DCM (3 mL), N,N–Diisopropylethylamine (DIPEA) (1.5 molar equivalents) and the appropriate benzoyl chloride derivative 52a–p (1 molar equivalent) was added in ice bath. The resulting mixture was brought to room temperature, stirred for different reaction times at room temperature and monitored by TLC until the disappearance of the starting materials. The reaction mixture was then cooled down to $0°C$, treated with trifluoroacetic acid (TFA) (8 molar equivalents) and consequently stirred for three hours at room temperature. After the reaction was completed

it was cooled into ice and diluted with DCM (2 mL) and 2M K_2CO_3 (2 mL). The mixture was extracted with DCM (3×5 mL), the combined organic layers were dried over Na_2SO_4, filtered, and concentrated under vacuo. The residue was purified by treatment with Et_2O giving the desired final compounds 53a–p . The registered CAS numbers for resulting compounds 53a–p have been already assigned and chemical properties, such as structural characterization, are available in literature.

Cmpds	CAS Number	Cmpds	CAS Number
53a	13754–38–6	53i	1016819–18–3
53b	139516–64–6	53j	59939–72–9
53c	179334–10–2	53k	100939–88–6
53d	102391–98–0	53l	100939–89–7
53e	13754–45–5	53m	94747–49–8
53f	100939–90–0	53n	885101–42–8
53g	54042–47–6	53o	341529–34–8
53h	926202–11–1	53p	72141–41–4

4.1.3 General procedures for the synthesis of 4–(4–benzoylpiperazine–1carbonyl) benzenesulfonamide derivatives 54a–p

To a solution of 4–(aminosulfonyl)benzoic acid 46 (2 molar equivalents) dissolved in dimethylformamide (DMF) (2 mL), HBTU was added (2 mmol). The mixture was stirred at room temperature for one hour. Then, TEA (2 molar equivalents) and appropriate 4-benzoylpiperazine derivatives 53a–p (2 molar equivalents) were added. The reaction mixture was left overnight at room temperature and then quenched with H_2O (10 mL) and extracted with EtOAc (3×10 mL). The organic phase was washed with saturated NaCl solution, dried with Na_2SO_4 and concentrated until dryness under reduced pressure. The residue was purified by crystallization from Et_2O and EtOH to give the desired final compounds 54a–p as white powder.

54a **4–(4–Benzoylpiperazine–1–carbonyl)benzenesulfonamide**

Yield: 45%; m.p.: 248 – 249°C; R_f = 0.24. ^{1}H-NMR (DMSO-d_6) (δ): 3.55-3.93 (m, 8H, CH_2), 7.40-7.47 (m, 5H, ArH), 7.50 (s, 2H, NH2), 7.62 (d, J= 8.2 Hz, 2H, ArH), 7.89 (d, J= 8.2 Hz, 2H, ArH); ^{13}CNMR (DMSO-d6): 42.13, 47.71, 125.64, 126.99, 127.65, 128.33, 129.64, 135.45, 138.62, 144.91, 169.33, 171.66. Anal. for $C_{18}H_{19}N_3O_4S$: C 57.89%; H 5.13%; N 11.25%; Found: C 57.99%; H 5.23%; N 11.35%.

54b **4–[4–(2–Fluorobenzoyl)piperazine–1–carbonyl]benzenesulfonamide**

Yield: 72%; m.p.: 268 – 269°C; R_f = 0.12. ^{1}H-NMR (DMSO-d_6) (δ): 3.55-3.76 (m, CH$_2$, 8H), 7.31-7.44 (m, 4H, ArH), 7.49 (s, 2H, NH$_2$), 7.57-7.65 (m, 2H, ArH), 7.88-7.95 (m, 2H, ArH). Anal. for C$_{18}$H$_{18}$FN$_3$O$_4$S: C 55.23%; H 4.64%; N 10.74%; Found: C 55.33%; H 4.74%; N 10.54%.

54c **4-[4-(3-Fluorobenzoyl)piperazine-1-carbonyl]benzenesulfonamide**

Yield: 43%; m.p.: 214 – 215°C; R_f = 0.11. ^{1}H-NMR (DMSO-d_6) (δ): 3.57-3.76 (m, 8H, CH$_2$), 7.23-7.33 (m, 3H, ArH), 7.49 (s, 2H, NH$_2$). 7.61-7.64 (m, 3H, ArH), 7.87-7.90 (m, 2H, ArH). Anal. for C$_{18}$H$_{18}$FN$_3$O$_4$S: C 55.23%; H 4.64%; N 10.74%. Found: C 55.03%; H 4.44%; N 10.54%.

54d **4–[4–(4–Fluorobenzoyl)piperazine–1–carbonyl]benzenesulfonamide**

Yield: 42%; m.p.: 212 – 213°C; R_f = 0.10. ^{1}H-NMR (DMSO-d_6) (δ): 3.03-3.40 (m, 8H, CH$_2$), 7.26-7.33 (m, 1H, ArH), 7.49 (s, 2H, NH$_2$), 7.60-7.74 (m, 2H, ArH), 7.83-8.01 (m, 4H, ArH), 8.11-8.14 (m, 1H, ArH) . Anal. for C$_{18}$H$_{18}$FN$_3$O$_4$S: C 55.23%; H 4.64%; N 10.74%. Found: C 55.13%; H 4.54%: N 10.64%.

54e **4–[4–(2–Chlorobenzoyl)piperazine–1–carbonyl]benzenesulfonamide**

Yield: 63%; m.p.: 249 – 250°C; R_f = 0.15. ^{1}H-NMR (DMSO-d_6) (δ): 3.16 (m, 2H, CH$_2$), 3.24 (m, 2H, CH$_2$), 3.67-3.73 (m, 4H, CH$_2$), 7.43 (m, 4H, ArH), 7.50 (s, 2H, NH$_2$), 7.62 (d, J= J= 8.2 Hz, 2H, ArH), 7.88 (d, J= 8.2 Hz, 2H, ArH). Anal. for C$_{18}$H$_{18}$ClN$_3$O$_4$S: C 53.01%; H 4.45%; N 10.30%. Found: C 52.91%; H 4.35%; N 10.20%.

54f **4–[4–(3–Chlorobenzoyl)piperazine–1–carbonyl]benzenesulfonamide**

Yield: 63%; m.p.: 193 – 194°C; R_f = 0.15. ^{1}H-NMR (DMSO-d_6) (δ): 3.27-3.41 (m, 4H, CH$_2$), 3.62-3.67 (m, 4H,), 7.37-7.43 (m, 2H, ArH), 7.49 (s, 2H, NH$_2$), 7.62-7.70 (m, 4H, ArH), 7.78-7.90 (m, 2H, ArH). Anal. for C$_{18}$H$_{18}$ClN$_3$O$_4$S: C 53.01%; H 4.45%; N 10.30%. Found: C 53.11%; H 4.55%; N 10.40%.

54g 4–[4–(4–Chlorobenzoyl)piperazine–1–carbonyl]benzenesulfonamide

Yield: 50%; m.p.: $245-246°C$; $R_f = 0.14$. ^{1}H-NMR (DMSO-d_6) (δ): 3.50-3.75 (m, 8H, CH$_2$), 7.41-7.48 (m, 2H, ArH), 7.50 (s, 2H, NH$_2$), 7.52-7.54 (m, 2H, ArH), 7.63 (d, J=8.2, 2H, ArH), 7.87 (d, J=8.2, 2H, ArH); ^{13}CNMR (DMSO-d6): 41.84, 46.94, 125.99, 127.76, 128.70, 129.20, 134.41, 134.55, 138.87, 145.04, 168.20, 168.41. Anal. for C$_{18}$H$_{18}$ClN$_3$O$_4$S: C 53.01%; H 4.45%; N 10.30%. Found: C 53.21%; H 4.65%; N 10.50%.

54h 4–[4–(2–Bromobenzoyl)piperazine–1–carbonyl]benzenesulfonamide

Yield: 49%; m.p.: $209-210°C$; $R_f = 0.19$. ^{1}H-NMR (DMSO-d_6) (δ): 3.22-3.40 (m, 4H, CH$_2$), 3.69-3.74 (m, 4H, CH$_2$), 7.32-7.39 (m, 3H, ArH), 7.49 (s, 2H, NH$_2$), 7.54-7.69 (m, 3H, ArH), 7.82-7.90 (m, 2H, ArH). Anal. for C$_{18}$H$_{18}$BrN$_3$O$_4$S: C 47.80%; H 4.01%; N 9.29%. Found: C 47.68%; H 4.21%; N 9.41%.

54i 4–[4–(3–Bromobenzoyl)piperazine–1–carbonyl]benzenesulfonamide

Yield: 86%; m.p.: $193-194°C$; $R_f = 0.18$. ^{1}H-NMR (DMSO-d_6) (δ): 3.52-3.87 (m, 8H, CH$_2$), 7.38-43 (m, 2H, ArH), 7.50 (s, 2H, NH$_2$), 7.59-7.68 (m, 4H, ArH), 7.83-7.92 (m, 2H, ArH). Anal. for C$_{18}$H$_{18}$BrN$_3$O$_4$S: C 47.80%; H 4.01%; N 9.29%. Found: C 47.98%; H 4.11%; N 9.39%.

54j 4–[4–(4–Bromobenzoyl)piperazine–1–carbonyl]benzenesulfonamide

Yield: 47%; m.p.: $222-223°CC$; $R_f = 0.18$. ^{1}H-NMR (DMSO-d_6) (δ): 3.51-3.75 (m, 8H, CH$_2$), 7.43- (m, 2H, ArH), 7.51 (s, 2H, NH$_2$), 7.53-7.58 (m, 2H, ArH), 7.63-7.70 (m, 2H, ArH), 7.87-7.93 (m, 2H, ArH). Anal. for C$_{18}$H$_{18}$BrN$_3$O$_4$S: C 47.80%; H 4.01%; N 9.29%. Found: C 47.70%; H 3.91%; N 9.19%.

54k 4–[4–(2–Methoxybenzoyl)piperazine–1–carbonyl]benzenesulfonamide

Yield: 56%; m.p.: $268-269°C$; $R_f = 0.13$. ^{1}H-NMR (DMSO-d_6) (δ): 3.24 (m, 4H, CH$_2$), 3.57 (m, 4H, CH$_2$), 3.90 (s, 3H, OCH$_3$), 6.98-7.38 (m, 4H, ArH), 7.50 (s, 2H, NH$_2$), 7.60-7.65 (m, 2H, ArH). 7.79-7.86 (m, 2H, ArH). Anal. for C$_{19}$H$_{21}$N$_3$O$_5$S: C 56.56%; H 5.25%; N 10.42%. Found: C 56.36%; H 5.05%; N 10.22%.

54l 4–[4–(3–Methoxybenzoyl)piperazine–1–carbonyl]benzenesulfonamide

Yield: 43%; m.p.: $144 - 145°C$°C; $R_f = 0.13$. ^{1}H-NMR (DMSO-d_6) (δ): 3.36-3.63 (m, 4H, CH$_2$), 3.77 (s, 3H, OCH$_3$), 4.23-4.63 (m, 4H, CH$_2$), 6.95-7.03 (m, 3H, ArH), 7.45-7.49 (m, 1H, ArH), 7.50 (s, 2H, NH$_2$), 7.61-7.64 (m, 2H, ArH). 7.87-7.90 (m, 2H, ArH). Anal. for C$_{19}$H$_{21}$N$_3$O$_5$S: C 56.56%; H 5.25%; N 10.42%. Found: C 56.36%; H 5.05%; N 10.22%.

54m 4–[4–(4–Methoxybenzoyl)piperazine–1–carbonyl]benzenesulfonamide

Yield: 52%; m.p.: $260 - 261°C$; $R_f = 0.12$. ^{1}H-NMR (DMSO-d_6) (δ): 3.34-3.47 (m, 4H, CH$_2$), 3.56-3.68 (m, 4H, CH$_2$), 3.71 (s, 3H, OCH$_3$), 6.97-7.01 (m, 2H, ArH), 7.37-7.41 (m, 2H, ArH), 7.50 (s, 2H, NH$_2$), 7.63-7.65 (d, J= 8.2 Hz, 2H, ArH). 7.86-7.90 (d, J= 8.2 Hz, 2H, ArH). Anal. for C$_{19}$H$_{21}$N$_3$O$_5$S: C 56.56%; H 5.25%; N 10.42%. Found: C 56.46%; H 5.15%; N 10.32%.

54n 4–[4–(2–Nitrobenzoyl)piperazine–1–carbonyl]benzenesulfonamide

Yield: 55%; m.p.: $231 - 232°C$; $R_f = 0.16$. ^{1}H-NMR (DMSO-d_6) (δ): 3.37-3.77 (m, 8H, CH$_2$), 7.48 (m, 2H, NH$_2$), 7.56-7.77 (m, 4H, ArH), 7.83-7.96 (m, 3H, ArH), 8.20-8.25 (m, 1H, ArH). Anal. for C$_{18}$H$_{18}$N$_4$O$_6$S: C 51.67%; H 4.34%; N 13.39%. Found: C 51.71%; H 4.39%; N 13.44%.

54o 4–[4–(3–Nitrobenzoyl)piperazine–1–carbonyl]benzenesulfonamide

Yield: 75%; m.p.: $243 - 244°C$; $R_f = 0.18$. ^{1}H-NMR (DMSO-d_6) (δ): 3.38-3.49 (m, 4H, CH$_2$), 3.65-3.74 (m, 4H, CH$_2$), 7.45 (s, 2H, NH$_2$), 7.61-8.29 (m, 8H, ArH). Anal. for C$_{18}$H$_{18}$N$_4$O$_6$S: C 51.67%; H 4.34%; N 13.39%.Found: C 51.70%, H 4.28%, N 13.53%.

54p 4–[4–(4–Nitrobenzoyl)piperazine–1–carbonyl]benzenesulfonamide

Yield: 77%; m.p.: $272 - 273°C$; $R_f = 0.18$. ^{1}H-NMR (DMSO-d_6) (δ): 3.30-3.40 (m, 4H, CH$_2$), 3.64-3.74 (m, 4H, CH$_2$), 7.46 (m, 2H, NH$_2$), 7.61-8.29 (m, 8H, ArH). Anal. for C$_{18}$H$_{18}$N$_4$O$_6$S: C 51.67%; H 4.34%; N 13.39%. Found: C 51.77%; H 4.44%; N 13.49%.

4.1.4 General procedures for the preparation of compounds 54q–s

To a suspension of the aroyl-nitro derivatives 54n–p (1 molar equivalent) and a catalytic amount of Pd/C in EtOH (15 *mL*), hydrazine hydrate (N$_2$H$_4 \cdot$ H$_2$O) (10 molar equivalents) was

slowly added. The reaction was stirred and refluxed ($70°C$) under nitrogen atmosphere. Then, the mixture was filtered through celite cake, which was washed with EtOAc. The solution was evaporated in vacuo to give the crude product, then dissolved in EtOAc and washed with H_2O (3×10 mL). The organic phase was dried over Na_2SO_4 and concentrated until dryness. The residue was purified by crystallization from Et_2O and EtOH to give the title compounds 54q–s.

54q **4–[4–(2–Aminobenzoyl)piperazine–1–carbonyl]benzenesulfonamide**

Yield: 99%; m.p.: $231 - 232°C$; $R_f = 0.10$. ^{1}H-NMR (DMSO-d_6) (δ): 3.36-3.76 (m, 8H, CH$_2$), 5.20 (bs, 2H, NH$_2$), 6.56 (t, $J= 7.6$ Hz, $J= 7.4$ Hz, 1H, ArH), 6.70 (d, $J= 8.1$ Hz, 1H, ArH), 7.01 (d, $J= 7.6$ Hz, 1H, ArH), 7.08 (t, J= 8.1, $J= 7.4$ Hz, 1H, ArH), 7.49 (s, 2H, NH$_2$), 7.60 (d, $J= 8.0$ Hz, 2H, ArH), 7.88 (d, $J= 8.0$ Hz, 2H, ArH). Anal. for C$_{18}$H$_{20}$N$_4$O$_4$S: C 55.66%; H 5.19%; N 14.42%. Found: C 55.63%; H 5.16%; N 14.39%.

54r **4–[4–(3–Aminobenzoyl)piperazine–1–carbonyl]benzenesulfonamide**

Yield: 87%; m.p.: $220 - 221°C$; $R_f =0.13$. ^{1}H-NMR (DMSO-d_6) (δ): 3.40-3.66 (m, 8H, CH$_2$), 5.26 (bs, 2H, NH$_2$), 6.50 (d, $J= 7.5$ Hz, 1H, ArH), 6.57 (s, 1H, ArH), 6.62 (d, $J= 7.5 Hz$, 1H, ArH,), 7.07 (t, 1H, ArH, $J= 7.5$ Hz), 7.48 (s, 2H, NH$_2$), 7.62 (d, $J= 8.2$ Hz, 2H, ArH), 7.89 (d, $J= 8.2$, Hz, 2H, ArH). Anal. for C$_{18}$H$_{20}$N$_4$O$_4$S: C 55.66%; H 5.19%; N 14.42%. Found: C 55.63%; H 5.16%; N 14.39%.

54s **4–[4–(4–Aminobenzoyl)piperazine–1–carbonyl]benzenesulfonamide**

Yield: 50%; m.p.: $229 - 230°C$; $R_f = 0.14$. 1H-NMR (DMSO-d_6) (δ): 3.49-3.65 (m, 8H, CH$_2$), 5.53 (bs, 2H, NH$_2$), 6.52 (d, $J= 8.4$ Hz, 2H, ArH), 7.13 (d, $J= 8.4$ Hz, 2H, ArH), 7.46 (s, 2H, NH$_2$), 7.59 (d, $J= 8.5$, Hz, 2H, ArH), 7.86 (d, $J= 8.5$, Hz, 2H, ArH). Anal. for C$_{18}$H$_{20}$N$_4$O$_4$S: C 55.66%; H 5.19%; N 14.42%. Found: C 55.62%; H 5.15%; N 14.38%.

4.1.5   Preparation of aroyl(piperazin–1–yl)methanone derivatives 56a-m

Pathway A: To a solution of 1–Boc–piperazine 51 (1 molar equivalent) in DCM/DMF (2 mL, 2:1, v/v) placed in a cylindrical quartz tube ($\varnothing$ 2 cm), DIPEA (1.5 molar equivalents) and the appropriate benzoyl chloride derivative 55a–c and 55h–k (1 molar equivalent) were added. The mixture was subjected to microwave irradiation at 250 W for 10 minutes at 25°C. Thus, TFA (8 molar equivalents) was added to the reaction mixture at 0°C and solution was irradiated in a microwave oven at 250 W for 5 minutes and at 25°C. After the reaction was completed, it was cooled into ice and diluted with DCM (2 mL) and 2M K_2CO_3 solution (2

mL). The mixture was extracted with DCM (3×5 *mL*), the combined organic layers were dried over Na_2SO_4, filtered, and concentrated under vacuo. The residue was purified by treatment with Et_2O giving the desired known intermediates 56a–c and 56h–k.

Pathway B: To a solution of the appropriate carboxylic acids 55d, 55f-g and 55l-m (1 molar equivalent) in DCM/DMF (2 *mL*, 2:1, v/v) placed in a cylindrical quartz tube (ø 2 *cm*), HBTU was added. The mixture was subjected to microwave irradiation at 250 *W* for 1 minute at 25°*C*. After this time, 1-Boc-piperazine 51 (1 molar equivalent) and DIPEA (2.5 molar equivalents) were added and solution was irradiated in a microwave oven at 250 W for 25 minutes and at 25°*C*. Thus, the reaction mixture was cooled down in ice bath, treated with TFA (8 molar equivalents) and irradiated in a microwave oven at 250 *W* for 5 minutes and at 25°*C*. When the reaction was completed, it was cooled into ice and diluted with DCM (2 *mL*) and 2M K_2CO_3 solution (2 *mL*). The mixture was extracted with DCM (3×5 *mL*), the combined organic layers were dried over Na_2SO_4, filtered and concentrated under vacuo. The residue was purified by treatment with Et_2O giving the desired known intermediates 56d, 56f and 56l–m. The chemical properties, as well as the structural assignments, for the resulting compounds 56a–m were in good agreement with the literature. The registered CAS numbers have been already assigned as reported below.

Cmpds	CAS Number		56g	1058149–42–0
56a	610802–12–5		56h	40172–95–0
56b	52063–83–9		56i	681837–54–7
56c	1016714–98–9		56j	864815–70–3
56d	1274828–07–7		56k	41717–31–1
56e	864815–96–3		56l	1038285–42–5
56f	104554–65–6		56m	136818–95–6

4.1.6 Synthesis of 4-(4-aroylpiperazine-1carbonyl)-benzenesulfonamide 57a-m

A solution of 4–(aminosulfonyl)benzoic acid 46 (1 molar equivalent) and HBTU (1 molar equivalent) dissolved in DMF (2 *mL*) was subjected to microwave irradiation at 250 *W* for 1 minute at 25°*C*. Then, TEA (2 molar equivalents) and appropriate 4–benzoylpiperazine derivatives 56a–m (1 molar equivalent) were added and the resulted mixture was irradiated in a microwave oven at 250 *W* for 25 minutes and at 25°*C*. The reaction crude was quenched H_2O (15 *mL*) and extracted with EtOAc (3×15 *mL*). The organic phase was washed with saturated NaCl solution, dried with Na_2SO_4 and concentrated until dryness under reduced pressure. The residue was purified by crystallization from Et_2O and EtOH to give the desired final compounds 57a–m as white powder.

57a 4–(4–(2–Naphthoyl)piperazine–1–carbonyl)benzenesulfonamide

Yield: 22%; m.p.: $273 - 275°C$; R_f (DCM/MeOH, 92:8, v/v): 1.39. ^{1}H–NMR (DMSO–d_6) (δ): 3.43–3.69 (m, 8H, CH$_2$), 7.51–7.62 (m, 5H, ArH), 7.84–7.86 (m, 2H, ArH), 7.93–7.99 (m, 4H, ArH). Anal. for C$_{22}$H$_{21}$N$_3$O$_4$S: C 62.40%; H 5.00%; N 9.92%. Found: C 62.00%; H 4.60%; N 9.52%.

57b 4–(4–(Tiophene–2–carbonyl–)piperazine–1carbonyl)benzenesulfonamide

Yield: 40%; m.p.: $224 - 226°C$; R_f (DCM/MeOH, 92:8, v/v): 1.49. ^{1}H–NMR (DMSO–d_6) (δ): 3.41–3.76 (m, 8H, CH$_2$), 7.14 (t, J_1= 3.2 Hz, textitJ_2= 4.8 Hz, 1H, ArH), 7.03 (d, J= 3.2 Hz, 1H, ArH), 7.48 (bs, 2H, NH$_2$), 7.64 (d, (d, J= 8.2 Hz, 2H, ArH), 7.78 (d, (d, J= 4.8 Hz, ArH), 7.89 (d, J= 8.2 Hz, 2H, ArH). Anal. for C$_{16}$H$_{17}$N$_3$O$_4$S$_2$: C 50.64%; H 4.52%; N 11.07%. Found: C 50.44%; H 5.32%; N 10.87%.

57c 4–(4–(3–Methylthiophene–2–carbonyl)piperazine–1–carbonyl)- benzenesulfonamide

Yield: 28%; m.p.: $248 - 250°C$; R_f (DCM/MeOH, 92:8, v/v): 1.34. ^{1}H–NMR (DMSO–d_6) (δ): 2.20 (m, 3H, CH$_3$), 3.54–3.68 (m, 8H, CH$_2$), 6.94 (m, 1H, ArH), 7.47 (bs, 2H, NH$_2$), 7.59 (m, 1H, ArH), 7.63 (d, J= 8.2 Hz, 2H, ArH), 7.89 (d, J= 8.2 Hz, 2H, ArH). Anal. for C$_{17}$H$_{19}$N$_3$O$_4$S$_2$: C 51.89%; H 4.87%; N 10.68%. Found: C 52.19%; H 5.17%; N 10.98%.

57d 4–(4–(3–Bromothiophene–2–carbonyl)piperazine–1–carbonyl)- benzenesulfonamide

Yield: 28%; m.p.: $218 - 220°C$; R_f (DCM/MeOH, 92:8, v/v): 1.40. ^{1}H–NMR (DMSO–d_6) (δ): 3.56–3.76 (m, 8H, CH$_2$), 7.15 (d, J= 5.1 Hz, 1H, ArH), 7.48 (bs, 2H, NH$_2$), 7.62 (d, J= 8.2 Hz, 2H, ArH), 7.79 (d, J= 5.1 Hzz, 1H, ArH), 7.88 (d, J= 8.2 Hz, 2H, ArH). Anal. for C$_{16}$H$_{16}$BrN$_3$O$_4$S$_2$: C 41.93%; H 3.52%; N 9.17%. Found: C 41.53%; H 3.12%; N 8.77%.

57e 4–(4–(5–Chlorothiophen–2–yl)carbonyl]piperazin–1–yl)carbonyl)- benzenesulfonamide

Yield: 44%; m.p.: $217 - 219°C$; R_f (DCM/MeOH, 92:8, v/v): 1.37. ^{1}H–NMR (DMSO–d_6) (δ): 3.68–3.77 (m, 8H, CH$_2$), 7.17 (d, J= 3.9 Hz, 1H, ArH), 7.35 (d, J= 3.9 Hz, 1H, ArH), 7.49 (bs, 2H, NH$_2$), 7.63 (d, J= 8.2 Hz, 2H, ArH), 7.89 (d, J= 8.2 Hz, 2H, ArH). Anal. for C$_{16}$H$_{16}$ClN$_3$O$_4$S$_2$: C 46.43%; H 3.90%; N 10.15%. Found: C 46.13%; H 3.60%; N 9.85%.

57f **4–(4–(5–Nitrothiophen–2–yl)carbonyl)piperazin–1–yl)carbonyl)-benzenesulfonamide**

Yield: 32%; m.p.: 252 – 254°C; R_f (DCM/MeOH, 92:8, v/v): 1.37. ^{1}H–NMR (DMSO–d_6) (δ): 3.66–3.74 (m, 8H, CH$_2$), 7.45–7.54 (m, 3H, ArH, NH$_2$), 7.63 (d, J= 8.2 *Hz*, 2H, ArH), 7.89 (d, J= 8.2 *Hz*, 2H, ArH), 8.11 (s, 1H, ArH). Anal. for C$_{16}$H$_{16}$N$_3$O$_6$S$_2$: C 45.28%; H 3.80%; N 13.20%. Found: C 45.48%; H 4.00%; N 13.60%.

57g **4–(4–(1–Benzothiophen–2–ylcarbonyl)piperazin–1–yl]carbonyl)-benzenesulfonamide**

Yield: 43%; m.p.: 244 – 246°C; R_f (DCM/MeOH, 92:8, v/v): 1.18. ^{1}H–NMR (DMSO–d_6) (δ): 3.66–3.82 (m, 8H, CH$_2$), 7.44–7.46 (m, 3H, ArH), 7.49 (bs, 2H, NH$_2$), 7.64 (d, J= 8.2 *Hz*, 2H, ArH), 7.77 (s, 1H, ArH), 7.90 (d, J= 8.2 *Hz*, 2H, ArH), 8.01–8.02 (m, 1H, ArH). ^{13}C–NMR (DMSO–d_6) (δ):: 122.76, 125.20, 125.26, 126.06, 126.08, 126.29, 127.88, 136.78, 128.83, 139.00, 139.60. 145.16, 163.00, 168.32. Anal. for C$_{20}$H$_{19}$N$_3$O$_4$S$_2$: C 55.93%; H 4.46%; N 9.78%. Found: C 55.83%; H 4.36%; N 9.68%.

57h **4–(4–(Furan–2–carbonyl)piperazine–1–carbonyl)benzenesulfonamide**

Yield: 30%; m.p.: 211 – 213°C; R_f (DCM/MeOH, 92:8, v/v): 1.68. ^{1}H–NMR (DMSO–d_6) (δ): 3.37–3.79 (m, 8H, CH$_2$), 6.63 (m, 1H, ArH), 7.03 (m, 1H, ArH), 7.48 (bs, 2H, NH$_2$), 7.64 (d, J= 8.2 *Hz*, 2H, ArH), 7.85 (m, 1H, ArH), 7.89 (d, J= 8.2 *Hz*, 2H, ArH). ^{13}C–NMR (DMSO–d_6) (δ): 168.29, 158.75, 146.90, 145.17, 145.14, 139.02, 127.89, 126.09, 116.21, 111.64, 47.19, 41.97. Anal. for C$_{16}$H$_{17}$N$_3$O$_5$S: C 54.10%; H 5.07%; N 11.13%. Found: C 53.70%; H 4.67%; N 10.73%.

57i **4–(4–(3–Methylfuran–2–yl)carbonyl]piperazin–1–yl)carbonyl)-benzenesulfonamide**

Yield: 20%; m.p.: 189 – 191°C; R_f (DCM/MeOH, 92:8, v/v): 1.43. ^{1}H–NMR (DMSO–d_6) (δ): 2.16 (s, 3H, CH$_3$), 3.60–3.70 (m, 8H, CH$_2$), 6.63 (m, 1H, ArH), 7.48 (bs, 2H, NH$_2$), 7.63 (d, J= 8.2 *Hz*, 2H, ArH), 7.69 (m, 1H, ArH), 7.88 (d, J= 8.2 *Hz*, 2H, ArH). Anal. for C$_{17}$H$_{19}$N$_3$O$_5$S: C 54.10%; H 5.07%; N 11.13%. Found: C 53.70%; H 4.67%; N 10.73%.

57j **4–(4–(5–Nitrofuran–2–yl)carbonyl)piperazin–1–yl)carbonyl)-benzenesulfonamide**

Yield: 38%; m.p.: 253 – 255°C; R_f (DCM/MeOH, 92:8, v/v): 1.40. ^{1}H–NMR (DMSO–d_6) (δ): 3.74–3.89 (m, 8H, CH$_2$), 7.28 (m, 1H, ArH), 7.48 (bs, 2H, NH$_2$), 7.65 (d, J= 8.2 *Hz*z, 2H, ArH), 7.76 (m, 1H, ArH), 7.89 (d, J= 8.2 *Hz*, 2H, ArH). Anal. for C$_{16}$H$_{16}$N$_4$O$_7$S: C 54.10%; H 5.07%; N 11.13%. Found: C 53.70%; H 4.67%; N 10.73%.

57k **4–(4–(1–Benzofuran–2–ylcarbonyl)piperazin–1–yl)carbonyl)-benzenesulfonamide**

Yield: 55%; m.p.: $209 - 211°C$; R_f (DCM/MeOH, 92:8, v/v): 1.24. ^{1}H–NMR (DMSO–d_6) (δ): 3.65–3.89 (m, 8H, CH$_2$), 7.30–7.33 (m, 1H, ArH), 7.43–7.46 (m, 4H, ArH, NH$_2$), 7.62–7.64 (m, 3H, ArH), 7.72–7–74 (m, 1H, ArH), 7.87–7.89 (m, 2H, ArH). Anal. for C$_{20}$H$_{19}$N$_3$O$_5$S: C 58.10%; H 4.63%; N 10.16%. Found: C 58.30%; H 4.83%; N 10.36%.

57l **4–(4–(1H–Pyrrole–2–carbonyl)piperazine–1–carbonyl)benzenesulfonamide**

Yield: 62%; m.p.: $247 - 249°C$; R_f (DCM/MeOH, 92:8, v/v): 2.42. ^{1}H–NMR (DMSO–d_6) (δ): 3.71–3.81 (m, 8H, CH$_2$), 6.12 (m, 1H, ArH), 6.53 (m, 1H, ArH), 6.90 (m, 1H, ArH), 7.49 (bs, 2H, NH$_2$2), 7.64 (d, J= 8.2 Hz, 2H, ArH), 7.90 (d, J= 8.2 Hz, 2H, ArH), 11.47 (bs, 1H, NH). Anal. for C$_{15}$H$_{16}$N$_2$O$_5$S: C 53.03%; H 5.01%; N 15.46%. Found: C 53.13%; H 5.11%; N 15.56%.

57m **4–(4–(1H–Indole–2–carbonyl)piperazine–1–carbonyl)benzenesulfonamide**

Yield: 73%; m.p.: $239 - 241°C$; R_f (DCM/MeOH, 92:8, v/v): 2.42. ^{1}H–NMR (DMSO–d_6) (δ): 3.22–4.00 (m, 8H, CH$_2$), 6.84 (bs, 1H, NH), 7.03–7.06 (m, 1H, ArH), 7.18–7.21 (m, 1H, ArH), 7.44–7.61 (m, 4H, ArH, NH$_2$), 7.65–7.66 (m, 2H, ArH), 7.91–7.94 (m, 2H, ArH), 11.66 (bs, 1H, NH). Anal. for C$_{20}$H$_{20}$N$_4$O$_5$S: C 58.24%; H 4.89%; N 13.58%. Found: C 58.19%; H 4.93%; N 13.47%.

4.1.7 General procedures for the synthesis of coumarin acetates 62a–64a

A solution of suitable starting compound 7–hydroxycoumarin (59), 6,7–dihydroxycoumarin (60) or 6–hydroxycoumarin (61) (1 molar equivalent) was stirred with acetic anhydride (3 *mL*) in ice bath for 5 minutes and then a catalytic amount of 96% sulfuric acid was added dropwise. After that, TEA (2.5 molar equivalents) was added to the mixture and stirred at 350 rpm until the disappearance of starting compounds (analyzed by TLC, CyHe/EtOAc 80:20 v/v). After reaction was completed, it was quenched with crushed ice flakes and the solid was filtered off and dried to afford the corresponding compounds 62a–64a that were recrystallized from Et$_2$O or EtOH.

62a **2–Oxo–2H–chromen–7–yl acetate**
(CAS Number: 10387–49–2)

Yield: 80%; m.p. (Et$_2$O): $133 - 145°C$; reaction time: 1.5 h; R_f (CyHe/EtOAc 80:20 v/v): 0.17; ^{1}H–NMR (CDCl$_3$) (δ): 2.34 (s, 3H, CH$_3$), 6,40 (d, J= 10.2 Hz, 1H, CH), 7.05 (dd, J_1= 8.4 Hz, J_2= 2.2 Hz, 1H,

ArH), 7.12 (d,*J*= 2.2 *Hz*, 1H, ArH), 7.49 (d, *J*= 8.4 *Hz*, 1H, ArH), 7.70 (d, *J*= 10.2 *Hz*, 1H, CH). Anal for. $C_{11}H_8O_4$: C 64.7%, H 3.9%; Found: C 64.3%, H 3.6%.

63a **2–Oxo–2*H*–chromene–6,7–diyl diacetate**
(CAS Number: **10387–49–2**)

Yield: 78%, m.p. (EtOH): 127 – 129°*C*; reaction time: 2 h;R_f (CyHe/EtOAc 80:20 v/v): 0.20; ^{1}H–NMR $(CDCl_3)$ (δ): 2.32 (s, 3H, CH_3), 2.34 (s, 3H, CH_3), 6.43 (d, J_2= 10.2 *Hz*, 1H, CH), 7.26 (s, 1H, ArH), 7.35 (s, 1H, ArH), 7.64 (d, J_2= 10.2 *Hz*, 1H, CH); ^{13}C–NMR $(CDCl_3)$ (δ): 20.8, 112.5, 117.0, 117.1, 121.8, 138.9, 142.5, 144.9, 151.8, 160.0, 167.7. Anal. for $C_{13}H_{10}O_6$:C 63.6%; H 3.5%. Found: C 63.2%; H 3.8%.

64a **2–Oxo–2*H*–chromen–6–yl acetate**
(CAS Number: **20690–03–3**)

Yield: 64%; m.p. (Et$_2$O): 143 – 145°*C*; reaction time: 1.5 h; R_f (CyHe/EtOAc, 80:20 v/v): 0.16; ^{1}H–NMR $(CDCl_3)$ (δ): 2.32 (s, 3H, CH_3), 6.45 (d, *J*= 10.1 *Hz*, 1H, CH), 7.23–7.25 (m, 2H, ArH), 7.36 (m, 1H, ArH), 7.65 (d, *J*= 10.1 *Hz*„ 1H, CH). Anal. for $C_{11}H_8O_4$: C 64.7%; H 3.9%. Found: C 64.3%; H 3.6%.

4.1.8   General procedures for synthesis of benzoate derivatives 62a–64b

To a well stirred solution of suitable starting material 7–hydroxycoumarin (59), 6,7–dihydroxy-coumarin (60) or 6–hydroxycoumarin (61) (1 molar equivalent) in DCM (2 *mL)* and TEA (2.5 molar equivalents), benzoyl chloride (5 molar equivalents) were slowly added in ice bath. After 10 minutes, the mixture was allowed to room temperature and stirred until the complete conversion of starting material (monitored by TLC, CyHe/EtOAc 80:20 v/v). Then, the solid in suspension was filtered off and recrystallized from appropriate solvent.

62b **2–Oxo–2*H*–chromen–7–yl benzoate**
(CAS Number: **31005–05–7**)

Yield: 78%; m.p. (MeOH): 158 – 160°*C* ; reaction time: 20h; R_f (CyHe/EtOAc 80:20 v/v): 0.22; ^{1}H–NMR $(CDCl_3)$ (δ): 6.42 (d, J= 9.6 Hz, 1H, CH), 7.19 (dd, J_1= 8.4 *Hz*, J_1= 2.2 *Hz*, 1H, ArH), 7.53 (d, *J*= 2.2 *Hz*, 1H, ArH), 7.48–760 (m, 3H, ArH), 7.66 (d, *J*= 8.4 *Hz*, 1H, ArH), 7.72 (d, *J*= 9.6 *Hz*, 1H, CH), 8.19–8.22 (m, 2H, ArH). Anal. for $C_{16}H_{10}O_4$: C 72.1%, H 3.7%; Trov: C 72.3%, H 3.9%.

63b **2–Oxo–2*H*–chromene–6,7–diyl dibenzoate**
(CAS Number: **87997–42–0**)

Yield: 82%, m.p. (MeCN): 185–187°*C*; reaction time: 20h; R_f (CyHe/EtOAc 80:20 v/v): 0.18; ^{1}H–NMR $(CDCl_3)$ (δ): 6.48 (d, *J*= 9.6 *Hz*, 1H, CH), 7.26 (s, 1H, ArH), 7.39 (m, 4H, ArH), 7.44 (s, 1H, ArH), 7.56

(m, 2H, ArH), 7.72 (d, J= 9.6 Hz, 1H, CH), 8.05 (m, 4H, ArH); ^{13}C–NMR (CDCl$_3$) (δ): 110.8, 116.3, 116.9, 118.7, 128.8, 128.9, 130.4, 134.2, 134.2, 143.0, 153.6, 154.9, 160.4, 164.6. Anal. for C$_{23}$H$_{14}$O$_6$: C 71.5%, H 3.65%; Trov: C 71.1%, H 3.9%.

64b   **2–Oxo–2H–chromen–6–yl benzoate**
(CAS Number: **35924–43–7**)

Yield: 60%; m.p. (MeOH): 137 – 139°C; reaction time: 20 h; R_f (CyHe/EtOAc 80:20 v/v): 0.23; ^{1}H–NMR (DMSO–d_6) (δ): 6.53 (m, 1H, CH), 6.56 (m, 1H, CH), 7.50–7.60 (m, 3H, ArH), 7.72–7.74 (m, 2H, ArH), 8.02–8.06 (m, 1H, ArH), 8.11–8.14 (m, 2H,ArH). Anal. for C$_{16}$H$_{10}$O$_4$: C 72.1%, H 3.7%. Found: C 72.3%, H 3.9%.

4.1.9   Synthesis of 4–arylcoumarins 69a–h, 70a–h, 71a and 71h

To an ice–cold solution of resorcinol **66**, 2–methylresorcinol **67** or 2–chlororesorcinol **68** (1 molar equivalent) in the appropriate ethylbenzoylacetate derivatives (**65a–h**, 1 molar equivalent), 96% w/v sulphuric acid (2 mL) was added drop wises. The mixture is brought to room temperature and stirred at 350 rpm by a stirring magnet bar for 24 hours, then time TLC (CyHe/EtOAc 80:20 v/v or 60:40 v/v) showed the disappearance of both starting materials. The reaction mixture was quenched with crushed ice, subsequently diluted with H$_2$O (10 mL) and extracted with EtOAc (3 × 10 mL). The organic layer was dried with Na$_2$SO$_4$and concentrated until dryness under reduced pressure. The targeted compounds **69a–h**, **70a–h**, **71a** and **71h** were isolated from the crude by crystallization from suitable solvent.

69a   **7–Hydroxy–4–phenyl–2H–chromen–2–one**

Yield: 53%. m.p. (Et$_2$O): 195 – 197°C; reaction time: 2.5 h; R_f (CyHe/EtOAc, 80:20 v/v): 0.16; ^{1}H–NMR (DMSO–d_6) (δ): 6.14 (s, 1H, CH), 6.76–6.80 (m, 2H, ArH), 7.27 (m, 1H, ArH), 7.49– 7.56 (m, 5H, ArH), 10.65 (bs, 1H, OH). Anal. for C$_{15}$H$_{10}$O$_3$: C 75.62%; H 4.23%; Found: C 75.72%; H 4.33%.

69b   **4–(2–Chlorophenyl)–7–hydroxy–2H–chromen–2–one**

Yield: 22%; m.p. (Et$_2$O): 218 – 220°C; reaction time: 2.5 h; R_f (CyHe/EtOAc, 80:20 v/v): 0.16; ^{1}H–NMR (DMSO–d_6) (δ): 6.16 (s, 1H, CH), 6.72–6.77 (m, 3H, ArH), 7.45–7.50 (m, 3H, ArH), 7.52–7.62 (m, 1H, ArH), 10.69 (bs, 1H, OH). Anal. for C$_{15}$H$_9$ClO$_3$: C 66.1% H 3.3%; Found: C 65.8%; H 3.0%.

69c **4–(3–Chlorophenyl)–7–hydroxy–2*H*–chromen–2–one**

Yield 31%; m.p. (EtOH): 237 – 239°*C*; reaction time: 2 h; R_f (CyHe/EtOAc, 80:20 v/v): 0.16; ^{1}H–NMR (DMSO–d_6) (δ): 6.18 (s, 1H, CH), 6.74–6.78 (m, 2H, ArH), 7.18 (m, 1H, ArH), 7.40 (m, 1H, ArH), 7.55–7.58 (m, 3H, ArH). Anal. for $C_{15}H_9ClO_3$: C 66.1%; H 3.3%; Found: C 65.9%; H 3.4%.

69d **4–(4–Chlorophenyl)–7–hydroxy–2*H*–chromen–2–one**

Yield: 33%; m.p. (EtOH): 280 – 282°C*C*; reaction time: 2.5 h; R_f (CyHe/EtOAc, 80:20 v/v): 0.16; ^{1}H–NMR (DMSO–d_6) (δ): 6.16 (s, 1H, CH), 6.76 (d, *J*= 8.8 *Hz*, 2H, ArH), 7.22 (m, 1H, ArH), 7,53 (d, *J*= 8.8 *Hz*, 2H, ArH), 7.59 (m, 2H, ArH), 10.70 (bs, 1H, OH). Anal. for $C_{15}H_9ClO_3$: C 66.1%; H 3.3%; Found: C 65.8%; H 3.1%.

69e **4–(2–Fluorophenyl)–7–hydroxy–2*H*–chromen–2–one**

Yield: 98%. m.p. (EtOH): 224 – 225°C; reaction time: 3 h; R_f (CyHe/EtOAc, 80:20 v/v): 0.16; ^{1}H–NMR (DMSO–d_6) (δ): 6.26 (s, 1H, CH), 6.76 (d, *J*= 8.7 *Hz*, 1H), 6.80 (s, 1H, ArH), 7.05 (d, *J*= 8.7 *Hz*, 1H, ArH), 7.50 (m, 4H, ArH), 10.76 (s, 1H, OH). Anal. for $C_{15}H_9O_3F$: C 70.31%, H 3.54%; Found: C 70.13%, H 3.85%.

69f **7–Hydroxy–4–(3–methylphenyl)–2*H*–chromen–2–one**

Yield: 32%; m.p. (Et$_2$O): 210 – 212°C; reaction time: 3 h; R_f (CyHe/EtOAc, 80:20 v/v): 0.18; ^{1}H–NMR (DMSO–d_6) (δ): 2.35 (s, 3H, CH$_3$), 5.98 (s, 1H, CH), 6.65 (m, 2H, ArH), 7.19 (d, 1H, ArH), 7.24–7.28 (m, 3H, ArH), 7.39 (m, 1H, ArH). Anal. for $C_{16}H_{12}O_3$: C 76.2%; H 4.8%. Found: C 75.9%; H 4.5%.

69g **7–Hydroxy–4–(4–methylphenyl)–2*H*–chromen–2–one**

Yield: 13%; m.p. ((Et$_2$O)/EtOH): 236 – 238°C; reaction time: 4 h; R_f (CyHe/EtOAc, 80:20 v/v): 0.16; ^{1}H–NMR (DMSO–d_6) (δ): 2.37 (s, 3H, CH$_3$), 6.09 (s, 1H, CH), 6.74–6.76 (m, 2H, ArH), 7.35–7.37 (m, 5H, ArH). Anal. for $C_{16}H_{12}O_3$: C 76.2%; H:4.8. Found: C 75.8%; H 4.6%.

69h **7–Hydroxy–4–(4–nitrophenyl)–2*H*–chromen–2–one**

Yield: 89%; m.p. (EtOAc): 178 – 180°C; reaction time: 1.5 h; R_f (CyHe/EtOAc, 80:20 v/v): 0.33; ^{1}H–NMR (DMSO–d_6) (δ): 6.24 (s, 1H, CH), 6.77 (m,1H, CH), 6.84 (m, 1H, CH), 7.15 (m, 1H, CH), 7.79 (d, J= 8.5 Hz, 2H, ArH), 8.35 (d, J= 8.5 Hz, 2H, ArH). Anal. for $C_{15}H_9NO_5$: C 63.6%; H 3.2%, N 4.9%. Found: C 63.4%; H 3.3%; N 4.7%.

70a **7–Hydroxy–8–methyl–4–phenyl–2*H*–chromen–2–one**

Yield: 50%; m.p. (EtOH): 223 – 225°C; reaction time: 4 h; R_f (CyHe/EtOAc 8:2): 0.20. ^{1}H–NMR (DMSO–d_6) (δ): 2.19 (s, 3H, CH$_3$), 6.13 (s, 1H, CH), 6.82 (d, J= 8.6 Hz, 1H, ArH), 7.10 (d,J= 8.6 Hz, 1H, ArH), 7.49–7.54 (m, 5H, ArH), 10.54 (bs, 1H, OH. Anal. For $C_{16}H_{12}O_3$: C 76.18%; H 4.79%; Found: C 75.88%, H: 4.49%.

70b **4–(2–Chlorophenyl)–7–hydroxy–8–methyl–2*H*–chromen–2– one**

Yield: 70%. m.p. (EtOH): 240 – 242°C; reaction time: 2.5 h; R_f (CyHe/EtOAc, 80:20 v/v): 0.22; ^{1}H–NMR (DMSO–d_6) (δ): 2.18 (s, 3H, CH$_3$), 6.15 (s, 1H, CH), 6.65 (d,J= 8.8 Hz, 1H, ArH), 6.77 (d, J= 8.8 Hz, 1H, ArH), 7.41–7.65 (m, 4H, ArH), 10.56 (bs, 1H, OH). Anal. for $C_{16}H_{11}ClO_3$: C 67.0%; H 3.9%. Found: C 66.8%; H 3.7%.

70c **4–(3–Chlorophenyl)–7–hydroxy–8–methyl–2*H*–chromen–2–one**

Yield: 79%; m.p. (EtOH): 315 – 317°C; reaction time: 2.5 h; R_f (CyHe/EtOAc, 80:20 v/v): 0.22; ^{1}H–NMR (DMSO–d_6) (δ): 2.18 (s, 3H, CH$_3$), 6.18 (s, 1H, CH), 6.83 (d, J= 8.5 Hz, 1H, ArH), 7.04 (m, 1H, ArH), 7.44 (d, J= 8.5 Hz, 1H, ArH), 7.53–7.59 (m, 3H, ArH), 10.59 (bs, 1H, OH). Anal. for $C_{16}H_{11}ClO_3$3: C 67.0%; H 3.9%. Found: C 66.7%; H 3.6%.

70d **4–(4–Chlorophenyl)–7–hydroxy–8–methyl–2*H*–chromen–2–one**

Yield 87%; m.p. (Et$_2$O): 253 – 255°C; reaction time: 3.5 h; R_f (CyHe/EtOAc, 80:20 v/v): 0.22; ^{1}H–NMR (DMSO–d_6) (δ): 2.19 (s, 3H, CH$_3$), 6.15 (s, 1H, CH), 6.83 (d, J= 9.0 Hz, 1H, ArH), 7.08 (d, J= 8.5 Hz, 1H, ArH), 7.50 (d, J= 9.0 Hz, 2H, ArH), 7.61 (d, J= 8.5 Hz, 2H, ArH), 10.55 (bs, 1H, OH). Anal. for $C_{16}H_{11}ClO_3$: C C 67.0%; H 3.9%. Found: C 67.2%; H 4.1%.

70e   4–(2–Fluorophenyl)–7–hydroxy–8–methyl–2*H*–chromen–2–one

Yield: 60%; m.p. (EtOH): 256 – 258°*C*; reaction time: 12 h; R_f (CyHe/EtOAc, 80:20 v/v): 0.19; ^{1}H–NMR (DMSO–d_6) (δ): 2.15 (s, 3H, CH$_3$), 6.17 (s, 1H, CH), 6.78–6.87 (m, 2H, ArH), 7.36–7.43 (m, 3H, ArH), 7.57 (m, 1H, ArH), 10.58 (bs, 1H, OH). Anal. for C$_{16}$H$_{11}$FO$_3$: C 65.0%; H 4.0%. Found: C 64.7%; H 3.75%.

70f   7–Hydroxy–8–methyl–4–(3–methylphenyl)–2*H*–chromen–2–one

Yield: 99%; m.p. (EtOAc): 185 – 187°*C*; reaction time: 3 h; R_f (CyHe/EtOAc, 80:20 v/v): 0.24; ^{1}H–NMR (DMSO–d_6) (δ): 2.19 (s, 3H, CH$_3$), 2.38 (s, 3H, CH$_3$), 6.10 (s, 1H, CH), 6.82 (d, *J*= 8.8 *Hz*, 1H, ArH), 7.12 (d, *J*= 8.8 *Hz*, 1H, ArH), 7.27–7.43 (m, 4H, ArH), 10.56 (bs, 1H, OH). Anal. for C$_{17}$H$_{14}$O$_3$: C: 76.7%; H 5.3%. Found: C 76.6%; H: 5.1%.

70g   7–Hydroxy–8–methyl–4–(4–methylphenyl)–2*H*–chromen–2–one

Yield: 63%; m.p. (EtOH): 259 – 261°*C*; reaction time: 2.5 h; R_f (CyHe/EtOAc, 80:20 v/v): 0.22; ^{1}H–NMR (DMSO–d_6) (δ): 2.19 (s, 3H, CH$_3$), 2.38 (s, 3H, CH$_3$), 6.09 (s, 1H, CH), 6.82 (d, *J*= 8.5 *Hz*, 1H, ArH), 7.13 (d, *J*= 8.5 *Hz*, 1H, ArH), 7.35–7.37 (m, 4H, ArH), 10.53 (bs, 1H, OH). Anal. for C$_{17}$H$_{14}$O$_3$: C 76.7%; H 5.3%. Found: C 76.8%; H 4.9%.

70h   7–Hydroxy–8–methyl–4–(4–nitrophenyl)–2*H*–chromen–2–one

Yield: 98%; m.p. (EtOAc): 360°*C* dec.; reaction time: 1.5 h; R_f (CyHe/EtOAc, 80:20 v/v): 0.15; ^{1}H–NMR (DMSO–d_6) (δ): 2.17 (s, 3H, CH$_3$), 6.22 (s, 1H, CH), 6.80 (d, *J*= 8.8 *Hz*, 1H, ArH), 6.90 (d, *J*= 8.8 *Hz*, 1H, ArH) 7.75 (d, *J*= 7.0 *Hz*, 2H, ArH), 8.34 (d, *J*= 7.0 *Hz*, 2H, ArH). Anal. for C$_{16}$H$_{11}$NO$_5$: C 64.6%; H 3.7%; N 4.7%. Found: C 64.2%; H 3.3%; N 4.4%.

71a   8–Chloro–7–hydroxy–4–phenyl–2*H*–chromen–2–one

Yield: 50%; m.p (EtOH): 214 – 215°*C*; R_f (CyHe/EtOAc 60:40 v/v) 0.63; ^{1}H–NMR (DMSO–d_6) (δ): 5.89 (s, 1H, CH), 6.66 (d, J=8.8, 1H, ArH), 6.95 (d, J=8.8, 1H, ArH), 7.15–7.25 (m, 5H, ArH). Anal. for C$_{15}$H$_9$ClO$_3$: C 66.04 %, H 3.33 %. Found: C 66.14%, H 3.43%.

71h 8–Chloro–7–hydroxy–4–(4–nitrophenyl)–2*H*–chromen–2–one

Yield: 55%; m.p.(EtOH): 303 – 305°C; R_f (CyHe/EtOAc 60:40 v/v): 0.29; ^{1}H–NMR (DMSO–d_6) (δ): 6.38 (s, 1H, CH), 6.98 (d, *J*= 8.7*Hz*, 1H, ArH), 7.15 (d, *J*= 8.7 *Hz*,1H, ArH), 7.82 (d, *J*= 8.2 *Hz*, 2H, ArH), 8.39 (d, *J*= 8.2 *Hz*, 2H, ArH). ^{13}C–NMR (DMSO–d_6) (δ): 111.55, 112.08. 113.36, 124.32, 125.99, 130.60, 141.74, 146.71. 148.54, 151.42, 153.76, 157.83, 159.46. Anal. for $C_{15}H_8NO_5$: C 56.71 %, H 2.54%, N 4.41%. Found: C 56.67%, H 2.59%, N 4.44%.

4.1.10 Synthesis of 4–(4–aminophenyl)–7–hydroxy-2*H*–chromen–2–one derivatives 72i-74i

To a suspension of the suitable arylnitro derivative 69h, 70h or 71h (1 molar equivalent) and a catalytic amount of Pd/C in EtOH (15 *mL*), $N_2H_4 \cdot H_2O$(10 mmol) was slowly added. The reaction was stirred and refluxed (70°*C*) for one hour. Then, the mixture was filtered through celite cake, which was later washed with EtOAc. The obtained solution was evaporated in vacuo to give the crude product, then diluted with EtOAc and washed with H_2O (3 × 10 *mL*). The organic layer was dried with $Na_2SO_4$and concentrated until dryness. The residue was purified by crystallization from suitable solvent to give the correspondent amines 72i–74i.

72i 4–(4–Aminophenyl)–7–hydroxychromen–2–one

Yield: 83%; m.p. (EtOH): 307 – 309°*C*; R_f (CyHe/EtOAc 80:20 v/v): 0.03; ^{1}H–NMR (DMSO–d_6) (δ): 5.60 (bs, 2H, NH$_2$), 5.96 (s, 1H, CH), 6.65 (d, *J*= 5.9 *Hz*, 2H), 6.73 (m, 2H, ArH), 7.17 (d, *J*= 5.9 *Hz*, 2H, ArH), 7.43 (m, 1H, ArH), 10.67 (bs, 1H, OH). Anal. for $C_{15}H_{11}NO_3$: C 71.1%; H 4.4%; N 5.5%. Found: C 70.8%; H 4.1%; N 5.2%.

73i 4–(4–Aminophenyl)–7–hydroxy–8–methyl–chromen–2–one

Yield: 90%; m.p. (EtOAc): 250 – 252°*C*; R_f (CyHe/EtOAc 80:20 v/v): 0.03; ^{1}H–NMR (DMSO–d_6) (δ): 2.15 (s, 3H, CH$_3$), 5.99 (bs, 2H, NH$_2$), 5.96 (s, 1H, CH), 6.64 (d, *J*= 8.5 *Hz*, 2H, ArH), 6.81 (d, *J*= 9.0 *Hz*, 1H, ArH), 7.17 (d, *J*= 8.5 *Hz*, 2H, ArH), 7.29 (d, *J*= 9.0 *Hz*, 1H, ArH). Anal. for $C_{16}H_{14}NO_3$: C 71.9%; H 4.9%; N 5.2%. Found: C 71.5%; H 4.4%; N 4.9%.

74i 4–(4–aminophenyl)–8–chloro–7–hydroxy–2H–chromen–2–one

Yield: 40%; m.p. (Et$_2$O): 313 – 315°*C*; R_f (CyHe/EtOAc 60:40 v/v): 0.14; ^{1}H–NMR (DMSO–d_6) (δ): 5.65 (bs, 2H, NH$_2$) 6.06 (s, 1H, CH), 6.67 (d, *J*= 8.2 *Hz*, 2H, ArH), 6.94 (m, 1H, ArH), 7.21 (d, *J*= 8.2 *Hz*,

2H, ArH), 7.47(d, 1H, ArH). Anal. for $C_{15}H_{10}ClNO_3$:C 62.62%; H 3.50%; N 4.87%; Found: C 62.60%; H 3.48%; N 4.85%.

4.1.11   Preparation of 2–oxo–4–phenyl–2*H*–chromen–7–yl acetate (75)

Derivative 75 has been prepared according to the procedure described above for compounds 62a–64a.

75   **2–oxo–4–phenyl–2*H*–chromen–7–yl acetate**

Yield: 79%; m.p.: $129 - -131°C$; R_f (CyHe/EtOAc 60:40 v/v): 0.64; ^{1}H–NMR (CDCl$_3$) (δ): 2.32 (s, 3H, CH$_3$) 6.44 (s, 1H,CH) 7.17 (m, 1H, ArH), 7.40 (s, 1H, ArH), 7.48 (m, 1H, ArH), 7.55–7.60 (m, 5H, ArH). Anal. for $C_{17}H_{12}O_4$: C 72.85%; H 4.32%; Found: C 72.88%; H 4.35%.

4.1.12   Synthesis of 2–oxo–4–phenyl–2*H*–chromen–7–yl propionate (76)

To a stirring solution of compound 69a (1 molar equivalent) in DCM (2 *mL*) and TEA (2.5 molar equivalents), propionyl chloride (5 molar equivalents) was slowly added in ice bath. After 10 minutes, the mixture was allowed to room temperature and stirred until the complete conversion of starting material (monitored by TLC, CyHe/EtOAc 60:40 v/v). Then, the solid in suspension was filtered off and recrystallized from Et$_2$O.

76   **2–oxo–4–phenyl–2*H*–chromen–7–yl propionate**

Yield: 20%; m.p. $172 - -174°C$; R_f (CyHe/EtOAc 60:40 v/v): 0.80; ^{1}H–NMR (DMSO–d_6) (δ): 1.16 (t,$J=$ 7.3 *Hz*, 3H, CH$_3$), 2.67 (q, $J=$ 7.3 *Hz*, 2H, CH2), 6.43 (s, 1H, CH), 7.17 (d, $J=$ 8.4 *Hz*, 2H, ArH), 7.40 (s, 1H, ArH) 7.48 (d, $J=$ 8.4 *Hz*, 2H, ArH), 7.55–7.63 (m, 5H, ArH). ^{13}C–NMR (DMSO–d_6) (δ): 8.77, 26.99, 110.71, 114.22. 116.37, 118.71, 127.82, 128.58, 128.99, 129.85. 134.71, 153.17, 154.26, 154.64, 159.56, 172.20. Anal. for $C_{18}H_{14}O_4$: C 73.46%; H 4.79%. Found: C 73.44%, H 4.77%.

4.1.13   Preparation of 2–oxo–4–phenyl–2*H*–chromen–7–yl benzoate (77)

Compound 77 was prepared according to the synthetic procedure reported for compounds 62i–64i.

77   **2–Oxo–4–phenyl–2*H*–chromen–7–yl benzoate**

Yield: 98%; m.p. $228 - 230°C$; R_f (CyHe /EtOAc 60:40 v/v): 0.76; ^{1}H–NMR (DMSO–d_6) (δ): 6.47 (s, 1H, CH), 7.32–7.79 (m, 11H, ArH), 8.16–8.18 (m, 2H, ArH). Anal. for $C_{22}H_{14}O_4$: C 77.18%, H 4.12%,

O 18.69%; Found: C 77.28%, H 4.22%, O 18.79%.

4.1.14 Synthesis of 8–acetyl–7–hydroxy–4–phenyl–2*H*–chromen–2–one (78) and 7–hydroxy–4–phenyl–8–propanoyl–2H–chromen–2–one (79)

A mixture of compound 75 or 76 (1 molar equivalent) and anhydrous AlCl$_3$ (5 molar equivalents) was heated to 320°C and stirred for 2h at the same temperature in solvent–free condition. When the reaction mixture was cooled to room temperature and a solution of 5% HCl (30 mL) was added. The resulted suspension was stirred for 1 h at room temperature and then heated under a steam bath for others 30 min. The precipitate formed was filtered off and purified by crystallization by EtOH to Yield compounds 78 and 79.

78 **8–Acetyl–7–hydroxy–4–phenyl–2*H*–chromen–2–one**

Yield: 25%; m.p.: 164 − 166°C; R_f (CyHe/EtOAc 60:40 v/v): 0.76; ^{1}H–NMR (DMSO–d_6) (δ): 1.10 (s, 3H, CH3), 6.14 (s, 1H, CH), 6.89 (d, J= 8.4 Hz, 2H, ArH), 7.33 (d, J= 8.4 Hz, 2H, ArH), 7.51–7.56 (m, 5H, ArH). ^{13}C–NMR (DMSO–d_6) (δ): 200.37, 159.16, 159.00, 155.37, 151.98, 134.85, 129.62, 129.48, 128.80, 128.33, 115.99, 113.26, 110.65, 39.52, 32.35. Anal. for C$_{17}$H$_{12}$O$_4$: C 72.85%, H 4.32%; Found: C 72.83%, H 4.30%.

79 **7–Hydroxy–4–phenyl–8–propanoyl–2*H*–chromen–2–one**

Yield: 20%; m.p.: 172 − 174°C; R_f (CyHe/EtOAc 60:4 v/v): 0.80. ^{1}H–NMR (DMSO–d_6) (δ): 1.10 (t, J= 7.3 Hz, 3H, CH$_3$), 2.90 (q, J= 7.3 Hz, 2H, CH$_2$), 6.14 (s, 1H, CH), 6.86 (d, J= 8.4 Hz, 2H, ArH), 7.31 (d, J= 8.4 Hz, 2H, ArH), 7.50–7.55 (m, 5H, ArH). Anal. for C$_{18}$H$_{14}$O$_4$: C 73.46%, H 4.79%. Found: C 73.56%, H 4.89%.

4.1.15 General synthetic procedures for aroyl derivatives 83a–g and 87a–c

The appropriate DL-amino acid derivative 82, 86a–c (1 molar equivalent) and NaOH pellets (3 molar equivalents), were dissolved in H$_2$O/CH$_3$CN(4:2 v/v, 6 mL) and the resulting mixture was cooled at 0°C. Then, the appropriate aroyl chloride (81a–g for glycine 82, 81a for valine, alanine and leucine 86a–c) (0.8 molar equivalent) was added in three divided portion within 1 hour by stirring vigorously at 450 rpm. The solution was brought to room temperature and kept under stirring for another 1.5 hour. Later, concentrated hydrochloric acid (37% w/w, HCl) was added slowly to the mixture with continuous stirring until it became acidic (pH= 3), which resulted into the precipitation of crude product which was collected by vacuum filtration, washed with cold Et$_2$Oand dried in vacuo at room temperature to give the desired

known intermediates 83a–g, 87a–c. The registered CAS numbers for resulting compounds have been already assigned as reported below. The experimental properties for 82a–g, 86a–c matched with those reported in literature.

Cmpds	CAS Number		Cmpds	CAS Number
83a	495–69–2		83f	5657–19–2
83b	16555–60–5		83g	33955–17–8
83c	57728–59–3		87a	2901–80–6
83d	13450–77–6		87b	17966–67–5
83e	366–79–0		87c	2901–76–0

4.1.16 Synthesis of N–(2–oxo–2–((4–sulfamoylphenyl)amino)ethyl)benzamide derivatives 84a–g

To a solution of the appropriate aroyl amino acid derivatives 83a–g in dimethylformamide (DMF) (2 *mL*), 1–[Bis(dimethylamino)methylene]–1*H*–1,2,3–triazolo[4,5–b]pyridinium 3–oxid hexafluorophosphate (HATU) (1 molar equivalent) or HBTU was added. The mixture was stirred at room temperature for 15 minutes. Then, 1,8–Diazabicyclo[5.4.0]undec–7–ene (DBU) (2.5 molar equivalents) and *p*–aminobenzenesulfonamide 84 (1 molar equivalent) were added. The reaction mixture was left overnight at room temperature, then quenched with H_2O(10 *mL*) and extracted with EtOAc (3 x 10 *mL*). The organic phase was washed with saturated NaCl solution, dried with $Na_2SO_4$and concentrated until dryness under reduced pressure. The crude was purified by crystallization from EtOH to give the desired final compounds 85a–g as white powder.

85a — **N–(2–oxo–2–((4–sulfamoylphenyl)amino)ethyl)benzamide**
(CAS Number: 63203–12–3)

Yield: 36%; m.p.: 214 – 216°*C*; ^{1}H–NMR (DMSO–d_6) (δ): 4.08 (d, *J*= 5.96 *Hz*, 2H, CH_2), 7.23 (bs, 2H, NH_2), 7.47–7.55 (m, 3H, ArH), 7.75 (m, 4H, ArH), 7.89 (m, 2H, ArH), 8.86 (t, *J*= 5.96 *Hz*, 1H, NH), 10.39 (s, 1H, NH); ^{13}C–NMR (DMSO–d_6): 43.83, 119.11, 120.28, 127.18, 127.76, 128.78, 131.88, 132.36, 134.30, 138.78, 142.58, 167.14, 168.87. Anal. for $C_{15}H_{15}N_3O_4S$: C, 54.04%; H, 4.54%; N, 12.61%; Found: C, 54.12%; H, 4.62%; N, 12.70%.

85b — **2–Chloro–N–(2–oxo–2–((4–sulfamoylphenyl)amino)ethyl)benzamide**

Yield: 27%; m.p.: 249 – 251°*C*; ^{1}H–NMR (DMSO–d_6) (δ): 4.08 (d, *J*= 5.87 *Hz*, 2H, CH_2), 7.26 (bs, 2H, NH_2), 7.42–7.53 (m, 4H, ArH), 7.77 (m, 4H, ArH), 8.77 (t, *J*= 5.87 *Hz*, 1H, NH), 10.49 (s, 1H, NH);

Anal. for $C_{15}H_{14}ClN_3O_4S$: C, 48.98%; H, 3.84%; N, 11.42%; Found: C, 48.90%; H, 3.76%; N, 11.38%.

85c 3–Chloro–N–(2–oxo–2–((4–sulfamoylphenyl)amino)ethyl)benzamide

Yield: 19%; m.p.: 262 – 264°C; ^{1}H–NMR (DMSO–d_6) (δ): 4.06 (d, J= 5.87 Hz Hz, 2H, CH$_2$), 7.22 (bs, 2H, NH$_2$), 7.31 (m, 2H, ArH), 7.74 (m, 4H, ArH), 7.96 (m, 2H, ArH), 8.66 (t,J= 5.96 Hz, 1H, NH), 10.55 (s, 1H, NH); Anal. for $C_{15}H_{14}ClN_3O_4S$: C, 48.98%; H, 3.84%; N, 11.42%; Found: C, 48.88%; H, 3.74%; N, 11.32%.

85d 4–Chloro–N–(2–oxo–2–((4–sulfamoylphenyl)amino)ethyl)benzamide

Yield: 41%; m.p.: 226 – 228°C; ^{1}H–NMR (DMSO–d_6) (δ): 4.07 (d, J= 5.87 Hz, 2H, CH$_2$), 7.23 (bs, 2H, NH$_2$), 7.51–7.93 (m, 8H, ArH), 9.01 (t, J= 5.87 Hz, 1H, NH), 10.39 (s, 1H, NH); Anal. for $C_{15}H_{14}ClN_3O_4S$: C, 48.98%; H, 3.84%; N, 11.42%; Found: C, 48.78%; H, 3.64%; N, 11.22%.

85e 4–Fluoro–N–(2–oxo–2–((4–sulfamoylphenyl)amino)ethyl)benzamide

Yield: 32%; m.p.: 269 – 271°C; ^{1}H–NMR (DMSO–d_6) (δ): 4.10 (d, J= 5.87 Hz, 2H, CH$_2$), 7.26 (bs, 2H, NH$_2$), 7.53–7.96 (m, 6H, ArH), 9.04 (t, J= 5.87 Hz, 1H, NH), 10.42 (s, 1H, NH); Anal. for $C_{15}H_{14}FN_3O_4S$: C, 51.28%; H, 4.02%; N, 11.96%; Found: C, 51.24%; H, 3.96%; N, 11.92%.

85f N–(2–oxo–2–((4–sulfamoylphenyl)amino)ethyl)furan–2–carboxamide

Yield: 24%; m.p.: 238 – 240°C; ^{1}H–NMR (DMSO–d_6) (δ): 4.03 (d, J= 5.96 Hz, 2H, CH$_2$), 6.62 (m, 1H, ArH), 7.14 (m, 1H, ArH), 7.23 (bs, 2H, NH$_2$), 7.74 (bs, 4H, ArH), 7.85 (m, 1H, ArH), 8.66 (t, J= 5.96 Hz, 1H, NH), 10.55 (s, 1H, NH); ^{13}C–NMR (DMSO–d_6): 43.07, 112.33, 114.23, 119.02, 127.10, 138.70, 142.40, 145.64, 148.05, 158.58, 168.66. Anal. for $C_{13}H_{13}N_3O_5S$: C, 48.29%; H, 4.05%; N, 13.00%; Found: C, 48.32%; H, 4.00%; N, 13.20%.

85g N–(2–oxo–2–((4–sulfamoylphenyl)amino)ethyl)thiophene–2–carboxamide

Yield: 21%; m.p.: 265 – 267°C; ^{1}H–NMR (DMSO–d_6) (δ): 4.08 (d, J= 5.96 Hz, 2H, CH$_2$), 7.17–7.19 (m, 1H, ArH), 7.26 (bs, 2H, NH$_2$), 7.77 (bs, 4H, ArH), 7.78–7.84 (m, 2H, ArH), 8.94 (t, J= 5.96 Hz, 1H, NH), 10.49 (s, 1H, NH); Anal. for $C_{13}H_{13}N_3O_4S_2$: C, 46.01%; H, 3.86%; N, 12.38%; Found: C, 46.11%; H, 3.96%; N, 12.46%.

4.1.17 Preparation of (9H–fluoren–9–yl)methyl (2–oxo–2–((4–sulfamoylphenyl) amino) ethyl) carbamate derivatives 89a–c

To a solution of N–α–Fmoc amino acids (1 molar equivalent) 88a–c in dry dimethylformamide (DMF) (2 *mL*), 1–[Bis(dimethylamino)methylene]–1H–1,2,3–triazolo[4,5–b]pyridinium 3–oxid hexafluorophosphate (HATU) (1 molar equivalent) was added in ice bath and by stirring vigorously at 450 rpm. Then, N,N–Diisopropylethylamine (DIPEA) (2.5 molar equivalents) and *p*–aminobenzenesulfonamide (1.25 molar equivalent) were added. The reaction mixture was vigorously stirred at room temperature overnight. Water (10 *mL*) was added and the mixture was extracted with EtOAc (3 × 10 *mL*). The organic phase was washed with acidic water (pH 4–5), dried with Na_2SO_4 and concentrated until dryness under reduced pressure. The crude was sonicated with Et_2O to give the desired intermediates 89a–c as white powder.

89a — **(9H–fluoren–9–yl)methyl(1–oxo–1–((4-sulfamoylphenyl)amino)propan-2-yl)-carbamate**

Yield: 58%; m.p.: 229 – 230°C; t_R: 5.52'; ^{1}H–NMR (DMSO–d_6) (δ): 1.33 (m, 3H, CH$_3$), 4.20–4.31 (m, 4H, CH$_2$, CH), 7.26 (bs, 2H, NH$_2$), 7.32–7.45 (m, 4H, ArH), 7.73–7.77 (m, 7H, ArH, NH), 7.86–7.91 (m, 2H, ArH), 10.34 (s, 1H, NH); ^{13}C–NMR (DMSO–d_6) (δ): 18.27, 47.11, 51.33, 66.11, 119.17, 120.59, 125.77, 127.08, 127.54, 128.11, 138.85, 141.19, 144.24, 144.34, 156.32, 172.68. Anal. for $C_{24}H_{23}N_3O_5S$: C, 61.92; H, 4.98; N, 9.03. Found: C, 62.05%; H, 4.85%; N, 9.09%. HRMS (ESI): m/z Calcd. for [MH]+ 465.14. Found: 466.00.

89b — **(9H–fluoren–9–yl)methyl (3–methyl–1–oxo–1–((4–sulfamoylphenyl)amino)-butan–2–yl)-carbamate**

Yield: 73%; m.p.: 230 – 231°C; t_R: 5.90'; ^{1}H–NMR (DMSO–d_6) (δ): 0.91–0.95 (m, 6H, CH$_3$), 4.01–4.10 (m, 2H, CH), 4.22–4.30 (m, 3H, CH$_2$, CH), 7.25 (bs, 2H, NH$_2$), 7.31–7.43 (m, 4H, ArH), 7.74–7.76 (m, 7H, ArH, NH), 7.88–7.90 (m, 2H, ArH), 10.41 (s, 1H, NH). Anal. for $C_{27}H_{27}N_3O_5S$: C, 63.27; H, 5.51; N, 8.51. Found: C, 63.39%; H, 5.28%; N, 8.63%. HRMS (ESI): m/z Calcd. for [MH]+ 493.17. Found: 494.00.

89c — **9H–fluoren–9–yl)methyl (4–methyl–1–oxo–1–((4–sulfamoylphenyl)amino)-pentan–2–yl)-carbamate**

Yield: 82%; m.p.: 200 – 201°C; t_R: 9.19'; ^{1}H–NMR (DMSO–d_6) (δ): 0.89–0.91 (m, 6H, CH$_3$), 3.16 (m, 2H, CH$_2$), 4.22–4.30 (m, 5H, CH$_2$, CH), 7.25 (bs, 2H, NH$_2$), 7.29–7.43 (m, 4H, ArH), 7.71–7.76 (m, 7H, ArH, NH), 7.88–7.90 (m, 2H, ArH), 10.37 (s, 1H, NH). ^{13}C–NMR (DMSO–d_6) (δ): 18.56, 23.49, 31.17, 47.14, 54.07, 66.08, 119.27, 120.59, 125.78, 127.14, 127.51, 128.11, 138.90, 141.19, 142.33, 144.21, 156.56, 172.65. Anal. for $C_{27}H_{29}N_3O_5S$: C, 63.89; H, 5.76; N, 8.28. Found: C, 63.65%; H, 5.63%; N, 8.37%. HRMS (ESI): m/z Calcd. for [MH]+ 507.18. Found: 508.00.

4.1.18 General procedures for the synthesis of compounds 90a–c

The F–moc protected intermediates 89a–c (250 *mg*) were treated with 2% (v/v) of 1,8–Diazabicyclo[5.4.0]undec–7–ene (DBU) in dimethylformamide (DMF, 2.5 *mL*). The reaction mixture was stirred at 25°*C* for 20 minutes. After the starting material has disappeared, the crude product was concentrated in vacuo and then subjected to sonication with a *n*–hexane (He)–DCM solution (50%, v/v) to provide the free amines 90a–c white powder.

90a **2–Amino–N–(4–sulfamoylphenyl)propanamide**

Yield: 68%; m.p.: $216 - 217°C$; t_R: 0.43'; ^{1}H–NMR(CD$_3$OD–d_4): (δ) 1.37 (m, 3H, CH$_3$), 3.58 (m, 1H, CH), 7.77–7.87 (m, 4H, ArH). $_{13}$C–NMR (DMSO–d_6): 21.53, 51.36, 118.86, 126.83, 138.44, 142.07, 175.81. Anal. for C$_9$H$_{13}$N$_3$O$_3$S : C, 44.43%; H, 5.39%; N, 17.27%. Found: C, 44.51%; H, 5.27%; N, 17.31%. HRMS (ESI): m/z, calcd. for [MH]+ 243.28. Found: 244.00.

90b **2–Amino–3–methyl–N–(4–sulfamoylphenyl)butanamide**

Yield: 62%; m.p.: $209 - 211°C$; t_R: 0.84'; ^{1}H–NMR (DMSO–d_6) (δ): 0.83–0.92 (m, 6H, CH$_3$), 1.88–1.96 (m, 2H, CH), 7.23 (bs, 2H, NH$_2$), 7.73–7.81 (m, 4H, ArH). Anal. for C$_{11}$H$_{17}$N$_3$O$_3$S: C, 48.69%; H, 6.32%; N, 15.49%. Found: C, 48.81%; H, 6.26%; N, 15.52%. HRMS (ESI): m/z, calcd. for [MH]$^+$ 271.34. Found: 272.00.

90c **2–Amino–4–methyl–N–(4–sulfamoylphenyl)pentanamide**

Yield: 71%; m.p.: $181 - 193°C$; t_R: 1.93'; ^{1}H–NMR (DMSO–d_6) (δ): 0.87–0.91 (m, 6H, CH$_3$), 1.29–1.50 (m, 2H, CH$_2$), 1.54–1.86 (m, 2H, CH), 7.26 (bs, 2H, NH$_2$), 7.72–7.81 (m, 4H, ArH). Anal. for C$_{12}$H$_{19}$N$_3$O$_3$S: C, 50.51%; H, 6.71%; N, 14.73%. Found: C, 50.38%; H, 6.60%; N, 14.81%. HRMS (ESI): m/z, calcd. for [MH]$^+$ 285.36. Found: 286.00.

4.1.19 General procedures for the synthesis of 91a–c

To a stirred solution of 90a–c (1 molar equivalent) in DMF/DCM (50%, v/v), benzoyl chloride (81a) (0.8 molar equivalent) was added in ice bath. The resulted mixture was stirred at room temperature for 1 hour. After the disappearence of the starting material, the organic solvent was evaporated in vacuo and purified by flash cromatography (eluting with 0–20% v/v of MeOH in DCM). The final crude was sonicated with petroleum ether (PE)/ethanol (EtOH) (50%, v/v) to afford the desired compounds 91a–c as white powder.

91a **N–(1–oxo–1–((4–sulfamoylphenyl)amino)propan–2–yl)benzamide**

Yield: 54%; m.p.: $260 - 261°C$; t_R: 4.09'; ^{1}H–NMR (DMSO–d_6) (δ): 1.96–1.98 (m, 3H, CH$_3$), 5.20–5.23 (m, 1H, CH), 6.89–6.90 (m, 1H, NH), 7.87–8.00 (m, 3H, ArH), 8.23–8.28 (m, 4H, ArH), 8.39–8.48 (m, 2H, ArH), 10.23 (bs, 1H, NH). Anal. for C$_{16}$H$_{17}$N$_3$O$_4$S: C, 55.32%; H, 4.93%; N, 12.10%. Found: C, 55.47%; H, 4.79%; N, 12.21%. HRMS (ESI): m/z Calcd. for [MH]$^+$ 347.09. Found: 348.00.

91b **N–(3–methyl–1–oxo–1–((4–sulfamoylphenyl)amino)butan–2–yl)benzamide**

Yield: 63%; m.p.: $279 - 280°C$; t_R: 4.09'; ^{1}H–NMR (DMSO–d_6) (δ): 0.97–1.02 (m, 6H, CH$_3$), 2.20–2.25 (m, 1H, CH), 4.39–4.45 (m, 1H, CH), 7.23 (bs, 2H, NH$_2$), 7.46–7.57 (m, 3H, ArH), 7.75–7.81 (m, 4H, ArH), 7.90–7.93 (m, 2H, ArH), 8.55–8.57 (m, 1H, NH), 10.54 (bs, 1H, NH). Anal. for C$_{18}$H$_{21}$N$_3$O$_4$S: C, 57.58%; H, 5.64%; N, 11.19%– Found: C, 57.62%; H, 5.58%; N, 11.26%. HRMS (ESI): m/z, Calcd. for [MH]$^+$ 376.13. Found: 376.00.

91c **N–(4–methyl–1–oxo–1–((4–sulfamoylphenyl)amino)pentan–2–yl)benzamide**

Yield: 48%; m.p.: $238 - 240°C$; t_R: 5.06'; ^{1}H–NMR (DMSO–d_6) (δ): 0.91–0.96 (m, 6H, CH$_3$), 1.54–1.60 (m, 1H, CH), 1.72–1.86 (m, 2H, CH$_2$), 4.63–4.69 (m, 1H, CH), 7.25 (bs, 2H, NH$_2$), 7.45–7.56 (m, 3H, ArH), 7.74–7.80 (m, 4H, ArH), 7.90–7.92 (m, 2H, ArH), 8.63–8.68 (m, 1H, NH), 10.46 (bs, 1H, NH). ^{13}C–NMR (DMSO–d_6) (δ): 21.87, 23.52, 25.04, 53.35, 119.31, 127.13, 128.07, 128.67, 131.86, 134.36, 138.87, 142.41, 167.10, 172.55. Anal. for C$_{19}$H$_{23}$N$_3$O$_4$S: C, 58.59%; H, 5.95%. N, 10.79%. Found: C, 58.48%; H, 5.99%; N, 10.83%. HRMS (ESI): m/z, Calcd. for [MH] $^+$ 390.14. Found: 390.00.

4.1.20 General procedures fo the synthesis of derivatives 93a–d

To a solution of the appropriate aroyl amino acids (87a–c) in dimethylformamide (DMF) (2 mL), N,N,N',N'–tetramethyl–O–(1H–benzotriazol–1–yl)–uroniumhexafluorophosphate (HBTU) was added. The mixture was stirred at room temperature for 15 minutes. Then, 1,8–Diazabicyclo[5.4.0]undec–7–ene (DBU) (2.5 molar equivalents) and 4–(aminomethyl)benzene-sulfonamide (92) (1 molar equivalent) were added. The reaction mixture was left overnight at room temperature and then quenched with H$_2$O(10 mL) and extracted with EtOAc (3×10 mL). The organic phase was washed with saturated NaCl solution, dried with Na$_2$SO$_4$and concentrated until dryness under reduced pressure. The crude was purified by crystallization from EtOH to give the desired final compounds 93a–d as white powder.

93a **N–(2–oxo–2–((4–sulfamoylbenzyl)amino)ethyl)benzamide**

Yield: 56%; m.p.: 211 – 213°C; ^{1}H–NMR (DMSO–d_6) (δ): 3.89–3.97 (m, 2H, CH$_2$), 4.32–4.40 (m, 2H,CH$_2$), 7.31 (bs, 2H, NH$_2$), 7.43–7.54 (5H, ArH), 7.75 (m, 2H, ArH), 7.91 (m, 2H, ArH), 8.55–8.63 (m, 1H, NH), 8.82–8.90 (m, 1H, NH); ^{13}C–NMR (DMSO–d_6) (δ): 42.20, 43.28, 126.10, 127.74, 128.78, 131.70, 134.42, 143.20, 144.24, 166.96, 169.88. Anal. for C$_{16}$H$_{17}$N$_3$O$_4$S: C 55.32%; H, 4.93%; N 12.10%. Found: C 55.23%; H 4.81%; N 12.24%.

93b **N–(1–oxo–1–((4–sulfamoylbenzyl)amino)propan–2–yl)benzamide**

Yield: 64%; m.p.: 178 – 180°C; ^{1}H–NMR (DMSO–d_6) (δ): 1.34–1.43 (m, 3H, CH$_3$), 4.32–4.42 (m, 1H, CH), 4.48–4.68 (m, 2H, CH$_2$), 7.30 (bs, 2H, NH$_2$), 7.42–7.54 (m, 5H, ArH), 7.74–7.84 (m, 2H, ArH), 7.88–7.98 (m, 2H, ArH), 8.47–8.65 (m, 1H, NH), 9.08–9.22 (m, 1H, NH); ^{13}C–NMR (DMSO–d_6) (δ): 18.27, 42.79, 49.67, 126.09, 127.69, 127.96, 128.58, 128.79, 131.80, 134.55, 143.01, 144.19, 166.80, 173.10. Anal. for C$_{17}$H$_{19}$N$_3$O$_4$S: C 56.50%; H 5.30%; N, 11.63%. Found: C 56.40%; H 5.43%; N 11.51%.

93c **N–(3–methyl–1–oxo–1–((4–sulfamoylbenzyl)amino)butan–2–yl)benzamide**

Yield: 61%; m.p.: 213 – 215°C; ^{1}H–NMR (DMSO–d_6) (δ): 0.90 (m, 3H, CH$_3$), 0.93 (m, 3H, CH$_3$), 2.12 (s, 1H, CH), 4.30 (m, 1H, CH), 4.36 (m, 2H, CH$_2$), 7.30 (s, 2H, NH$_2$), 7.43–7–74 (m, 5H, ArH), 7.75 (m, 2H, ArH), 7.89 (m, 2H, ArH), 8.31 (m, 1H, NH), 8.66 (m, 1H, NH); ^{13}C–NMR (DMSO–d_6) (δ): 19.34, 19.83, 42.17, 59.80, 126.02, 127.92, 127.97, 128.62, 131.72, 134.63, 142.96, 143.98, 167.13, 171.80. Anal. for C$_{19}$H$_{23}$N$_3$O$_4$S: C 58.59%; H 5.95%; N 10.79%. Found: C 58.47%; H 6.03%; N 10.66%.

93d **N–(1–oxo–3–phenyl–1–((4–sulfamoylbenzyl)amino)propan–2–yl)benzamide**

Yield: 48%; m.p.: 229 – 230°C; ^{1}H–NMR (DMSO–d_6) (δ): 3.02–3.17 (m, 2H, CH$_2$), 4.36–4.38 (m, 2H, CH$_2$), 4.72–4.76 (m, 1H, CH), 7.16–7.20 (m, 1H, ArH), 7.25–7.28 (m, 2H, ArH), 7.30 (bs, 2H, NH$_2$), 7.34–7.53 (m, 7H, ArH), 7.74 (m, 2H, ArH), 7.82 (m, 2H, ArH), 8.64–8.65 (m, 1H, NH), 8.68–8.70 (m, 1H, NH); ^{13}C–NMR (DMSO–d_6) (δ): 37.33, 41.97, 56.32, 125.77, 126.43, 127.51, 127.63, 128.28, 128.32, 129.34, 131.46, 134.18, 138.50, 142.71, 143.65, 166.52, 171.65. Anal. for C$_{23}$H$_{23}$N$_3$O$_4$S: C 63.14%; H 5.30%; N 9.60%. Found: C 63.28%; H 5.18%; N 9.72%.

4.1.21   Synthesis of N–(4–sulfamoylbenzyl) amides 104a–i

Pathway i (A): To a solution of 4–aminomethylbenzenesulfonamide hydrochloride (92) (1 molar equivalent) in a mixture of DCM/DMF (6 *mL*, 2:1, v/v) placed in a cylindrical quartz tube (∅ 2 *cm*), N,N–Diisopropylethylamine (DIPEA) (2.5 molar equivalents) and the appropriate acyl chloride (0.8 molar equivalent) were added. The mixture was subjected to microwave irradiation at 250 *W* for 10 minutes at 25°*C*. The reaction progresses were monitored by TLC, by using a solution of DCM/MeOH (9:1, v/v) as eluent. Then, the solvent was removed under *vacuum*, the resulted residue diluted with of H_2O(10 *mL*) and extracted with EtOAc (3 × 10 *mL*). The combined organic extracts were washed with brine solution, dried (Na_2SO_4) and concentrated until dryness under reduced pressure. The crude product was purified by crystallization with $Et_2O$and EtOH to afford compounds 104a–e and 104h as white powders.
Pathway i (B): The suitable carboxylic acids (1 molar equivalent) and N,N,N,N–tetramethyl–O–(1*H*–benzotriazol–1–yl)uronium hexafluorophosphate (HBTU) (1 molar equivalent) in DMF (2 *mL*) were placed in a cylindrical quartz tube (∅ 2 *cm*), stirred and irradiated in a microwave oven at 250 *W* for 5 minutes at 25°*C*. Then, N,N–Diisopropylethylamine (DIPEA) (2.5 molar equivalents) and 4–aminomethylbenzenesulfonamide hydrochloride (92) (1 molar equivalent) were added and the resulted solution was stirred and subjected to microwave irradiation for 25 minutes in the same condition reported above. The solvent was removed under *vacuum*, the resulted residue diluted with of H_2O(10 *mL*) and extracted with EtOAc (3 × 10 *mL*). The combined organic extracts were washed with brine solution, dried (Na_2SO_4) and concentrated until dryness under reduced pressure. The crude product was purified by crystallization with $Et_2O$and EtOH to afford compounds 104f–g and 104i as white powders.

104a **3–Methyl–N–(4–sulfamoylbenzyl)benzamide**
(CAS Number: 349136–13–6)

Yield: 68%; m.p.: 197 − 199°*C*; ^{1}H–NMR (DMSO–d_6) (δ): 2.36 (s, 3H, CH$_3$), 4.52 (d, *J*= 5.9 *Hz*, 2H, CH$_2$), 7.30 (bs, 2H, NH$_2$), 7.36–7.37 (m, 2H, ArH), 7.48 (d, *J*= 8.3 *Hz*, 2H, ArH), 7.68–7.72 (m, 2H, ArH), 7.78 (d, *J*= 8.3 *Hz*, 2H, ArH), 9.07 (t, *J*= 5.9 *Hz*, 1H, NH). ^{13}C–NMR (DMSO–d_6) (δ): 21.12, 42.50, 124.57, 125.86, 127.66, 127.98, 128.42, 132.07, 134.30, 137.79, 142.74, 143.96, 166.60. Anal. for $C_{15}H_{16}N_2O_3S$: C 59.19%, H 5.30%, N 9.20%; Found: C 59.09%, H 5.20%, N 9.10%.

104b **3–Chloro–N–(4–sulfamoylbenzyl)benzamide**
(CAS Number: 349136–17–0)

Yield: 59%; m.p.: 157−159°*C*; ^{1}H–NMR (DMSO–d_6) (δ): 2.36 (s, 3H, CH$_3$), 4.52 (d, *J*= 5.5 *Hz*, 2H,CH$_2$), 7.31 (bs, 2H, NH$_2$), 7.49 (d, *J*= 8.3 *Hz*, 2H, ArH), 7.51–7.54 (m, 1H, ArH), 7.62–7.64 (m, 1H, ArH), 7.78 (d, *J*= 8.3 *Hz*, 2H, ArH), 7.85–7.87 (m, 1H, ArH), 7.94 (m, 1H, ArH), 9.25 (t, *J*= 5.5 *Hz*,1H, NH). ^{13}C–NMR (DMSO–d_6) (δ): 39.52, 42.47, 125.74, 126.06, 127.10, 127.58, 130.41, 131.22, 133.26, 136.10, 142.67, 143.40, 164.94. Anal. for $C_{14}H_{13}ClN_2O_3S$: C 51.77%; H 4.03%; N 8.63%;. Found: C 51.87%; H 4.13%; N 8.73%.

104c **2,5–Dichloro–N–(4–sulfamoylbenzyl)benzamide**
(CAS Number: 349136–29–4)

Yield: 57%; m.p.: 213 – 215°C; ^{1}H–NMR (DMSO–d_6) (δ): 4.52 (d, J= 5.5 Hz, 2H, CH$_2$), 7.33 (bs, 2H, NH$_2$), 7.53–7.61 (m, 5H, ArH), 7.80 (m, 2H, ArH), 9.16 (t, J= 5.5 Hz,1H, NH). Anal. for C$_{14}$H$_{12}$Cl$_2$N$_2$O$_3$S: C 46.81%; H 3.37%; N 7.80%. Found: C 46.91%; H 3.47%; N 7.90%.

104d **4–Bromo–N–(4–sulfamoylbenzyl)benzamide**
(CAS Number: 349136–03–4)

Yield: 97% m.p.: 233 – 235°C; ^{1}H–NMR (DMSO–d_6) (δ): 4.52 (d, J= 5.5 Hz, 2H, CH$_2$), 7.30 (bs, 2H, NH$_2$), 7.47 (d, J= 8.1 Hz, 2H, ArH), 7.69 (d, J= 8.3 Hz, 2H, ArH), 7.77 (d, J= 8.1 Hz, 2H, ArH), 7.83 (d, J= 8.3 Hz, 2H, ArH), 9.20 (t, J= J= 5.9 Hz, 1H, NH). Anal. for C$_{14}$H$_{13}$BrN$_2$O$_3$S: C 45.54%; H 3.55%; N 7.59%. Found: C 45.44%; H 3.45%; N 7.49%.

104e **N–(4–sulfamoylbenzyl)–[1,1'–biphenyl]–4–carboxamide**
(CAS Number: 349084–68–0)

Yield: 88%; m.p.: 367 – 369°C; ^{1}H–NMR (DMSO–d_6) (δ): 4.55 (d, J= 5.9 Hz, 2H, CH$_2$), 7.32–7.51 (m, 7H, ArH), 7.61–7.74 (m, 4H, ArH), 7.78 (d, J= 8.3 Hz, 2H, ArH), 8.01 (d, J= 8.3 Hz, 2H, ArH), 9.27 (t, J= 5.9 Hz, 1H, NH). ^{13}C–NMR (DMSO–d_6) (δ): 39.52, 42.41, 125.11, 125.71, 125.72, 127.55, 129.41, 131.39, 133.22, 142.64, 143.50, 165.41. Anal. for C$_{20}$H$_{18}$N$_2$O$_3$S: C 65.55%; H 4.95%; N 7.64%. Found: C 65.45%; H 4.85%; N 7.54%.

104f **2–Benzyl–N–(4–sulfamoylbenzyl)benzamide**
(CAS Number: 848052–23–3)

Yield: 85%; m.p.: 197 – 199°C; ^{1}H–NMR (DMSO–d_6) (δ): 4.12 (s, 2H, CH$_2$), 4.47 (d, J= 5.9 Hz, 2H,CH$_2$), 7.13–7.30 (m, 7H, ArH), 7.33 (bs, 2H, NH$_2$), 7.36–7.43 (m, 4H, ArH), 7.75 (m, 2H, ArH), 8.94 (t, J= 5.9 Hz, 1H, NH).^{13}C–NMR (DMSO–d_6) (δ): 37.60, 39.52, 42.00, 125.56, 125.76, 125.94, 127.39, 127.41, 128.14, 128.65, 129.62, 130.41, 136.27, 138.94, 140.91, 142.44, 143.42, 169.15. Anal. for C$_{21}$H$_{20}$N$_2$O$_3$S: C 66.29%; H 5.30%; N 7.36%. Found: C 66.19%; H 5.20%; N 7.26%.

104g **2–(2–Fluorophenyl)–N–(4–sulfamoylbenzyl)acetamide**
(CAS Number: 794539–67–6)

Yield: 58%; m.p.: 196 – –198°C; ^{1}H–NMR (DMSO–d_6) (δ): 4.34 (d, J= 5.9 Hz 2H, CH$_2$), 7.15–7.16 (m, 2H, ArH), 7.30–7.35 (m, 4H, ArH and NH$_2$), 7.42 (d, J= 8.3 Hz, 2H, ArH), 8.66 7.76 (d, J= 8.3 Hz, 2H, ArH). ^{13}C–NMR (DMSO–d_6) (δ): 35.48, 39.52, 42.09, 115.09, 115.26, 124.36, 125.83, 127.62, 128.78, 128.84, 132.04, 132.08, 142.79, 143.75, 169.44. Anal. for C$_{15}$H$_{15}$FN$_2$O$_3$S: C 55.89%; H 4.69%; N 8.69%. Found: C 55.79%; H 4.59%; N 8.59%.

104h **N–(4–sulfamoylbenzyl)thiophene–3–carboxamide**
(CAS Number: 1090372–43–2)

Yield: 76%; m.p.: 222 – 224°C; ^{1}H–NMR (DMSO–d_6) (δ): 4.50 (d, J= 5.9 *Hz*, 2H, CH_2), 7.31 (bs, 2H, NH_2), 7.48 (d, *J*= 8.3 *Hz* 2H, ArH), 7.55 (dd, *J*= 7.8 *Hz*, *J*= 1.2 *Hz*, 1H, ArH), 7.60 (dd, *J*= 7.8 *Hz*, *J*= 2.9 *Hz*, 1H, ArH), 7.78 (d, *J*= 8.3 *Hz* 2H, ArH), 8.18 (dd, *J*= 2.9 *Hz*, *J*= 1.2 *Hz*), 9.00 (t, *J*= 5.9 *Hz*, 1H, NH).^{13}C–NMR (DMSO–d_6) (δ): 39.52, 41.86, 125.69, 126.73, 126.94, 127.56, 129.07, 137.53, 142.58, 143.85, 162.14. Anal. for $C_{12}H_{12}N_2O_3S_2$: C 48.63%; H 4.08%; N 9.45%. Found: C 48.73%; H 4.18%; N 9.55%.

104i **3–(methylthio)–N–(4–sulfamoylbenzyl)propanamide**
(CAS Number: 851629–70–4)

Yield: 84%; m.p.: 128 – 130°C; ^{1}H–NMR (DMSO–d_6) (δ): 2.06 (s, 3H, CH_3), 2.46 (d, *J*= 6.9 *Hz*, 2H, CH_2), 2.69 (d, *J*= 6.9 *Hz*, 2H, CH_2), 4.33 (d, *J*= 5.9 *Hz*, 2H, CH_2), 7.30 (bs, 2H, NH_2), 7.43 (d, *J*= 8.3 *Hz*, 2H, ArH), 7.76 (d, *J*= 8.3 *Hz*, 2H, ArH), 8.50 (t, *J*= 5.9 *Hz*, 1H, NH). Anal. for $C_{11}H_{16}N_2O_3S_2$: C 45.81%; H 5.59%; N 9.71%. Found: C 45.61%; H 5.39%; N 9.51%.

4.2 CA Inhibition assay

The CA catalysed CO_2 hydration activity has been tested by an Applied Photophysics *stopped–flow* instrument. Phenol red (at a concentration of 0.2 *mM*) has been used as indicator, working at the absorbance maximum of 557 *nm*, with 10–20 *mM* Tris (pH 8.3) or Hepes (pH 7.5) as buffers, and 20 *mM* Na_2SO_4or 20 *mM* $NaClO_4$ (for maintaining constant the ionic strength), following the initial rates of the CA–catalyzed CO_2 hydration reaction for a period of 10–100 *s*. The CO_2 concentrations ranged from 1.7 to 17 *mM* for the determination of kinetic parameters and inhibition constants. For each inhibitor six traces of the initial 5–10% of the reaction have been used for determining the initial velocity. The uncatalyzed rates were determined in the same manner and subtracted from the total observed rates. Stock solutions of inhibitor (10 *mM*) were prepared in distilled–deionized water and dilutions up to 0.01 *nM* were done thereafter with distilled–deionized water. Inhibitor and enzyme solutions were preincubated together for 15 min at room temperature prior to assay, in order to allow for the formation of the E–I complex. The inhibition constants were obtained by non–linear least–squares methods using PRISM 3, as reported earlier, and represent the mean from at least three different determinations. CA isoforms were recombinant ones produced in house [116]. The bacterial classes were prepared by the novel protonography techniques [114].

4.3 Anticonvulsant test

Male ICR CD–1 mice (n= 80) were purchased from Charles River Laboratories s.r.l. (Calco, Lecco, Italy). Animals were housed four/five per cage and kept under controlled environmental conditions (60 ± 5% humidity; 22°C ±2°C; 12/12 h reversed light/dark cycle; lights on at 8 pm). Animals were allowed free access to standard laboratory chow and tap water. This experimental protocol was approved by the local ethics committee of University of Catanzaro and all procedures involving animals and their care were in compliance with international and national regulations (EU Directive 2010/63/EU for animal experiments, ARRIVE guidelines and the Basel declaration including the 3R concept). Male ICR CD–1 mice (30–35 *g*, 35–40 days old) were pretreated with a solution of 49a, 49c, 50b and 50c (groups of 10 mice per dose) 30 *min* before the i.p. administration of pentylenetetrazole (PTZ) 60 *mg/kg* (inducing clonus in 80% of mice) in order to test the efficacy against clonus [117].

4.4 Docking analysis

4.4.1 Molecular docking studies using Gold

Molecular docking studies for 4–[4–(2–Fluorobenzoyl)piperazine–1–carbonyl]benzenesulfonamide 54b have been carried out by means of Gold Suite 5.7.1. [118]. The structure of the ligand was built and energy minimized by using VEGA ZZ [119]. The crystal structures of CA XII in complex with the inhibitor acetazolamide was retrieved from the RCSB Protein Data Bank (PDB code: 1JD0). The region of interest was defined in order to contain residues within 10 AngstromÅ from the mass of the co–crystallized ligand. A scaffold constraint (penalty= 5.0) was used to restrict the solutions in which the sulfonamide moiety was able to coordinate the metal within the catalytic binding site. ChemPLP was chosen as fitness function and the standard default settings were used in all calculations. Ligands were submitted to 100 genetic algorithm runs and the "allow early termination" command was deactivated. Results differing by less than 0.75 AngstromÅ in ligand–all atom RMSD, were clustered together. The best GOLD–calculated conformation was considered both for analysis and representation. The same docking protocol has been used for compounds 57h by using the crystal structures of CAVII in complex with 4–(4–phenylpiperidine–1–carbonyl)benzenesulfonamide 49a (PDB code: 6H36). Interactions were analyzed by using LigandScout V4.4.2 [120] and the figure were prepared by using opensource software PyMOL.

4.4.2 Molecular docking studies using AutoDock

Docking analysis has been carried out by means of AUTODOCK 4.2 software [121] for compounds 59–61, 62a–64a, 62b–64b, 69a–i, 70a–i, 71a, 71h–i. The crystal structures used have been retrieved from the Protein Data Bank (PDB code: 1JCZ and 1JD0). The ligand and

water molecules were discarded, and hydrogen atoms were added to protein with Discovery Studio 2.5.5. Structures of the ligand were constructed and energy minimized using VEGA ZZ [119]. The regions of interest used by AUTODOCK were defined by considering the suitable ligand docked into the CA XII receptor as the central group; in particular, a grid of 60, 60, and 60 points in the x, y, and z directions has been constructed centered on the mass of Zn ion. A grid spacing of 0.375 Å and a distance–dependent function of the dielectric constant were used for the energetic map calculations. Using the Lamarckian Genetic Algorithm, docked compound have been subjected to 100 runs of the AUTODOCK search, in which the default values of the other parameters were used. Cluster analysis was performed on the docked results using an RMS tolerance of 2.0 Å. The Lamarckian genetic algorithm (LGA) was applied to model the interaction between ligands and CA XII active site. For the Lamarckian genetic algorithm: 27,000 maximum generations, a gene mutation rate of 0.02 and a crossover rate of 0.8 were used. Cluster analysis was performed on the docked results using an RMSD (Root Mean Square Deviation) tolerance of 2 Å. The CA XII/ligand complex obtained by docking studies was minimized using 1000 iterations of SD and 1000 interaction of Polak–Ribiere Conjugate Gradient. Interactions were identified using the LigPlot software [121] and the figures were prepared using opensource software PyMOL or UCSF Chimera.

4.4.3   Modeling of VchCAβ active site

The crystal structure of β–CA from *V. cholerae* is not available in RCSB PDB in its "*open*" active site form. Therefore, the crystal structure of *closed* VchCAβ was downloaded from the PDB (PDB code: 5CXK). The suitable template for modeling VchCAβ active site was identified in β–CA from the unicellular green alga Coccomyxa (*Co*CA, PDB code: 3UCJ). A superimposition of residues C42, D44, R46, H98, C101, Zn301 of β–CA from *V. cholerae* on corresponding residues C7, D49, R51, H103, C106, Zn228 of chain A of X–ray complex of AAZ with *Co*CA was performed using PyMOL software (https://pymol.org). The above–mentioned superimposition was useful to modify the orientation of the side–chains of the two amino acids D44 and R46 of β–CA from *V. cholera*e using as template the conformation of D49 and R51 of *Co*CA. The modified structure of VchCAβ was minimized using the conjugate gradient algorithm of NAMD. Minimization was performed for 500 steps keeping all atoms fixed except for the backbones of residue 43–47 and the side–chains of D44 and R46: in detail, to maintain the correct orientation of carboxylate moiety of D44 and guanidinium group of R46 also these groups were kept fixed. The atom types were assigned using force field CHARMM v22 and the atomic charges according to Gasteiger–Marsili method by Vega ZZ [119]. Furthermore, in the obtained structure, assuming a similar binding mode of the AAZ in both of the β–CAs, we inserted in the catalytic site of VchCAβ the X–ray conformation of the acetazolamide retrieved from *Co*CA. The side–chains of the residues around the inhibitor AAZ have been minimized by LigandScout [120]. The obtained complex was used to perform docking studies for all compounds reported in section 2.4 according to the procedures

reported above (Section 4.4.2).

4.4.4 Pharmacophore Modelling and Virtual Screening

LigandScout V4.4.2 [120] has been used for the pharmacophore generation and the virtual screening process. All selected molecules (Training Setand Test Set, Figure 2.25–2.26) were constructed by Vega 3.1.1 [119]. The ligand–based pharmacophore model was generated using "merged features" option and maintaining the default parameters. Our model was validated by using two datasets a) the first one containing 72 inhibitors of the β–class of VchCA presenting a sulfonamide moiety and with a K_i value < 10,000 nM; b) the second one was generated throughout a web tool online DUD–E obtaining 3899 decoys. The ligand–based pharmacophore model has been used for a virtual screening against a SciFinder database containing 8.208 *para*–benzenesulfonamide derivatives. All virtual screening runs were conducted by setting the option "Get best matching conformation" as retrieval mode and the obtained hits from screening were ranked based on their pharmacophore fit scores.

4.5 X-ray crystallographic studies

Crystals of the hCA II and hCA VII with 49a, 49b, 50b adducts were obtained by co–crystallization. The complexes were prepared by adding a 5 M excess of the inhibitor to a 10 mg/mL protein solution. This mixture, equilibrated for 1 h at room temperature, was used for the crystallization experiments. Drops were prepared by mixing 1 μl of enzyme/inhibitor solution with 1 μl of precipitant solution containing 1.3 M sodium citrate, 0.1 M Tris–HCl, pH 8.5 and further equilibrated over a well containing 1 mL of precipitant buffer. Crystals appeared in the drops within 2–3 days and grew to a maximum dimension of $0.2 \times 0.3 \times 0.2$ mm^3 in about one week. Crystals of the hCA II–49a adduct were instead obtained by using the soaking technique. In particular, native hCA II crystals were grown at room temperature by the hanging drop vapor diffusion technique using a protein concentration of 10 mg/mL and 1.3 M sodium citrate, 0.1 M Tris–HCl, pH 8.5 as precipitant solution. A few hCA II crystals were then transferred in a 2 μl drop of freshly prepared precipitant solution containing also the inhibitor at the concentration of 2.5 mM and glycerol (15% v/v) as cryoprotectant. These crystals were kept in the soaking solution for one night and finally flash–frozen in liquid nitrogen. A very similar experimental strategy was used to obtain crystals of the hCA VII–inhibitor complexes. For crystallographic studies a mutated form of hCA VII, where the cysteine residues in position 183 and 217 were mutated to serines, was used, since we previously reported that this mutant was more suitable for crystallization experiments hCA VII crystals were grown at room temperature by the vapor diffusion hanging drop method. Equal volumes of protein (5 mg/mL in 0.02 M Tris–HCl pH 8.0 and 0.1 M NaCl) and precipitant solutions (25% v/v Peg3350, 0.2 M Ammonium acetate and 0.1 M Tris pH 8.5) were mixed and equilibrated against 1 mL reservoir containing the same precipitant solution. A few crystals

of hCA VII were then transferred into a 2 *μl* drop of the freshly prepared precipitant solution containing the inhibitor at a concentration of 40 *mM* for inhibitors 49a and 49b and 10 *mM* for 50b. Moreover, 25% (v/v) glycerol was used as cryoprotectant agent. These crystals were kept in the soaking solution overnight and then flash–frozen in a gaseous nitrogen stream prior to the diffraction experiment. All X–ray data sets were collected at 100 K by a copper rotating anode generator developed by Rigaku and equipped with a Rigaku Saturn CCD detector. Diffraction data were indexed, integrated and scaled using the HKL2000 software package. Data collection statistics are reported in Table 4.1. The initial phases of all structures were calculated using the atomic coordinates of hCA VII and hCA II (PDB accession code 6G4T and 1CA2 for hCA VII and II, respectively) with waters removed. The structures were refined using the CNS program as previously described, whereas model building and map inspections were performed using the program O. Topology files for inhibitors 49a, 49b, 50b generated using the PRODRG server. The same experimental procedures was used to obtain the crystal structures of 54a in complex with hCA II (PDB code: 6XXT) and 57h with hCA VII (not yet deposited in PDB). Table 4.2 collected the data statistics for hCAII/54a complex.

	hCA II in complex with			hCA VII in complex with		
	49a	**49b**	**50b**	**49a**	**49b**	**50b**
Cell parameters						
Space group	$P2_1$	$P2_1$	$P2_1$	$P2_12_12$	$P2_12_12$	$P2_12_12$
Cell dimensions (Å, °)	a= 42.4	a= 42.3	a= 42.3	a= 66.0	a= 66.0	a= 66.1
	b= 41.1	b= 41.4	b= 41.3	b= 88.1	b= 88.6	b= 89.2
	c= 71.7	c= 72.0	c= 72.1	c= 44.0	c= 44.1	c= 44.2
	β= 104.2	β= 104.2	β= 104.3			
Number of independent molecules	1	1	1	1	1	1
Data collection statistics	1.54178	1.54178	1.54178	1.54178	1.54178	1.54178
Resolution limits (Å)	34.7-1.94	29.1-1.58	29.1-1.55	31.1-1.85	30.9-1.90	34.0-1.70
Total reflections	70015	136858	121412	91414	69324	138766
Unique reflections	17564	30160	33156	21202	19303	28527
Redundancy	4.0	4.5	3.7	4.3	3.6	4.9
Completeness (%)	98.6 (90.2)	90.7 (77.2)	93.8 (82.5)	94.1 (88.9)	92.1 (69.4)	96.6 (90.2)
R-merge[*]	0.114 (0.418)	0.045 (0.147)	0.055 (0.228)	0.067 (0.459)	0.046 (0.181)	0.046 (0.503)
Rmeas[§]	0.131 (0.521)	0.050 (0.173)	0.062 (0.280)	0.074 (0.573)	0.052 (0.213)	0.051 (0.590)
Rpim[¶]	0.063 (0.306)	0.021 (0.089)	0.028 (0.161)	0.032 (0.338)	0.024 (0.108)	0.021 (0.301)
$<I>/<\sigma(I)>$	11.5 (2.3)	29.9 (9.0)	21.8 (4.4)	18.0 (2.2)	22.3 (7.4)	27.3 (2.6)
Refinement statistics						
Resolution limits (Å)	34.7-1.94	29.1-1.58	29.1-1.55	31.1-1.85	30.9-1.90	34.0-1.70
R-work[**] (%)	17.9	16.6	17.1	19.5	19.4	19.3
R-free[**] (%)	21.4	19.4	20.6	23.3	23.6	24.5
r.m.s.d. from ideal geometry:						
Bond lengths (Å)	0.006	0.008	0.009	0.008	0.007	0.006
Bond angles (°)	1.4	1.5	1.6	1.5	1.5	1.5
Number of protein atoms	2039	2093	2063	2066	2057	2055
Number of inhibitor atoms	24	25	26	24	25	26
Number of water molecules	158	225	229	116	115	144
Average B factor (Å²)						
All atoms	16.04	12.51	11.88	22.91	19.45	21.27
Protein atoms	15.42	11.52	10.78	22.61	19.22	20.75
Inhibitor atoms	16.97	15.50	20.29	21.45	19.60	19.92
Waters	23.30	21.33	20.57	28.68	23.68	28.32
PDB accession code	**6H2Z**	**6H33**	**6H34**	**6H36**	**6H37**	**6H38**

[*]R–merge=$\sum_{hkl}\sum_i |I_i(hkl) - \langle I(hkl)\rangle|/\sum_{hkl}\sum_i I_i(hkl)$, where $I_i(hkl)$ is the intensity of an observation and $\langle I(hkl)\rangle$ is the mean value for its unique reflection; summations are over all reflections; [§]Rmeans= $\sum_{hkl}\{N(hkl)/[N(hkl) - 1]\}^{1/2} \times \sum_i |I_i(hkl) - \langle I(hkl)\rangle|/\sum_{hkl}\sum_i I_i(hkl)$; [¶]Rpim=$\sum_{hkl}\{1/[N(hkl) - 1]\}^{1/2} \times \sum_i |I_i(hkl) - \langle I(hkl)\rangle|/\sum_{hkl}\sum_i I_i(hkl)$; [**]R–work=$\sum_{hkl} |Fo(hkl)| - |Fc(hkl)|/|\sum hkl Fo(hkl)|$ calculated for the working set of reflections. R–free is calculated as for R–work, but from data of the test set that was not used for refinement (Test Set Size (%) = 5.7% for hCA II/49a, 3.5% for hCA II/49b, 3.0% for hCA II/50b, 5.0% for hCA VII/49a and hCA VII/49b, 4.0% for hCA VII/50b). Values in parentheses are referred to the highest resolution shell (2.01–1.94 Å for hCA II/7a, 1.64–1.58 Å for hCA II/49b and 1.61–1.55 Å for hCA II/50b, 1.92-1.85 Å for hCA VII/49a, 1.97-1.90 Å for hCA VII/49b, 1.76-1.70 Å for hCA VII/50a).

Table 4.1: *Data collection statistics and refinement statistics.*

	hCA II/54a
Cell parameters	
Space group	$P2_1$
Cell dimensions (Å, °)	a= 42.3
	b= 41.5
	c= 72.1
	β= 104.3
Number of independent molecules	1
Data collection statistics	
Wavelength (Å)	1.0
Resolution limits (Å)	35.7-1.05
Total reflections	652807
Unique reflections	112517
Redundancy	5.8
Completeness (%)	99.2 (86.9)
R-merge[*]	0.072 (0.277)
Rmeas[§]	0.078 (0.323)
Rpim[¶]	0.031 (0.159)
$<I>/<\sigma(I)>$	22.1 (4.3)
Refinement statistics	
Resolution limits (Å)	35.7-1.05
R-work[**] (%)	13.5
R-free[**] (%)	14.6
r.m.s.d. from ideal geometry:	
Bond lengths (Å)	0.008
Bond angles (°)	1.5
Number of protein atoms	2129
Number of inhibitor atoms	26
Number of water molecules	271
Average B factor (Å^2)	
All atoms	16.03
Protein atoms	10.54
Inhibitor atoms	13.49
Waters	21.36
PDB accession code	6XXT

[*]R–merge=$\sum_{hkl}\sum_{\tau}|I_i(hkl) - \langle I(hkl)\rangle|/\sum_{hkl}\sum_i I_i(hkl)$, where $I_i(hkl)$ is the intensity of an observation and $\langle I(hkl)\rangle$ is the mean value for its unique reflection; summations are over all reflections; [§]Rmeans= $\sum_{hkl}\{N(hkl)/[N(hkl) - 1]\}^{1/2} \times \sum_i|I_i(hkl) - \langle I(hkl)\rangle|/\sum_{hk\lambda}\sum_i I_i(hkl)$; [¶]Rpim=$\sum_{hkl}\{1/[N(hkl) - 1]\}^{1/2} \times \sum_i|I_i(hkl) - \langle I(hkl)\rangle|/\sum_{hk\lambda}\sum_i I_i(hkl)$; [**]R–work=$\sum_{hkl}|Fo(hkl)| - |Fc(hkl)|/|\sum hklFo(hkl)|$ calculated for the working set of reflections. R–free is calculated as for R–work, but from data of the test set that was not used for refinement (Test Set Size (%) = 1.0%). Values in parentheses refer to the highest resolution shell (1.07-1.05 Å for hCA II/54a).).

Table 4.2: *Data collection statistics and refinement statistics.*

BIBLIOGRAPHY

[1] C. T. Supuran, "Structure and function of carbonic anhydrases", *Biochemical Journal*, **473**(14), pp. 2023–2032, (2016). doi: 10.1042/BCJ20160115.

[2] V. Alterio, A. Di Fiore, K. D'Ambrosio, C. T. Supuran, and G. De Simone, "Multiple binding modes of inhibitors to carbonic anhydrases: How to design specific drugs targeting 15 different isoforms?", *Chemical reviews*, **112**(8), pp. 4421–4468, (2012). doi: 10.1021/cr200176r.

[3] V Alterio, "Di fiore, a., d'ambrosio, k., supuran, ct, de simone, g. multiple binding modes of inhibitors to carbonic anhydrases: How to design specific drugs targeting 15 different isoforms", *Chem. Rev*, **112**, pp. 4421–4468, (2012). doi: 10.1021/cr200176r.

[4] A. Nocentini and C. T. Supuran, "Advances in the structural annotation of human carbonic anhydrases and impact on future drug discovery", *Expert opinion on drug discovery*, **14**(11), pp. 1175–1197, (2019). doi: 10.1080/17460441.2019.1651289.

[5] V. Alterio, P. Pan, S. Parkkila, M. Buonanno, C. T. Supuran, S. M. Monti, and G. De Simone, "The structural comparison between membrane-associated human carbonic anhydrases provides insights into drug design of selective inhibitors", *Biopolymers*, **101**(7), pp. 769–778, (2014). doi: 10.1002/bip.22456.

[6] M. Y. Mboge, B. P. Mahon, N. Lamas, L. Socorro, F. Carta, C. T. Supuran, S. C. Frost, and R. McKenna, "Structure activity study of carbonic anhydrase ix: Selective inhibition with ureido-substituted benzenesulfonamides", *European journal of medicinal chemistry*, **132**, pp. 184–191, (2017). doi: 10.1016/j.ejmech.2017.03.026.

[7] E. Bruno, M. R. Buemi, L. De Luca, S. Ferro, A.-M. Monforte, C. T. Supuran, D. Vullo, G. De Sarro, E. Russo, and R. Gitto, "In vivo evaluation of selective carbonic anhydrase inhibitors as potential anticonvulsant agents", *ChemMedChem*, **11**(16), pp. 1812–1818, (2016). doi: 10.1002/cmdc.201500596.

[8]   E. Bruno, M. R. Buemi, A. Di Fiore, L. De Luca, S. Ferro, A. Angeli, R. Cirilli, D. Sadutto, V. Alterio, S. M. Monti, et al. "Probing molecular interactions between human carbonic anhydrases (hcas) and a novel class of benzenesulfonamides", *Journal of medicinal chemistry*, **60**(10), pp. 4316–4326, (2017). doi: 10.1021/acs.jmedchem.7b00264.

[9]   L. De Luca, S. Ferro, F. M. Damiano, C. T. Supuran, D. Vullo, A. Chimirri, and R. Gitto, "Structure-based screening for the discovery of new carbonic anhydrase vii inhibitors", *European Journal of Medicinal Chemistry*, **71**, pp. 105–111, (2014). doi: 10.1016/j.ejmech.2013.10.071.

[10] R. Gitto, F. M. Damiano, P. Mader, L. De Luca, S. Ferro, C. T. Supuran, D. Vullo, J. Brynda, P. Rezacova, and A. Chimirri, "Synthesis, structure–activity relationship studies, and x-ray crystallographic analysis of arylsulfonamides as potent carbonic anhydrase inhibitors", *Journal of medicinal chemistry*, **55**(8), pp. 3891–3899, (2012). doi: 10.1021/jm300112w.

[11] R. Gitto, F. M. Damiano, L. De Luca, S. Ferro, D. Vullo, C. T. Supuran, and A. Chimirri, "Synthesis and biological profile of new 1, 2, 3, 4-tetrahydroisoquinolines as selective carbonic anhydrase inhibitors", *Bioorganic & medicinal chemistry*, **19**(23), pp. 7003–7007, (2011). doi: 10.1016/j.bmc.2011.10.015.

[12] P. Mader, J. Brynda, R. Gitto, S. Agnello, P. Pachl, C. T. Supuran, A. Chimirri, and P. Rezacova, "Structural basis for the interaction between carbonic anhydrase and 1, 2, 3, 4-tetrahydroisoquinolin-2-ylsulfonamides", *Journal of medicinal chemistry*, **54**(7), pp. 2522–2526, (2011). doi: 10.1021/jm2000213.

[13] R. Gitto, S. Agnello, S. Ferro, D. Vullo, C. T. Supuran, and A. Chimirri, "Identification of potent and selective human carbonic anhydrase vii (hca vii) inhibitors", *ChemMedChem*, **5**(6), pp. 823–826, (2010). doi: 10.1002/cmdc.201000044.

[14] R. Gitto, S. Agnello, S. Ferro, L. De Luca, D. Vullo, J. Brynda, P. Mader, C. T. Supuran, and A. Chimirri, "Identification of 3, 4-dihydroisoquinoline-2 (1 h)-sulfonamides as potent carbonic anhydrase inhibitors: Synthesis, biological evaluation, and enzyme-ligand x-ray studies", *Journal of medicinal chemistry*, **53**(6), pp. 2401–2408, (2010). doi: 10.1021/jm9014026.

[15] M. Aggarwal, C. D. Boone, B. Kondeti, and R. McKenna, "Structural annotation of human carbonic anhydrases", *Journal of enzyme inhibition and medicinal chemistry*, **28**(2), pp. 267–277, (2013). doi: https://doi.org/10.3109/14756366.2012.737323.

[16] C. T. Supuran, "Carbonic anhydrases: Novel therapeutic applications for inhibitors and activators", *Nature reviews Drug discovery*, **7**(2), pp. 168–181, (2008). doi: 10.1038/nrd2467.

[17] C. T. Supuran, "How many carbonic anhydrase inhibition mechanisms exist?", *Journal of enzyme inhibition and medicinal chemistry*, **31**(3), pp. 345–360, (2016). DOI: [10.3109/14756366.2015.1122001](10.3109/14756366.2015.1122001).

[18] V. De Luca, D. Vullo, A. Scozzafava, V. Carginale, M. Rossi, C. T. Supuran, and C. Capasso, "An α–carbonic anhydrase from the thermophilic bacterium sulphurihydrogenibium azorense is the fastest enzyme known for the CO_2 hydration reaction", *Bioorganic & medicinal chemistry*, **21**(6), pp. 1465–1469, (2013). DOI: [10.1016/j.bmc.2012.09.047](10.1016/j.bmc.2012.09.047).

[19] S. Del Prete, D. Vullo, A. Scozzafava, C. Capasso, and C. T. Supuran, "Cloning, characterization and anion inhibition study of the δ–class carbonic anhydrase (tweca) from the marine diatom thalassiosira weissflogii", *Bioorganic & Medicinal Chemistry*, **22**(1), pp. 531–537, (2014). DOI: [10.1016/j.bmc.2013.10.045](10.1016/j.bmc.2013.10.045).

[20] Y. Xu, L. Feng, P. D. Jeffrey, Y. Shi, and F. M. Morel, "Structure and metal exchange in the cadmium carbonic anhydrase of marine diatoms", *Nature*, **452**(7183), pp. 56–61, (2008). DOI: 10.1038/nature06636.

[21] S. Del Prete, D. Vullo, G. M. Fisher, K. T. Andrews, S.-A. Poulsen, C. Capasso, and C. T. Supuran, "Discovery of a new family of carbonic anhydrases in the malaria pathogen plasmodium falciparum—the η-carbonic anhydrases", *Bioorganic & medicinal chemistry letters*, **24**(18), pp. 4389–4396, (2014). DOI: 10.1016/j.bmcl.2014.08.015.

[22] V. Alterio, E. Langella, G. De Simone, and S. M. Monti, "Cadmium-containing carbonic anhydrase cdca1 in marine diatom thalassiosira weissflogii", *Marine drugs*, **13**(4), pp. 1688–1697, (2015). DOI: [10.3390/md13041688](10.3390/md13041688).

[23] A. S. Covarrubias, A. M. Larsson, M. Högbom, J. Lindberg, T. Bergfors, C. Björkelid, S. L. Mowbray, T. Unge, and T. A. Jones, "Structure and function of carbonic anhydrases from mycobacterium tuberculosis", *Journal of Biological Chemistry*, **280**(19), pp. 18 782–18 789, (2005). DOI: [10.1074/jbc.M414348200](10.1074/jbc.M414348200).

[24] G. De Simone, A. Di Fiore, C. Capasso, and C. T. Supuran, "The zinc coordination pattern in the η-carbonic anhydrase from plasmodium falciparum is different from all other carbonic anhydrase genetic families", *Bioorganic & medicinal chemistry letters*, **25**(7), pp. 1385–1389, (2015). DOI: 10.1016/j.bmcl.2015.02.046.

[25] B. E. Alber and J. G. Ferry, "A carbonic anhydrase from the archaeon methanosarcina thermophila", *Proceedings of the National Academy of Sciences*, **91**(15), pp. 6909–6913, (1994). DOI: 10.1073/pnas.91.15.6909.

[26] J.-Y. Winum, A. Scozzafava, J.-L. Montero, and C. T. Supuran, "Design of zinc binding functions for carbonic anhydrase inhibitors", *Current pharmaceutical design*, **14**(7), pp. 615–621, (2008). DOI: [10.2174/138161208783877848](10.2174/138161208783877848).

[27]   F. Carta, M. Aggarwal, A. Maresca, A. Scozzafava, R. McKenna, E. Masini, and C. T. Supuran, "Dithiocarbamates strongly inhibit carbonic anhydrases and show antiglaucoma action in vivo", *Journal of medicinal chemistry*, **55**(4), pp. 1721–1730, (2012). doi: 10.1021/jm300031j.

[28]   A. Di Fiore, A. Maresca, C. T. Supuran, and G. De Simone, "Hydroxamate represents a versatile zinc binding group for the development of new carbonic anhydrase inhibitors", *Chemical Communications*, **48**(70), pp. 8838–8840, (2012). doi: 10.1039/C2CC34275H.

[29]   V. Alterio, R. Cadoni, D. Esposito, D. Vullo, A. Di Fiore, S. M. Monti, A. Caporale, M. Ruvo, M. Sechi, P. Dumy, et al. "Benzoxaborole as a new chemotype for carbonic anhydrase inhibition", *Chemical communications*, **52**(80), pp. 11 983–11 986, (2016). doi: 10.1039/c6cc06399c.

[30]   A. Nocentini, P. Gratteri, and C. T. Supuran, "Phosphorus versus sulfur: Discovery of benzenephosphonamidates as versatile sulfonamide-mimic chemotypes acting as carbonic anhydrase inhibitors", *Chemistry–A European Journal*, **25**(5), pp. 1188–1192, (2019). doi: 10.1002/chem.201805039.

[31]   A. Innocenti, D. Vullo, A. Scozzafava, and C. T. Supuran, "Carbonic anhydrase inhibitors: Interactions of phenols with the 12 catalytically active mammalian isoforms (ca i–xiv)", *Bioorganic & medicinal chemistry letters*, **18**(5), pp. 1583–1587, (2008). doi: 10.1016/j.bmc.2008.06.013.

[32]   F. Carta, C. Temperini, A. Innocenti, A. Scozzafava, K. Kaila, and C. T. Supuran, "Polyamines inhibit carbonic anhydrases by anchoring to the zinc-coordinated water molecule", *Journal of Medicinal Chemistry*, **53**(15), pp. 5511–5522, (2010). doi: 10.1021/jm1003667.

[33]   K. Tars, D. Vullo, A. Kazaks, J. Leitans, A. Lends, A. Grandane, R. Zalubovskis, A. Scozzafava, and C. T. Supuran, "Sulfocoumarins (1, 2-benzoxathiine-2, 2-dioxides): A class of potent and isoform-selective inhibitors of tumor-associated carbonic anhydrases", *Journal of medicinal chemistry*, **56**(1), pp. 293–300, (2013). doi: 10.1021/jm301625s.

[34]   A. Nocentini, F. Carta, M. Tanc, S. Selleri, C. T. Supuran, C. Bazzicalupi, and P. Gratteri, "Deciphering the mechanism of human carbonic anhydrases inhibition with sulfocoumarins: Computational and experimental studies", *Chemistry–A European Journal*, **24**(31), pp. 7840–7844, (2018). doi: 10.1002/chem.201800941.

[35]   A. Maresca, C. Temperini, H. Vu, N. B. Pham, S.-A. Poulsen, A. Scozzafava, R. J. Quinn, and C. T. Supuran, "Non-zinc mediated inhibition of carbonic anhydrases: Coumarins are a new class of suicide inhibitors", *Journal of the American Chemical Society*, **131**(8), pp. 3057–3062, (2009). doi: 10.1021/ja809683v.

[36] A. Maresca, C. Temperini, L. Pochet, B. Masereel, A. Scozzafava, and C. T. Supuran, "Deciphering the mechanism of carbonic anhydrase inhibition with coumarins and thiocoumarins", *Journal of medicinal chemistry*, **53**(1), pp. 335–344, (2010). DOI: 10.1021/jm901287j.

[37] A. Nocentini, F. Carta, M. Ceruso, G. Bartolucci, and C. T. Supuran, "Click-tailed coumarins with potent and selective inhibitory action against the tumor-associated carbonic anhydrases ix and xii", *Bioorganic & Medicinal Chemistry*, **23**(21), pp. 6955–6966, (2015). DOI: 10.1016/j.bmc.2015.09.041.

[38] K. D'Ambrosio, S. Carradori, S. M. Monti, M. Buonanno, D. Secci, D. Vullo, C. T. Supuran, and G. De Simone, "Out of the active site binding pocket for carbonic anhydrase inhibitors", *Chemical Communications*, **51**(2), pp. 302–305, (2015). DOI: 10.1039/C4CC07320G.

[39] A. Scozzafava, F. Carta, and C. T. Supuran, "Secondary and tertiary sulfonamides: A patent review (2008–2012)", *Expert opinion on therapeutic patents*, **23**(2), pp. 203–213, (2013). DOI: 10.1517/13543776.2013.742065.

[40] A. D. Scott, C. Phillips, A. Alex, M. Flocco, A. Bent, A. Randall, R. O'Brien, L. Damian, and L. H. Jones, "Thermodynamic optimisation in drug discovery: A case study using carbonic anhydrase inhibitors", *ChemMedChem*, **4**(12), pp. 1985–1989, (2009). DOI: 10.1002/cmdc.200900386.

[41] D. Keilin and T Mann, "Carbonic anhydrase. purification and nature of the enzyme", *Biochemical Journal*, **34**(8-9), pp. 1163–1176, (1940). DOI: 10.1042/bj0341163.

[42] C. Temperini, A. Innocenti, A. Guerri, A. Scozzafava, S. Rusconi, and C. T. Supuran, "Phosph (on) ate as a zinc-binding group in metalloenzyme inhibitors: X-ray crystal structure of the antiviral drug foscarnet complexed to human carbonic anhydrase i", *Bioorganic & medicinal chemistry letters*, **17**(8), pp. 2210–2215, (2007). DOI: 10.1016/j.bmcl.2007.01.113.

[43] M. Abellán-Flos, M. Tanç, C. T. Supuran, and S. P. Vincent, "Multimeric xanthates as carbonic anhydrase inhibitors", *Journal of enzyme inhibition and medicinal chemistry*, **31**(6), pp. 946–952, (2016). DOI: 10.3109/14756366.2015.1072177.

[44] D. P. Martin and S. M. Cohen, "Nucleophile recognition as an alternative inhibition mode for benzoic acid based carbonic anhydrase inhibitors", *Chemical Communications*, **48**(43), pp. 5259–5261, (2012). DOI: 10.1039/c2cc32013d.

[45] R. A. Davis, A. Hofmann, A. Osman, R. A. Hall, F. A. Muhlschlegel, D. Vullo, A. Innocenti, C. T. Supuran, and S.-A. Poulsen, "Natural product-based phenols as novel probes for mycobacterial and fungal carbonic anhydrases", *Journal of medicinal chemistry*, **54**(6), pp. 1682–1692, (2011). DOI: 10.1021/jm1013242.

[46] C. Temperini, A. Innocenti, A. Scozzafava, S. Parkkila, and C. T. Supuran, "The coumarin-binding site in carbonic anhydrase accommodates structurally diverse inhibitors: The antiepileptic lacosamide as an example and lead molecule for novel classes of carbonic anhydrase inhibitors", *Journal of medicinal chemistry*, **53**(2), pp. 850–854, (2010). doi: 10.1021/jm901524f.

[47] C. T. Supuran, "Carbonic anhydrase activators", *Future Medicinal Chemistry*, **10**(5), pp. 561–573, (2018). doi: 10.4155/fmc-2017-0223.

[48] G. De Simone, C. Capasso, and C. T. Supuran, "Amine, amino acid and oligopeptide carbonic anhydrase activators", (2014). doi: 10.4155/fseb2013.13.42.

[49] F. Briganti, S. Mangani, P. Orioli, A. Scozzafava, G. Vernaglione, and C. T. Supuran, "Carbonic anhydrase activators: X-ray crystallographic and spectroscopic investigations for the interaction of isozymes i and ii with histamine", *Biochemistry*, **36**(34), pp. 10 384–10 392, (1997). doi: 10.1021/bi970760v.

[50] C. Temperini, A. Scozzafava, D. Vullo, and C. T. Supuran, "Carbonic anhydrase activators. activation of isozymes i, ii, iv, va, vii, and xiv with l-and d-histidine and crystallographic analysis of their adducts with isoform ii: Engineering proton-transfer processes within the active site of an enzyme", *Chemistry–A European Journal*, **12**(27), pp. 7057–7066, (2006). doi: 10.1002/chem.200600159.

[51] C. Temperini, A. Scozzafava, D. Vullo, and C. T. Supuran, "Carbonic anhydrase activators. activation of isoforms i, ii, iv, va, vii, and xiv with l-and d-phenylalanine and crystallographic analysis of their adducts with isozyme ii: Stereospecific recognition within the active site of an enzyme and its consequences for the drug design", *Journal of medicinal chemistry*, **49**(10), pp. 3019–3027, (2006). doi: 10.1021/jm0603320.

[52] C. Temperini, A. Innocenti, A. Scozzafava, and C. T. Supuran, "Carbonic anhydrase activators: Kinetic and x-ray crystallographic study for the interaction of d-and l-tryptophan with the mammalian isoforms i–xiv", *Bioorganic & medicinal chemistry*, **16**(18), pp. 8373–8378, (2008). doi: 10.1016/j.bmc.2008.08.043.

[53] G. N. Shah, G. Bonapace, P. Y. Hu, P. Strisciuglio, and W. S. Sly, "Carbonic anhydrase ii deficiency syndrome (osteopetrosis with renal tubular acidosis and brain calcification): Novel mutations in ca2 identified by direct sequencing expand the opportunity for genotype-phenotype correlation", *Human mutation*, **24**(3), pp. 272–272, (2004). doi: 10.1002/humu.9266.

[54] N. Meldrum and F. Roughton, "The state of carbon dioxide in blood", *The Journal of physiology*, **80**(2), p. 143, (1933). doi: 10.1113/jphysiol.1933.sp003078.

[55] C. Supuran and G. De Simone, *Carbonic anhydrases as biocatalysts: from theory to medical and industrial applications*. Elsevier, 2015.

[56]   W. Kong and J. Yang, "The complete chloroplast genome sequence of morus mongolica and a comparative analysis within the fabidae clade", *Current genetics*, **62**(1), pp. 165–172, (2016). doi: 10.1007/s00294-009-0238-x.

[57]   A. Nocentini, R. Cadoni, P. Dumy, C. T. Supuran, and J.-Y. Winum, "Carbonic anhydrases from trypanosoma cruzi and leishmania donovani chagasi are inhibited by benzoxaboroles", *Journal of Enzyme Inhibition and Medicinal Chemistry*, **33**(1), pp. 286–289, (2018). doi: 10.1080/14756366.2017.1414808.

[58]   A. Bertucci, A. Moya, S. Tambutté, D. Allemand, C. T. Supuran, and D. Zoccola, "Carbonic anhydrases in anthozoan corals—a review", *Bioorganic & medicinal chemistry*, **21**(6), pp. 1437–1450, (2013). doi: 10.1016/j.bmc.2012.10.024.

[59]   R. J. DiMario, M. C. Machingura, G. L. Waldrop, and J. V. Moroney, "The many types of carbonic anhydrases in photosynthetic organisms", *Plant science*, **268**, pp. 11–17, (2018). doi: 10.1016/j.plantsci.2017.12.002.

[60]   C. T. Supuran, "Carbonic anhydrase inhibition and the management of hypoxic tumors", *Metabolites*, **7**(3), p. 48, (2017). doi: 10.3390/metabo7040056.

[61]   B.-B. Gao, X. Chen, N. Timothy, L. P. Aiello, and E. P. Feener, "Characterization of the vitreous proteome in diabetes without diabetic retinopathy and diabetes with proliferative diabetic retinopathy", *Journal of proteome research*, **7**(6), pp. 2516–2525, (2008). doi: 10.1021/pr800112g.

[62]   F. Mincione, A. Scozzafava, and C. T. Supuran, "The development of topically acting carbonic anhydrase inhibitors as antiglaucoma agents", *Current pharmaceutical design*, **14**(7), pp. 649–654, (2008). doi: 10.2174/138161208783877866.

[63]   N. Hen, M. Bialer, B. Yagen, A. Maresca, M. Aggarwal, A. H. Robbins, R. McKenna, A. Scozzafava, and C. T. Supuran, "Anticonvulsant 4-aminobenzenesulfonamide derivatives with branched-alkylamide moieties: X-ray crystallography and inhibition studies of human carbonic anhydrase isoforms i, ii, vii, and xiv", *Journal of medicinal chemistry*, **54**(11), pp. 3977–3981, (2011). doi: 10.1021/jm200209n.

[64]   C. T. Supuran, "Diuretics: From classical carbonic anhydrase inhibitors to novel applications of the sulfonamides", *Current pharmaceutical design*, **14**(7), pp. 641–648, (2008). doi: 10.2174/138161208783877947.

[65]   E. R. Swenson and L. J. Teppema, "Prevention of acute mountain sickness by acetazolamide: As yet an unfinished story", *Journal of Applied Physiology*, **102**(4), pp. 1305–1307, (2007). doi: 10.1152/japplphysiol.01407.2006.

[66]   C. T. Supuran, A. S. A. Altamimi, and F. Carta, "Carbonic anhydrase inhibition and the management of glaucoma: A literature and patent review 2013-2019", *Expert Opinion on Therapeutic Patents*, **29**(10), pp. 781–792, (2019). doi: 10.1080/13543776.2019.1679117.

[67] D. M. Monti, M. M. Rigano, S. M. Monti, and H. S. Peixoto, "Role of antioxidants in the protection from aging-related diseases", *Oxidative medicine and cellular longevity*, **2019**, (2019). doi: 10.1155/2018/2018306.

[68] T. O. Price, N. Sheibani, and G. N. Shah, "Regulation of high glucose-induced apoptosis of brain pericytes by mitochondrial ca va: A specific target for prevention of diabetic cerebrovascular pathology", *Biochimica et Biophysica Acta (BBA)-Molecular Basis of Disease*, **1863**(4), pp. 929–935, (2017). doi: 10.1016/j.bbadis.2017.01.025.

[69] G. D. Simone, A. D. Fiore, and C. T. Supuran, "Are carbonic anhydrase inhibitors suitable for obtaining antiobesity drugs?", *Current pharmaceutical design*, **14**(7), pp. 655–660, (2008). doi: 10.2174/138161208783877820.

[70] M. Patrikainen, P. Pan, N. Kulesskaya, V. Voikar, and S. Parkkila, "The role of carbonic anhydrase vi in bitter taste perception: Evidence from the car6-/- mouse model", *Journal of biomedical science*, **21**(1), pp. 1–7, (2014). doi: 10.1186/s12929-014-0082-2.

[71] C. T. Supuran, "Carbonic anhydrase inhibition and the management of neuropathic pain", *Expert review of neurotherapeutics*, **16**(8), pp. 961–968, (2016). doi: 10.1080/14737175.2016.1193009.

[72] S. Singh, C. L. Lomelino, M. Y. Mboge, S. C. Frost, and R. McKenna, "Cancer drug development of carbonic anhydrase inhibitors beyond the active site", *Molecules*, **23**(5), p. 1045, (2018). doi: 10.3390/molecules23051045.

[73] S. Liao, S Ivanov, A Ivanova, S Ghosh, M. Cote, K Keefe, M Coca-Prados, E. Stanbridge, and M. Lerman, "Expression of cell surface transmembrane carbonic anhydrase genes ca9 and ca12 in the human eye: Overexpression of ca12 (caxii) in glaucoma", *Journal of medical genetics*, **40**(4), pp. 257–261, (2003). doi: 10.1136/jmg.40.4.257.

[74] J. M. Ogilvie, K. K. Ohlemiller, G. N. Shah, B. Ulmasov, T. A. Becker, A. Waheed, A. K. Hennig, P. D. Lukasiewicz, and W. S. Sly, "Carbonic anhydrase xiv deficiency produces a functional defect in the retinal light response", *Proceedings of the National Academy of Sciences*, **104**(20), pp. 8514–8519, (2007). doi: 10.1073/pnas.0702899104.

[75] S. Huang, B. Sjöblom, A. E. Sauer-Eriksson, and B.-H. Jonsson, "Organization of an efficient carbonic anhydrase: Implications for the mechanism based on structure-function studies of a t199p/c206s mutant", *Biochemistry*, **41**(24), pp. 7628–7635, (2002). doi: 10.1021/bi020053o.

[76] J. Zheng, B. S. Avvaru, C. Tu, R. McKenna, and D. N. Silverman, "Role of hydrophilic residues in proton transfer during catalysis by human carbonic anhydrase ii", *Biochemistry*, **47**(46), pp. 12 028–12 036, (2008). doi: 10.1021/bi801473w.

[77] J. F. Domsic and R. McKenna, "Sequestration of carbon dioxide by the hydrophobic pocket of the carbonic anhydrases", *Biochimica et Biophysica Acta (BBA)-Proteins and Proteomics*, **1804**(2), pp. 326–331, (2010). doi: 10.1016/j.bbapap.2009.07.025.

[78] F. Carta and C. T. Supuran, "Diuretics with carbonic anhydrase inhibitory action: A patent and literature review (2005–2013)", *Expert opinion on therapeutic patents*, **23**(6), pp. 681–691, (2013). doi: 10.1517/13543776.2013.780598.

[79] F. Carta, C. T. Supuran, and A. Scozzafava, "Novel therapies for glaucoma: A patent review 2007–2011", *Expert opinion on therapeutic patents*, **22**(1), pp. 79–88, (2012). doi: 10.1517/13543776.2012.649006.

[80] E. Masini, F. Carta, A. Scozzafava, and C. T. Supuran, "Antiglaucoma carbonic anhydrase inhibitors: A patent review", *Expert opinion on therapeutic patents*, **23**(6), pp. 705–716, (2013). doi: 10.1517/13543776.2013.794788.

[81] M. Aggarwal, B. Kondeti, and R. McKenna, "Anticonvulsant/antiepileptic carbonic anhydrase inhibitors: A patent review", *Expert opinion on therapeutic patents*, **23**(6), pp. 717–724, (2013). doi: 10.1517/13543776.2013.782394.

[82] C. T. Supuran, "Applications of carbonic anhydrases inhibitors in renal and central nervous system diseases", *Expert Opinion on Therapeutic Patents*, **28**(10), pp. 713–721, (2018). doi: 10.1080/13543776.2018.1519023.

[83] C. T. Supuran, "Drug interaction considerations in the therapeutic use of carbonic anhydrase inhibitors", *Expert Opinion on Drug Metabolism & Toxicology*, **12**(4), pp. 423–431, (2016). doi: 10.1517/17425255.2016.1154534.

[84] S. J. Dodgson, R. P. Shank, and B. E. Maryanoff, "Topiramate as an inhibitor of carbonic anhydrase isoenzymes", *Epilepsia*, **41**, pp. 35–39, (2000). doi: 10.1111/j.1528-1157.2000.tb06047.x.

[85] G. De Simone, A. Di Fiore, V. Menchise, C. Pedone, J. Antel, A. Casini, A. Scozzafava, M. Wurl, and C. T. Supuran, "Carbonic anhydrase inhibitors. zonisamide is an effective inhibitor of the cytosolic isozyme ii and mitochondrial isozyme v: Solution and x-ray crystallographic studies", *Bioorganic & medicinal chemistry letters*, **15**(9), pp. 2315–2320, (2005). doi: 10.1016/j.bmcl.2005.03.032.

[86] A. Weber, A. Casini, A. Heine, D. Kuhn, C. T. Supuran, A. Scozzafava, and G. Klebe, "Unexpected nanomolar inhibition of carbonic anhydrase by cox-2-selective celecoxib: New pharmacological opportunities due to related binding site recognition", *Journal of medicinal chemistry*, **47**(3), pp. 550–557, (2004). doi: 10.1021/jm030912m.

[87] K. Köhler, A. Hillebrecht, J. Schulze Wischeler, A. Innocenti, A. Heine, C. T. Supuran, and G. Klebe, "Saccharin inhibits carbonic anhydrases: Possible explanation for its unpleasant metallic aftertaste", *Angewandte Chemie International Edition*, **46**(40), pp. 7697–7699, (2007). doi: 10.1002/anie.200701189.

[88] A. Angeli, M. Ferraroni, A. Nocentini, S. Selleri, P. Gratteri, C. T. Supuran, and F. Carta, "Polypharmacology of epacadostat: A potent and selective inhibitor of the tumor associated carbonic anhydrases ix and xii", *Chemical Communications*, **55**(40), pp. 5720–5723, (2019). doi: 10.1039/C8CC09568J.

[89] P. C. McDonald, S. Chia, P. L. Bedard, Q. Chu, M. Lyle, L. Tang, M. Singh, Z. Zhang, C. T. Supuran, D. J. Renouf, et al. "A phase 1 study of slc-0111, a novel inhibitor of carbonic anhydrase ix, in patients with advanced solid tumors", *American Journal of Clinical Oncology*, (2020). doi: 10.1097/COC.0000000000000691.

[90] B. C. C. Agency. (2018). A study of slc-0111 and gemcitabine for metastatic pancreatic ductal cancer in subjects positive for caix (slc-0111-17-01), [Online]. Available: https://clinicaltrials.gov/ct2/show/NCT03450018 (visited on 09/25/2020).

[91] B.-B. Gao, A. Clermont, S. Rook, S. J. Fonda, V. J. Srinivasan, M. Wojtkowski, J. G. Fujimoto, R. L. Avery, P. G. Arrigg, S.-E. Bursell, et al. "Extracellular carbonic anhydrase mediates hemorrhagic retinal and cerebral vascular permeability through prekallikrein activation", *Nature medicine*, **13**(2), pp. 181–188, (2007). doi: 10.1038/nm1534.

[92] N. Oksala, M. Levula, M. Pelto-Huikko, L. Kytömäki, J. T. Soini, J. Salenius, M. Kähönen, P. J. Karhunen, R. Laaksonen, S. Parkkila, et al. "Carbonic anhydrases ii and xii are up-regulated in osteoclast-like cells in advanced human atherosclerotic plaques—tampere vascular study", *Annals of medicine*, **42**(5), pp. 360–370, (2010). doi: 10.3109/07853890.2010.486408.

[93] A. D. Kenny, "Role of carbonic anhydrase in bone: Plasma acetazolamide concentrations associated with inhibition of bone loss", *Pharmacology*, **31**(2), pp. 97–107, (1985). doi: 10.1159/000138104.

[94] H.-Y. Dai, C.-C. Hong, S.-C. Liang, M.-D. Yan, G.-M. Lai, A.-L. Cheng, and S.-E. Chuang, "Carbonic anhydrase iii promotes transformation and invasion capability in hepatoma cells through fak signaling pathway", *Molecular Carcinogenesis: Published in cooperation with the University of Texas MD Anderson Cancer Center*, **47**(12), pp. 956–963, (2008). doi: 10.1002/mc.20448.

[95] G. Rebello, R. Ramesar, A. Vorster, L. Roberts, L. Ehrenreich, E. Oppon, D. Gama, S. Bardien, J. Greenberg, G. Bonapace, et al. "Apoptosis-inducing signal sequence mutation in carbonic anhydrase iv identified in patients with the rp17 form of retinitis pigmentosa", *Proceedings of the National Academy of Sciences*, **101**(17), pp. 6617–6622, (2004). doi: 10.1073/pnas.0401529101.

[96] Y. Ikeda, T. Hisatomi, N. Yoshida, S. Notomi, Y. Murakami, H. Enaida, and T. Ishibashi, "The clinical efficacy of a topical dorzolamide in the management of cystoid macular edema in patients with retinitis pigmentosa", *Graefe's Archive for Clinical and Experimental Ophthalmology*, **250**(6), pp. 809–814, (2012). doi: 10.1007/s00417-011-1904-5.

[97] C. T. Supuran, "Carbonic anhydrase inhibitors in the treatment and prophylaxis of obesity", *Expert Opinion on Therapeutic Patents*, **13**(10), pp. 1545–1550, (2003). doi: 10.1517/13543776.13.10.1545.

[98] E. Ruusuvuori, H. Li, K. Huttu, J. M. Palva, S. Smirnov, C. Rivera, K. Kaila, and J. Voipio, "Carbonic anhydrase isoform vii acts as a molecular switch in the development of synchronous gamma-frequency firing of hippocampal ca1 pyramidal cells", *Journal of Neuroscience*, **24**(11), pp. 2699–2707, (2004). doi: 10.1523/JNEUROSCI.5176-03.2004.

[99] A. Nocentini and C. T. Supuran, "Carbonic anhydrase inhibitors for the treatment of neuropathic pain and arthritis", in *Carbonic Anhydrases*, Elsevier, 2019, pp. 367–386. doi: 10.1016/B978-0-12-816476-1.00017-4.

[100] C. L. Lomelino, J. T. Andring, and R. McKenna, "Crystallography and its impact on carbonic anhydrase research", *International journal of medicinal chemistry*, **2018**, (2018). doi: 10.1155/2018/9419521.

[101] N. K. Tafreshi, M. C. Lloyd, M. M. Bui, R. J. Gillies, and D. L. Morse, "Carbonic anhydrase ix as an imaging and therapeutic target for tumors and metastases", in *Carbonic Anhydrase: Mechanism, Regulation, Links to Disease, and Industrial Applications*, Springer, 2014, pp. 221–254. doi: 10.1007/978-94-007-7359-2_12.

[102] S. Pastorekova and R. J. Gillies, "The role of carbonic anhydrase ix in cancer development: Links to hypoxia, acidosis, and beyond", *Cancer and Metastasis Reviews*, **38**(1-2), pp. 65–77, (2019). doi: 10.1007/s10555-019-09799-0.

[103] H. M. Berman, J. Westbrook, Z. Feng, G. Gilliland, T. N. Bhat, H. Weissig, I. N. Shindyalov, and P. E. Bourne, "The Protein Data Bank", *Nucleic Acids Research*, **28**(1), pp. 235–242, (2000). doi: 10.1093/nar/28.1.235.

[104] RCSB-PDB. (2000). Protein data bank, biological macromolecular structures enabling breakthroughs in research and education, [Online]. Available: https://www.rcsb.org/ (visited on 09/27/2020).

[105] C. T. Supuran and C. Capasso, "An overview of the bacterial carbonic anhydrases", *Metabolites*, **7**(4), p. 56, (2017). doi: 10.3390/metabo7040056.

[106] S. Morishita, I. Nishimori, T. Minakuchi, S. Onishi, H. Takeuchi, T. Sugiura, D. Vullo, A. Scozzafava, and C. T. Supuran, "Cloning, polymorphism, and inhibition of β-carbonic anhydrase of helicobacter pylori", *Journal of gastroenterology*, **43**(11), pp. 849–857, (2008). doi: 10.1007/s00535-008-2240-3.

[107] I. Nishimori, S. Onishi, H. Takeuchi, and C. T. Supuran, "The α and β classes carbonic anhydrases from helicobacter pylori as novel drug targets", *Current pharmaceutical design*, **14**(7), pp. 622–630, (2008). doi: 10.2174/138161208783877875.

[108] B. Kusian, D. Sültemeyer, and B. Bowien, "Carbonic anhydrase is essential for growth of ralstonia eutropha at ambient CO_2 concentrations", *Journal of bacteriology*, **184**(18), pp. 5018–5026, (2002). DOI: 10.1128/JB.184.18.5018-5026.2002.

[109] C. Merlin, M. Masters, S. McAteer, and A. Coulson, "Why is carbonic anhydrase essential to escherichia coli?", *Journal of Bacteriology*, **185**(21), pp. 6415–6424, (2003). DOI: 10.1128/JB.185.21.6415-6424.2003.

[110] S. Del Prete, S. Isik, D. Vullo, V. De Luca, V. Carginale, A. Scozzafava, C. T. Supuran, and C. Capasso, "Dna cloning, characterization, and inhibition studies of an α-carbonic anhydrase from the pathogenic bacterium vibrio cholerae", *Journal of medicinal chemistry*, **55**(23), pp. 10 742–10 748, (2012). DOI: 10.1021/jm301611m.

[111] A. Akdemir, C. Supuran, A Angeli, Ö Güzel-Akdemir, et al. "Novel indole-based hydrazones as potent inhibitors of the α-class carbonic anhydrase from pathogenic bacterium vibrio cholerae.", (2020). DOI: 10.3390/ijms21093131.

[112] M. Ferraroni, S. Del Prete, D. Vullo, C. Capasso, and C. T. Supuran, "Crystal structure and kinetic studies of a tetrameric type ii β-carbonic anhydrase from the pathogenic bacterium vibrio cholerae", *Acta Crystallographica Section D: Biological Crystallography*, **71**(12), pp. 2449–2456, (2015). DOI: 10.1107/S1399004715018635.

[113] S. Del Prete, D. Vullo, V. De Luca, V. Carginale, M. Ferraroni, S. M. Osman, Z. AlOthman, C. T. Supuran, and C. Capasso, "Sulfonamide inhibition studies of the β-carbonic anhydrase from the pathogenic bacterium vibrio cholerae", *Bioorganic & medicinal chemistry*, **24**(5), pp. 1115–1120, (2016). DOI: 10.1016/j.bmc.2016.01.037.

[114] V. De Luca, S. Del Prete, C. T. Supuran, and C. Capasso, "Protonography, a new technique for the analysis of carbonic anhydrase activity", *Journal of enzyme inhibition and medicinal chemistry*, **30**(2), pp. 277–282, (2015). DOI: 10.3109/14756366.2014.917085.

[115] C. Capasso and C. T. Supuran, "An overview of the α–, β– and γ–carbonic anhydrases from bacteria: Can bacterial carbonic anhydrases shed new light on evolution of bacteria?", *Journal of enzyme inhibition and medicinal chemistry*, **30**(2), pp. 325–332, (2015). DOI: 10.3109/14756366.2014.910202.

[116] I. Nishimori, D. Vullo, A. Innocenti, A. Scozzafava, A. Mastrolorenzo, and C. T. Supuran, "Carbonic anhydrase inhibitors: Inhibition of the transmembrane isozyme xiv with sulfonamides", *Bioorganic & medicinal chemistry letters*, **15**(17), pp. 3828–3833, (2005). DOI: 10.1016/j.bmcl.2005.06.055.

[117] E. Russo, A. Constanti, G. Ferreri, R. Citraro, and G. De Sarro, "Nifedipine affects the anticonvulsant activity of topiramate in various animal models of epilepsy", *Neuropharmacology*, **46**(6), pp. 865–878, (2004). DOI: 10.1016/j.neuropharm.2003.11.028.

[118] G. Jones, P. Willett, R. C. Glen, A. R. Leach, and R. Taylor, "Development and validation of a genetic algorithm for flexible docking", *Journal of molecular biology*, **267**(3), pp. 727–748, (1997). doi: 10.1006/jmbi.1996.0897.

[119] G. Vistoli, A. Mazzolari, B. Testa, and A. Pedretti, "Binding space concept: A new approach to enhance the reliability of docking scores and its application to predicting butyrylcholinesterase hydrolytic activity", *Journal of chemical information and modeling*, **57**(7), pp. 1691–1702, (2017). doi: 10.1021/acs.jcim.7b00121.

[120] G. Wolber and T. Langer, "Ligandscout: 3-d pharmacophores derived from protein-bound ligands and their use as virtual screening filters", *Journal of chemical information and modeling*, **45**(1), pp. 160–169, (2005). doi: 10.1021/ci049885e.

[121] G. M. Morris, R. Huey, W. Lindstrom, M. F. Sanner, R. K. Belew, D. S. Goodsell, and A. J. Olson, "Autodock4 and autodocktools4: Automated docking with selective receptor flexibility", *Journal of computational chemistry*, **30**(16), pp. 2785–2791, (2009). doi: 10.1002/jcc.21256.

Appendix

Transition-Metal-Mediated versus Tetrazine-Triggered Bioorthogonal Release Reactions: Direct Comparison and Combinations Thereof

Francesca Mancuso,[a] Michal Rahm,[b] Rastislav Dzijak,[b] Helena Mertlíková-Kaiserová,[b] and Milan Vrabel*[b]

Bioorthogonal cleavage reactions are gaining popularity in chemically inducible prodrug activation and in the control of biomolecular functions. Despite similar applications, these reactions were developed and optimized on different substrates and under different experimental conditions. Reported herein is a side-by-side comparison of palladium-, ruthenium- and tetrazine-triggered release reactions, which aims at comparing the reaction kinetics, efficiency and overall advantages and limitations of the methods. In addition, we disclose the possibility of mutual combination of the cleavage reactions. Finally, we compare the efficiency of the bioorthogonal deprotections in cellular experiments, which revealed that among the three methods investigated, the palladium- and the tetrazine-promoted reaction can be used for efficient prodrug activation, but only the tetrazine-triggered reactions proceed efficiently inside cells.

Biocompatible cleavage reactions complement bioorthogonal bond forming reactions by enabling control and activation of molecular functions in response to specific chemical stimuli.[1] One of the earliest examples of bioorthogonal cleavage reactions is based on the Ru-catalyzed cleavage of allylcarbamate-protected amines. This reaction can be performed under biological conditions as originally shown by deprotection of fluorogenic alloc-caged rhodamine dye in HeLa cells.[2] Careful structural optimization of the Ru-complex further led to improved catalytic turnover number and efficiency of the reaction.[3] Embedding of organelle-targeting groups to such catalytic systems enables performing the cleavage reaction even in an organelle-specific manner.[4] Inspired by the great success of Pd-mediated chemical transformations in organic

synthesis,[5] Pd-assisted deprotections were employed as alternative organometallic decaging reactions.[6] Pd-mediated deprotections were mainly used for prodrug activation[7] and for chemically-induced rescuing of molecular function of proteins.[8]

The click-to-release strategy based on the inverse electron-demand Diels-Alder (IEDDA) reaction of alkene dienophiles with 1,2,4,5-tetrazines (Tz) was developed as an alternative to the metal-promoted deprotection reactions. A pioneering work from the Robillard's group showed that allylic trans-cyclooctene (TCO)-caged carbamates undergo after initial Diels-Alder reaction with tetrazines a set of electron-cascade elimination steps leading to the release of free amino group. The power of the concept was demonstrated by bioorthogonal activation of TCO-caged doxorubicin, which was successfully reactivated after TCO elimination from the respective TCO-caged prodrug.[9] Later, the same group reported that other functional groups including carbonates, esters and ethers can be activated using the same strategy.[10] Recently, the approach was extended to the release of tetrazine-caged compounds.[11] In combination with the targeting ability of antibodies, the activation strategy was successfully applied for targeted release of biologically active compounds from antibody-drug conjugates.[12] Another example showed that the chemistry can be used for chemically-induced control over T-cell activation by bioorthogonal deprotection of TCO-caged epitopes.[13] In addition to the strained TCO, vinyl ethers,[14] benzonorbornadienes[15] and 3-isocyanopropyl groups[16] were employed as alternative dienophiles in tetrazine-promoted deprotection reactions.[17]

All these examples illustrate the great potential of bioorthogonal cleavage reactions for non-enzymatic, chemically-inducible prodrug activation or for on-demand controlled switch of biomolecular function. Various experimental conditions and model systems were used throughout these studies to optimize the reaction conditions and to achieve best possible release yield and efficiency. This makes it very difficult to compare the individual methods in a broader context. With the aim to fill this gap, we herein report a side-by-side comparison of two different metal-promoted and the tetrazine-triggered decaging reaction with the focus on overall release efficacy and reaction kinetics. In addition, we explore the possibility of mutual combinations of the methods in an effort to further expand the scope of these chemical transformations toward simultaneous multi-decaging applications.

To enable direct comparison of various bioorthogonal deprotection reactions we first needed a test releasing system containing variable caging moieties. Fluorogenic reagents

[a] F. Mancuso
University of Messina
Department of Chemical, Biological
Pharmaceutical and Environmental Sciences (CHIBIOFARAM)
Viale Palatucci 13, I-98168, Messina (Italy)
[b] M. Rahm, Dr. R. Dzijak, Dr. H. Mertlíková-Kaiserová, Dr. M. Vrabel
Institute of Organic Chemistry
and Biochemistry of the Czech Academy of Sciences
Flemingovo nám. 2, 166 10, Prague (Czech Republic)
E-mail: vrabel@uochb.cas.cz

leading to formation of fluorescent dyes during the decaging reaction represent a convenient strategy for monitoring the process. Indeed, previous studies have utilized various fluorogenic probes based mainly on coumarine, rhodamine or naphthalene scaffolds to optimize the reaction conditions.[18] To

avoid errors that could arise by the use of different fluorophore systems for different decaging reactions we designed a 'universal' probe that incorporates the actual bioorthogonal protecting group attached via N,N'-dimethylethylenediamine spacer to resorufin dye (Figure 1A). Resorufin is well established
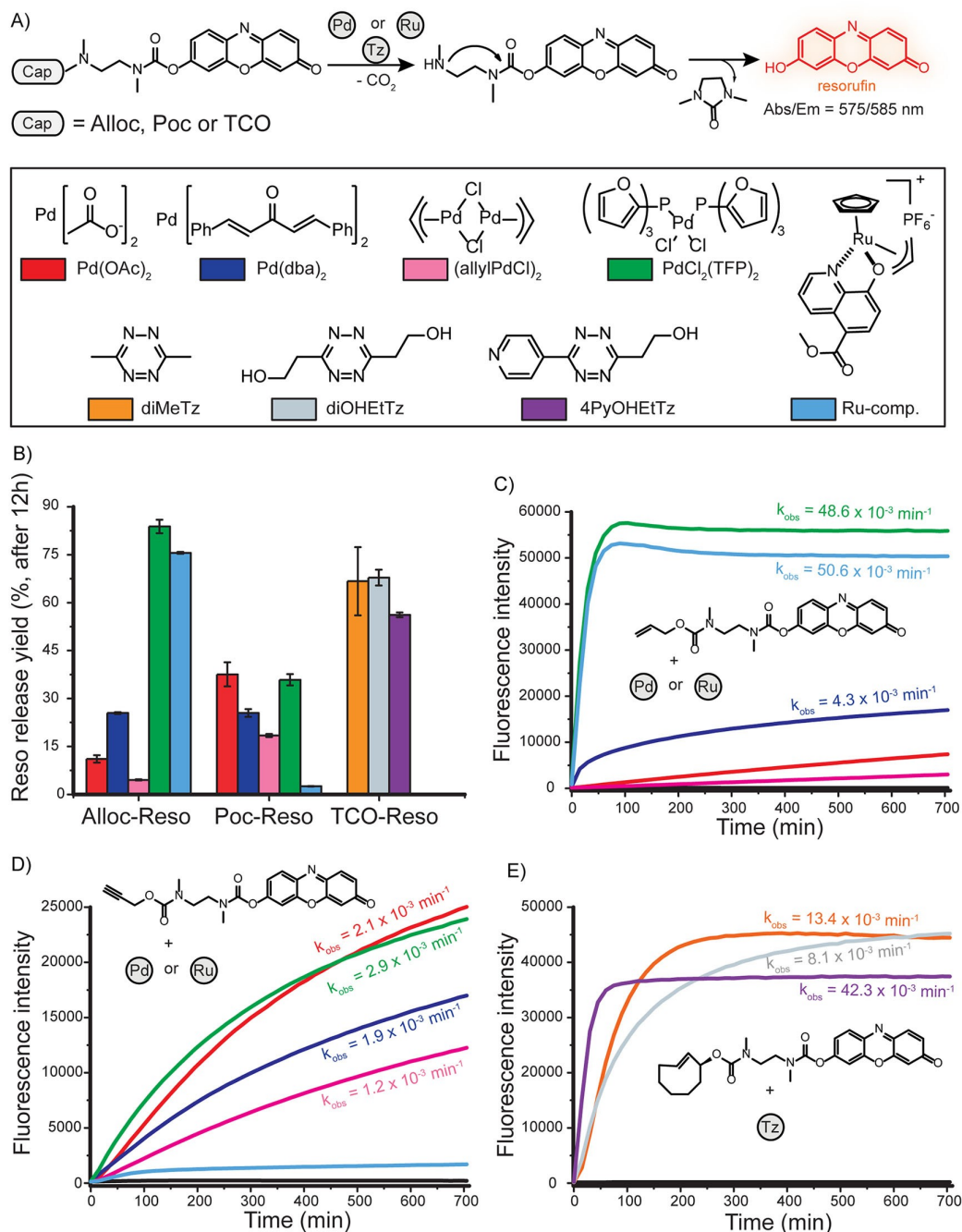

Figure 1. A) Structure of the 'universal' resorufin probes used in this study and mechanism of the dye release from the caged compounds. B) Endpoint release yields of the resorufin dye after 12 hours using different triggers. The experiment was performed in PBS buffer (pH = 7.4) containing 5% DMSO at 25 C using 10 μM final concentration of the caged resorufin and 15 μM final concentration of the metal complexes or tetrazines. Release of the dye was followed on plate reader using 555 ± 10 nm excitation and 595 ± 20 nm emission window. C) Release of resorufin from Alloc-Reso. D) Release of resorufin from Poc-Reso. E) Release of resorufin from TCO-Reso. Black lines at the bottom of the graphs represent control experiments where Alloc-, Poc- or TCO-Reso were incubated in the absence of the activator. The observed rate constants of the reactions are indicated above or below the curves.

ChemPlusChem

Communications
doi.org/10.1002/cplu.202000477

Chemistry
Europe
European Chemical
Societies Publishing

fluorophore being used in many biological assays e.g. in the form of resazurin in cell viability assays[19] or as Amplex red for monitoring the cellular production of reactive oxygen species.[20] The absorption maximum of resorufin centered around 575 nm and the fluorescence emission maximum at 585 nm enables convenient monitoring of the reaction by absorbance and/or fluorescence spectrophotometry and is well suited also for cellular experiments. The N,N'-dimethylethylenediamine spacer is a commonly used self-immolative linker.[21] This linker contains a methyl group at the amino substituent, which should prevent formation of the previously described dead-end product formed in certain TCO/Tz decaging reactions.[22]

Considering these criteria, we synthesized three resorufin releasing probes containing propargyloxycarbonyl (Poc-Reso), allyoxycarbonyl (Alloc-Reso) or trans-cyclooctene (TCO-Reso) caps (Figure 1A). The synthesis is straightforward and includes attachment of the spacer to resorufin using Boc-protected imidazolium active ester, Boc deprotection and subsequent capping of the free methylamino group using the respective chloroformates (for Poc and Alloc) or the TCO-NHS active ester under basic conditions (see the Supporting Information for details). It is important to use highly reactive acylating agents in the last step as the intramolecular cyclization of the generated free methylamino group of the self-immolative N,N'-dimethylethylenediamine linker on the resorufin system is very fast under basic conditions. For example, using equivalent amounts of para-nitrophenyl (PNP) active ester instead of the NHS active ester of TCO yielded only traces of the desired product under identical reaction conditions (data not shown).

With the three caged resorufin-containing probes in hand, we next moved to investigate different triggers to release the dye from the constructs. Based on previous reports, we chose four different palladium species,[6–7,8b] Ru-complex developed by the Meggers group[3b] and three different model tetrazines, dimethyl-tetrazine (diMeTz), dihydroxyethyl tetrazine (diOHEtTz) and 4-pyridyl-hydroxyethyl tetrazine (4PyOHEtTz) (Figure 1B). The decaging experiments were performed in phosphate buffered saline (PBS, pH = 7.4) containing 5 % DMSO and progress of the reaction was monitored in fluorescence plate reader over the course of twelve hours. Alternatively, the reaction can be monitored by UV/Vis spectrophotometry, which gave similar results (see Figure S7 in the Supporting Information).

Our measurements showed that $PdCl_2(TFP)_2$ is the most effective trigger for Alloc-Reso and led to formation of the free resorufin dye in 80 % yield after twelve hours. This is in good agreement with previous studies using caged-rhodamine.[7a] We obtained the second best release yield in reaction of the same alloc protected compound with the Ru-complex. The decaging reaction was in both cases fast and the release reaction under these conditions finished within ca. two hours (Figure 1C).

In the case of Poc-Reso, the most effective metal complex was $Pd(OAc)_2$ together with $PdCl_2(TFP)_2$. However, the release yield did not exceed 45 % in this case with any of the complexes within the time frame. Other palladium complexes performed modestly and gave only low decaging yields. As expected, the Ru-complex was not effective in promoting the Poc deprotec-

tion from Poc-Reso. The Poc-deprotection reactions were also slower when compared to deprotection of the alloc-caged resorufin (Figure 1D).

Among the three tetrazines investigated with TCO-Reso, diMeTz and diOHEtTz gave the free resorufin dye in slightly better yield when compared to 4PyOHEtTz (ca. 70 % vs. 60 %) (Figure 1E). However, the release reaction promoted by the pyridyl-containing tetrazine was faster. Considering that the rate of the first Diels-Alder cycloaddition with EWG-group or aryl containing tetrazines is higher when compared to alkyl substituted tetrazines, it is reasonable to assume that this step is also responsible for the observed overall enhanced release rate of the resorufin dye (Figure S12). The different propensity of substituted tetrazines to form the head-to-head versus head-to-tail adduct is another important factor that can influence the outcome of the tetrazine-promoted release reaction.[22–23] Importantly, our control experiments using Alloc-Reso, Poc-Reso or TCO-Reso without any trigger did not yield free resorufin demonstrating that the constructs are stable under the experimental conditions.

These initial release experiments showed that the Alloc group can be removed more efficiently when compared to the Poc group using either palladium or ruthenium complexes. We therefore continued our study with Alloc-Reso and the two most efficient metal-based triggers, the $PdCl_2(TFP)_2$ and the Ru-complex. One of the potential advantages of the metal-promoted deprotections is the catalytic nature of the reaction. We therefore performed a series of experiments with Alloc-Reso using various concentrations/equivalents of the metal complexes. As shown in Figure 2A and 2B, both metal complexes release the resorufin dye even at 10 mol%, but the yield drops significantly by lowering the amount of the catalyst. The effect is more pronounced for the palladium complex even though the actual deprotection reaction is faster in this case. This experiment demonstrates that the reaction can be performed with catalytic amounts of the metal complexes however, the overall efficiency of the process as well as the final release yields decrease by lowering the amount of the metal complexes. One possible explanation for the observed reduced efficiency could be in that the catalyst decomposes over time. Indeed, we obtained best results when both metal complexes were prepared freshly before the experiment. Even simple pre-incubation of the complexes for one hour in PBS buffer before adding Alloc-Reso resulted in reduction of the release yield and rate. The $PdCl_2(TFP)_2$ seems to be more sensitive than the Ruthenium complex in this regard (Figure 2C). Decomposition of the active catalytic species under these conditions indicates potential limitation for biological applications. However, the use of specific formulations of the metal complexes could provide systems with increased stability and advanced performance.[7a,h]

We performed similar experiment using different equivalents of tetrazines, which promote liberation of the resorufin dye from TCO-Reso (Figure 2D). In this case, we used two or five equivalents of the tetrazine since the reaction is not catalytic. The release of resorufin from TCO-Reso was faster in the presence of five equivalents of the tetrazine, presumably as a result of enhanced reaction rate of the first Diels-Alder reaction
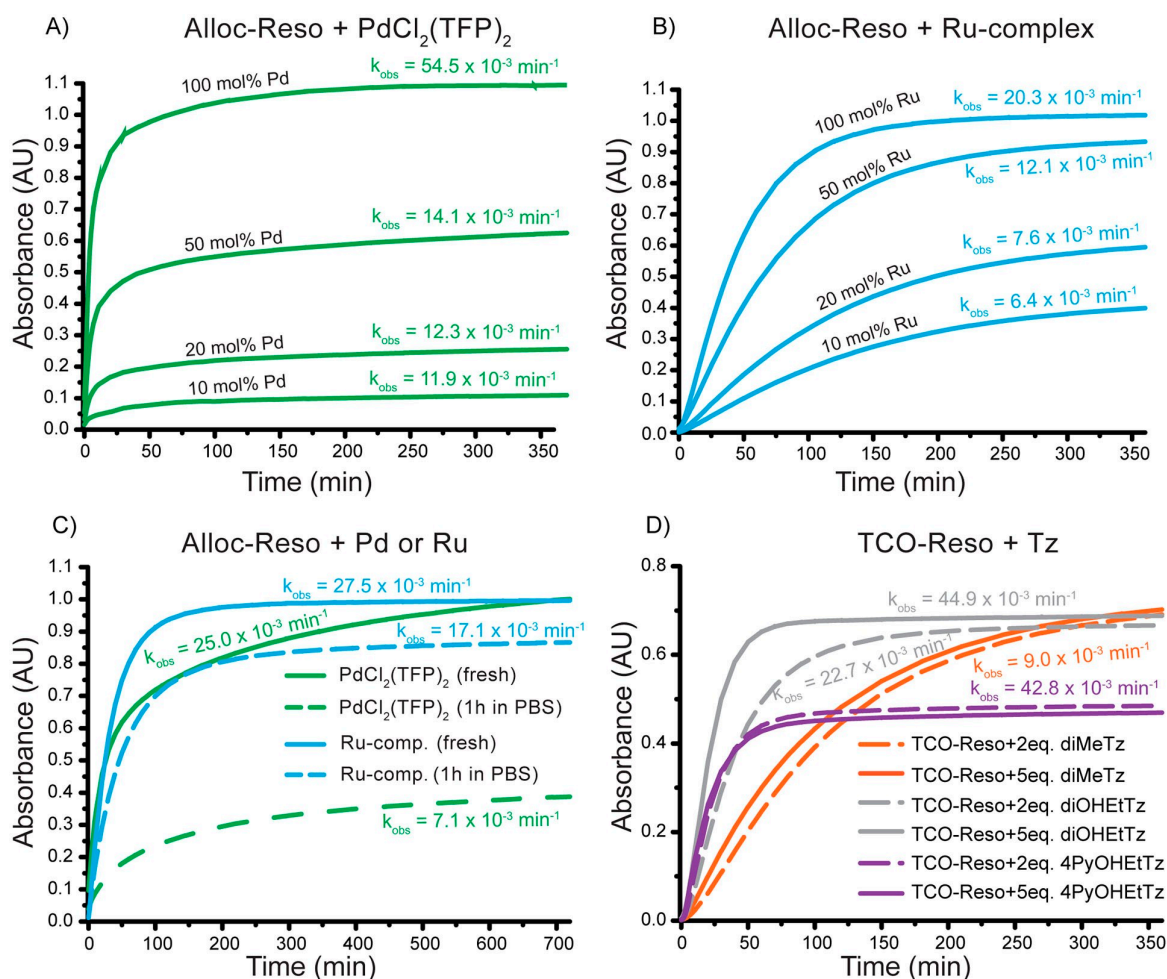
ChemPlusChem

Communications
doi.org/10.1002/cplu.202000477

Chemistry
Europe
European Chemical
Societies Publishing

Figure 2. Comparison of the release reactions using different equivalents of the activators. The experiments were performed at room temperature in PBS buffer containing 5 % DMSO using 20 μM final concentration of the caged-resorufin. Release of the dye was followed by UV/Vis spectrophotometry (575 nm). A) Deprotection of Alloc-Reso using different equivalents of $PdCl_2(TFP)_2$. B) Deprotection of Alloc-Reso using different equivalents of the Ru-complex. C) Experiment showing that the performance of the metal complex is influenced by the experimental setup. Pre-incubation in PBS buffer lowers the efficiency of the reaction and influences the release yield. Reproducible results can be obtained by the use of freshly prepared metal complex solutions. D) Deprotection of TCO-Reso using different equivalents of the tetrazines. The observed rate constants of the reactions are indicated above or below the curves.

step (Figure S12). The effect was most pronounced for diOHEtTz. As expected, there was no significant difference in the final release yield since the subsequent steps leading to release of the dye are intramolecular and therefore independent from the tetrazine concentration.

In an effort to further compare the various release reactions we next explored the possibility to combine the metal-promoted and the Tz-triggered decaging reaction. To have a system that would allow for such comparison, we synthesized Alloc-caged Nile blue dye (Alloc-Nile blue). The absorption and emission spectra of nile blue ($Abs_{max} = 635$ nm and $Em_{max} = 674$ nm) do not overlap with that of resorufin. We therefore thought that it should be possible to simultaneously monitor release of the two dyes in a one pot reaction. We chose 4PyOHEtTz tetrazine for resorufin release from TCO-Reso, because it combines fast reaction rate comparable to the best palladium and ruthenium catalysts. The two metal complexes,

$PdCl_2(TFP)_2$ and the Ru-comp. were used to promote release of nile blue from Alloc-Nile blue. The experiments were performed in PBS buffer containing 5 % DMSO and progress of the release reaction was followed by the scanning kinetics method in UV/Vis spectrophotometer (Figure 3). Similar experiments were also analyzed by HPLC equipped with a fluorescence detector (Figure S8).

As observed in all previous experiments, 4PyOHEtTz leads to efficient release of the resorufin dye from TCO-Reso. The Alloc-Nile blue can be deprotected with both metal catalysts, but the reaction is more efficient with the Ru-complex. The observed difference when compared to the resorufin release could be in that Alloc-Nile blue bears the substituent on aromatic amino group. When we combined TCO-Reso and Alloc-Nile blue and added only 4PyOHEtTz we observed efficient release of the resorufin dye. Although not directly visible in the UV/Vis spectrum, the HPLC analysis revealed that small amounts of nile
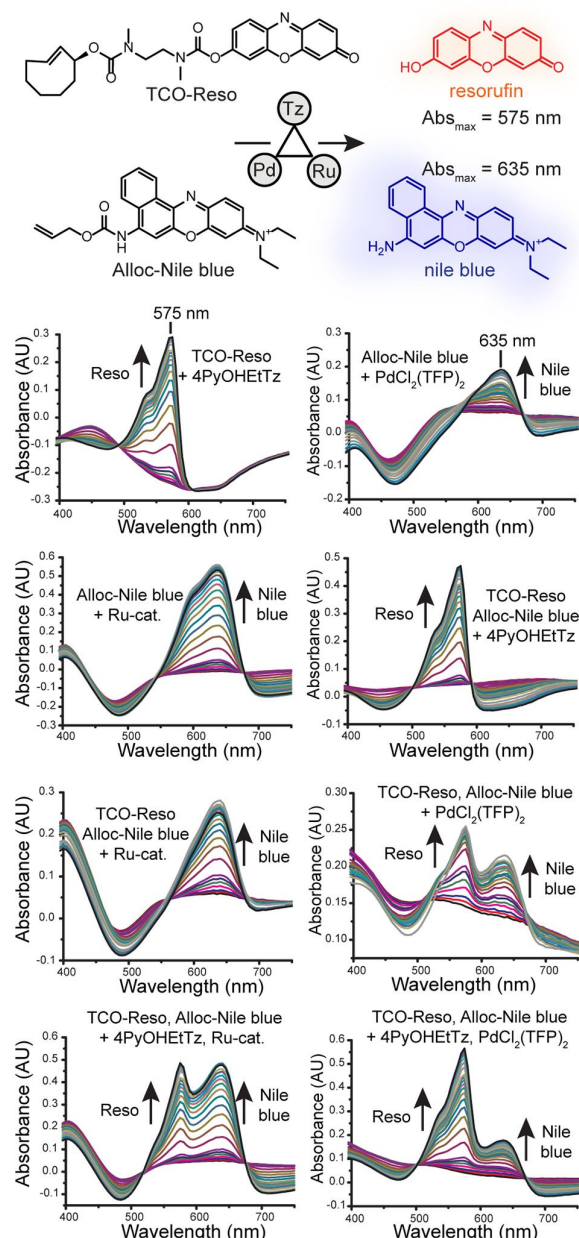
ChemPlusChem

Communications
doi.org/10.1002/cplu.202000477

Chemistry Europe
European Chemical
Societies Publishing

Figure 3. Simultaneous release of resorufin and nile blue dyes using different combinations of activators. The tetrazine-triggered reaction is orthogonal to the Ru-promoted release, but it is not orthogonal to the palladium-promoted cleavage. The later combination leads to 'unspecific' release of the resorufin possibly promoted by allyl palladium species formed during the alloc deprotection (Figure S8). These experiments were performed in PBS buffer containing 5% DMSO at room temperature using 20 μM final concentrations of TCO-Reso or Alloc-Nile blue and 30 μM concentration of the activator. Release of the dyes was followed by UV/Vis spectrophotometry (Abs max. 575 nm for resorufin or 635 nm for nile blue). Similar experiments were analyzed by HPLC using fluorescence detection (Figure S8).

blue formed in this case as well (Figure S8). This can be a result of the reaction of tetrazine with the alloc group which leads to subsequent release of the dye similarly to the known reaction of tetrazines with vinyl ethers.[14c,24] When we combined TCO-

Reso and Alloc-Nile blue with the Ru-catalyst we observed specific formation of the free nile blue dye without concomitant resorufin release demonstrating that the Ru-complex does not release resorufin from TCO-Reso and that this metal-promoted decaging reaction is orthogonal to the tetrazine-triggered chemistry.

The outcome was different when we combined the mixture of TCO-Reso and Alloc-Nile blue with PdCl$_2$(TFP)$_2$. In this case, we observed the release of both dyes, resorufin and nile blue. This was confirmed also by HPLC analysis using fluorescence detection (Figure S8). To find out if PdCl$_2$(TFP)$_2$ is able to release resorufin from TCO-Reso we mixed these two reagents under the same conditions and analyzed the mixture by HPLC. Surprisingly, we did not observe resorufin release even after 24 hours, showing that this palladium complex alone is not responsible for resorufin release from TCO-Reso (Figure S9). We therefore hypothesized that other active species must form when the three reagents, TCO-Reso, Alloc-Nile blue and PdCl$_2$(TFP)$_2$, are all present in the reaction mixture. One possibility is that the alloc substituent in the form of an allyl group coordinates to the palladium and that this complex then leads to the release of resorufin from TCO-Reso. To test this hypothesis, we incubated TCO-Reso with allyl palladium dichloride dimer complex (Pd$_2$Cl$_2$allyl$_2$). Indeed, we observed clear resorufin release in this case (Figure S9). To the best of our knowledge this is the first example of a metal-promoted release reaction from a TCO-caged compound. The efficiency and practicability of the process especially in connection with and compared to the tetrazine-promoted reaction is currently under investigation and will be reported elsewhere.

We next evaluated the release reactions in cells. Live HeLa cells were loaded with 5 μM of Alloc-Reso, Poc-Reso or TCO-Reso for 30 min. The cells were then washed to remove excess of the probe from the extracellular space and were incubated with the activators for 24 hours. The fluorescence intensity of released resorufin was measured by a flow cytometer (Figure S10). Assuming that all caged resorufin constructs penetrated the cells, this experiment showed that PdCl$_2$(TFP)$_2$ does not release the dye from Alloc-Reso inside the cells even when used at 10 μM concentration. Similarly, we did not observe resorufin release from Poc-Reso by Pd(OAc)$_2$. A series of additional confocal microscopy experiments corroborated these results and showed that even higher doses of the metal complexes do not lead to resorufin release in the cells (Figure S11). These data clearly indicate that the palladium complexes are not suitable for intracellular applications. In contrast, the Ru-complex led to resorufin release from Alloc-Reso even at 0.5 μM concentration. However, we noticed altered cell morphology at this concentration possibly due to toxicity of the metal complex (see below). Both diMeTz and 4PyOHEtTz successfully released resorufin from TCO-Reso as confirmed by both, flow cytometry and confocal microscopy.

To further compare the efficiency of various release reactions in a cellular context, we prepared alloc- and TCO-caged doxorubicins (Alloc-Doxo and TCO-Doxo). These compounds were previously used on different cell lines to demonstrate the potential of release reactions for prodrug

activation.[3,9] In agreement with previous studies, blocking the amino group of doxorubicin with alloc or TCO yields compounds with lower IC$_{50}$ when compared to free doxorubicin (Table 1, Figure S13).[3b,9] We first assessed the toxicity of the metals and the tetrazines after 72 h on HeLa cells. The Ru-complex was by far the most toxic among the activators with an IC$_{50}$ of 70 nM exceeding even the free doxorubicin. PdCl$_2$(TFP)$_2$ and the tetrazines all showed modest toxicity with IC$_{50}$ values well above the doxorubicins.

Based on these preliminary data, we next combined Alloc-Doxo with PdCl$_2$(TFP)$_2$ (10 μM) and TCO-Doxo with the three tetrazines (10 μM) using otherwise identical experimental conditions. We did not use the Ru-complex in this experiment due to its high toxicity. On the other hand, we used the palladium complex even though it is probably not cell permeable. In this case, even if the activation reaction will be extracellular the released doxorubicin can enter the cells. We determined the IC$_{50}$ values of the respective combination of reagents on HeLa cells after 72 hours (Table 1, Figure S13). As expected, all compounds were able to release free doxorubicin from the respective precursors as can be deduced from the increased IC$_{50}$ values. The lower IC$_{50}$ determined in the release experiments when compared to the parent doxorubicin indicates that the doxorubicin release is only partial, which agrees with the resorufin release experiments and with previous studies.[3,9]

Altogether, these data show that PdCl$_2$(TFP)$_2$ and all tetrazines tested can be used as triggers for prodrug activation and that these reactions are similarly efficient. In addition, the tetrazines efficiently promote release of the dye inside the cells. Hence, they could be used for release of intracellularly localized prodrugs. The significant toxicity of the Ru-complex severely limits its utility in and on biological systems. The palladium complexes used in this study are not sufficiently cell permeable (or decompose inside the cells) and are better suited for extracellular applications.[6,8b] It is worth noting that for many applications (e.g. metal-triggered prodrug activation) the release reaction does not need to be intracellular. Indeed, several groups showed that organometallic activators can be used in the form of nano-formulations that can be implanted during surgery or has the ability to accumulate at the tumor site based on the enhanced permeability and retention effect. After prodrug administration, these organometallic devices serve to produce the active drugs locally, which can have beneficial therapeutic effect.[7a,e] For intracellular applications, the metal catalyst can be fused to e.g. cell-penetrating peptides.[25]

In conclusion, we have performed a comparison of two metal-promoted and the tetrazine-triggered bioorthogonal release reactions with the aim to identify the pros and cons of each methodology under the same experimental conditions. Using new fluorogenic resorufin derivatives, we show that the allyloxycarbonyl protecting group can be removed more efficiently when compared to propargyloxycarbonyl group using either palladium or ruthenium complexes. All tetrazines investigated efficiently release the resorufin dye from the TCO-caged compound under the same conditions. Our results indicate that although the metal-promoted reactions can be performed using catalytic amounts of the complexes, the efficiency and the reaction rates significantly decrease when these reagents are used sub-stoichiometrically. Therefore, the true catalytic nature of the reactions under biologically relevant conditions remains questionable. We found that the Ru-promoted and the tetrazine-triggered reactions are mutually orthogonal, which opens new avenues toward multi-decaging applications. However, the high toxicity of the Ru-complex limits its utility mainly to non-biological systems. Unexpectedly, we discovered that resorufin can be released from the TCO-caged compound by certain palladium complexes. This observation may lead to development of new decaging reactions. Our experiments on HeLa cells revealed that the elimination reactions promoted by PdCl$_2$(TFP)$_2$ take place rather in the extracellular space. In contrast, the tetrazine-triggered reactions efficiently proceed inside the cells. Except for the Ru-complex, which showed significant toxicity, the PdCl$_2$(TFP)$_2$ and all tetrazines investigated can be used for prodrug activation as demonstrated by doxorubicin release from the respective alloc- and TCO-caged derivatives. We believe that this study will serve as useful guideline for scientists who consider using these chemical activation reactions, but have difficulties by choosing the right method for a given application.

Conflict of Interest

The authors declare no conflict of interest.

Table 1. IC$_{50}$ values for doxorubicin derivatives, the activators and combinations thereof as determined on HeLa cells after 72 hours.

Compound	IC$_{50}$ [μM][a]
Doxo	0.22 ± 0.02
Alloc-Doxo	2.37 ± 0.17
TCO-Doxo	1.00 ± 0.03
PdCl$_2$(TFP)$_2$	78.0 ± 22[b]
Ru-complex	0.07 ± 0.005
diMeTz	>100
diOHEtTz	84.0 ± 2[b]
4PyOHEtTz	31.0 ± 1
Alloc-Doxo + 10 μM PdCl$_2$(TFP)$_2$	0.66 ± 0.12
TCO-Doxo + 10 μM diMeTz	0.52 ± 0.04
TCO-Doxo + 10 μM diOHEtTz	0.45 ± 0.04
TCO-Doxo + 10 μM 4PyOHEtTz	0.45 ± 0.04

[a] Determined by CellTiter Glo® ATP assay. [b] Estimated values because of the concentration range used in the experiment (maximum concentration tested was 100 μM).

[1] a) J. Li, P. R. Chen, *Nat. Chem. Biol.* **2016**, *12*, 129–137; b) X. Ji, Z. Pan, B. Yu, L. K. De La Cruz, Y. Zheng, B. Ke, B. Wang, *Chem. Soc. Rev.* **2019**, *48*, 1077–1094; c) T. Volker, E. Meggers, *Curr. Opin. Chem. Biol.* **2015**, *25*, 48–54.

[2] C. Streu, E. Meggers, *Angew. Chem. Int. Ed.* **2006**, *45*, 5645–5648; *Angew. Chem.* **2006**, *118*, 5773–5776.

[3] a) T. Volker, F. Dempwolff, P. L. Graumann, E. Meggers, *Angew. Chem. Int. Ed.* **2014**, *53*, 10536–10540; *Angew. Chem.* **2014**, *126*, 10705–10710; b) T. Volker, E. Meggers, *ChemBioChem* **2017**, *18*, 1083–1086.

[4] M. Tomas-Gamasa, M. Martinez-Calvo, J. R. Couceiro, J. L. Mascarenas, *Nat. Commun.* **2016**, *7*, 12538.

[5] E. i Negishi, *Handbook of Organopalladium Chemistry for Organic Synthesis*, John Wiley & Sons, **2002**.

[6] R. M. Yusop, A. Unciti-Broceta, E. M. Johansson, R. M. Sanchez-Martin, M. Bradley, *Nat. Chem.* **2011**, *3*, 239–243.

[7] a) M. A. Miller, B. Askevold, H. Mikula, R. H. Kohler, D. Pirovich, R. Weissleder, *Nat. Commun.* **2017**, *8*, 15906; b) J. T. Weiss, J. C. Dawson, K. G. Macleod, W. Rybski, C. Fraser, C. Torres-Sanchez, E. E. Patton, M. Bradley, N. O. Carragher, A. Unciti-Broceta, *Nat. Commun.* **2014**, *5*, 3277 ; c) J. T. Weiss, J. C. Dawson, C. Fraser, W. Rybski, C. Torres-Sanchez, M. Bradley, E. E. Patton, N. O. Carragher, A. Unciti-Broceta, *J. Med. Chem.* **2014**, *57*, 5395–5404; d) C. Adam, A. M. Perez-Lopez, L. Hamilton, B. Rubio-Ruiz, T. L. Bray, D. Sieger, P. M. Brennan, A. Unciti-Broceta, *Chem. Eur. J.* **2018**, *24*, 16783–16790; e) T. L. Bray, M. Salji, A. Brombin, A. M. Perez-Lopez, B. Rubio-Ruiz, L. C. A. Galbraith, E. E. Patton, H. Y. Leung, A. Unciti-Broceta, *Chem. Sci.* **2018**, *9*, 7354–7361; f) J. T. Weiss, C. Fraser, B. Rubio-Ruiz, S. H. Myers, R. Crispin, J. C. Dawson, V. G. Brunton, E. E. Patton, N. O. Carragher, A. Unciti-Broceta, *Front. Chem.* **2014**, *2*; g) G. Y. Tonga, Y. D. Jeong, B. Duncan, T. Mizuhara, R. Mout, R. Das, S. T. Kim, Y. C. Yeh, B. Yan, S. Hou, V. M. Rotello, *Nat. Chem.* **2015**, *7*, 597–603; h) J. T. Weiss, N. O. Carragher, A. Unciti-Broceta, *Sci. Rep.* **2015**, *5*, 9329.

[8] a) J. Li, J. T. Yu, J. Y. Zhao, J. Wang, S. Q. Zheng, S. X. Lin, L. Chen, M. Y. Yang, S. Jia, X. Y. Zhang, P. R. Chen, *Nat. Chem.* **2014**, *6*, 352–361; b) J. Wang, S. Zheng, Y. J. Liu, Z. Y. Zhang, Z. Lin, J. F. Li, G. Zhang, X. Wang, J. Li, P. R. Chen, *J. Am. Chem. Soc.* **2016**, *138*, 15118–15121.

[9] R. M. Versteegen, R. Rossin, W. ten Hoeve, H. M. Janssen, M. S. Robillard, *Angew. Chem. Int. Ed.* **2013**, *52*, 14112–14116; *Angew. Chem.* **2013**, *125*, 14362–14366.

[10] R. M. Versteegen, W. Ten Hoeve, R. Rossin, M. A. R. de Geus, H. M. Janssen, M. S. Robillard, *Angew. Chem. Int. Ed.* **2018**, *57*, 10494–10499; *Angew. Chem.* **2018**, *130*, 10654–10659.

[11] a) A. H. A. M. van Onzen, R. M. Versteegen, F. J. M. Hoeben, I. A. W. Filot, R. Rossin, T. Zhu, J. Wu, P. J. Hudson, H. M. Janssen, W. ten Hoeve, M. S. Robillard, *J. Am. Chem. Soc.* **2020**, doi.org/10.1021/jacs.0c00531; b) J. Tu, D. Svatunek, S. Parvez, H. J. Eckvahl, M. Xu, R. T. Peterson, K. N. Houk, R. M. Franzini, *Chem. Sci.* **2020**, *11*, 169–179.

[12] a) R. Rossin, R. M. Versteegen, J. Wu, A. Khasanov, H. J. Wessels, E. J. Steenbergen, W. Ten Hoeve, H. M. Janssen, A. van Onzen, P. J. Hudson, M. S. Robillard, *Nat. Commun.* **2018**, *9*, 1484; b) R. Rossin, S. M. J. van Duijnhoven, W. ten Hoeve, H. M. Janssen, L. H. J. Kleijn, F. J. M. Hoeben, R. M. Versteegen, M. S. Robillard, *Bioconjugate Chem.* **2016**, *27*, 1697–1706.

[13] A. M. F. van der Gracht, M. A. R. de Geus, M. G. M. Camps, T. J. Ruckwardt, A. J. C. Sarris, J. Bremmers, E. Maurits, J. B. Pawlak, M. M. Posthoorn, K. M. Bonger, D. V. Filippov, H. S. Overkleeft, M. S. Robillard, F. Ossendorp, S. I. van Kasteren, *ACS Chem. Biol.* **2018**, *13*, 1569–1576.

[14] a) H. X. Wu, S. C. Alexander, S. J. Jin, N. K. Devaraj, *J. Am. Chem. Soc.* **2016**, *138*, 11429–11432; b) K. Neumann, S. Jain, A. Gambardella, S. E. Walker, E. Valero, A. Lilienkampf, M. Bradley, *ChemBioChem* **2017**, *18*, 91–95; c) E. Jimenez-Moreno, Z. J. Guo, B. L. Oliveira, I. S. Albuquerque, A. Kitowski, A. Guerreiro, O. Boutureira, T. Rodrigues, G. Jimenez-Oses, G. J. L. Bernardes, *Angew. Chem. Int. Ed.* **2017**, *56*, 243–247; *Angew. Chem.* **2017**, *129*, 249–253; d) K. Neumann, A. Gambardella, A. Lilienkampf, M. Bradley, *Chem. Sci.* **2018**, *9*, 7198–7203.

[15] M. H. Xu, J. L. Tu, R. M. Franzini, *Chem. Commun.* **2017**, *53*, 6271–6274.

[16] J. L. Tu, M. H. Xu, S. Parvez, R. T. Peterson, R. M. Franzini, *J. Am. Chem. Soc.* **2018**, *140*, 8410–8414.

[17] K. Neumann, A. Gambardella, M. Bradley, *ChemBioChem* **2019**, *20*, 872–876.

[18] a) X. Y. Fan, Y. Ge, F. Lin, Y. Yang, G. Zhang, W. S. C. Ngai, Z. Lin, S. Q. Zheng, J. Wang, J. Y. Zhao, J. Li, P. R. Chen, *Angew. Chem. Int. Ed.* **2016**, *55*, 14046–14050; *Angew. Chem.* **2016**, *128*, 14252–14256; b) M. A. R. de Geus, E. Maurits, A. J. C. Sarris, T. Hansen, M. S. Kloet, K. Kamphorst, W. ten Hoeve, M. S. Robillard, A. Pannwitz, S. A. Bonnet, J. D. C. Codée, D. V. Filippov, H. S. Overkleeft, S. I. van Kasteren, *Chem. Eur. J.* **2020**, doi:10.1002/chem.201905446.

[19] R. D. Fields, M. V. Lancaster, *Am. Biotechnol. Lab.* **1993**, *11*, 48–50.

[20] M. Zhou, Z. Diwu, N. Panchuk-Voloshina, R. P. Haugland, *Anal. Biochem.* **1997**, *253*, 162–168.

[21] A. Alouane, R. Labruere, T. Le Saux, F. Schmidt, L. Jullien, *Angew. Chem. Int. Ed.* **2015**, *54*, 7492–7509; *Angew. Chem.* **2015**, *127*, 7600–7619.

[22] J. C. T. Carlson, H. Mikula, R. Weissleder, *J. Am. Chem. Soc.* **2018**, *140*, 3603–3612.

[23] A. J. C. Sarris, T. Hansen, M. A. R. de Geus, E. Maurits, W. Doelman, H. S. Overkleeft, J. D. C. Codee, D. V. Filippov, S. I. van Kasteren, *Chem. Eur. J.* **2018**, *24*, 18075–18081.

[24] M. Staderini, A. Gambardella, A. Lilienkampf, M. Bradley, *Org. Lett.* **2018**, *20*, 3170–3173.

[25] E. Indrigo, J. Clavadetscher, S. V. Chankeshwara, A. Megia-Fernandez, A. Lilienkampf, M. Bradley, *Chem. Commun.* **2017**, *53*, 6712–6715.

A thesis submitted for the degree of

Doctor of Philosophy

in

Applied Biology and Experimental Medicine

UNIVERSITY OF MESSINA

DEPARTMENT OF CHEMICAL, BIOLOGICAL,
PHARMACEUTICAL AND ENVIRONMENTAL SCIENCES